To the Graduate Council:

I am submitting herewith a thesis written by Hideho Tanaka entitled "Rheological Properties of Polymer Melts Reinforced with Small Particles." I recommend that it be accepted in partial fulfillment of the requirements for the degree of Master of Science, with a major in Polymer Engineering.

J. L. White, Major Professor

We have read this thesis and recommend its acceptance:

Accepted for the Council:

Vice Chancellor
Graduate Studies and Research

RHEOLOGICAL PROPERTIES OF POLYMER MELTS REINFORCED WITH SMALL PARTICLES

A Thesis

Presented for the

Master of Science

Degree

The University of Tennessee, Knoxville

Hideho Tanaka

August 1979

ACKNOWLEDGMENTS

The author gives his thanks to the many people who have made this study possible.

First of all, hearty appreciation is expressed to Professor James L. White, the author's advisor throughout his graduate study at The University of Tennessee, for his helpful comments and suggestions and patient encouragement in all aspects of the author's graduate work.

Appreciation is also expressed to Professor Donald C. Bogue for his helpful comments and suggestions.

The author is very thankful to UBE Industries, LTD. for providing the opportunity to study at this university.

The author is also grateful to all faculty members and student colleagues who have given useful suggestions and discussions, particularly to Mr. W. Minoshima for melt spinning study methods. The author owes his study to the members of the Laboratory Service Shops. Appreciation is also extended to Mr. B. L. McGill for his help in obtaining the scanning electron micrographs.

Financial support for this study was provided by UBE Industries, LTD., and the National Science Foundation.

Finally, the author expresses his thanks to du Pont, Dow Chemical, Monsanto Co. and Pfizer Inc. for providing samples.

ABSTRACT

An experimental investigation of rheological properties during both shear and elongational flow and melt spinning characteristics for polystyrene melts reinforced with small rigid particles and high impact polystyrene (HIPS) is reported.

The influences of loading level, particle size and surface treatment were discussed. These systems exhibit yield values for both shear and elongational flow. Experimental values for the ratio of the tensile to the shear yield stress give satisfactory agreement with the production of the von Mises yield criterion. The yield value appears to increase with decreasing particle size and may lower with surface treatment. The first normal stress difference at fixed shear stress decreased with loading level. The spinline elongational viscosity for filled systems shows a strong elongational rate thinning behavior compared with unfilled systems, the same trend as in the steady state elongational viscosity. It has been found that an addition of small particles makes the spinline unstable under both isothermal and nonisothermal conditions.

A theoretical approach to shear viscosity was attempted from a mechanistic viewpoint. A cell theory model of concentrated suspensions involving particle-particle interaction was developed. This theory suggests that a yield stress is related to the particle-particle interaction energy per unit volume. The predicted values give satisfactory agreements with experimental data concerning the effects

of particle characteristics on shear viscosity and yield stress. Then, the phenomenological theory of White which is largely consistent with the mechanistic theory was compared with experimental data on both shear and elongational flow. A proposal for flow mechanism was made.

TABLE OF CONTENTS

CHAPTER		PAGE
I.	INTRODUCTION	1
II.	LITERATURE SURVEY	3
	A. Experimental Investigations of Rheological Properties of Suspensions	3
	B. Phenomenological Theory for Polymer Melts Highly-Filled with Small Particles	16
	C. Mechanistic Theory for Concentrated Suspensions of Small Particles	37
III.	THEORETICAL APPROACH TO THE VISCOSITY OF CONCENTRATED SUSPENSIONS OF SMALL PARTICLES	47
	A. Introduction	47
	B. Viscous Dissipation Due to Flow	49
	C. Energy Dissipation Due to Other Force Fields	57
	D. Theory of Viscosity	61
	E. Summary of View of Viscosity Behavior of Polymer Melts Reinforced with Small Particles	66
IV.	MATERIALS AND EXPERIMENTAL PROCEDURES	67
	A. Materials	67
	B. Preparation of Samples	67
	C. Rheological Measurements	78
	D. Melt Spinning	84
V.	EXPERIMENTAL STUDIES ON SHEAR FLOW	92
	A. Shear Viscosity	92
	B. First Normal Stress Difference	105
VI.	EXPERIMENTAL STUDIES ON ELONGATIONAL FLOW	128
	A. Transient Elongational Viscosity	128
	B. Steady State Elongational Viscosity	140
	C. Elongation to Break	152
VII.	COMPARISON OF EXPERIMENTAL DATA WITH RHEOLOGICAL THEORIES	161
	A. Yield Surface	161
	B. Comparison of Mechanistic Theory with Experiment	169

CHAPTER PAGE

C. Comparison of Phenomenological Theory with Experiment 179

VIII. MELT SPINNING 192

A. Introduction 192
B. Spinline Elongational Viscosity During Isothermal Melt Spinning 192
C. Draw Resonance Phenomena 201

IX. CONCLUSIONS AND RECOMMENDATIONS 213

A. Conclusions 213
B. Recommendations 215

LIST OF REFERENCES 217

APPENDIX 230

VITA 234

LIST OF TABLES

TABLE		PAGE
II.1.	Yield Values for Polymer Melts Reinforced with Small Particles	10
II.2.	Reduced Elastic Recoveries of Polymer Melts Reinforced with Small Particles	11
IV.1.	Description of Polymers Used	68
IV.2.	Characteristics of Fillers Studied	69
IV.3.	Weight Fraction of Fillers in Compounds Prepared	77
IV.4.	Densities of Samples Used and Ratio of Cross Section of Filament at 180°C to That at 25°C After Annealing	83
VII.1.	Experimental Yield Values	166
VII.2.	Comparison of Experimental Yield Stress with Theoretical Value	172
VIII.1.	Critical Draw Ratio During Isothermal Melt Spinning . . .	204
VIII.2.	Critical Draw Ratio During Nonisothermal Melt Spinning . .	207

LIST OF FIGURES

FIGURE		PAGE
II.1.	Bingham Plastic Model	26
II.2.	Schwedoff Body	28
III.1.	Relative Motion of Two Spheres	50
IV.1.	Scanning Electron Micrograph of Carbon Black Used	70
IV.2.	Scanning Electron Micrograph of TiO_2 Used	71
IV.3.	Scanning Electron Micrograph of Untreated $CaCO_3$ Used	72
IV.4.	Scanning Electron Micrograph of Treated $CaCO_3$ Used	73
IV.5.	Transmission Electron Micrograph of HIPS-A Sample	74
IV.6.	Transmission Electron Micrograph of HIPS-B Sample	75
IV.7.	Elongational Flow Apparatus	80
IV.8.	Nonisothermal Melt Spinning Apparatus	85
IV.9.	Isothermal Melt Spinning Apparatus	87
V.1.	Shear Viscosity as a Function of Shear Rate for CB-Filled PS Melts	93
V.2.	Shear Viscosity as a Function of Shear Rate for TiO_2-Filled PS Melts	94
V.3.	Shear Viscosity as a Function of Shear Rate for $CaCO_3$-Filled PS Melts	95
V.4.	Shear Viscosity as a Function of Shear Rate for HIPS Melts	96
V.5.	Shear Viscosity as a Function of Shear Rate for HDPE/PS Melts	98
V.6.	Shear Viscosity as a Function of Shear Stress for CB-Filled PS Melts	99
V.7.	Shear Viscosity as a Function of Shear Stress for TiO_2-Filled PS Melts	100

FIGURE PAGE

V.8. Shear Viscosity as a Function of Shear Stress for $CaCO_3$-Filled PS Melts 101

V.9. Shear Viscosity as a Function of Shear Stress for HIPS Melts 103

V.10. Shear Viscosity as a Function of Shear Stress for HDPE/PS Melts 104

V.11. First Normal Stress Difference as a Function of Shear Rate for CB-Filled PS Melts 106

V.12. First Normal Stress Difference as a Function of Shear Rate for TiO_2-Filled PS Melts 107

V.13. First Normal Stress Difference as a Function of Shear Rate for $CaCO_3$-Filled PS Melts 108

V.14. First Normal Stress Difference as a Function of Shear Stress for CB-Filled PS Melts 109

V.15. First Normal Stress Difference as a Function of Shear Stress for TiO_2-Filled PS Melts 110

V.16. First Normal Stress Difference as a Function of Shear Stress for $CaCO_3$-Filled PS Melts 111

V.17. First Normal Stress Difference Coefficient as a Function of Shear Rate for CB-Filled PS Melts 112

V.18. First Normal Stress Difference Coefficient as a Function of Shear Rate for TiO_2-Filled PS Melts 113

V.19. First Normal Stress Difference Coefficient as a Function of Shear Rate for $CaCO_3$-Filled PS Melts 114

V.20. First Normal Stress Difference as a Function of Shear Rate for HIPS Melts 115

V.21. First Normal Stress Difference as a Function of Shear Stress for HIPS Melts 116

V.22. First Normal Stress Difference Coefficient as a Function of Shear Rate for HIPS Melts 117

V.23. First Normal Stress Difference as a Function of Shear Rate for HDPE/PS Melts 119

FIGURE		PAGE
V.24.	First Normal Stress Difference as a Function of Shear Stress for HDPE/PS Melts	120
V.25.	First Normal Stress Difference Coefficient as a Function of Shear Rate for HDPE/PS Melts	121
V.26.	First Normal Stress Difference as a Function of Shear Stress for Various Filled PS Melts at the Same Loading Level	123
V.27.	First Normal Stress Difference Coefficient as a Function of Shear Stress for CB-Filled PS Melts	125
V.28.	First Normal Stress Difference Coefficient as a Function of Shear Stress for TiO_2-Filled PS Melts	126
V.29.	First Normal Stress Difference Coefficient as a Function of Shear Stress for $CaCO_3$-Filled PS Melts	127
VI.1.	Transient Elongational Viscosity at Various Elongational Rates for PS Melt	129
VI.2.	Transient Elongational Viscosity at Various Elongational Rates for 10% CB-Filled PS Melt	130
VI.3.	Transient Elongational Viscosity at Various Elongational Rates for 20% CB-Filled PS Melt	131
VI.4.	Transient Elongational Viscosity at Various Elongational Rates for 30% CB-Filled PS Melt	132
VI.5.	Transient Elongational Viscosity at Various Elongational Rates for 20% TiO_2-Filled PS Melt	133
VI.6.	Transient Elongational Viscosity at Various Elongational Rates for 30% TiO_2-Filled PS Melt	134
VI.7.	Transient Elongational Viscosity at Various Elongational Rates for 30% Untreated $CaCO_3$-Filled PS Melt	135
VI.8.	Transient Elongational Viscosity at Various Elongational Rates for 30% Treated $CaCO_3$-Filled PS Melt	136
VI.9.	Transient Elongational Viscosity at Various Elongational Rates for HIPS-A Melt	137
VI.10.	Transient Elongational Viscosity at Various Elongational Rates for HIPS-C Melt	138

FIGURE		PAGE
VI.11.	Transient Elongational Viscosity at Various Elongational Rates for 50% HDPE-Blended PS Melt	139
VI.12.	Steady State Elongational Viscosity as a Function of Elongational Rate for CB-Filled PS Melts	142
VI.13.	Steady State Elongational Viscosity as a Function of Elongational Rate for TiO_2-Filled PS Melts	143
VI.14.	Steady State Elongational Viscosity as a Function of Elongational Rate for $CaCO_3$-Filled PS Melts	144
VI.15.	Steady State Elongational Viscosity as a Function of Elongational Rate for HIPS Melts	145
VI.16.	Steady State Elongational Viscosity as a Function of Elongational Rate for HDPE/PS Melts	146
VI.17.	Steady State Elongational Viscosity as a Function of Tensile Stress for CB-Filled PS Melts	147
VI.18.	Steady State Elongational Viscosity as a Function of Tensile Stress for TiO_2-Filled PS Melts	148
VI.19.	Steady State Elongational Viscosity as a Function of Tensile Stress for $CaCO_3$-Filled PS Melts	149
VI.20.	Steady State Elongational Viscosity as a Function of Tensile Stress for HIPS Melts	151
VI.21.	Steady State Elongational Viscosity as a Function of Tensile Stress for HDPE/PS Melts	153
VI.22.	Elongation to Break as a Function of Elongational Rate for CB-Filled PS Melts	154
VI.23.	Elongation to Break as a Function of Elongational Rate for TiO_2-Filled PS Melts	155
VI.24.	Elongation to Break as a Function of Elongational Rate for $CaCO_3$-Filled PS Melts	156
VI.25.	Elongation to Break as a Function of Elongational Rate for HIPS Melts	157
VI.26.	Elongation to Break as a Function of Elongational Rate for HDPE/PS Melts	158

FIGURE PAGE

VI.27. Elongation to Break as a Function of Elongational Rate for Various Filled PS Melts at the Same Loading Level 160

VII.1. Viscosity as a Function of Stress During Both Shear and Elongational Flow for 30% CB-Filled PS Melt 162

VII.2. Viscosity as a Function of Stress During Both Shear and Elongational Flow for 30% TiO_2-Filled PS Melt 163

VII.3. Viscosity as a Function of Stress During Both Shear and Elongational Flow for 30% Untreated $CaCO_3$-Filled PS Melt 164

VII.4. Viscosity as a Function of Stress During Both Shear and Elongational Flow for 30% Treated $CaCO_3$-Filled PS Melt 165

VII.5. Empirical Correlations Between Yield Stress and Particle Size 167

VII.6. Plot of η^* versus Shear Rate for Small Rigid Particle-Filled PS Melts 173

VII.7. Plot of η^*/η_0^* versus Shear Rate for Small Rigid Particle-Filled PS Melts 174

VII.8. Plot of η^*/η^0 versus Shear Rate for Small Rigid Particle-Filled PS Melts 176

VII.9. $f(\phi)$ as a Function of Volume Fraction of Small Rigid Particles 177

VII.10. η^*/η^0 as a Function of $\eta_0^*\dot{\gamma}$ for Small Particle-Filled PS Melts 180

VII.11. Characteristic Relaxation Time as a Function of Shear Rate for Matrix PS Melt 185

VII.12. Comparison of Experimental Data with Phenomenological Theory for Plot of Shear Viscosity versus Shear Rate . . 186

VII.13. Comparison of Experimental Data with Phenomenological Theory for Plot of Elongational Viscosity versus Elongational Rate 187

FIGURE		PAGE
VII.14.	Comparison of Experimental Data with Phenomenological Theory for Plot of First Normal Stress Difference versus Shear Stress	188
VIII.1.	Typical Photograph of the Spinline During the Isothermal Melt Spinning for HIPS-A	194
VIII.2.	Profiles of Fiber Diameter along Spinline for HIPS under Isothermal Conditions	195
VIII.3.	Profiles of Fiber Velocity along Spinline for HIPS under Isothermal Conditions	196
VIII.4.	Profiles of Elongational Rate along Spinline for HIPS under Isothermal Conditions	197
VIII.5.	Spinline Elongational Viscosity as a Function of Elongational Rate for HIPS	198
VIII.6.	Comparison of Spinline Elongational Viscosity with Steady State Elongational Viscosity for HIPS	199
VIII.7.	Typical Spinline Tension Variation with Time under Isothermal Conditions for HIPS-A	203
VIII.8.	Diameter Fluctuation as a Function of Draw Ratio for Various Filled PS under Nonisothermal Conditions	208
VIII.9.	Period of Draw Resonance as a Function of Draw Ratio for Various Filled PS under Nonisothermal Conditions . .	209
VIII.10.	Ratio of Wavelength of Draw Resonance to Spinline Length as a Function of Draw Ratio for Various Filled PS under Nonisothermal Conditions	210

CHAPTER I

INTRODUCTION

In many polymer products, reinforcement with small particles is used to improve properties and performance. Examples are reinforcement with carbon black, calcium carbonate, talc, etc. as well as rubber modification. In these systems, small particles are dispersed in a continuous phase.

Although we have considerable information on the properties in the solid state for such reinforced polymers, there have appeared little study on rheological properties in the molten state. Most of these have been limited to capillary rheometers involving high shear rate measurements. Few studies of this type involving a range of instruments or systems have appeared.

It has long been recognized that an addition of fillers brings a change in processing conditions. It has also been said that fillers improve the extrusion characteristics. For example, as we know well, carbon black makes natural rubber extrudable.

In order to better understand the behavior of these materials in processing, we need more basic rheological characterization studies to investigate the influence of an addition of small particles on melt properties. There is a need to develop a general picture of the rheological properties of highly-filled polymer melt systems, and to develop quantitative representation of such behavior. It is the

purpose of this thesis to fill this need. We present both an extensive experimental study of polymer melts reinforced with small particles and a theoretical study of the shear viscosity of suspensions of small particles in viscoelastic fluids. We also investigate processing characteristics in melt spinning.

CHAPTER II

LITERATURE SURVEY

A. Experimental Investigations of Rheological Properties of Suspensions

A.1. Suspensions of Particles in Newtonian Fluids

It had been observed by the turn of the century that all fluids did not necessarily obey Newton's theory. In 1885 Reynolds (192) reported volumetric dilatation resulted from shearing rigid particle suspensions in water. Bingham and Green (20) reported in 1919 that points exhibited yield values in shear flow.

$$\sigma_{12} = Y + \eta_B \dot{\gamma} \qquad (II.1)$$

where Y is a yield value, η_B a plastic viscosity, σ_{12} shear stress and $\dot{\gamma}$ shear rate. They proposed similar observations were made on other concentrated suspensions in succeeding years.

Since that early period, there have appeared many studies on rheological behavior of suspensions. They have been mainly related to the effects of particle size and concentration on the suspension viscosity and viscosity changes with the shear rate.

Freundlich et al. (63) (64) obtained many important results on the time dependent behaviors of colloidal systems. The viscosity change with shear rate and time were expressed as "thixotropy (decreasing viscosity)" and "rheopexy (increasing viscosity)." In some systems, the

viscosity was found to decrease with shear rate, which in others it increased. This, Freundlich and Roder (64) termed "dilatancy."

During the 1950s, Maron and Krieger and their co-workers (137) (138) (139) and Mooney (156) among others made extensive studies of the viscosity of latices investigating particle size, volume fraction and shear rate dependence. Mooney developed a useful semiempirical equation for the influence of volume fraction on viscosity. Other investigators studied the suspension of inorganic particulates confirming the existence of yield values (190). Metzner and Whitlock (147) studied the occurrence of the Reynolds (192) and Freundlich-Roder (64) dilatancy effects and concluded they are independent.

In 1959, Casson (35) proposed a viscosity equation for suspensions exhibiting yield stresses.

$$\sigma_{12}^{1/2} = Y + \eta_{\infty} \dot{\gamma}^{1/2} \qquad \text{(II.2)}$$

where η_{∞} is the high shear limiting viscosity. A plot of $\sigma_{12}^{1/2}$ against $\dot{\gamma}^{1/2}$ gives Y as an intercept.

In the 1960s, much study on the influence of particle concentration and particle-particle interaction was reported by several investigators (65) (207). Electrostatic forces on latex particles was found very important by Fryling (66). Enormous differences in viscosity were reported by this author with the addition and removal of salts from rubber latices. These changes in viscosity are produced by altering the concentration of ions in the surrounding fluid.

Brodnyan et al. (31) (32) reported that the addition of an electrolyte diminishes non-Newtonian character of lattices, and the suspension viscosity may obey Mooney's equation (156) independent of particle size, in the Newtonian region.

Summarizing experimental data for viscosity as a function of volume fraction in 1965, Thomas (207) indicates the scatter mainly resulted from particle size distribution, and that for small particles with diameter less than 1 to 10μ, colloidal forces become dominant. He points out that in such cases the viscosity increases with decreasing particle size and also depends on the shear rate.

Extensive studies on time dependent rheological behaviors of suspensions such as thixotropy and rheopexy were reported by several investigators (11) (215) in the 1960s. In these papers, the behavior was argued to be due to the formation and break-up of aggregated structures. Thixotropy was considered to be due to break-up of the structures with deformation.

Several important papers during the 1970s on concentrated suspensions have appeared. Notable studies on the dilatancy of suspensions were reported by Hoffman (92) (93). He reports that a discontinuity in the viscosity as a function of the shear rate, which can be seen in a dilatant flow, is caused by a flow instability at which an order-disorder transition occurs. He has developed arguments accounting for nonhydrodynamic interparticle effects such as Van der Waals and electrostatic force. He has emphasized the effect of nonhydrodynamic forces on rheological behavior of concentrated suspensions of small particles.

Several studies on rubber latices by Krieger et al. (115) (116) should be noted. For lattices of monodisperse particles without electroviscous effects, Krieger (115) reports that a graph of the relative viscosities of lattices plotted against a Péclet number, a nondimensional group combining shear rate and Brownian diffusion constant, for fixed volume fraction enables one to superpose results for different suspending fluids. From these experiments, he points out the effect of Brownian motion on the viscosity of concentrated suspensions. The non-Newtonian character induced by removing salts reported by Fryling (66) and Brodnyan (31) (32) was again investigated by Krieger and Eguiluz (116) who refer to it as the second electroviscous effect. They report that the latex exhibits a yield stress which decreases with decreasing particle concentration and with increasing electrolyte concentration.

More recently, rheological behavior of suspensions of particles in Newtonian fluids have been extensively studied by Umeya and his co-workers (210) (211). The dilatancy, thixotropy and rheopexy on rigid small particles suspensions in water have been reported.

A.2. Suspensions of Particles in Polymer Solutions

Matsumoto, Onogi and their co-workers (140) (142) (174) (175) have investigated polymer solutions containing carbon black, crosslinked polymer beads, etc. as small particles and pointed out the appearance of yield values in both dynamic experiments and in steady shear flow. In other words, the storage modulus becomes constant at low frequencies,

and the dynamic viscosity does infinite at finite shear stress levels. It has also been found that dynamic properties have a strong amplitude dependency, decreasing at larger amplitude. They have reported that the yield value may increase with particle content and polymer concentration in the disperse medium. The smaller the particle size, the larger the yield value. The system also becomes more thixotropic. In addition, they have studied the temperature dependence of the yield stress. In their articles they have attempted to interpret small strain behavior in terms of linear viscoelasticity. Onogi et al. (141) have argued more recently that there is no yield value in carbon black filled polymer solutions. They consider the system to form a pseudo-gel, which has a higher maximum relaxation time causing a long memory, but it still flows at very low stresses.

The possibility of yield values in suspensions of particles in polymer solutions has also been reported by Nicodemo and Nicolais (164) (165). They point out a viscosity increase with decreasing shear rate owing to particle aggregate formation for glass bead and short glass fiber suspensions in polymer solutions. They report that this effect appears to be imperfect in glass bead suspensions.

It has been found by Hutton and his co-workers (18) (97) (98) that greases possess yield stresses. In addition, they point out some problem existing in normal stress measurement in the systems with yield stresses such as grease. They indicate that the abnormal effects interfering with the normal stress measurement at low shear rates are due to interactions between the instrument and the yield stress property. As

a result, a proper zero point for measurement cannot be obtained. Furthermore, the uncertainty is proportional to the level of the yield stress.

Casson's equation, Equation II.2, was modified for the case of non-Newtonian media by Matsumoto et al. (175)

$$\sigma_{12}^{1/2} = Y + \eta_{\infty}\left(\frac{\eta_a}{\eta_0}\dot{\gamma}\right)^{1/2} \qquad \text{(II.3)}$$

where η_a and η_0 denote the apparent and zero shear viscosity, respectively. They have obtained yield values of small particle suspensions in polymer solutions using an above equation.

Several investigations on fiber suspensions in polymer solutions have been reported by Mikami, Matsumoto and Onogi (149) (176). They point out that suspensions of powdered glass fibers and titanate fibers in polystyrene solutions exhibit yield values. In addition, the suspensions of titanate fibers tend to show remarkable rheopectic behavior at low shear rate after being sheared at high shear rates (176).

A.3. Suspensions of Particles in Polymer Melts

Particle reinforced polymers have been extensively studied by many investigators, because those systems have not only scientific, but industrial importance. However, most investigators have measured viscosity either at single shear rates or in a high shear rate range. Reinforcing particles may be divided into two groups: rigid particles and deformable particles.

A.3.1. Polymer Melts Reinforced with Rigid Particles

It has long been recognized that the loading of rigid particles to polymer melts increases the shear viscosity. It has been found that small rigid particles such as carbon black, titanium dioxide and calcium carbonate increase the viscosity of systems to the greatest extent at low shear rates. As a result, a careful investigation of the data indicates that these systems exhibit yield values. These phenomena have been reported in shear flow by several investigators as summarized in Table II.1. Yield values have been observed for not only small spherical particle-filled systems, but also small disc-shaped (22) and their rod-shaped particle suspensions (51). Some papers (111) (112) report yield values for glass bead-filled polymer melts, but the situation is ambiguous, for other investigators report low shear rate Newtonian viscosity (51) (59) (157) (158). Yield values are generally found in systems with particle sizes less than 1μ, that is, colloidal particles, as seen in Table II-1. It has been reported that yield stresses increase with loading level for carbon black-reinforced rubber unvulcanizates (213) (229).

As shown in Table II.2, it has also been reported that small particles may reduce the elastic recovery of polymer melts following flow. Han (75) reports that calcium carbonate reduces the first normal stress difference in shear flow at constant shear stress. Lobe and White (131) report a reduced normal stress difference at fixed shear stresses, although it exhibits an increase at fixed shear rates. Although

Table II.1. Yield Values for Polymer Melts Reinforced with Small Particles

Flow	Measurement	Particle	Size (μ)	Polymer Matrix	References
Shear Flow	Steady	TiO_2	0.18 ~ 0.25	PE, PS	Minagawa and White (151)
		Talc	?	PP	Chapman and Lee (40)
		Mica	D: -70+ 100 mesh L/D: 30	PP	Boaira and Chaffey (22)
		$CaSO_4$ anhydrite fiber	D: 4 ~ 6 L/D: ~100	PS	Czarnecki and White (51)
		Carbon black	0.02	PIB	Vinogradov et al. (213)
		Carbon black	0.1	PIB	Zakharenko et al. (229)
		Rubber globule	?	(HIPP, HIPS)	Lee (126)
	Steady,Dynamic	Carbon black	0.025	PS	Lobe and White (131)
	Dynamic	$CaCO_3$	0.15	PS	Münstedt (157)(158)
		TiO_2	?	PS	Zosel (232)
		Rubber globule	0.08	(ABS, ASA)	Münstedt (157)(158)
		Rubber globule	0.08 ~ 0.1	(ABS)	Zosel (232)
		Rubber globule	1 ~ 2	(HIPS)	Chang and Takahashi (39)
Elongational Flow	Steady	Carbon black	0.025	PS	Lobe and White (131)
		Rubber globule	?	(ABS)	Cogswell (44)

Table II.2. Reduced Elastic Recoveries of Polymer Melts Reinforced with Small Particles

Particle	Polymer Matrix	Elastic Properties* Measured	References
Carbon black	PS	N_1, B	Lobe and White (131)
	BR, SBR	B, ΔP_{ent}	White and Crowder (219)
	SBR, NBR	B	Collins and Oetzel (47)
	SBR	B	Hopper (96)
	CR	B	McCabe and Mueller (144)
	NBR	B	Nakajima and Collins et al. (160)(161)(162)
	PIB	B	Vinogradov et al. (213)
	NR	B	Bagchi and Sirkar (4)
TiO_2	PS, PE	N_1, B, ΔP_{ent}	Minagawa and White (151)
$CaCO_3$	PP	P_{exit}	Han (75)
Glass bead $CaSiO_3$ Cross linked polymer bead	AS	B	Newman and Trementozzi (163)
Mica $CaSO_4$ anhydrite fiber	PS	N_1	Czarnecki and White (51)
Rubber globule	(ABS, HIPS)	B	Casale et al. (34)
Rubber globule	(ABS, HIPS)	P_{exit}	Han (74)
Rubber globule	(ABS,ASA,HIPS)	B	Münstedt (157)(158)

*N_1: First normal stress difference; B: Extrudate swell; ΔP_{ent}: Entrance pressure drop; P_{exit}: Exit pressure.

generally fiber reinforcements tend to increase the normal stresses (37) (38) (50) (218), a very small diameter fiber has been found to decrease it (51). The effects of carbon black structure on the elastic properties of rubber components have been studied by White and Crowder (219). The smaller carbon black decreases the elastic properties. Recently, Bagchi and Sirkar (4) have related extrudate swell to the free rubber volume fraction obtained from unextractable rubber measurements.

Few studies concerned with elongational flow of filled polymer melts have appeared in the literature. Cotten and Thiele (48) have presented transient elongational viscosity data, but have not obtained the steady state values. Lobe and White (131) measure the elongational viscosity at a constant elongational rate and strikingly, obtain yield values for carbon black-filled polystyrene melts. Han and Kim (77) have investigated isothermal melt spinning of calcium carbonate-filled polypropylene. They report that the fillers increase apparent elongational viscosity which decreases more rapidly with elongational rate in contrast with polypropylene melts.

There have been few studies of the small strain viscoelastic properties of filled polymer systems. Lobe and White (131) report dynamic and stress relaxation studies for carbon black-filled polystyrene. They find the introduction of carbon black to reduce the rate of stress relaxation and to make at low frequencies storage modulus tend to a finite value and dynamic viscosity tend to infinity. This indicates the formation of a gel structure. Payne (177) (178) discusses carbon black-reinforced rubber vulcanizates. He finds that the dynamic moduli of

such systems are strongly amplitude dependent suggesting the existence of a gel. He suggests that at low strains the system may behave almost elastically with the modulus independent of the strain, namely, tends to form a gel by a carbon black-carbon black structure.

Reinforcing particles often receive a prior surface treatment intended to improve the dispersion of particles in the polymer matrix and eventually, the mechanical properties of final molded products. A reduction in viscosity by surface treatment has been reported by several investigators (22) (40) (82). It has also been reported that surface treatment may slightly increase the extrudate swell of polymer melts during extrusion (231).

A.3.2. Polymer Melts Reinforced with Deformable Particles

In order to improve mechanical properties of polymers such as impact strength, reinforcement with deformable particles has been widely used. This can be mainly classified into two groups: polymer blends (mechanical blends) and rubber-modified polymers by graft polymerization. These have commonly the structure in which deformable particles are dispersed in a polymer matrix. However, the particles dispersed in the latter case are generally very small compared with those of the former.

It has been reported that rubber-modified polymers tend to exhibit yield values in the steady shear flow as shown in Table II.1. Lee (126) reports that high impact polypropylene (HIPP) and high impact polystyrene (HIPS) show an increase of viscosity with decreasing shear rate. He suggests the aggregation of the dispersed elastomer domains

and the formation of a kind of loose network structure at low shear rates, which eventually is broken under high shear. Yield values have also been found in dynamic measurements for these polymers. At low frequencies, dynamic viscosity tends to infinity and storage modulus to a finite value in ABS melts (3) (157) (158) (232). Similar results have also been reported in HIPS melts (39). As indicated by Itoyama and Soda (105), a marked increase in viscosity at low shear rates for these polymer melts may depend on rubber globule size. For example, Münstedt (157) (158) points out that HIPS melts with large rubber globules did not exhibit yield values in his experiments.

There have been few studies on elongational flow of rubber-modified polymer melts. Cogswell (44) reports that ABS melts have no definable region of constant elongational viscosity at low shear stress, that is, a tendency to a yield value.

Few papers have reported on elastic properties of these materials as shown in Table II.2 (p. 11). Casale, Moroni and Spreafico (34) find that increasing rubber contents reduces extrudate swell of ABS melts. Han (74) studied the rheological properties at high shear rate of HIPS and ABS melts using slit rheometer. He indicates that the sample containing a higher amount of rubbery component appears less elastic than that with a lower amount. Münstedt (157) (158) has also reported a reduced extrudate swell in HIPS, ABS and acrylonitrile-styrene-acrylester copolymer (ASA) melts.

Several studies on polymer blends, especially extensive investigations by Han and his co-workers (76), have been reported. In

contrast with rubber-modified polymers, blend polymers show Newtonian regions in the steady shear flow experiments (78) (127) (150) (182). Han and Kim (78) point out that the composition dependence of viscosity at constant shear rate has a minimum and a maximum for high density polyethylene (HDPE)-polystyrene (PS) blend system. Similar trends have been obtained by Plochocki (182) for polyethylene (PE)-polypropylene (PP) blend.

Several studies on elastic properties of blend polymer melts have appeared in the literature. Han and Kim (78) report that elastic properties such as normal stress or exit pressure have a maximum and a minimum against blending ratio in HDPE-PS systems. The influence of composition on extrudate swell has also been studied for PE-PP blends by Plochocki (182).

From investigations on the effect of mixing on the rheological properties of polymer melts, Han, Kim and Chen (79) conclude that these viscoelastic properties depend on the mode of dispersion. For instance, two-phase fluids containing deformable droplets tend to give a lower viscosity and a higher elastic property than a single phase-fluid or the two-phase fluid containing nondeformable particles.

Experimental studies on melt spinning of HDPE-PS blend polymer have been carried out by Han and Kim (77). They interpret the observed elongational flow behavior in terms of the interaction between components in the molten state, which can be obtained only when the microstructure of the fiber spun can be examined.

B. Phenomenological Theory for Polymer Melts Highly-Filled with Small Particles

There are two approaches to the rheological properties of suspensions of small particles. One is a phenomenological approach which intends to correlate stress with deformation history. Another is a mechanistic theory which interprets flow behavior in terms of structure and mechanisms, and is based on hydrodynamic analysis for a system of particles surrounded by a continuous fluid phase. Before proceeding, we describe briefly the phenomenological nonlinear viscoelasticity theory.

B.1. Nonlinear Viscoelasticity Theory and Basic Flow Fields

Polymer melts show elastic or memory effects in the sense that the present stress state depends on the previous history of deformation. In other words, they are viscoelastic fluids. Viscoelasticity theory has been extended from one-dimensional linear model for small strains to three-dimensional large strain models. Viscoelastic models are classified into two groups: differential type models and integral type models.

The total stress $\underset{\sim}{\sigma}$ is usually divided into two parts for convenience:

$$\underset{\sim}{\sigma} = -p\underset{\sim}{I} + \underset{\sim}{P} \qquad \text{(II.4)}$$

where p is an isotropic pressure and $\underset{\sim}{P}$ is the extra stress tensor

associated with deformation. $\underset{\sim}{I}$ is a unit tensor. When a fluid is in the static condition ($\underset{\sim}{P} = 0$), p is identified as the hydrostatic pressure. In a dynamic situation for incompressible fluid p should be considered as a scalar value to be determined by boundary conditions.

The differential type constitutive equations are based on Maxwell's equation (143), which is the simplest one-dimensional linear viscoelastic fluid model.

$$P + \tau \frac{dP}{dt} = G\tau \frac{d\gamma}{dt} , \quad G\tau = \eta \tag{II.5}$$

where P is the stress, γ is the strain, G is the elastic modulus and τ denotes the relaxation time.

Various investigations have tried to extend Equation II.5 to large strains. The first successful generalization was given by Zaremba (230). He considered an embedded coordinate system which translates and rotates with a material point and rewrite Equation II.5 in such a manner in three-dimensional form. Zaremba's equation is able to predict non-Newtonian viscosity and normal stresses in simple shear flow.

Modern research in this area begins with the paper of Oldroyd (173) in 1950, who presented a convected coordinate system introduced first by Hencky (88) which translates, rotates and deforms with the fluid. In succeeding years, other generalizations were reported by several investigators (166) (200) (201) (221) (224). Of them, the equation proposed by White and Metzner (221) is useful for analysis of various flow problems in spite of the simple expression. This has the form

$$\underset{\sim}{P} + \tau \frac{\delta \underset{\sim}{P}}{\delta t} = 2n\underset{\sim}{d} \ , \ G\tau = n \tag{II.6a}$$

where $\underset{\sim}{d}$ is the rate of deformation tensor given by

$$\underset{\sim}{d} = \frac{1}{2} [\nabla \underline{v} + (\nabla \underline{v})^T] \tag{II.6b}$$

and

$$\frac{\delta \underset{\sim}{P}}{\delta t} = \frac{\partial \underset{\sim}{P}}{\partial t} + (\underline{v} \cdot \nabla)\underset{\sim}{P} - \nabla \underline{v} \cdot \underset{\sim}{P} - \underset{\sim}{P} \cdot \nabla \underline{v} \tag{II.6c}$$

where τ is taken as a function of deformation rate invariants

$$\tau = \tau(\mathrm{tr}\underset{\sim}{d}^2) \ . \tag{II.6d}$$

Integral models are based on Boltzmann's superposition principle (26) given by

$$P(t) = \int_{-\infty}^{t} G(t-s) \frac{d\gamma}{dt} ds \tag{II.7}$$

where G(t) is a relaxation modulus at time t and s is time. This equation can be rewritten as

$$P(t) = \int_{-\infty}^{t} \phi(t-s)\gamma(s)ds \tag{II.8a}$$

where

$$\phi(t) = - \frac{dG(t)}{dt} \qquad \text{(II.8b)}$$

The Maxwell model is a special case of the Boltzmann equation for which

$$G(t) = G_0 e^{-t/\tau} \qquad \text{(II.9a)}$$

$$\phi(t) = \frac{G_0}{\tau} e^{-t/\tau} \; . \qquad \text{(II.9b)}$$

The function $\phi(t)$ is usually written by

$$\phi(t) = \sum \frac{G_i}{\tau_i} e^{-t/\tau_i} = \int_{-\infty}^{t} \frac{H(\tau)}{\tau} e^{-t/\tau} d\ell n\tau \qquad \text{(II.10)}$$

where $H(\tau)$ is called the relaxation spectrum.

The generalization of Boltzmann's principle to large deformation has been carried out by many rheologists (25) (228). Oldroyd (173) and more specifically Lodge (132) first presented possible generalization of the single integral form to large strains. Lodge used convected coordinate systems developed by Hencky-Oldroyd. In the same period, Yamamoto (226) (227) and Lodge (133) developed nonlinear generalization of Boltzmann's equation based on network theories of flexible polymer chains.

A general theory accounting for nonlinear effects was developed by Green and Rivlin (68) who presumed that the stress was general hereditary functional of the deformation history. A similar presentation was given

by Noll (166) and Coleman and Noll (46). This is represented by a functional of strain history, which can be expressed by a Frechet expansion of the functional giving an expansion of multiple integrals. Further, under certain conditions as pointed out by White and Tokita (223) this multiple integral may be simplified to a single integral as follows.

$$\underset{\sim}{P}(t) = \int_{-\infty}^{t} [a_1(t-s, \mathrm{tr}\underset{\sim}{e}, \mathrm{tr}\underset{\sim}{e}^2)\underset{\sim}{e}(s) + a_2(t-s, \mathrm{tr}\underset{\sim}{e}, \mathrm{tr}\underset{\sim}{e}^2)\underset{\sim}{e}^2(s)]ds \tag{II.11}$$

where $\underset{\sim}{e}(t)$ is a Finger type strain tensor, and a_1 and a_2 denoting relaxation moduli are dependent on time and deformation invariants.

Single integral type constitutive equation can be expressed as the following equation which is in general equivalent to Equation II.11,

$$\underset{\sim}{P}(t) = \int_{-\infty}^{t} [m_1(t-s)\underset{\sim}{c}^{-1}(t-s) - m_2(t-s)\underset{\sim}{c}(t-s)]ds \tag{II.12}$$

where $\underset{\sim}{c}^{-1}$ and $\underset{\sim}{c}$ are the Finger and Cauchy deformation tensor, respectively. The above equation was first used by Bernstein, Kearsley and Zapas (BKZ) (16). m_1 and m_2 are called memory functions depending on the invariant of deformation, rate of deformation or the stress tensor. Many equations of this type have been proposed (228). The nature of these equations may be dependent on the memory functions used.

One widely used form of the memory function has been presented by Bogue (23) and Bogue and White (25). This form has been found to successfully correlate data on bulk polymers (41) (42) (67) (99) (102) (148) (202). This takes the following form

$$m(t-s) = \sum_i \frac{G_i}{\tau_{i\ eff}} \exp(-\frac{t}{\tau_{i\ eff}}) \qquad \text{(II.13a)}$$

$$\tau_{i\ eff} = \frac{\tau_i}{1 + a\tau_i \langle II_d^{1/2} \rangle} \qquad \text{(II.13b)}$$

$$\langle II_d^{1/2} \rangle = \frac{1}{z} \int_0^z (2tr\underset{\sim}{d}^2)^{1/2} dz \qquad \text{(II.13c)}$$

where $z = t - s$ is a time variable running backward from the present.

Tanner (203) (204) presented the theory in which if the applied strain in a system reached a critical value, the memory would drop to zero. Hence, he changed the lower limit in time integral from $-\infty$ to $t - mI_c^{-1}$, where I_c means the first invariant of Finger tensor and m a coefficient.

We here consider two basic steady flow fields. One is simple shear flow. The imposed velocity field can be written as

$$\underline{v} = (v_1(x_2), 0, 0) \qquad \text{(II.14)}$$

where "1" denotes the flow direction, "2" the normal direction and "3"

the neutral direction. Therefore, the rate of deformation tensor is given by

$$\underset{\sim}{d} = \begin{pmatrix} 0 & \frac{\dot{\gamma}}{2} & 0 \\ \frac{\dot{\gamma}}{2} & 0 & 0 \\ 0 & 0 & 0 \end{pmatrix} \tag{II.15}$$

where $\dot{\gamma} = \frac{\partial v_1}{\partial x_2}$ is the shear rate. The stress field in a viscoelastic fluid can be expressed by (45)

$$\underset{\sim}{\sigma} = -p\underset{\sim}{I} + \begin{pmatrix} \beta_1\dot{\gamma}^2 & \eta\dot{\gamma} & 0 \\ \eta\dot{\gamma} & \beta_2\dot{\gamma}^2 & 0 \\ 0 & 0 & 0 \end{pmatrix} \tag{II.16}$$

where η, $\beta_1 - \beta_2 \equiv \Psi_1$ and $\beta_2 \equiv \Psi_2$ are the shear viscosity, the first and second normal stress difference coefficient, respectively. These functions can be predicted from nonlinear theory. For instance, a single integral form gives

$$\sigma_{12} = \eta\dot{\gamma} = \dot{\gamma}\int_0^\infty z_1[m_1(z) + m_2(z)]dz \tag{II.17a}$$

$$N_1 = \sigma_{11} - \sigma_{22} = \Psi_1\dot{\gamma}^2 = \dot{\gamma}^2\int_0^\infty z^2[m_1(z) + m_2(z)]dz \tag{II.17b}$$

$$N_2 = \sigma_{22} - \sigma_{33} = \Psi_2 \dot{\gamma}^2 = -\dot{\gamma}^2 \int_0^\infty z^2 m_2(z) dz \qquad \text{(II.17c)}$$

where N_1 and N_2 are called the first and second normal stress difference, respectively.

Another flow field is uniaxial elongational flow. The velocity field can be written as

$$\underline{v} = (v_1(x_1),\ v_2(x_2),\ v_2(x_2)) \qquad \text{(II.18)}$$

where "1" denotes the flow direction. The rate of deformation tensor takes the following form after presuming incompressibility.

$$\underset{\sim}{d} = \begin{pmatrix} \dot{E} & 0 & 0 \\ 0 & -\frac{\dot{E}}{2} & 0 \\ 0 & 0 & -\frac{\dot{E}}{2} \end{pmatrix} \qquad \text{(II.19)}$$

where $\dot{E} = \frac{\partial v_1}{\partial x_1}$ is the elongational rate. If $\dot{E}$ is constant with time, a cylinder deforms with time according to

$$L(t) = L(0)e^{\dot{E}t} \qquad \text{(II.20a)}$$

$$R(t) = R(0)e^{-\frac{\dot{E}}{2}t} \qquad \text{(II.20b)}$$

where L and R are the filament length and radius, respectively. The corresponding stress field can be expressed as

$$\underset{\sim}{\sigma} = -p\underset{\sim}{I} + \begin{pmatrix} P_{11} & 0 & 0 \\ 0 & P_{22} & 0 \\ 0 & 0 & P_{22} \end{pmatrix} . \qquad \text{(II.21)}$$

The stress components must be satisfied with the boundary conditions:

$$\sigma_{11} = -p + P_{11} = \frac{F}{\pi R^2} \qquad \text{(II.22a)}$$

$$\sigma_{22} = -p + P_{22} = 0 . \qquad \text{(II.22b)}$$

Therefore, a true elongational viscosity can be defined under a constant elongational rate in the following way:

$$\chi = \frac{\sigma_{11}}{\dot{E}} \qquad (\dot{E} = \text{constant}) . \qquad \text{(II.23)}$$

The steady state elongational viscosity can be predicted from the various nonlinear constitutive equations mentioned above. All of these give the relationship

$$\chi = 3\eta_0 \qquad \text{(II.24)}$$

at low elongational rates, but may predict different behavior at high elongational rates. Some models which tend to show unbounded values are based on Lodge's theory (134) or its generalization. In the Bogue and White model (25), the steady state viscosity behavior depends on

"a" value given in Equation II.13b and rises infinity for small values of "a". A White and Metzner model (221) with a time average deformation dependent relaxation time leads to similar trends. The BKZ (16), Yamamoto (226) (227) and Tanner's theory (203) (204) never take infinite value. At some elongational rates the value may take the maximum and then decreases with elongational rate.

B.2. Constitutive Equations for Polymer Melts Highly-Filled with Small Particles

B.2.1. One-Dimensional Rheological Model

It has long been said that concentrated suspensions of small particles in Newtonian fluids show quite different flow behavior from that of the suspending media. Bingham (19) and Bingham and Green (20) proposed the model:

$$\sigma < Y \qquad \dot{\gamma} = 0 \qquad \text{(II.25a)}$$

$$\sigma \geq Y \qquad \sigma = Y + \eta_B \dot{\gamma} \ . \qquad \text{(II.25b)}$$

As long as the shear stress σ remains below a certain constant Y called yield stress, the material responds as a solid. When σ reaches Y, the material flows in a Newtonian manner. η_B in Equation II.25b is called a plastic viscosity. Mechanical analogues have been used in the representation of the rheological models. The Bingham plastic equation can be represented by the mechanical model in Fig. II.1. We may call this a visco-plastic material (109) (183) (186).

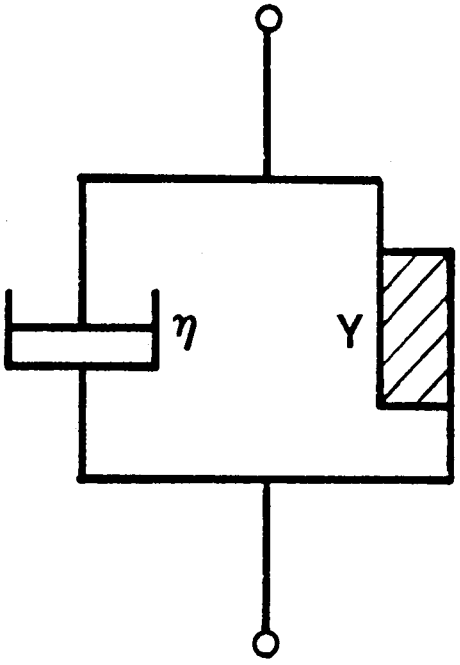

Figure II.1. Bingham Plastic Model.

If we modify the Bingham plastic model of Fig. II.1 to respond as a viscoelastic fluid above the yield value, we obtain the models shown in Fig. II.2. These are called Schwedoff bodies (135) (183) (191) which represent plastic gels (183), namely, viscoelastic-plastic materials. The equation of the model of Fig. II.2a can be written as (131)

$$\sigma < Y \qquad \frac{d\gamma}{dt} = 0 \tag{II.26a}$$

$$\sigma \geq Y \qquad \frac{d\sigma}{dt} = G \frac{d\gamma}{dt} - \frac{(\sigma - Y)}{\tau} \tag{II.26b}$$

Above a yield value, the material behaves as a Maxwell fluid. Solving Equation II.26b yields

$$\sigma = Y + \int_0^\infty G\, e^{-z/\tau} \frac{d\gamma}{dz}\, dz \ . \tag{II.27}$$

Equation II.27 has the same form as the Bingham plastic fluid theory given by Equation II.25b except that material behaves as a linear viscoelastic fluid above a yield value.

The equation of the model of Fig. II.2b can also be written (217)

$$\sigma < Y \qquad \sigma = G_1 \gamma_1 \tag{II.28a}$$

$$\sigma \geq Y \qquad \frac{d\sigma}{dt} = G_2 \frac{d\gamma_2}{dt} - \frac{(\sigma - Y)}{\tau} \ . \tag{II.28b}$$

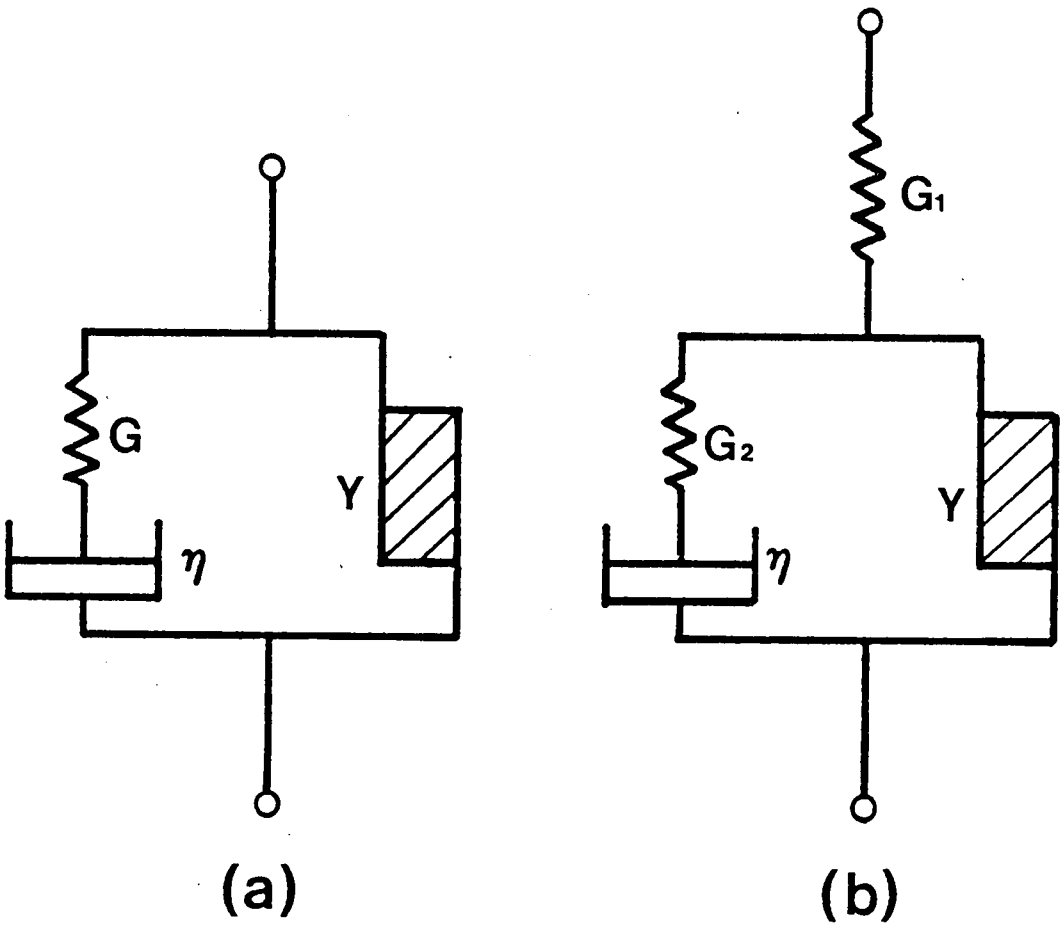

Figure II.2. Schwedoff Body.

Similarly, Equation II.28b leads to

$$\sigma = Y + \int_0^\infty G_2 \, e^{-t/\tau} \, \frac{d\gamma_2}{dz} \, dz \ . \qquad \text{(II.29)}$$

Equations II.28a and II.29 give the rheological response of the material of the model of Fig. II.2b. Using Equation II.28, the total strain γ should be represented by (217)

$$\gamma = \gamma_1 + \gamma_2 = \frac{\sigma}{G_1} + \frac{\sigma - Y}{G_2} + \int_0^t \frac{(\sigma - Y)}{\eta} \, dt \ . \qquad \text{(II.30)}$$

For a simple Maxwell model, as G_1 becomes larger, the elastic recovery following flow goes to zero.

B.2.2. Three-Dimensional Large Strain Theory

B.2.2.1. Constitutive equation. Our concern has been limited to one-dimensional and to small strain in the previous sections. However, our main interest is with the large strain nonlinear behavior. This requires the constitutive equation to be represented in a tensor form.

Classical plasticity theory (89) (159) shows how one-dimensional yielding such as mentioned in the previous section may be replaced by three-dimensional yielding. In the von Mises criterion (155), this is done through the second invariant of the deviatoric stress tensor. In the Tresca criterion (208) (209), this is done through the maximum shear stress.

Hohemser and Prager (95) (186) and Oldroyd (168) gave a tensor formulation for a Bingham plastic model using the von Mises yield criterion. If $\underset{\sim}{P}$ is defined as a deviatoric stress tensor, namely,

$$\underset{\sim}{P} = \underset{\sim}{\sigma} - \frac{1}{3}(\text{tr}\ \underset{\sim}{\sigma})\underset{\sim}{I} \tag{II.31a}$$

or

$$\text{tr}\ \underset{\sim}{P} = 0 \tag{II.31b}$$

it can be expressed as

$$II_P < Y^2 \qquad \underset{\sim}{d} = 0 \tag{II.32a}$$

$$II_P \geq Y^2 \qquad \underset{\sim}{P}\left(1 - \frac{Y}{II_P^{1/2}}\right) = 2\eta\, \underset{\sim}{d} \tag{II.32b}$$

where II_P is the second invariant of the deviatoric stress tensor, i.e.,

$$II_P = \frac{1}{2}\,\text{tr}\ \underset{\sim}{P}^2 \ . \tag{II.32c}$$

Equation II.32 has been applied to the analysis of hydrodynamic problems by Oldroyd (169) (170) (171) (172).

Recently, Equations II.26 and II.28 have been generalized by White (217) and Lobe and White (131). They give

$$II_P < Y^2 \qquad \underset{\sim}{\sigma} = -p\underset{\sim}{I} + G_{11}\underset{\sim}{c}^{-1} - G_{12}\underset{\sim}{c} \tag{II.33a}$$

$$II_P \geq Y^2 \qquad \underset{\sim}{P}\left(1 - \frac{Y}{II_P^{1/2}}\right) = \underset{\sim}{H} \tag{II.33b}$$

where G_{11} and G_{12} are moduli. Here

$$\underset{\sim}{H} = \underset{\sim}{H}\ (\text{deformation history}) \tag{II.34}$$

and is defined so that

$$\text{tr}\ \underset{\sim}{H} = 0\ . \tag{II.35}$$

Equation II.33a would be taken as equivalent to

$$II_P < Y^2 \qquad \underset{\sim}{d} = 0\ . \tag{II.36}$$

It can be shown that Equation II.33b can be rewritten in the following form (217)

$$\underset{\sim}{P} = \left(1 + \frac{Y}{\sqrt{\frac{1}{2}\ \text{tr}\ \underset{\sim}{H}^2}}\right)\underset{\sim}{H}\ . \tag{II.37}$$

If $\underset{\sim}{H}$ is considered to be a nonlinear single memory integral, then

$$\underset{\sim}{H} = \int_0^\infty [m_1(z)\underset{\sim}{\bar{C}}^{-1} - m_2(z)\underset{\sim}{\bar{C}}]dz \tag{II.38a}$$

where

$$\bar{\underset{\sim}{C}}^{-1} = \underset{\sim}{C}^{-1} - \frac{1}{3}(\mathrm{tr}\ \underset{\sim}{C}^{-1})\underset{\sim}{I} \qquad \text{(II.38b)}$$

$$\bar{\underset{\sim}{C}} = \underset{\sim}{C} - \frac{1}{3}(\mathrm{tr}\ \underset{\sim}{C})\underset{\sim}{I} \ . \qquad \text{(II.38c)}$$

$m_1(z)$ and $m_2(z)$ are relaxation functions. Equation II.38 is defined so that Equation II.35 is satisfied.

We here consider theoretical predictions for basic steady flow. These calculations for the simple case were carried out by White (217) and Lobe (130). These tend to predict viscoelastic behaviors at high deformation rates. The behavior at low deformation rates can also be predicted from these viscoelastic-plastic constitutive equations. In simple shear flow

$$\lim_{\dot{\gamma}\to 0} \sigma_{12} = Y \qquad \text{(II.39a)}$$

$$\lim_{\dot{\gamma}\to 0} \eta = \infty \qquad \text{(II.39b)}$$

$$\lim_{\dot{\gamma}\to 0} N_1 = 0 \qquad \text{(II.39c)}$$

$$\lim_{\dot{\gamma}\to 0} \Psi_1 = \infty \ . \qquad \text{(II.39d)}$$

In uniaxial elongational flow

$$\lim_{\dot{E}\to 0} \sigma_{11} = \sqrt{3}\, Y \qquad \text{(II.39e)}$$

$$\lim_{\dot{E}\to 0} \chi = \infty \ . \tag{II.39f}$$

These relationships can be rewritten as follows

$$\lim_{\sigma_{12}\to Y} \eta = \infty \tag{II.40a}$$

$$\lim_{\sigma_{12}\to Y} \Psi_1 = \infty \tag{II.40b}$$

$$\lim_{\sigma_{12}\to Y} N_1 = 0 \tag{II.40c}$$

$$\lim_{\sigma_{11}\to\sqrt{3}\,Y} \chi = \infty \ . \tag{II.40d}$$

That is, if these rheological functions are plotted against the stress, η, Ψ_1 and χ go to infinity, and N_1 to zero at a yield stress.

B.2.2.2. Yield surface. Most of the rate-independent theories of continuum plasticity presume that for a given state of a given material, there exists a function $f(\underset{\sim}{\sigma})$ of the stress such that the material is elastic for

$$f(\underset{\sim}{\sigma}) < 0 \text{ and } \frac{\partial f}{\partial \sigma_{ij}} \frac{\partial \sigma_{ij}}{\partial t} < 0 \tag{II.41a}$$

and plastic for

$$f(\underset{\sim}{\sigma}) = 0 \text{ and } \frac{\partial f}{\partial \sigma_{ij}} \frac{\partial \sigma_{ij}}{\partial t} \geq 0 \ . \tag{II.41b}$$

$f(\underset{\sim}{\sigma})$ is called a yield function (135) (186).

The yield condition can be interpreted geometrically in terms of a surface, i.e., a yield surface

$$f(\underset{\sim}{\sigma}) = 0 \ . \tag{II.42}$$

For example, the von Mises yield criterion (155) is given by

$$f(\underset{\sim}{\sigma}) = II_P - k_M^2 = \frac{1}{2} \text{tr } \underset{\sim}{P}^2 - k_M^2 \tag{II.43}$$

where k_M is critical shear stress for flow in pure shear. Now the corresponding yield surface is represented by

$$\text{tr } \underset{\sim}{P}^2 = 2k_M^2 \ . \tag{II.44}$$

In other words (185) (214),

$$(\sigma_{11} - \sigma_{22})^2 + (\sigma_{22} - \sigma_{33})^2 + (\sigma_{33} - \sigma_{11})^2 + 6(\sigma_{12}^2 + \sigma_{23}^2 + \sigma_{13})^2 = 6k_M^2 . \tag{II.45}$$

The yield surface is represented by a cylinder. In the case of simple shear flow, the stress tensor $\underset{\sim}{\sigma}$ is given by

$$\underset{\sim}{\sigma} = \begin{pmatrix} 0 & \sigma_{12} & 0 \\ \sigma_{12} & 0 & 0 \\ 0 & 0 & 0 \end{pmatrix} \tag{II.46}$$

we get

$$\sigma_{12} = k_M \cdot \tag{II.47}$$

In the case of uniaxial elongational flow, $\underset{\sim}{\sigma}$ is given by

$$\underset{\sim}{\sigma} = \begin{pmatrix} \sigma_{11} & 0 & 0 \\ 0 & 0 & 0 \\ 0 & 0 & 0 \end{pmatrix} \tag{II.48}$$

we obtain

$$\sigma_{11} = \sqrt{3}\, k_M \cdot \tag{II.49}$$

Equations II.47 and II.49 lead to that the von Mises yield criterion gives the relationship

$$Y_e = \sqrt{3}\, Y_s \tag{II.50}$$

where Y_s and Y_e are the yield stress during simple shear and uniaxial elongational flow, respectively.

In the Tresca yield criterion (208) (209), the yield function is given by

$$f(\underset{\sim}{\sigma}) = (\sigma_{12})_{max} - k_T = \sqrt{\left(\frac{\sigma_{11} - \sigma_{22}}{2}\right)^2 + \sigma_{12}^2} - k_T \tag{II.51}$$

where $(\sigma_{12})_{max}$ denotes the maximum shear stress and k_T is a critical

shear stress. The yield surface is represented by a hexagonal prism. Similarly, we get

$$Y_e = 2\ Y_s \ . \tag{II.52}$$

The Tresca yield criterion exhibits a higher ratio Y_e/Y_s as compared with the von Mises yield criterion.

In the Tresca yield criterion, the critical shear stress for yield is independent of the normal pressure on the plane in which yield is occurring. Coulomb (49) had proposed a more general criterion for the failure of soils in 1773. According to his theory, the critical shear stress k_T for yielding to occur in any plane increases linearly with the pressure σ_N applied normal to this plane.

$$k_T = k_C + \mu_C \sigma_N \tag{II.53}$$

where μ_C is a coefficient of friction, and k_C "cohesion" of the material.

One should consider the pressure dependence of the yield behavior which is neglected in the von Mises and Tresca criterion. The modifications have been attempted in such a manner that k_M and k_T are expressed by arbitrary functions of the hydrostatic pressure. The von Mises criterion has been modified to incorporate the effect of pressure on the state of the material by substituting in Equation II.45 a value of k_M that increases linearly with the hydrostatic compound p of the stress tensor

$$k_{mM} = k_M + \mu_M p \ . \qquad \text{(II.54)}$$

The yield surface is a right circular cone if μ_M is constant. This modification was first suggested for polymers in a theoretical model by Bauwens (12) (13).

The Tresca criterion can also be modified by making the quantity k_T in Equation II.51 depend on the state of the material as determined by the hydrostatic component p of the stress tensor (197).

$$k_{mT} = k_T + \mu_T p \ . \qquad \text{(II.55)}$$

If μ_T is constant, the yield surface can be represented by a hexagonal pyramid.

C. Mechanistic Theory for Concentrated Suspensions of Small Particles

It is often possible to regard suspensions as homogeneous fluids and to describe their certain effective fluid properties. This is correct if the length of the motion of the suspension as a whole is much larger than the average size or separation of the particles. Since the particles are usually very small, this condition is satisfied, if the suspension can be treated as homogeneous. The effective flow properties can be derived by theoretical considerations on the known structure of the suspension. Many attempts at theoretical developments have been carried out (9) (71) (106) (108). First of all, theories for dilute systems are described here.

C.1. Dilute Suspensions

Einstein (55) (56) derived the following equation for an effective viscosity η of a dilute suspension of spherical rigid particles.

$$\eta/\eta_0 = 1 + \frac{5}{2}\phi \qquad \text{(II.56)}$$

where ϕ is the volume fraction of the particles, and η_0 is the viscosity of the suspending Newtonian fluid. He assumed that the particles are too far apart to interact with each other, and the flow around each particle can be described in terms of hydrodynamics by Stokes equation.

Many attempts have been made to extend Einstein's theory (65) (86). Hydrodynamic models for nonspherical particles such as ellipsoids suspended in Newtonian fluids have been extensively developed by many investigators (107) (118) (119) (184). The viscosity of suspensions of deformable droplets dispersed in Newtonian fluids was investigated by Taylor (205) (206).

There are two ways for calculating the effective properties of a suspension. One, which was first used by Einstein (55) (56), is related to the energy dissipated in the suspension. This method gives only the effective viscosity of the suspension, not a complete constitutive equation. Another approach is to relate the average stress tensor in the suspension to the average rate of deformation tensor. The original idea was proposed by Burgers (33) and developed extensively by Batchelor (7). Batchelor shows that the former approach is included into the latter one, that is, energy dissipation can be derived from the average stress and rate of deformation tensor.

A general theory for dilute suspensions of rigid particles accounting for fluid microscopic structure was proposed by Hand (83) (84). He gave a function composed of the rate of deformation tensor and a symmetric tensor describing the microscopic structure of a fluid. By limiting the type of terms in the constitutive equations, various stress components were evaluated for simple shear flow, exhibiting non-Newtonian behavior. Jeffrey's (107), Prager's theories (184) of suspensions and Ericksen's theory of anisotropic fluids (57) (58) are contained in Hand's theory. Later, Barthès-Biesel and Acrivos (6) attempted to recast many of the existing constitutive equations for dilute suspensions into the form suggested by Hand involving an anisotropy described in terms of a single second-order tensor. Recently, from combination of the standard phenomenological techniques and the basic formulation of suspension mechanics, Hinch and Leal (90) (91) have developed a general constitutive equation for a dilute suspension of rigid spherical particles with Brownian rotations.

It has long been known that nonhydrodynamic forces, which do not exist in the Einstein theory, act on particles in a suspension. In such a case, Equation II.56 is no longer valid. According to the Derjaguin-Landau-Verwey-Overbeek theory (DVLO theory) (53) (212) of colloid stability, these forces consist of thermal (Brownian) forces, electrical forces and London-van der Waals forces.

Brownian forces arise from the random collision of particles due to thermal agitation and fluctuate on a very short time scale. By taking a time average, this can be replaced by the force associated with

a diffusion process on a long time scale, which is represented by a diffusion constant. It increases with decreasing the particle size. Therefore, Brownian force is more important in small particles than in large ones. However, in the case of polymer melts, thermal agitation is supposed to be unimportant, or even if it exists, very small. Thus, Brownian force may be negligible compared with other nonhydrodynamic forces in such cases.

If the particles have electric charges, these create an electric double layer of charge which can store energy, with the opposite charges in the ionic cloud. The cloud has two layers: an immobile inner layer and a diffuse outer layer. It screens the charge on the particle and then, decreases the repulsive force between particles. The effect of electric forces on the suspension viscosity, so-called electroviscous effects are divided into two: a resistance to distortion of the diffuse layer, the primary effect (27) (28) (114); electrostatic repulsions between neighboring particles, the second (36) (66) (93) (116) (194) (195). The effective viscosity is increased through both these effects. However, for colloidal suspensions the second effect dominates the others. As with thermal effects, this becomes more important as the particle size decreases.

Van der Waals forces are weak attractive forces which act between all particles (36) (93). These forces are often used to interpret the aggregation of particles, for van der Waals forces act in a short range.

Generally, the effective viscosity of suspensions can be expressed as

$$\eta/\eta_0 = 1 + O_1(\phi) + O_2(\phi^2) + \ldots . \qquad (II.57)$$

To obtain the term, $O_2(\phi^2)$, we must consider interactions between particles. First, this problem was started from assumptions that interaction was solely due to be hydrodynamic. Guth and Simha (72) extended Einstein's method by calculating the additional energy dissipation. This expression was later corrected by Simha (199). He gave the following equation for the effective viscosity of suspensions.

$$\eta/\eta_0 = 1 + 2.5\phi + 12.6\phi^2 . \qquad (II.58)$$

The most recent attempt was carried out by Batchelor and Green (10). Also extending Einstein's equation, they obtained the equation

$$\eta/\eta_0 = 1 + 2.5\phi + 7.60\phi^2 . \qquad (II.59)$$

They also indicated that Brownian and electroviscous effects should be taken into account.

Studies of electroviscous effects in dilute solutions have been carried out by Krasny-Ergen (114), Booth (27) (28) and Russel (194) (195). Assuming that Brownian effect is negligible compared to the second electroviscous effect, Russel (194) (195) gives the following equation in low-shear limit in the case of electrostatically dilute suspension

where a is the particle radius, κ^{-1} is called Debye length which means the thickness of ionic cloud, β the factor found by Booth (27) (28) and B' depends on the ratio, electrostatic forces to Brownian forces. Equation II.60 shows that the suspension has a Newtonian viscosity.

C.2. Concentrated Suspensions

Although the theories presented above for dilute systems have been extended to concentrated systems, there have been no exact theories compared with those of dilute suspensions. The results which have been proposed do not give general three-dimensional tensor constitutive equation. These are classified into two large groups from the point of theoretical approaches: the cell model and lubrication theory.

Before describing them, it is very useful to note the empirical equations proposed for concentrated suspensions.

C.2.1. Empirical Equations for the Effective Viscosity

Many empirical equations have been proposed by some investigators. These are described in a recent review by Jinescu (108). Of them, two equations are most widely used, that is, Mooney's equation (156) and Eiler's equation (54):

$$n/n_0 = \exp\left(\frac{2.5\phi}{1 - f\phi}\right) \tag{II.61}$$

$$n/n_0 = \frac{25}{16}\left[\frac{\phi^2}{(1 - \phi/\phi_m)^2}\right] \tag{II.62}$$

where f is an empirical parameter and ϕ_m is the maximum concentration.

Recently, Quemada (187) (188) (189) has proposed semiempirical equations for the effective viscosity of concentrated disperse systems. The equation takes the form

$$n/n_0 = (1 - \frac{1}{2}\tilde{k}\phi)^{-2} \qquad \text{(II.63)}$$

where $\tilde{k}$ is a generalized intrinsic viscosity, function of a relative shear rate and structural parameters. This equation approaches a Casson law type (35) at the high shear limit, but does not exhibit any yield stress at the low shear limit. It means that this equation may be correct only when the yield stress is very small.

C.2.2. Theoretical Investigations

Many models have been proposed to calculate the rheological properties of concentrated suspensions. Of them, the cell model (86) has been most well known. This model has been first proposed by Simha (199), and later used by several investigators (2) (85). A cell consists of a particle surrounded by fluid. It is assumed that the cell is a sphere with radius, $a/\phi^{1/3}$. The Stokes equations for creeping flow are solved in the fluid inside the cell under consideration of such boundary conditions that there is no slip on the particle surface and no normal flow at the outer boundary. Thus, Simha derived

$$n/n_0 = 1 + \frac{5}{2}\lambda(y)\phi \qquad \text{(II.64a)}$$

where $\lambda(y)$ is a function of y defined as

$$y^3 = \frac{\phi}{f^3\left[1 - \frac{\phi^{1/3}}{f}\right]^3} . \qquad \text{(II.64b)}$$

f is an empirical parameter. For the limit of high concentration Equation II.64 reduces to

$$\eta/\eta_0 = \frac{54}{5f^3}\left[\frac{\phi^2}{1 - (\phi/\phi_m)^3}\right] \text{ as } \phi \to \phi_m \qquad \text{(II.65)}$$

where ϕ_m is the maximum concentration depending on the arrangement of the particles.

In spite of advantages in mathematical treatment, the cell model has some problems in it (106). One is concerned with the arbitrary choice for the shape of cell and the boundary conditions. The other is the most important thing in the case of concentrated suspensions, namely, this model implies that the particles are far apart each other, in other words, it is impossible to consider the close approach. Therefore, the cell model cannot be expected to fully interpret experimental data at high concentration.

Recently, Adler (2) has applied a cell model to concentrated suspensions of porous spheres. He considered the spherical aggregates as a porous medium, and used the cell model to solve the flow fields. He used the von Mises yield criterion to determine the break-up of the

aggregates, and predicted a yield stress in the case of breakable aggregates. He has considered only hydrodynamic problem, but not taken into account nonhydrodynamic particle-particle interactions, which are important in concentrated suspensions.

The cell model was also used to analyze elongational flow of concentrated fiber suspensions of Newtonian fluids by Batchelor (8), which has extended recently to those of non-Newtonian fluids by Goddard (69). In elongational flow of oriented fiber suspensions shearing motions are set up between the fibers which result in increased resistance to elongational flow. Batchelor realized that under the conditions, fiber diameter << average separation << fiber length, the velocity field would be constant entirely along flow direction. The problem reduces to one in the plane perpendicular to flow direction, where the particles are dilute in a noninteracting sense. Thus, he derived the effective Trouton viscosity by solving the two-dimensional hydrodynamic problem.

In concentrated suspensions, one can assume that the typical nearest distance separating neighboring particles is small but nonzero, such that the minimum thickness of the interstitial liquid phase is much smaller than the typical linear dimension of the typical radius of curvature of the adjacent particle surfaces. We then may adopt the classical Reynolds' theory of hydrodynamic lubrication (120) (122) in order to describe the viscous flow and stress as generated in the neighborhood of points of near contact, and to calculate the energy dissipated there.

Frankel and Acrivos (62) derived a theory for viscosity for concentrated suspensions of rigid particles. They provided an asymptotic theory to explain the experimental observations of an ultimate sharp increase of viscosity with particle concentration. Namely, they presented

$$\eta/\eta_0 \sim \frac{(\phi/\phi_m)^{1/3}}{1 - (\phi/\phi_m)^{1/3}} \quad \text{as} \quad \phi \to \phi_m \tag{II.66}$$

and gave 9/8 as a proportional constant in the case of a simple cubical packing.

For slightly deformable elastic particles, Goddard (70) (71) has derived the full stress tensor using a so-called elastohydrodynamic lubrication theory (43). He obtained the same form for the viscosity as that of Frankel and Acrivos.

Although these approaches using lubrication theory are supposed to be more adequate than the others such as the cell model in interpretation of flow mechanism of concentrated suspensions, it is very important to note that the theories mentioned above are concerned with only Newtonian fluid medium and do not consider nonhydrodynamic interparticle effects, but only hydrodynamic interaction.

CHAPTER III

THEORETICAL APPROACH TO THE VISCOSITY OF CONCENTRATED SUSPENSIONS OF SMALL PARTICLES

A. Introduction

Few hydrodynamic theories of suspensions involving particle-particle interactions in concentrated suspensions have appeared. We can only mention two papers. Hoffman (93) has taken into account van der Waals attraction and electrostatic repulsion to interpret the discontinuous rise in viscosity observed with concentrated suspensions. He presumed that nonhydrodynamic interaction would lead to indicated flow instability causing the viscosity rise above.

More recently, Adler (2) has analyzed the stresses in a porous solid matrix, applying a free-cell model (85) to a suspension of porous spheres and assuming the deformation of the porous particles to be negligible. This model predicts shear thinning when the aggregate of particles is broken by the shear flow. In addition, if the shear is small enough, the aggregates can grow without any limit, that is, this is closely associated with the existence of a yield stress in aggregable suspensions. He uses a von Mises yield condition for the determination of the break-up of the aggregates.

In this chapter, we treat a suspension of uniform rigid solid spheres in which each sphere moves with the average velocity of the surrounding fluid medium. Wall effects are assumed to be negligible and

the continuous phase is considered to behave macroscopically as a non-Newtonian continuum whose shear viscosity η^0 is given by (21)

$$\eta^0 = \frac{\eta_0^0}{1 + \frac{\eta_0^0}{K}\dot{\gamma}^{1-n}} \qquad \text{(III.1)}$$

where η_0^0 and n are zero shear viscosity and a parameter characteristic to non-Newtonian behavior ($0 < n \leq 1$). K is a constant.

According to Frankel and Acrivos (62) approach, the viscous dissipation of energy, which is related to the effective viscosity, results from hydrodynamic interaction by the flow with the small gap separating the various particles from one another. According to Einstein (55) (56), if we assume steady flow,

$$\eta/\eta^0 = E_T/E_T^0 \qquad \text{(III.2)}$$

where E_T and E_T^0 denote the total rate of viscous dissipation energy of the suspension and that of an equivalent volume of pure fluid, respectively.

In addition to hydrodynamic interaction, we have to consider the contribution of nonhydrodynamic interparticle effects to viscous dissipation. Therefore, Equation III.2 should be rewritten as

$$\eta/\eta^0 = E_T/E_T^0 = \frac{E_H + E_{NH}}{E_T^0} \qquad \text{(III.3)}$$

where E_H and E_{NH} denote the viscous dissipation due to the hydrodynamic and nonhydrodynamic particle-particle interaction energy (> 0), respectively.

B. Viscous Dissipation Due to Flow

First, we consider hydrodynamic interaction caused by the relative motion of two spheres within each gap. Furthermore, this motion can be decomposed into two types: a relative sliding motion of two spheres and a motion along their lines of centers.

First, we consider the contribution of the former type to the viscous dissipation. Here, a cylindrical coordinate (r, θ, z) should be taken as Fig. III.1. We consider two spheres with radius a, one having the velocity $\frac{u}{2}$ and another $-\frac{u}{2}$ (these are normal to center axis). This is replaced by the same two spheres, one has velocity u and the other stationary. An origin is fixed at the surface of the stationary sphere. Since the rate of viscous dissipation per unit volume, ϕ is defined by (120)

$$\phi = \underset{\sim}{\sigma} : \underset{\sim}{d} \tag{III.4}$$

the rate of energy dissipated, E is given by

$$E = \int_V \phi dV = \int_0^a \phi \cdot 2\pi r h dr \tag{III.5}$$

where h is a separation of two spheres at an arbitrary r. From Equation III.1, ϕ is expressed as

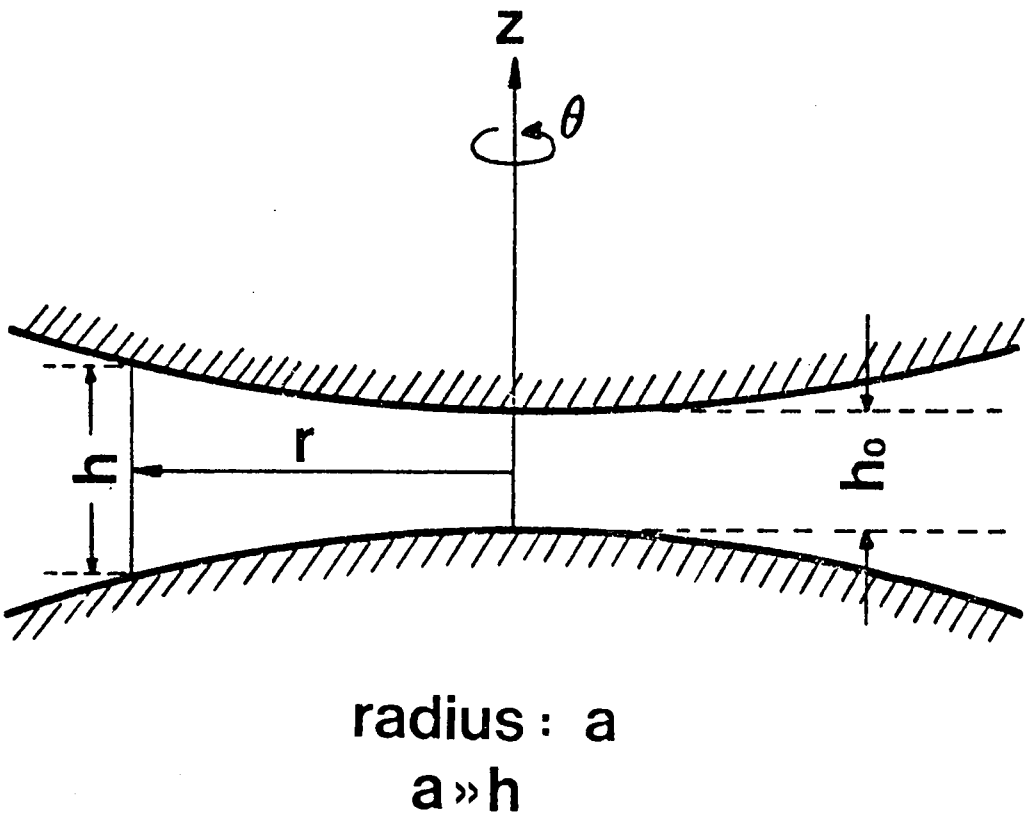

Figure III.1. Relative Motion of Two Spheres.

$$\phi = \frac{\eta_0^0 \dot{\gamma}^2}{1 + \frac{\eta_0^0}{K} \dot{\gamma}^{1-n}} \quad . \tag{III.6}$$

From $\dot{\gamma} = u/h$, Equation III.5 reduces to

$$E = 2\pi\eta_0^0 \int_0^a \frac{(\frac{u}{h})^2}{1 + \frac{\eta_0^0}{K} (\frac{u}{h})^{1-n}} rhdr \quad . \tag{III.7}$$

If we take $K \to \infty$, we obtain the result of Frankel and Acrivos (62). If instead we assume

$\frac{\eta_0^0}{K} (\frac{u}{h})^{1-n} >> 1$, we obtain

$$E = 2\pi K u^{n+1} \int_0^a \frac{r}{h^n} dr \tag{III.8a}$$

where

$$h(r) = h_0 + 2a\left[1 - \sqrt{1 - (\frac{r}{a})^2}\right] \quad . \tag{III.8b}$$

After integration, in the limit of $\frac{h_0}{a} \to 0$ for E, we obtain

$$E = \frac{\pi K}{|n-1|} u^{n+1} a^{2-n} (\frac{a}{h_0})^{n-1} \quad (n \neq 1) \quad . \tag{III.9}$$

Next, we consider the case of a motion along line of centers of two spheres. The problems of normal approach of two parallel plates is so-called squeeze flow problems and has been investigated by many researchers using lubrication theory (17) (30) (128) (129). Similarly, we take a cylindrical coordinate shown in Fig. III.1. A normal approach of two spheres, whose velocity are given by $\frac{u}{2}$ and $-\frac{u}{2}$, respectively, is considered, but as in the sliding motion, this is equivalent to the state in which one sphere is approaching with velocity u and another is stationary. The origin is fixed at the surface of the stationary sphere. It should be noted that in this case h and h_0 are dependent of time, i.e., $h(r,t)$ and $h_0(t)$.

Velocity fields in the surrounding fluid can be represented by (121).

$$v_r = v_r(r,z),\ v_\theta = 0,\ v_z = v_z(z)\ . \tag{III.10}$$

Since the flow is supposed to be dominant in radial direction and axisymmetric because the fluid has a small thickness, i.e., $a >> h$,

$$v_z << v_r,\quad \frac{\partial v_r}{\partial r} << \frac{\partial v_r}{\partial z}\ . \tag{III.11}$$

A force balance for the r-component gives

$$0 = -\frac{\partial p}{\partial r} + \frac{\partial}{\partial z}\left(\eta 0\ \frac{\partial v_r}{\partial z}\right)\ . \tag{III.12}$$

From Equation III.1 using the following boundary conditions

$$v_r(0) = 0 \quad \text{and} \quad v_r(h) = 0 \tag{III.13}$$

we obtain the velocity profile. If $K \to \eta_0$, we obtain the Frankel and Acrivos result (62). If we consider $\frac{\eta_0}{K} \dot{\gamma}^{1-n} >> 1$ $\left(\dot{\gamma} = \frac{\partial v_r}{\partial z}\right)$ and $p = p(r)$,

$$v_r(z) = K^{\frac{1}{n}} \left(\frac{dp}{dr}\right)^{\frac{1}{n}} \frac{n}{n+1} \left[z^{\frac{n+1}{n}} - h^{\frac{1}{n}} z\right] \tag{III.14}$$

Continuity gives

$$\frac{1}{r} \frac{\partial}{\partial r} (r\, v_r) + \frac{\partial v_z}{\partial z} = 0 \ . \tag{III.15}$$

Integrating this using the boundary conditions,

$$v_z(0) = 0 \quad \text{and} \quad v_z(h) = -u \tag{III.16}$$

the following equation can be obtained

$$u = \frac{1}{r} \frac{d}{dr} \int_0^h r\, v_r \, dz \ . \tag{III.17}$$

Substituting Equation III.14 into Equation III.17, we obtain

$$u = -K^{\frac{1}{n}} \frac{n}{2(n+1)(2n+1)} \frac{1}{r} \frac{d}{dr} \left[r\, h^{\frac{2n+1}{n}} \left(\frac{dp}{dr}\right)^{\frac{1}{n}}\right] \ . \tag{III.18}$$

If we define $x \equiv \sqrt{1 - \left(\frac{r}{a}\right)^2}$ and $B \equiv 1 + \frac{h_0}{2a}$,

$$p(x) = p_0 + K \left[\frac{(n+1)(2n+1)}{n}\right]^n u^n 2^{-(2n+1)} a^{-n} \left(f(0) - f(x)\right) \quad \text{(III.19a)}$$

where

$$f(x) = \int_x^1 \frac{x(1-x^2)^{\frac{n-1}{2}}}{(B-x)^{2n+1}} dx \ . \quad \text{(III.19b)}$$

The force due to this pressure rise is

$$F = \int_0^a (p(r) - p_0) 2\pi r dr \ . \quad \text{(III.20)}$$

Since the rate of the energy dissipated can be expressed by (62)

$$E = \left|\frac{1}{2} u F\right| \quad \text{(III.21)}$$

and using the approximation for $0 \leq x \leq 1$

$$\frac{x(1-x^2)^{\frac{n-1}{2}}}{(B-x)^{2n+1}} \cong \frac{x}{(B-x)^{2n+1}} \quad \text{(III.22)}$$

we obtain the following equation in the limit of $\frac{h_0}{a} \to 0$ (see Appendix).

$$E = \alpha K a^{2-n} u^{n+1} \left(\frac{a}{h_0}\right)^{2n-1} \quad \text{(III.23a)}$$

where

$$\alpha = \frac{\pi}{4}\left[\frac{(n+1)(2n+1)}{n}\right]^{n}\left|\frac{1}{(2n)(2n-1)}\right| . \qquad \text{(III.23b)}$$

From a comparison of Equation III.9 with Equation III.23, it is reasonable to assume that the contribution of a relative sliding motion is negligible compared to that of a normal approaching motion.

Since Equation III.23 involves the viscous dissipation energy concerned with one particle, total energy, E_H associated with all particles contained are given by

$$E_H \sim \sum_i E_i = \alpha m K a^{2-n} \left(\frac{a}{h_0}\right)^{2n-1} \sum_i u_i^{n+1} \qquad \text{(III.24)}$$

where u_i is the velocity of i-th particle, and m is the number of the nearest neighboring contacts. If the particles would take a simple configuration such as a cubic packing, a relative velocity $\frac{u_i}{2}$ can be expressed by

$$\left\langle \left(\frac{u_i}{2}\right)^2 \right\rangle \sim (2a + h_0)^2 \, \underset{\sim}{d}_i : \underset{\sim}{d}_i \qquad \text{(III.25)}$$

where $\langle \ \ \rangle$ means the average over possible orientation of neighboring spheres and $\underset{\sim}{d}_i$ is the rate of deformation tensor corresponding to the i-th particle. Since we can put as

$$\sum_i \left(\underset{\sim}{d}_i : \underset{\sim}{d}_i\right)^{\frac{n+1}{2}} \sim N\dot{\gamma}^{n+1} \qquad \text{(III.26)}$$

where N is the number of particles in suspensions. Equation III.24 can be rewritten as

$$E_H \sim mNKa^{2-n} \left(\frac{a}{h_0}\right)^{2n-1} (2a + h_0)^{n+1} \dot{\gamma}^{n+1} \quad . \tag{III.27}$$

As mentioned before, E_T^0 can be represented by

$$E_T^0 = \int_V (\underset{\sim}{\sigma} : \underset{\sim}{d}) dV = \int_V \eta^0(\dot{\gamma})\dot{\gamma}^2 \, dV \quad . \tag{III.28}$$

Substituting Equation III.1 and using the approximation $\frac{\eta_0^0}{K} \dot{\gamma}^{1-n} >> 1$,

$$E_T^0 = \eta_0^0 \int \frac{\dot{\gamma}^2}{1 + \frac{\eta_0^0}{K} \dot{\gamma}^{1-n}} dV = K \dot{\gamma}^{n+1} \frac{4}{3}\pi \left(a + \frac{h_0}{2}\right)^3 N \quad . \tag{III.29}$$

From Equation III.2, Equation III.27 and Equation III.29, we obtain the effective viscosity of concentrated suspension in the limit of $\frac{h_0}{a} \to 0$

$$\eta/\eta^0 \sim \left(\frac{a}{h_0}\right)^{2n-1} \quad . \tag{III.30}$$

The case of n = 1 (Newtonian fluid) corresponds to Frankel and Acrivos result (62). They have proposed the following relationship between $\frac{h_0}{a}$ and volume fraction of small particles, ϕ,

$$\frac{h_0}{a} = 2\left[\left(\frac{\phi_m}{\phi}\right)^{1/3} - 1\right] \text{ as } \frac{\phi}{\phi_m} \to 1 \tag{III.31}$$

where ϕ_m is the maximum volume fraction attainable. Therefore, we can write

$$\eta/\eta^0 = f(n,\phi) \tag{III.32a}$$

where

$$f(n,\phi) \sim \left[\left(\frac{\phi_m}{\phi}\right)^{1/3} - 1\right]^{1-2n} \quad (0 < n \leq 1) \; . \tag{III.32b}$$

Therefore, as ϕ increases, η increases. A smaller n gives a higher η.

C. Energy Dissipation Due to Other Force Fields

Next, we treat nonhydrodynamic effects. The most important two effects are presumed to be van der Waals forces and electrostatic forces.

First, we consider the effect of van der Waals forces between two spheres. This problem has been solved by Hamaker (73). He carried out this calculation using London-type potential. The interaction energy between two particles containing q atoms per unit volume, $\bar{E}_{VW}$ is given by

$$\bar{E}_{VW} = - \iint \frac{q^2\lambda}{r^6} \, dV_1 \, dV_2 \tag{III.33}$$

where dV_1 and dV_2 designate volume elements of two particles, r denotes the distance between dV_1 and dV_2, and λ is the London-van der Waals constant. The potential energy of an atom at a point outside a sphere at some distance is first calculated. Accordingly, the total energy of interaction between two spheres, $\bar{E}_{VW}$ can be obtained by applying the

same method with respect to a second sphere, the centers being a distance h_0 apart, namely

$$\bar{E}_{VW} = - \frac{A}{12} \left[\frac{1}{y^2+2y} + \frac{1}{(y+1)^2} + 2\ell n \frac{(y^2+2y)}{(y+1)^2} \right] \qquad \text{(III.34a)}$$

where

$$y = \frac{h_0}{2a} \qquad \text{(III.34b)}$$

$$A = \pi^2 q^2 \lambda > 0 \quad \text{(called Hamaker's constant)} . \qquad \text{(III.34c)}$$

Therefore, the rate of the energy dissipated due to van der Waals force, E_{VW} is

$$E_{VW} = \frac{mN}{2} \left| \frac{\partial \bar{E}_{VW}}{\partial t} \right| = \frac{mNA}{12} \left[\frac{2}{y(y+1)(y+2)} - \frac{1}{(y+1)^3} - \frac{1}{4y^2} + \frac{1}{4(y+2)^2} \right] \left(\frac{dy}{dt} \right) . \qquad \text{(III.35)}$$

From Fig. III.1 (p. 50),

$$\frac{dy}{dt} = \frac{1}{2a} \frac{dh_0}{dt} = - \frac{u}{2a} \qquad \text{(III.36)}$$

Furthermore, combination of Equation III.11 and Equation III.15 gives

$$\frac{\partial v_z}{\partial z} = - \frac{1}{r} \frac{\partial}{\partial r} (r v_r) \sim - \frac{v_z}{r} - \frac{\partial v_r}{\partial z} \quad - \frac{\partial v_r}{\partial z} = - \dot{\gamma} . \qquad \text{(III.37)}$$

and from

$$u = -(2a + h_0) \frac{\partial v_z}{\partial z} \tag{III.38}$$

we obtain

$$u \sim (2a + h_0)\dot{\gamma} = 2a(y + 1)\dot{\gamma} \ . \tag{III.39}$$

Therefore

$$\frac{dy}{dt} \sim -(y + 1)\dot{\gamma} \ . \tag{III.40}$$

Substituting this into Equation III.35

$$E_{VW} = - \frac{mNA\dot{\gamma}}{12} \left(\frac{2}{y(y+2)} - \frac{1}{(y+1)^2} - \frac{y+1}{4y^2} + \frac{y+1}{4(y+2)^2} \right) \ . \tag{III.41}$$

Combination of Equation III.1, Equation III.29 and Equation III.41 leads to

$$\frac{E_{VW}}{E_T^0} \sim \frac{mA}{a^3 y^2} \frac{1}{n^0 \dot{\gamma}} \text{ for } \frac{h_0}{a} \to 0 \ . \tag{III.42}$$

Next, we discuss electrostatic effects. Energy stored by electric double layer depends on the electrolyte concentration, the surface electrostatic potential, the particle size relative to the thickness of cloud of ions, the particle separation and so on. It has been well known that the following general equation may be satisfied for the electrostatic potential ψ

$$\nabla^2\psi = f(\psi) \ . \qquad \text{(III.43)}$$

For the case where the supporting electrolyte is symmetrical, i.e., cations and anions have the same valence, this reduces to the Poisson-Boltzmann equation

$$\nabla^2\psi = \kappa^2 \sinh \psi \qquad \text{(III.44)}$$

where κ^{-1} is called Debye length. We consider the simplest case here, that is, for small potential above equation can be rewritten as

$$\nabla^2\psi = \kappa^2\psi \ . \qquad \text{(III.45)}$$

These are the so-called Debye-Hückel equations for small potentials. The solution for the case of the thin ionic cloud ($\kappa a >> 1$) and small particle separation ($h_0 << a$), which are now of interest, was first obtained by Derjaguin (52) (53). In this case he has presumed that the two spheres can be replaced by a set of parallel rings, each pair of rings being treated as sections of infinite parallel plates. If $\overline{E}(H)$ is defined as the potential energy of interaction between two parallel plates, interaction energy between spherical double layers, $\overline{E}_{e\ell}$ is given by (52) (53)

$$\overline{E}_{e\ell} = \pi a \int_{h_0}^{\infty} \overline{E}(H)dH \qquad \text{(III.46)}$$

where H is a distance between two plates. The potential energy of

interaction between flat double layers, $\bar{E}(H)$ has also been investigated by several researchers (94) (123). $\bar{E}(H)$ can be given by (94)

$$\bar{E}(H) = \frac{\varepsilon\kappa}{4\pi}\psi_0^2\left[1 + \text{cosech}\,(\kappa H) - \coth\,(\kappa H)\right] \qquad \text{(III.47)}$$

where ε is a dielectric constant of medium and ψ_0 is a surface potential of two plates. Therefore, from Equation III.46, we obtain (14) (53) (94) (212)

$$\bar{E}_{e\ell} = \frac{\varepsilon a\psi_0^2}{2}\ell n(1 + e^{-\kappa h_0}) \; . \qquad \text{(III.48)}$$

The rate of heat dissipation due to motion of the sphere can be expressed, taking into account Equation III.40,

$$E_{e\ell} = \frac{mN}{2}\left|\frac{\partial\bar{E}_{e\ell}}{\partial t}\right| = \varepsilon a^2\kappa\psi_0^2\frac{mN}{2}\frac{y+1}{1 + e^{\kappa h_0}}\dot{\gamma} \qquad \text{(III.49)}$$

Combining Equation III.1, Equation III.29 and Equation III.49,

$$\frac{E_{e\ell}}{E_T^0} \sim \frac{m\varepsilon\kappa\psi_0^2}{a}\frac{1}{\eta^0\dot{\gamma}} \quad \text{for } \frac{h_0}{a} \to 0 \; . \qquad \text{(III.50)}$$

D. Theory of Viscosity

In the presence of nonhydrodynamic interactions including van der Waals force and electrostatic force, Equation III.3 should be rewritten in general as follows

$$\frac{\eta}{\eta^0} = \frac{E_T}{E_T^0} = \frac{E_H}{E_T^0} + \frac{E_{VW}}{E_T^0} + \frac{E_{e\ell}}{E_T^0} \quad . \tag{III.51}$$

Finally, we propose the effective viscosity for concentrated suspensions of a non-Newtonian fluid medium under consideration of nonhydrodynamic interaction from Equation III.30, Equation III.42 and Equation III.51

$$\frac{\eta}{\eta^0} = C_1 y^{1-2n} + \left(C_2 \frac{\varepsilon\kappa\psi_0^2}{a} + C_3 \frac{A}{a^3 y^2} \right) \frac{1}{\eta^0 \dot{\gamma}} \tag{III.52}$$

where C_1, C_2 and C_3 are positive constants. If we define the following equations using Equation III.32

$$\eta^*(\phi,\dot{\gamma},n) \equiv \eta^0(\dot{\gamma},n) f(n,\phi) \tag{III.53a}$$

$$Y \equiv C_2 \frac{\varepsilon\kappa\psi_0^2}{a} + C_3 \frac{A}{a^3 y^2} \tag{III.53b}$$

where as derived by Equation III.31

$$y = \left(\frac{\phi_m}{\phi}\right)^{1/3} - 1 \quad \text{as} \quad \frac{\phi}{\phi_m} \to 1 \quad . \tag{III.53c}$$

From Equation III.52 and Equation III.53, we finally obtain

$$\eta = \eta^*(\phi,\dot{\gamma},n) + \frac{Y}{\dot{\gamma}} \quad . \tag{III.54}$$

This equation is very similar to the Bingham equation derived from phenomenological approach except that η_B in the Bingham equation is replaced by η^* in Equation III.54. Therefore, the Y defined in Equation III.53b should be a yield stress. That is, it supposedly results from nonhydrodynamic particle-particle interaction such as van der Waals force and electrostatic force. Equation III.53 would predict that increasing dielectric constant of medium fluid, surface potential on the particles, particle concentration and Hamaker's constant, in other words, van der Waals constant increases the yield stress, eventually, the effective viscosity, but increasing particle size and ionic cloud thickness decreases them.

Here, we develop the relationship between the yield stress and particle diameter. If we assume ε, κ, ψ_0, A and y in Equation III.53b to be independent of particle diameter, we obtain

$$Y = \frac{C_4}{a} + \frac{C_5}{a^3} \qquad \text{(III.55)}$$

where C_4 and C_5 are positive constants. This suggests that small particles lead to the large yield stress.

Let us attempt to evaluate the actual magnitude of the yield stress. If we use a = 1μ, A = $10^{-12} \sim 10^{-13}$ erg (73) and ϕ/ϕ_m = 0.8 $\sim$ 0.9, the term due to van der Waals force takes the order of magnitude, $10^2 \sim 10^3$ dyne/cm^2. Assuming that ψ_0 = 1 mV, ε = 2 $\sim$ 3 Farad/m for polystyrene (29) and κa = 10, the term due to electrostatic force gives 10^7 dyne/cm^2 in magnitude. Therefore, in the presence of electrostatic

interaction the contribution of van der Waals effect can be neglected to electrostatic effect. Next, we consider the system without electrostatic interaction. As yield stresses, we obtain $10^5 \sim 10^6$ dyne/cm^2 for $a = 0.05\mu$ and $10^4 \sim 10^5$ dyne/cm^2 for $a = 0.1\mu$ from Equation III.53b.

Furthermore, Equation III.54 suggests that nonhydrodynamic particle-particle interaction could be dominant at low shear rates, but normal hydrodynamic interaction becomes much more important at high shear rates.

From Equation III.53a, the following relationship can be obtained

$$\frac{\eta^*(\phi,\dot{\gamma},n)}{\eta^*(\phi,0,n)} \equiv \frac{\eta^*}{\eta_0^*} = \frac{\eta^0(\dot{\gamma},n)}{\eta^0(0,n)} = \frac{\eta^0}{\eta_0^0}$$

that is

$$\frac{\eta^*}{\eta_0^*} = \frac{\eta^0}{\eta_0^0} . \qquad \text{(III.56)}$$

This means that the value, $\eta - \frac{Y}{\dot{\gamma}}$, which is obtainable from experiments, is solely due to hydrodynamic effects.

In the above discussions, we used the power law approximation, $\frac{\eta_0^0}{K}\dot{\gamma}^{1-n} >> 1$. We attempt to obtain a general solution using Equation III.1. However, this may not be attainable, for it is impossible to integrate mathematically Equation III.12 necessary for calculation of hydrodynamic problems. As a result. rate of energy dissipation due to hydrodynamic interaction, E_H can be obtained by

numerical method. Other terms can be evaluated mathematically using Equation III.1. E_T^0 in Equation III.29 can be replaced by

$$E_T^0 \sim \frac{\eta_0^0 \dot{\gamma}^2}{1 + \frac{\eta_0^0}{K} \dot{\gamma}^{1-n}} \frac{4}{3}\pi (a + \frac{h_0}{2})^3 N . \qquad \text{(III.57)}$$

Therefore, the hydrodynamic term can be represented by

$$\frac{E_H}{E_T^0} \sim (\frac{a}{h_0})^{2n-1} g(\dot{\gamma}) \qquad \text{(III.58)}$$

where $g(\dot{\gamma})$ is a function of the shear rate only. For nonhydrodynamic terms, the calculation gives the same equations as the power law approximation given by Equation III.42 and Equation III.50. Finally, we get

$$\eta = \eta^* g(\dot{\gamma}) + \frac{\gamma}{\dot{\gamma}} . \qquad \text{(III.59)}$$

The case which $g(\dot{\gamma})$ is close to a unity corresponds to power law approximation given by Equation III.54. An approximation by Newtonian fluid media takes the form

$$\eta = \eta_0^* + \frac{\gamma}{\dot{\gamma}} . \qquad \text{(III.60)}$$

This is equivalent to a Bingham equation.

E. Summary of View of Viscosity Behavior of Polymer Melts Reinforced with Small Particles

In a previous section, we proposed that the flow behavior of suspension systems at low shear rates would be chiefly dependent upon nonhydrodynamic interparticle interaction such as van der Waals and electrostatic forces associated with the yield stresses. Flow properties at high shear rates can be purely characterized by normal hydrodynamic interaction essentially dependent upon only particle concentration.

We should remember the phenomenological theory based on von Mises yield criterion mentioned in Chapter II and its interpretation of it given by Hencky (87) (191). He shows it is equivalent to a critical distortional strain energy. We can view viscosity behavior of these systems. At low shear stresses, nonhydrodynamic interparticle interaction tends to produce a gel-like structure causing the yield stress. As high shear stresses are applied, the structure formed is disrupted by a critical distortional strain energy. Then, the melts behave similar to a viscoelastic fluid dominated by hydrodynamic interaction.

CHAPTER IV

MATERIALS AND EXPERIMENTAL PROCEDURES

A. Materials

Four kinds of particulate-filled polystyrene (PS), several types of commercial high-impact polystyrene (HIPS) and PS blended with high density polyethylene (HDPE) were used in this study. Carbon black (CB), titanium dioxide (TiO_2) and two types of calcium carbonate ($CaCO_3$). One of the calcium carbonates had received an unknown surface treatment. Table IV.1 and Table IV.2 show the polymers and fillers investigated here, respectively. Scanning electron micrographs for each filler are shown in Fig. IV.1 to Fig. IV.4. From these figures and information given by suppliers, the fillers used in this study are considered to be roughly spherical and order in particle size

$$CaCO_3 > TiO_2 > CB \ .$$

Figure IV.5 and Fig. IV.6 show transmission electron micrographs of two Dow's HIPS grades taken by Berko-Boateng (15). Rubber particle size determined from the pictures is also given in Table IV.1. Codes for HIPS samples are shown in the same table.

B. Preparation of Samples

The fillers were blended into PS melts using a two roll laboratory mill (D = 3" and L = 7") at 150°C; 0.03 wt % of Irganox 1010 was added

Table IV.1. Description of Polymers Used

Polymer	Supplier	Grade	Code	Rubber Content (vol %)	Rubber Particle Size (μ)	
PS	Dow	678u		0		M_w = 240,000 M_n = 80,000 (102)
HDPE	Phillips	EHM6001		0		MI = 0.1 (151)
HIPS	Dow	430	A	4.8	5.2	--
		470	B	6.7	4.8	--
		492u	C	9.6 (15)	4.5 (15)	--
		495	D	14.5	--	--
	Monsanto	(a)	E	27.0	--	M_w = 217,000 M_w = 165,000 (117) (b)
			F	27.0 (117)	--	

(a) Not commercial products.

(b) Values for matrix polystyrene.

Table IV.2. Characteristics of Fillers Studied

Filler	Supplier	Grade	Particle Size (μ)	
CB	Continental Carbon	FEF-LS N542	0.045	(219)
TiO_2	du Pont	R101	0.18	(151)
Untreated $CaCO_3$	Pfizer	Uncoated PCC Control (a)	0.5	(181)
Treated $CaCO_3$	Pfizer	Super-pflex 200	0.5	

(a) Not a commercial product.

Figure IV.1. Scanning Electron Micrograph of Carbon Black Used.

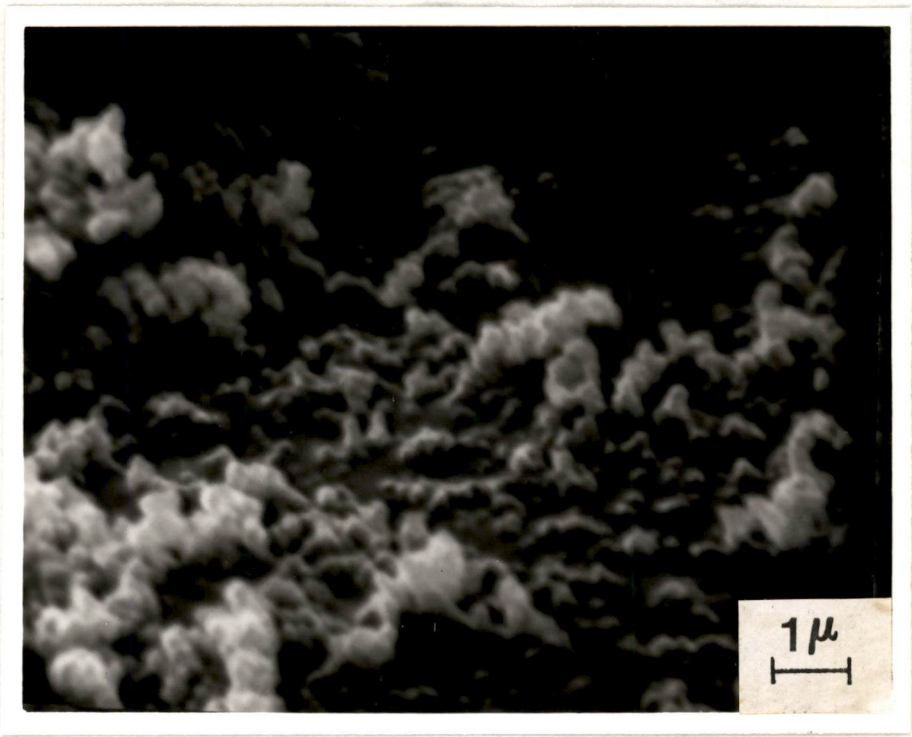

Figure IV.2. Scanning Electron Micrograph of TiO_2 Used.

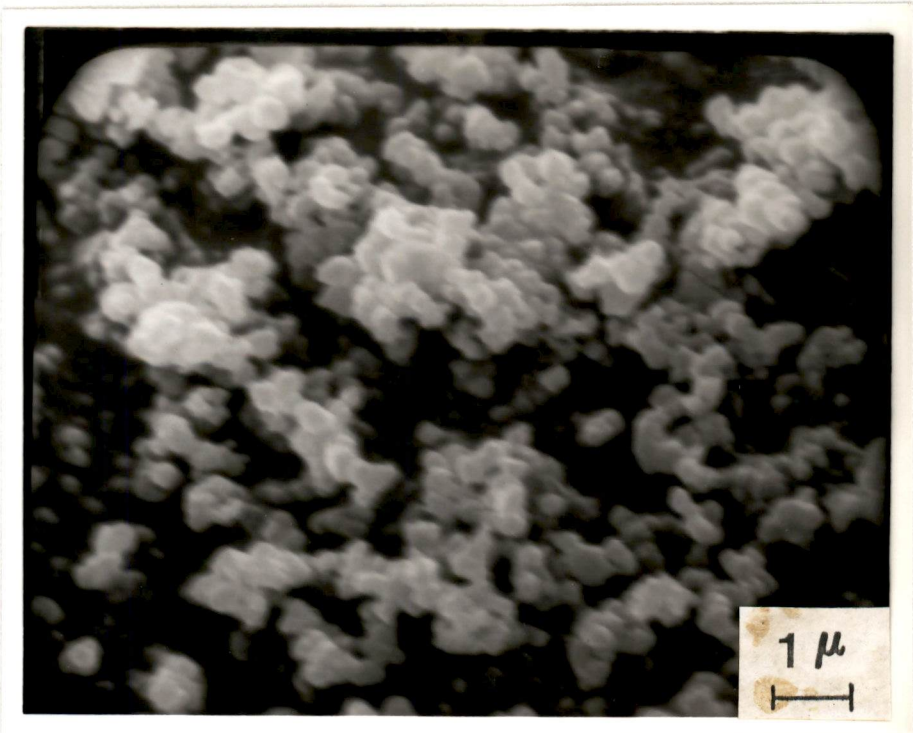

Figure IV.3. Scanning Electron Micrograph of Untreated $CaCO_3$ Used.

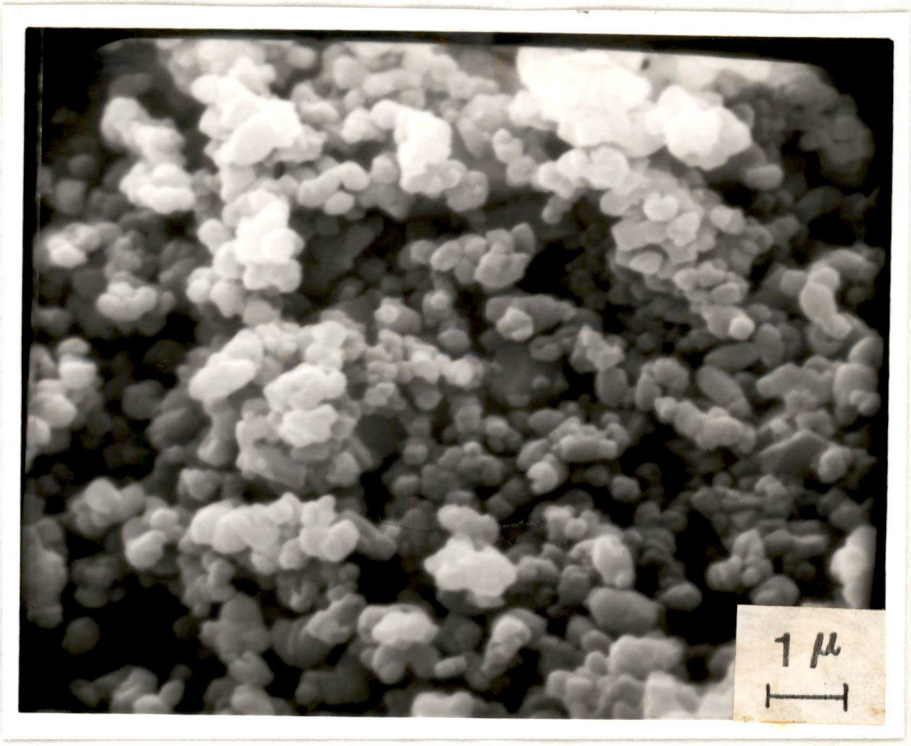

Figure IV.4. Scanning Electron Micrograph of Treated $CaCO_3$ Used.

Figure IV.5. Transmission Electron Micrograph of HIPS-A Sample.

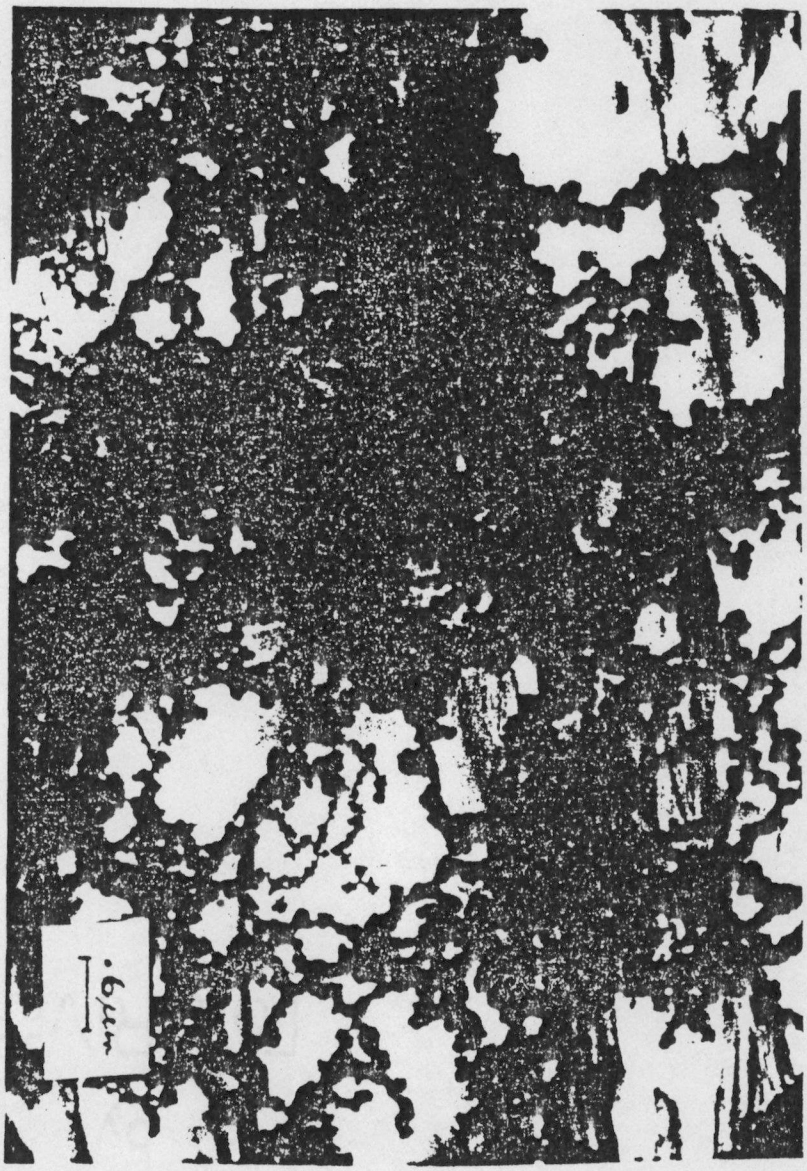

Figure IV.6. Transmission Electron Micrograph of HIPS-B Sample.

as an antioxidant. The mixing time was about 20 minutes at 15 rpm for one batch (300g of compounds), after adding the filler. Blends with filler contents of 10, 20 and 30 volume percent at 180°C were prepared. The volume fraction of the fillers at 180°C, at which the rheological measurements were carried out, was determined from

$$\phi = \frac{\frac{W_f}{\rho_f}}{\frac{W_f}{\rho_f} + \frac{1-W_f}{\rho_{PS}}} \qquad \text{(IV.1)}$$

where W_f is weight fraction of the filler, ρ_f the density of filler at 180°C and ρ_{PS} the density of PS at 180°C. Here, ρ_{TiO_2} = 4.1 g/cm^3 (151), ρ_{CaCO_3} = 2.7 g/cm^3 (113), ρ_{CB} = 1.8 g/cm^3 (225), ρ_{PS} = 0.96 g/cm^3 (151) and ρ_{HDPE} = 0.77 g/cm^3 (151) were used. Rubber contents of HIPS in Table IV.1 are values at 25°C. However, assuming that HIPS can be approximated to be a blend of PS and polybutadiene (PB), values at 180°C were calculated. As a result, it was shown that the rubber contents at 180°C were almost equal to those at 25°C. The filled polymers prepared are summarized in Table IV.3.

The prepared compounds were crushed into small pieces and compression molded at 180°C to form sheet samples of about 1.5 mm thickness. Samples prepared in this way were used for shear flow measurements. Other small pieces of compounds were extruded at 180°C by a Brabender extruder (D = 3/4" and L/D = 10) to make strands. A die with D = 0.081 mm and L/D = 15 was used. The extrusion speed was

Table IV.3. Weight Fraction of Fillers in Compounds Prepared

	PS/TiO_2	PS/CB	$PS/CaCO_3$	PS/HDPE
ϕ = 0.1	0.32	0.17	0.24	0.08
ϕ = 0.2 (0.3)	0.52	0.32	0.41	0.26
ϕ = 0.3 (0.5)	0.65	0.45	0.55	0.45

( ): PS/HDPE.

usually 30 rpm. No take-up devices were used. The strands obtained were used as specimens for uniaxial elongational flow measurements.

C. Rheological Measurements

C.1. Shear Flow Measurement

Rheological measurements in the low shear rates were carried out at 180°C by a Mechanical Spectrometer (Rheometrics Inc., Union, NJ). A cone-and-plate apparatus was used to measure the shear stress and the first normal stress difference. The cone had a 25 mm diameter and a 0.1 radian cone angle was used in this study.

The analysis of data is the same as mentioned in previous work (152) (153) in our laboratories. The shear viscosity η and the first normal stress difference N_1 were evaluated from the following equations.

$$\dot{\gamma} = \frac{\Omega}{\alpha} \qquad \text{(IV.2a)}$$

$$\eta = \frac{\sigma_{12}}{\dot{\gamma}} = \frac{3T}{2\pi R^3 \dot{\gamma}} \qquad \text{(IV.2b)}$$

$$N_1 = \frac{2F}{\pi R^2} \qquad \text{(IV.2c)}$$

where Ω is the angular velocity of the cone, α the cone angle (0.1 rad.), T the torque, F the thrust and R the radius of the cone (25 mm). An average of the values in the clockwise and counterclockwise direction was taken. All measurements were repeated three times.

C.2. Elongational Flow Measurement

Elongational flow measurements were carried out at 180°C in an Ide rheometer shown in Fig. IV.7 (99). This enables us to stretch the samples at a constant deformation rate. Several studies with this instrument have been carried out in our laboratories (38) (100) (101) (102) (131) (153) (218) (220).

This instrument essentially consists of three parts. The first part is a constant temperature silicone oil bath which is controlled by a Hallikinen tube block heater at the bottom and a variac. In addition, another immersion type heater was used and controlled by a temperature controller. A thermocouple was put close to the sample. The temperature fluctuation was within ±2°C at a maximum. The second part is a 500 gm Instron load cell, and the third one is a rotating roll operated by a motor with a controller. Three $\frac{1}{15}$ HP B and B motors were used: One is for low speeds, a second for intermediate speeds and a third for high speeds. The motor speed was controlled by a B and B controller. An elongational rate was obtained in a range of 0.005 sec^{-1} to 3.0 sec^{-1} using the 63.5 mm diameter roll. The highest sensitivity range for the tension was a full-scale of 2 gm. A silicone oil (Dow Corning, Fluid 200®, kinetic viscosity: 100 centistokes at 25°C, density: 0.968 g/cm^3 at 25°C) was used as an oil bath medium.

The samples were first annealed for 7 minutes at 180°C in a silicone oil bath to eliminate residual stresses and orientation. If the annealed filament has length L_0 and the cross section A_0 at 25°C, it changes to length L and the cross section A at 180°C, A is given by

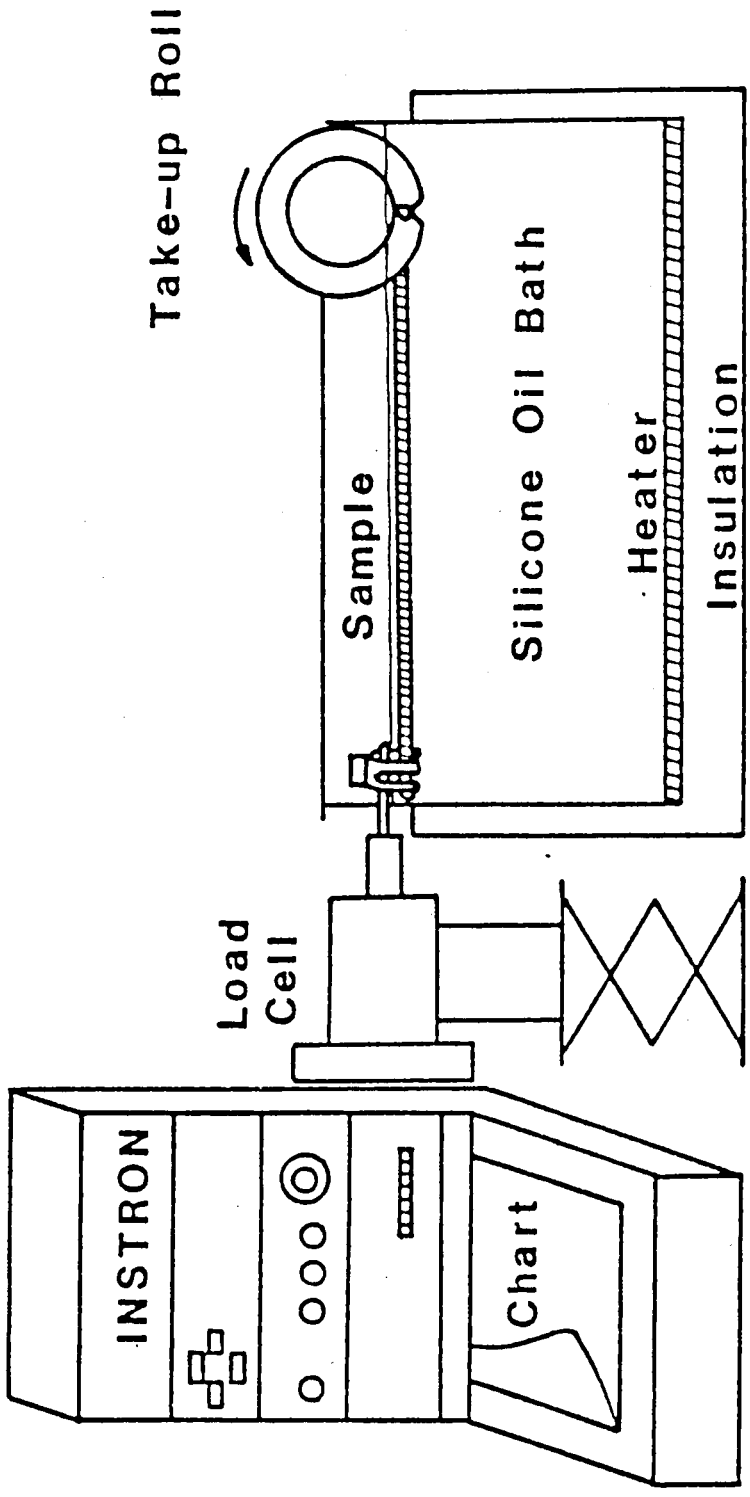

Figure IV.7. Elongational Flow Apparatus.

$$A = \frac{L_0}{L}\frac{\rho_0}{\rho}A_0 = \frac{1}{1 + \int_{25}^{100}\alpha dT}\frac{1}{\rho}\frac{W}{L_0} \qquad \text{(IV.3)}$$

where W and α are the weight and the linear thermal expansion coefficient of the filament. An average value of A was calculated from the measurement of five samples using Equation IV.3. Here, the following assumptions were made:

1. The densities of fillers are unchanged.
2. The fillers make no contribution to the thermal expansion, i.e., that of the compound is assumed

   $$\alpha = (1 - \phi)\alpha_{PS} \qquad \text{(IV.4)}$$

   where α_{PS} is the thermal expansion of PS, equal to 1.85×10^{-4}/°C (29) for above T_g.
3. HIPS is approximated to be a blend of PS and PB for evaluation of α. If we use $\alpha_{PB} = 2.2 \times 10^{-4}$/°C (29) for above T_g, α can be given by

   $$\alpha = (1 - \phi)\alpha_{PS} + \phi\alpha_{PB} \; . \qquad \text{(IV.5)}$$

4. Densities of HIPS at 180°C were also evaluated using the same approximation. Here, the following values were used: $\rho_{0,PB} = 1.01$ g/cm^3 (29), $\rho_{PB} = 0.90$ g/cm^3 (29) and $\rho_{0,PS} = 1.07$ g/cm^3 (151).
5. The linear thermal expansion factor for HDPE-PS blend polymer was calculated by

$$\alpha = (1 - \phi)\alpha_{PS} + \phi\alpha_{HDPE} \cdot \qquad \text{(IV.6)}$$

If the volumetric expansion factor β is assumed to be nearly equal to 3α, we obtain $\alpha_{HDPE} = 5.4 \times 10^{-4}$°C using β value in the literature (136).

6. To determine the density of blended polymer at 180°C, we took 0.96 g/cm^3 (151) as the density of HDPE at 25°C.

Hence, cross section A can be obtained from Equation IV.3. Ratio of cross section of filament at 180°C to that at 25°C, A/A_0 is summarized in Table IV.4 together with the densities at both 25°C and 180°C calculated by Equation IV.1.

The filament was attached between the clamp connected with a load cell and the take-up roller. After 10 minutes, which is necessary for thermal equilibrium, the filament was stretched in a constant elongational rate. The elongational rate $\dot{E}$ is defined by

$$\dot{E} = \frac{\partial v_1}{\partial x_1} = \frac{1}{L}\frac{dL}{dt} = \frac{v_L}{L} = \frac{R\Omega}{L} \qquad \text{(IV.7)}$$

where in this experiment R = 63.5 mm, L = 22 cm and Ω is the angular velocity of a roller. $\dot{E}$ is independent of time, namely, this instrument provides a constant elongational rate. Under an assumption of uniform deformation, the tensile stress $\sigma_{11}(t)$ and the elongational viscosities $\chi(t)$ can be calculated taking into account for Equation II.20.

$$\sigma_{11}(t) = \frac{F(t)}{A(t)} = \frac{F(t)}{A(o)} e^{\dot{E}t} \qquad \text{(IV.8a)}$$

Table IV.4. Densities of Samples Used and Ratio of Cross Section of Filament at 180°C to That at 25°C After Annealing

Systems	Loading Level at 180°C (vol %)	$\rho_{25°}$ (g/cm^3)	$\rho_{180°C}$ (g/cm^3)	A/A_0
PS	--	1.07	0.96	1.08
PS/TiO_2	10	1.40	1.27	1.07
	20	1.70	1.59	1.07
	30	2.06	1.91	1.05
PS/CB	10	1.15	1.04	1.08
	20	1.23	1.12	1.08
	30	1.31	1.22	1.05
PS/$CaCO_3$	10	1.25	1.14	1.07
	20	1.42	1.30	1.07
	30	1.60	1.49	1.05
PS/HDPE	10	1.06	0.942	1.09
	30	1.04	0.902	1.09
	50	1.02	0.864	1.10
HIPS-A	5 (a)	1.07	0.957	1.09
-B	7 (a)	1.07	0.956	1.09
-C	10 (a)	1.06	0.950	1.08
-D	15 (a)	1.06	0.951	1.08

(a) Rubber content.

$$\chi(t) = \frac{\sigma_{11}(t)}{\dot{E}} \tag{IV.8b}$$

where F(t) is the total force and A(o) is given by Equation IV.3. The elongation to break was evaluated from the breaking time t_B, measured by a stopwatch. We obtain from Equation II.20,

$$\ell n \frac{L_B}{L_0} = \dot{E} t_B \tag{IV.9}$$

where L_B and L_0 denote sample length at the breaking time and in the initial state, respectively.

D. Melt Spinning

The melt spining experiments were carried out using an Instron capillary rheometer and take-up device under both isothermal and nonisothermal conditions.

D.1. Nonisothermal Melt Spinning

Nonisothermal melt spinning experiments were carried out to measure the melt spinning instability. The apparatus is shown in Fig. IV.8. The samples were extruded through a die at 180°C into room air and then into an iced water quench bath. The die used had a 0.059" diameter and a 10 L/D ratio. The flow rate was constant throughout the experiment at 1.508×10^{-3} cm^3/sec.

The diameter of the take-up roll was 63.5 mm. That roll was driven by two types of $\frac{1}{15}$ HP B and B motor, 345 rpm and 12 rpm at the maximum

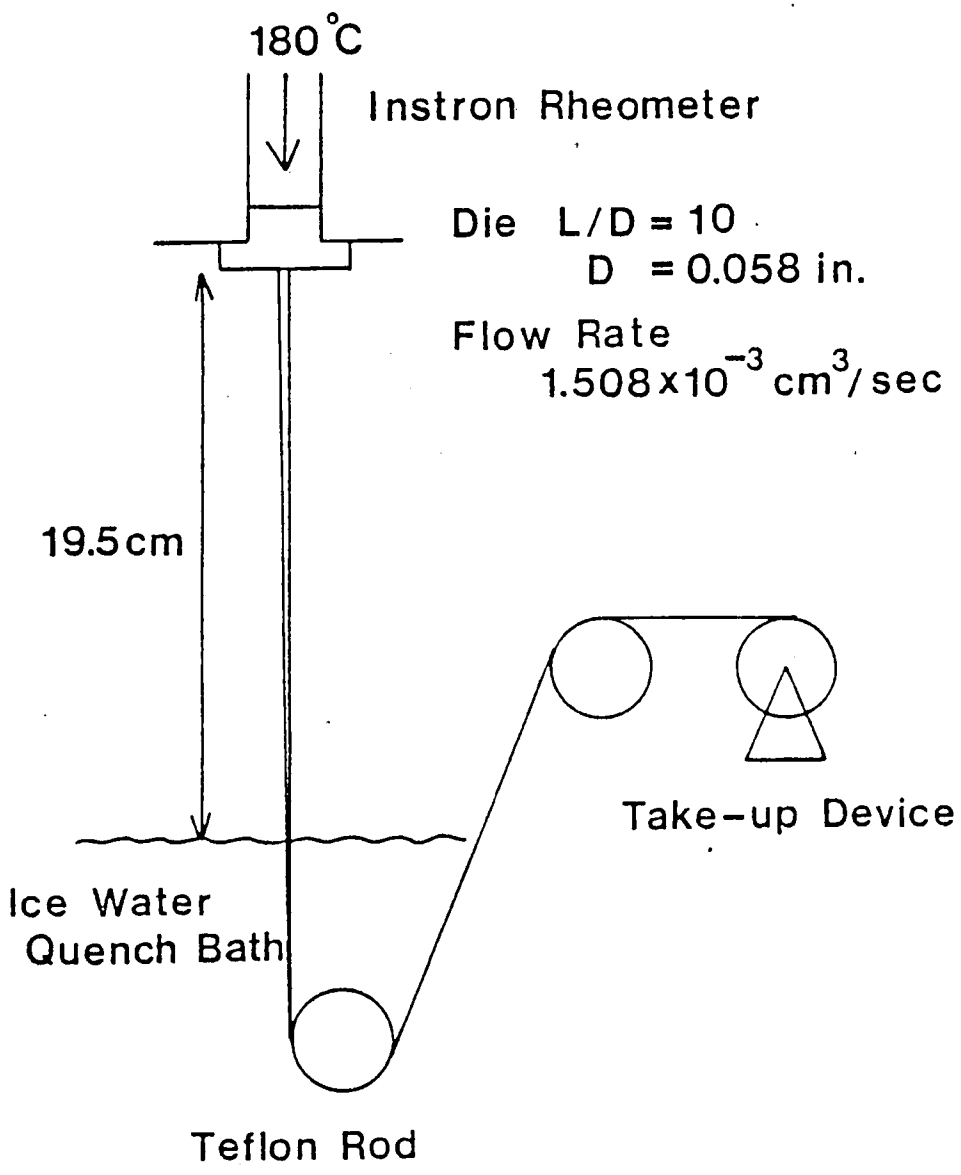

Figure IV.8. Nonisothermal Melt Spinning Apparatus.

speed and a B and B motor controller. The spinpath from the die exit to the water surface was always kept constant at 19.5 cm.

The diameter of the fiber taken up was measured using a thickness gauge. From the diameter variation along the fiber, the ratio of maximum diameter to minimum one, D_{max}/D_{min}, was determined and the period T obtained by

$$T = \frac{\lambda}{v_L} \tag{IV.10}$$

where v_L and λ are take-up velocity and wave length, respectively, were evaluated as a function of draw ratio given by v_L/v_0, where v_0 is the fiber velocity at die exit.

D.2. Isothermal Melt Spinning

Isothermal melt spinning experiments were carried out to measure the elongational viscosity. The apparatus used is shown in Fig. IV.9. The samples were extruded through a die at 180°C. The die used had a 0.01" diameter and a 22 L/D ratio. The fiber extruded passed into a 1.0" inside diameter by 3" long heated chamber and then into a water quench bath. Two sets of heaters were used to heat that chamber. Two thermocouples were located at 0.25" and 1.5" from the die exit, respectively, and connected with temperature controllers. The flow rate was always kept 1.508×10^{-3} cm^3/sec. The diameter of the take-up roll was 63.5 mm, which was operated by a $\frac{1}{15}$ HP B and B motor and a motor controller.

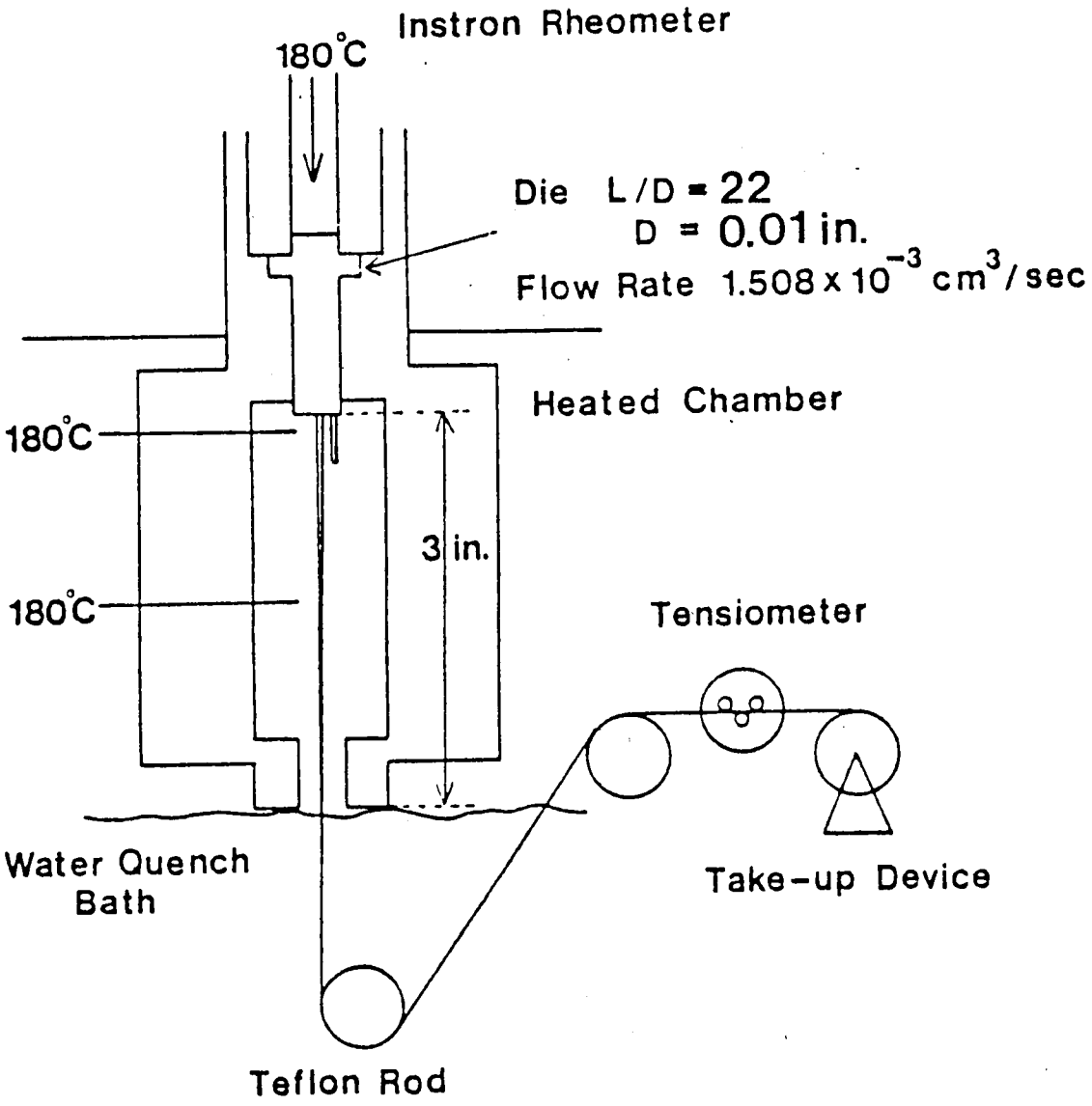

Figure IV.9. Isothermal Melt Spinning Apparatus.

A Rothschild tensiometer (10 gm full scale) was placed near the take-up roll. A calibration was required to obtain the spinline tension due to the presence of the teflon rods. This was done using Minoshima's procedure (152). The measured tension was recorded by a strip chart recorder (Model EV-205-11, Heath Co., Benton Harbor, Mich.) and a potentiometric amplifier (Model EV-200-01, Health Co., Benton Harbor, Mich.).

In conditions as mentioned above, isothermal melt spinning experiments for filled-PS were carried out. However, except for HIPS and HDPE-blended PS, all other samples were not available for measurements of the elongational viscosity, because they broke at the tensiometer. This may be due to brittleness of these samples. Therefore, isothermal melt spinning experiments were carried out for only the HIPS and HDPE-blended PS.

Measurements of the diameter along the spinline were carried out by taking a photograph of the fiber. Data were taken between 1 mm from the die exit and 40 mm from the die exit.

In isothermal melt spinning, the tensile stress σ_{11} is given by

$$\sigma_{11}(x_1) = \frac{4\ F_{rheo}(x_1)}{\pi\ D^2(x_1)} \qquad \text{(IV.11)}$$

where $D(x_1)$ is the fiber diameter at a position x_1 along the fiber. The spinline elongational viscosity χ_{sp} taken from isothermal melt spinning experiments is not a steady state value, but an apparent one (24) (216).

$$\chi_{sp}(x_1) = \frac{\sigma_{11}(x_1)}{\dot{E}(x_1)} \tag{IV.12a}$$

$$\dot{E}(x_1) = \frac{\partial v_1(x_1)}{\partial x_1} \tag{IV.12b}$$

$$v_1(x_1) = \frac{4Q}{\pi D^2(x_1)} \tag{IV.12c}$$

where Q is the volumetric flow rate. Now, F_{rheo} mentioned in Equation IV.11, the actual rheological force, can be expressed as

$$F_{rheo} = F_L + F_{grav} - F_{drag} - F_{inert} \tag{IV.13}$$

where F_L, F_{grav}, F_{drag} and F_{inert} are take-up force, gravity force, drag force and inertial force, respectively. These forces can be expressed as

$$F_{grav}(x_1) = \int_{x_1}^{L} \rho g \frac{\pi}{4} D^2(x_1)dx_1 = \frac{\pi\rho g}{4} \int_{x_1}^{L} D^2(x_1)dx_1 \tag{IV.14}$$

where ρ is the density of fiber at 180°C.

$$F_{inert}(x_1) = \rho Q(v_L - v_1(x_1)) = \rho Q(v_L - \frac{4Q}{\pi D^2(x_1)}) \tag{IV.15}$$

$$F_{drag}(x_1) = \int_{x_1}^{L} \sigma_f \pi D(x_1) dx_1 = \int_{x_1}^{L} C_f \frac{\rho v_1^2(x_1)}{2} \pi D(x_1) dx_1 \ . \qquad (IV.16)$$

Following the approximation by Sano and Orii (5) (196), we may write

$$F_{drag}(x_1) \cong 0.34 \pi D(x_1) \rho v_f^2 \, Re^{-0.8} (L - x_1) \qquad (IV.17)$$

where v_f is the fiber velocity. This equation reduces to

$$F_{drag}(x_1) = \begin{cases} 0.34\pi \left(D \rho v_f^2 \ell \, Re^{-0.8} \right)_{\text{in water}} & \text{for drag force between fiber and water} \qquad (IV.18a) \\ 0.34\pi \left(D \rho v_f^2 \ell \, Re^{-0.8} \right)_{\text{in air}} & \text{for drag force between fiber and air} \qquad (IV.18b) \end{cases}$$

where Reynolds number, Re, is given by

$$Re(\text{in water}) = \frac{(Dv_f)_{\text{in water}} \rho_{\text{water}}}{\eta_{\text{water}}} \qquad (IV.18c)$$

$$Re(\text{in air}) = \frac{(Dv_f)_{\text{in air}} \rho_{\text{air}}}{\eta_{\text{air}}} \qquad (IV.18d)$$

and the take-up force F_L is

$$F_L = k F \qquad (IV.19)$$

where k is a coefficient determined from the calibration mentioned above,

and F is the experimentally measured tension. It was assumed that fibers were suddenly solidified at the water surface and the correction due to buoyancy for gravity force could be neglected.

Values shown in Table IV.4 (p. 83) were used as densities necessary for the above calculations. In addition, the following values were used to calculate Reynolds number given by Equation IV.18: ρ_{H_2O} = 0.997 g/cm^3, η_{H_2O} = 0.01 poise, ρ_{air} = 1.2 × 10^{-3} g/cm^3 (196) and η_{air} = 1.8 × 10^{-4} poise (196). Then, as a value for ℓ, 20 cm and 7.62 cm were used in Equation IV.18a and Equation IV.18b, respectively. From these numerical values and the diameter $D(x_1)$ along the spinline, F_{grav}, F_{inert}, and F_{drag} can be calculated. Thus, the rheological force F_{rheo} can be evaluated, and eventually the spinline elongational viscosity χ_{sp}.

CHAPTER V

EXPERIMENTAL STUDIES ON SHEAR FLOW

Experimental studies on rheological behavior on shear flow are presented in this chapter. The shear viscosity η and the first normal stress difference N_1 were determined as discussed earlier (Chapter IV) on a Rheometrics Mechanical Spectrometer. There was an upper limit in the Mechanical Spectrometer due to a flow instability at about 1 sec^{-1}. Accordingly, the measurable shear rate range was from 0.01 to 1 sec^{-1}.

A. Shear Viscosity

A.1. Results

A.1.1. Polystyrene (PS) Melts Reinforced with Small Rigid Particles

Figures V.1 to V.3 show the shear viscosity as a function of the shear rate for carbon black (CB), TiO_2 and $CaCO_3$-filled PS melts. The shear viscosity increases with loading level. The highly-filled systems do not possess Newtonian region at low shear rates, but are always non-Newtonian. The shear viscosity function at high shear rates exhibits behavior similar to unfilled melts.

A.1.2. High Impact Polystyrene (HIPS) Melts

The viscosity of HIPS melts are summarized in Fig. V.4. While there is not a clear tendency for the present samples to exhibit a zero shear viscosity, it is also unsure if they will possess non-Newtonian region at low shear rates.

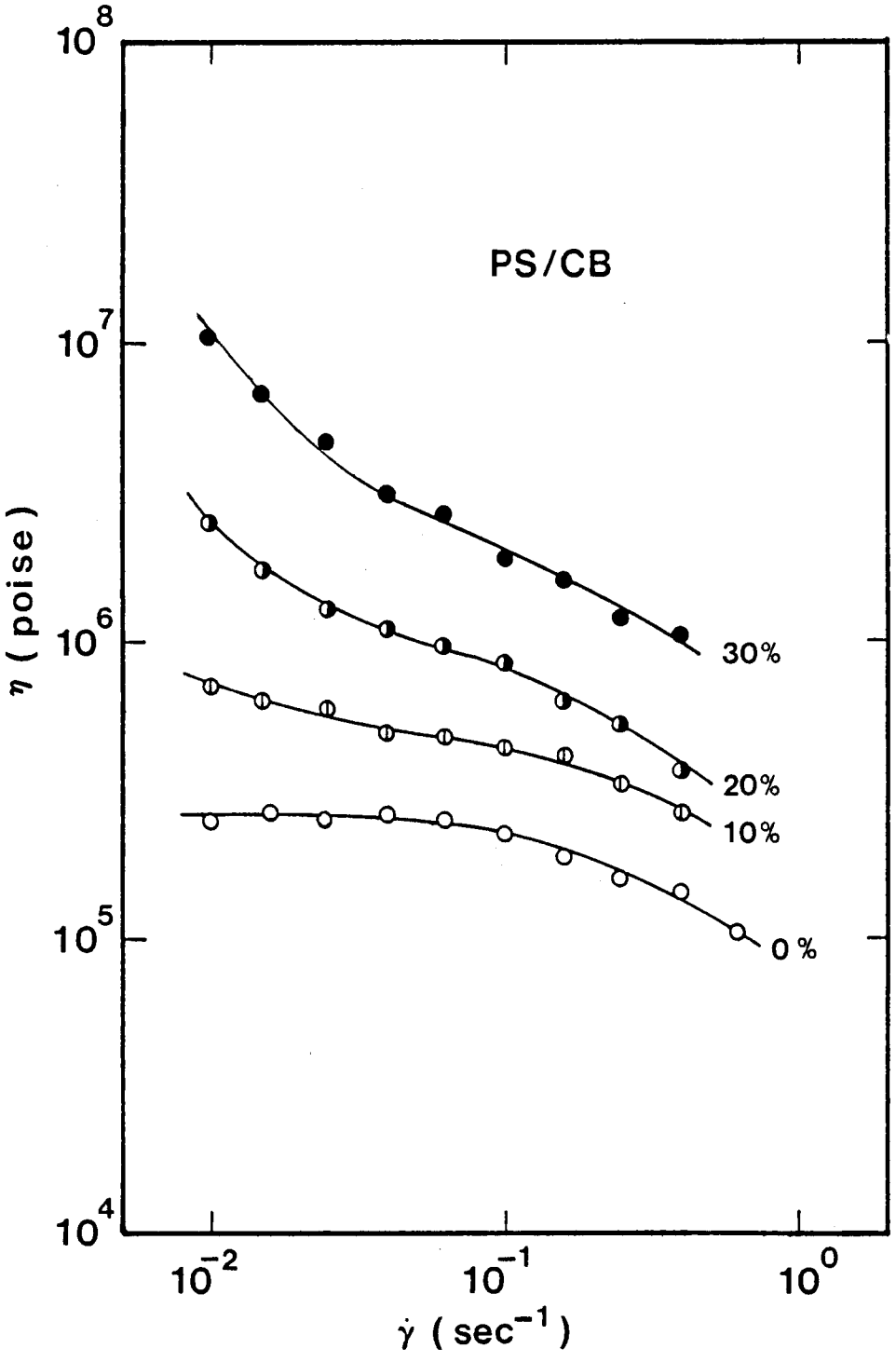

Figure V.1. Shear Viscosity as a Function of Shear Rate for CB-Filled PS Melts.

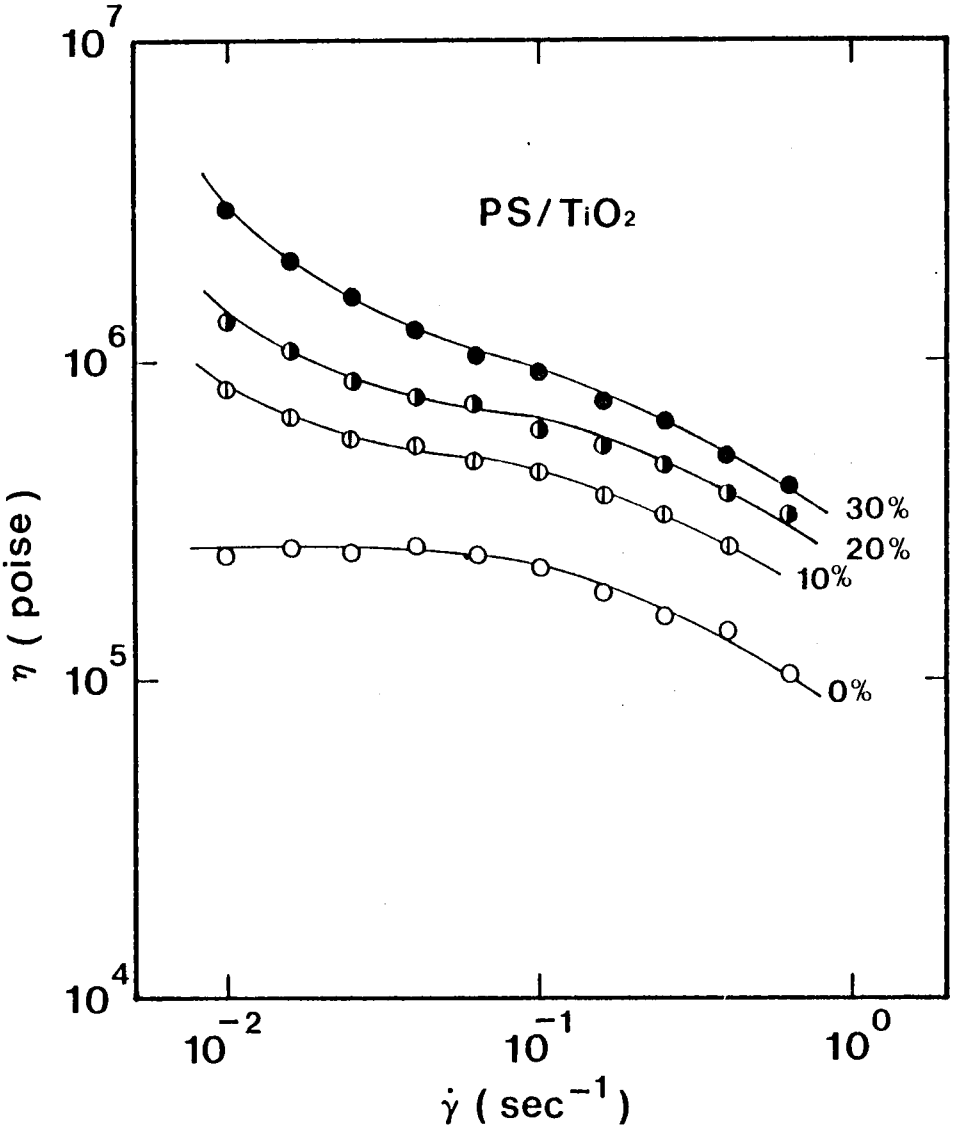

Figure V.2. Shear Viscosity as a Function of Shear Rate for TiO_2-Filled PS Melts.

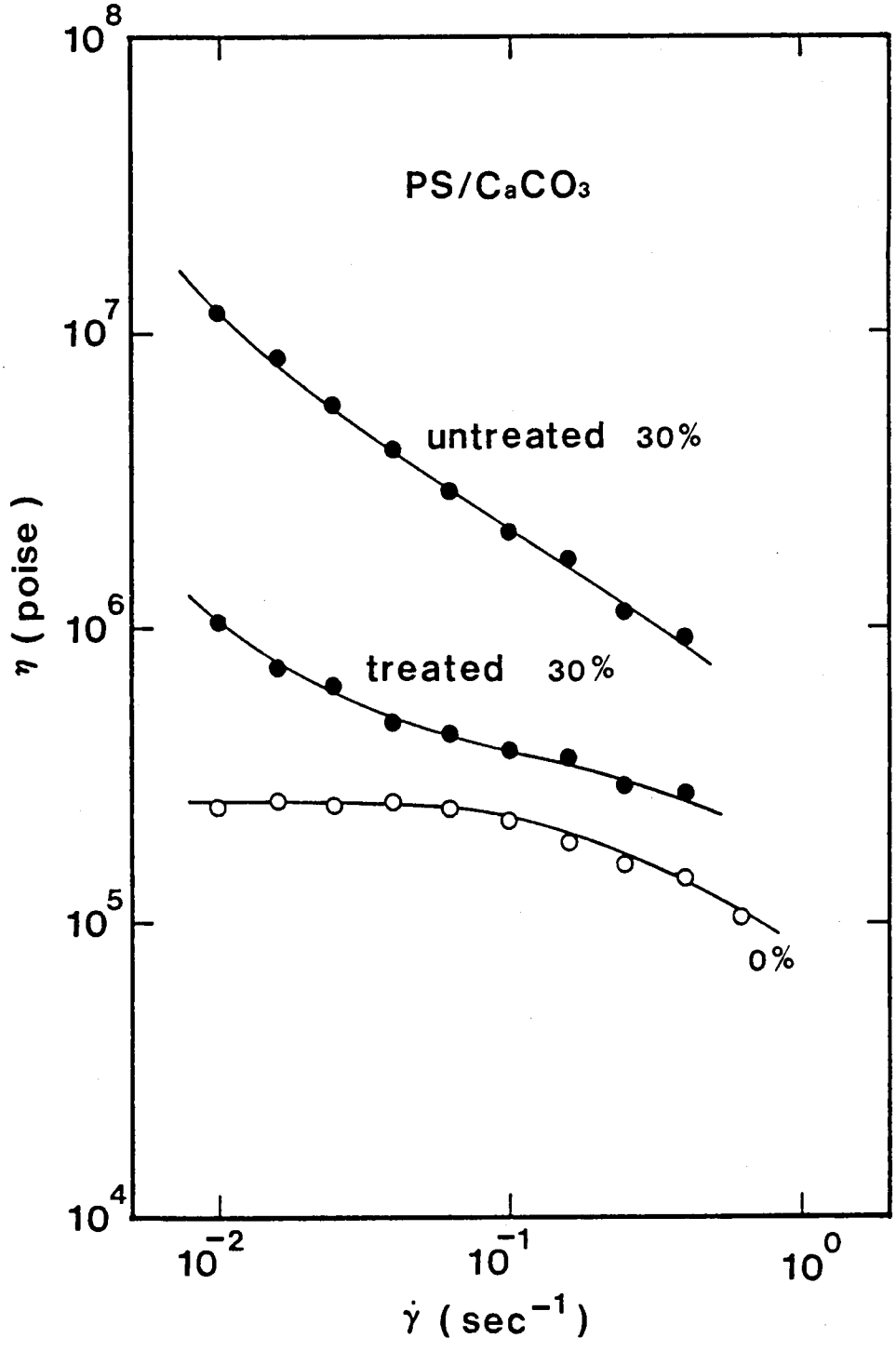

Figure V.3. Shear Viscosity as a Function of Shear Rate for $CaCO_3$-Filled PS Melts.

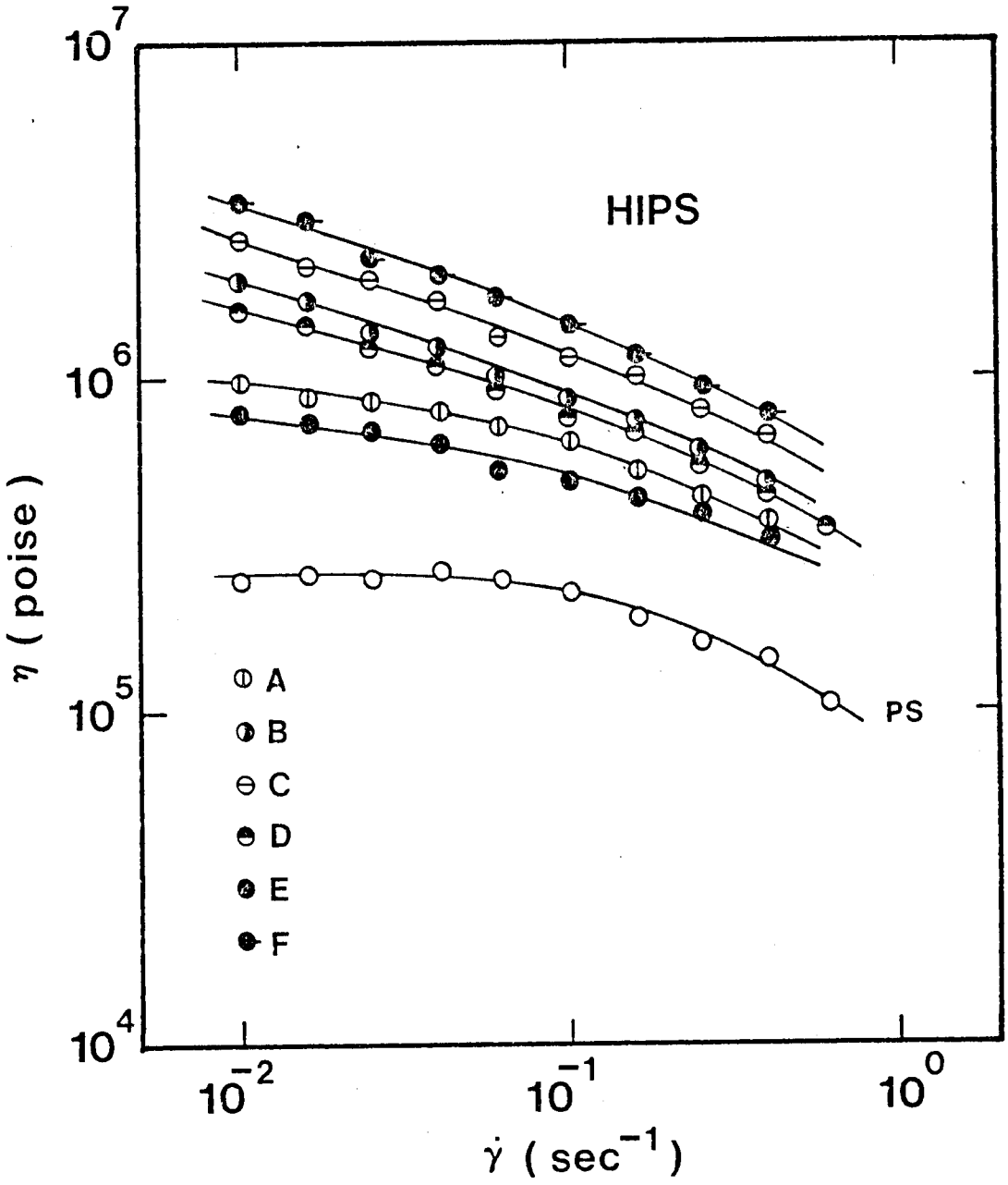

Figure V.4. Shear Viscosity as a Function of Shear Rate for HIPS Melts.

A.1.3. High Density Polyethylene (HDPE)-PS Blend Polymer Melts

Figure V.5 represents the shear viscosity as a function of the shear rate for HDPE-PS blend polymer melts. This system shows a higher viscosity than PS and does not appear to exhibit a Newtonian viscosity.

A.2. Discussion

A.2.1. PS Melts Reinforced with Small Rigid Particles

The nature of the abnormal behavior at low shear rates for highly-filled systems may be made distinct in a plot against shear stress, as presented in Fig. V.6 to Fig. V.8. At high loading levels, the shear viscosity goes to infinity at certain shear stress levels, that is, it exhibits a yield value. Yield values in TiO_2-filled melts have been observed by Minagawa and White (151) and in CB-filled melts by Zakharenko et al. (229), Vinogradov et al. (213) and by Lobe and White (131).

From the above figures, we can discuss the effects of the particle characteristics used. First, comparing the shear viscosities of different systems at the same loading level and the shear rate, these increase in magnitude in the order of

$$CB \geq \text{untreated } CaCO_3 > TiO_2 > \text{treated } CaCO_3 .$$

This difference is considered to result from not only particle size and surface treatment, but other structural factors.

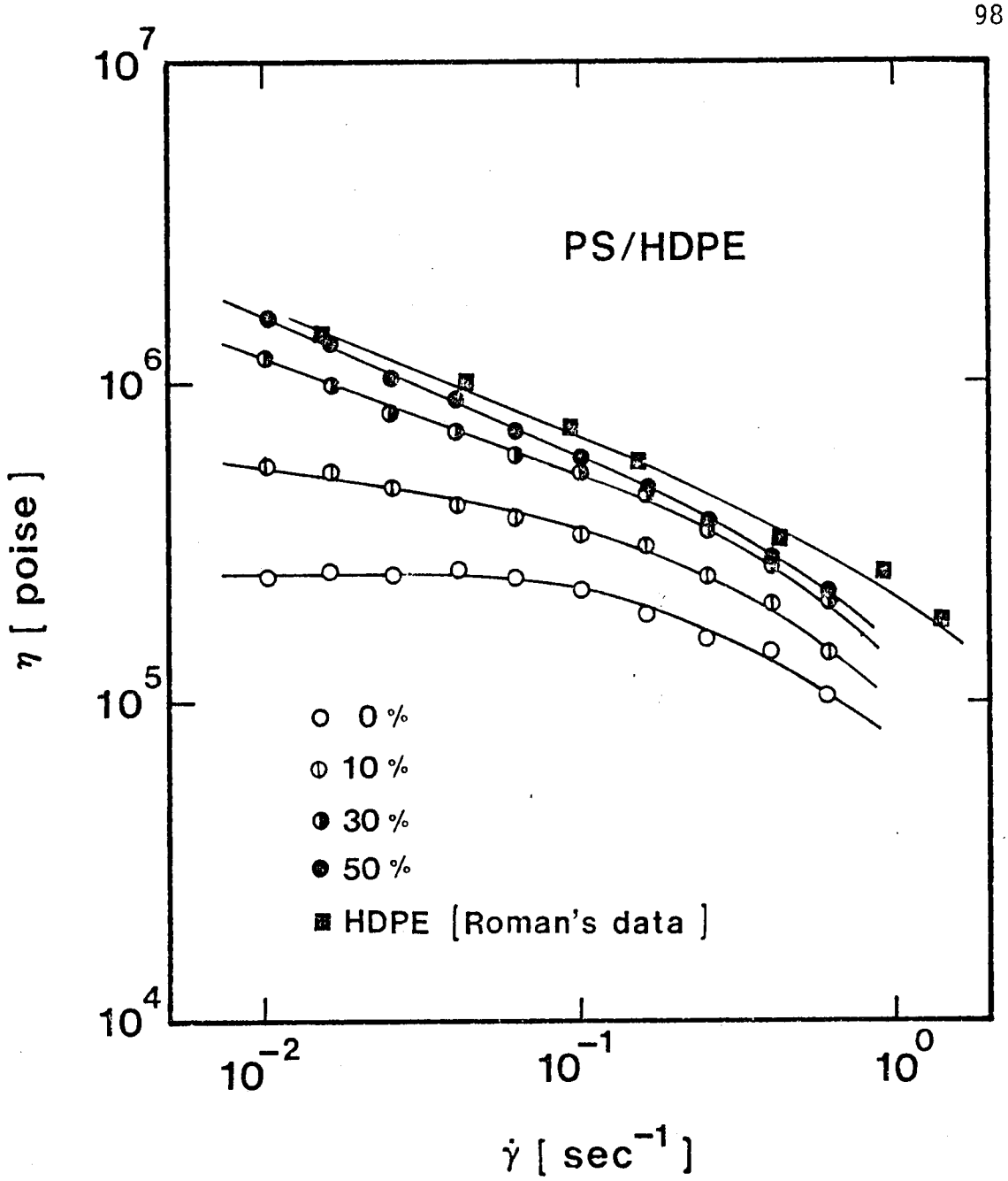

Figure V.5. Shear Viscosity as a Function of Shear Rate for HDPE/PS Melts.

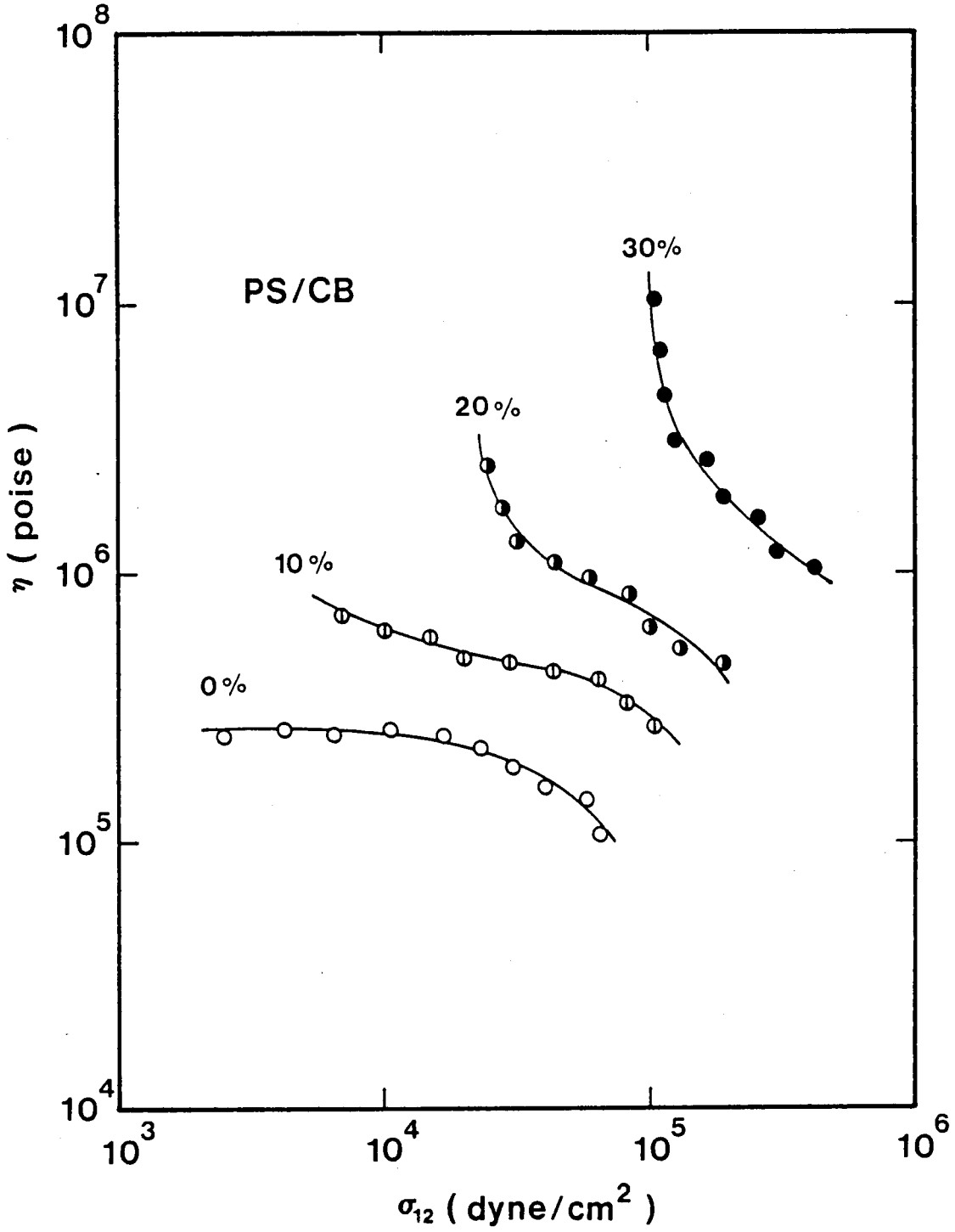

Figure V.6. Shear Viscosity as a Function of Shear Stress for CB-Filled PS Melts.

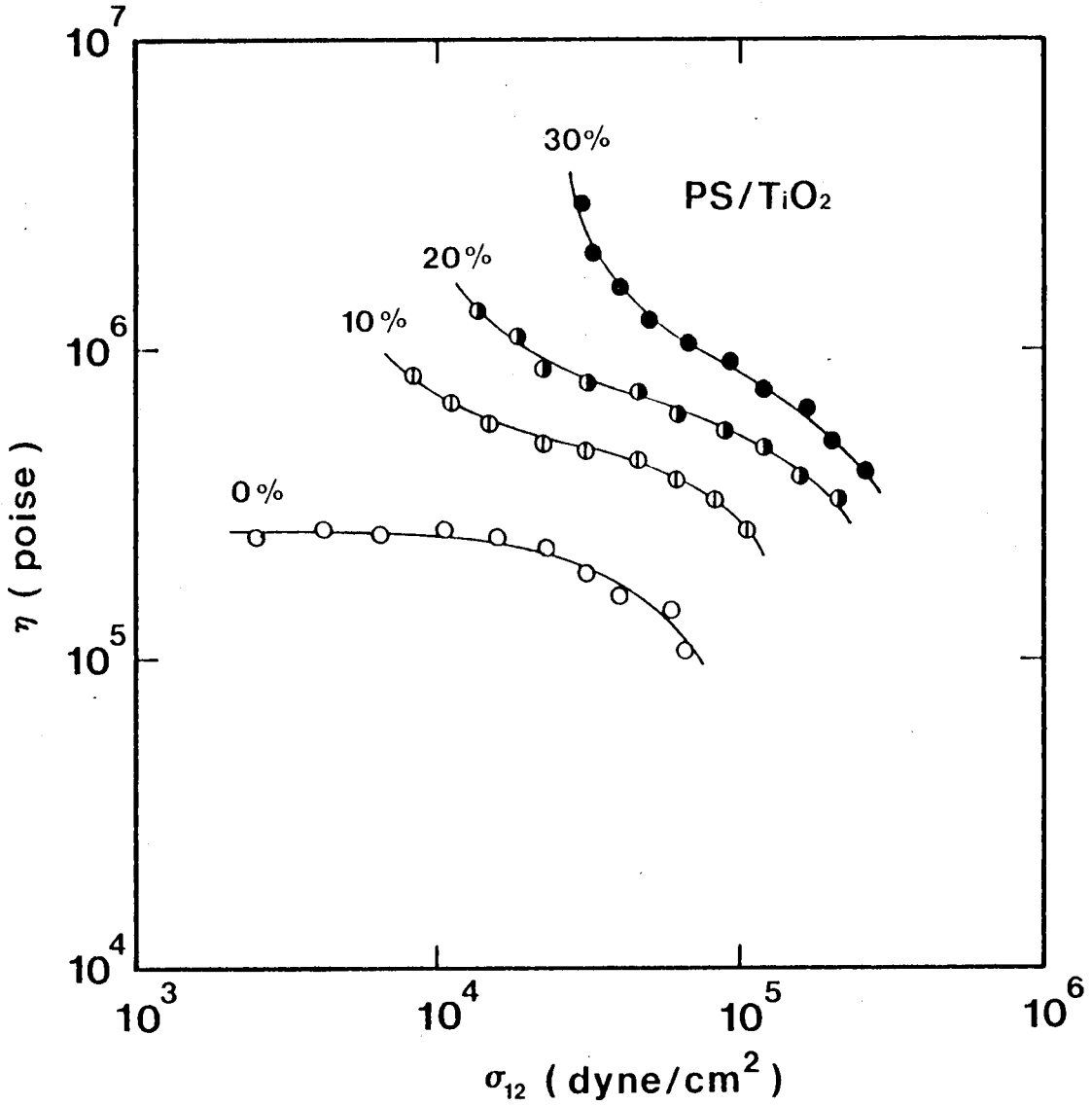

Figure V.7. Shear Viscosity as a Function of Shear Stress for TiO_2-Filled PS Melts.

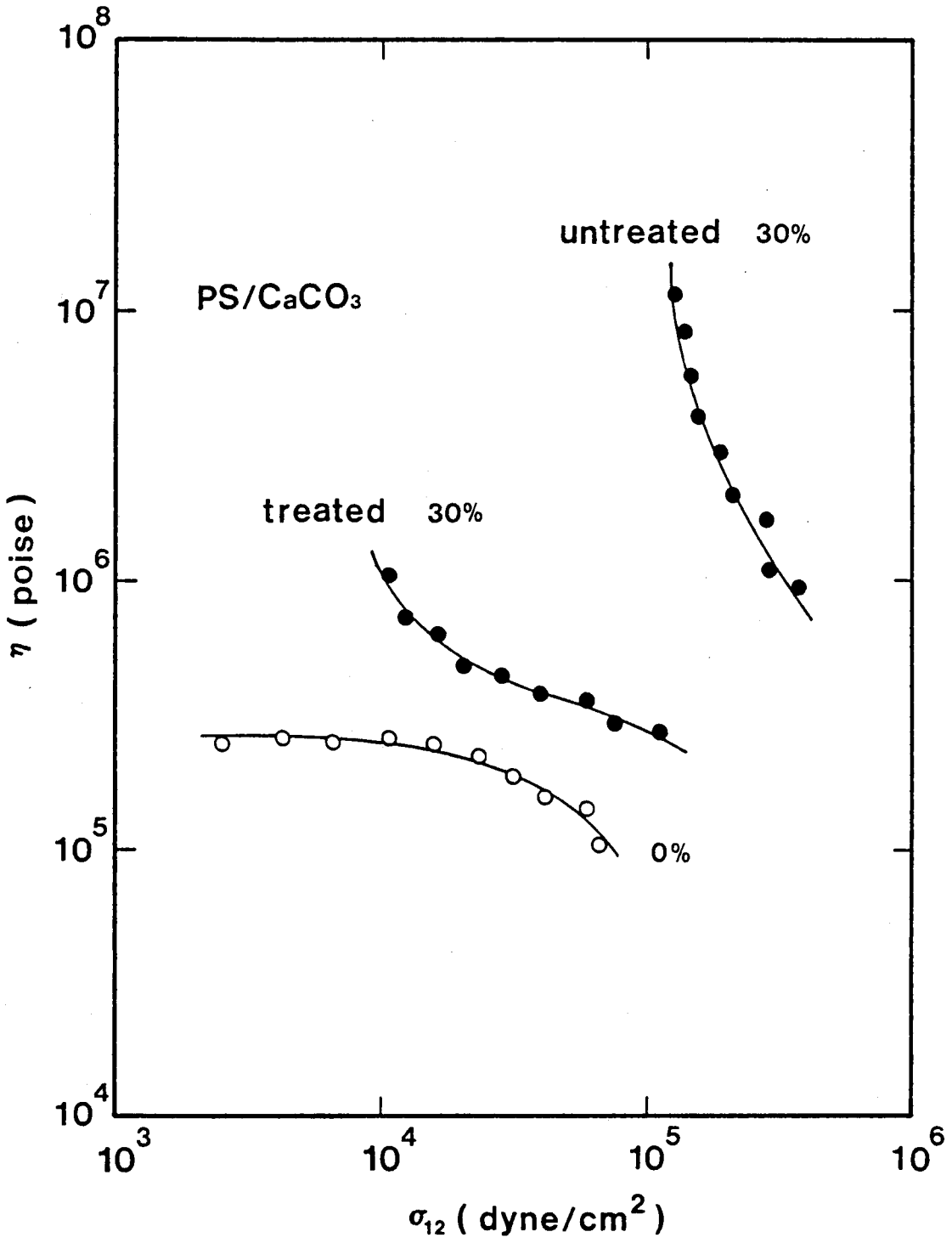

Figure V.8. Shear Viscosity as a Function of Shear Stress for $CaCO_3$-Filled PS Melts.

Comparison of the present data on CB-filled PS with those of Lobe and White (131) enables us to argue the effect of the particle size. We may conclude that the smaller the size, the higher the viscosity and smaller particles give higher yield stresses.

Figure V.3 (p. 95) and Fig. V.8 show that loading level increases yield stress as well as viscosity. These effects of particle characteristics on the shear viscosity and yield stress are exactly identical to those described in Chapter II.

The low shear rate behavior of the viscosity in the systems studied seems largely interpretable in terms of the formation of gel structures characterized by a yield value determined by three factors: loading, particle size and surface character. Other factors such as particle aspect ratio, occluded polymer, etc. have been discussed in the literature. We have not looked at a sufficiently broad range of systems here to check this.

A.2.2. HIPS Melts

Figure V.9 plots viscosity versus shear stress for HIPS melts. Trends to yield values cannot be observed there. These are presumably due to the large rubber particle size dispersed in the PS matrix ($4.5 \sim 5\mu$), as indicated by Münstedt (157) (158) and perhaps rubber flexibility. The role of graft rubber is not known.

A.2.3. HDPE-PS Blend Polymer Melts

Figure V.10 shows the shear viscosity as a function of the shear stress for HDPE-PS blends. Values for pure HDPE were measured by Roman

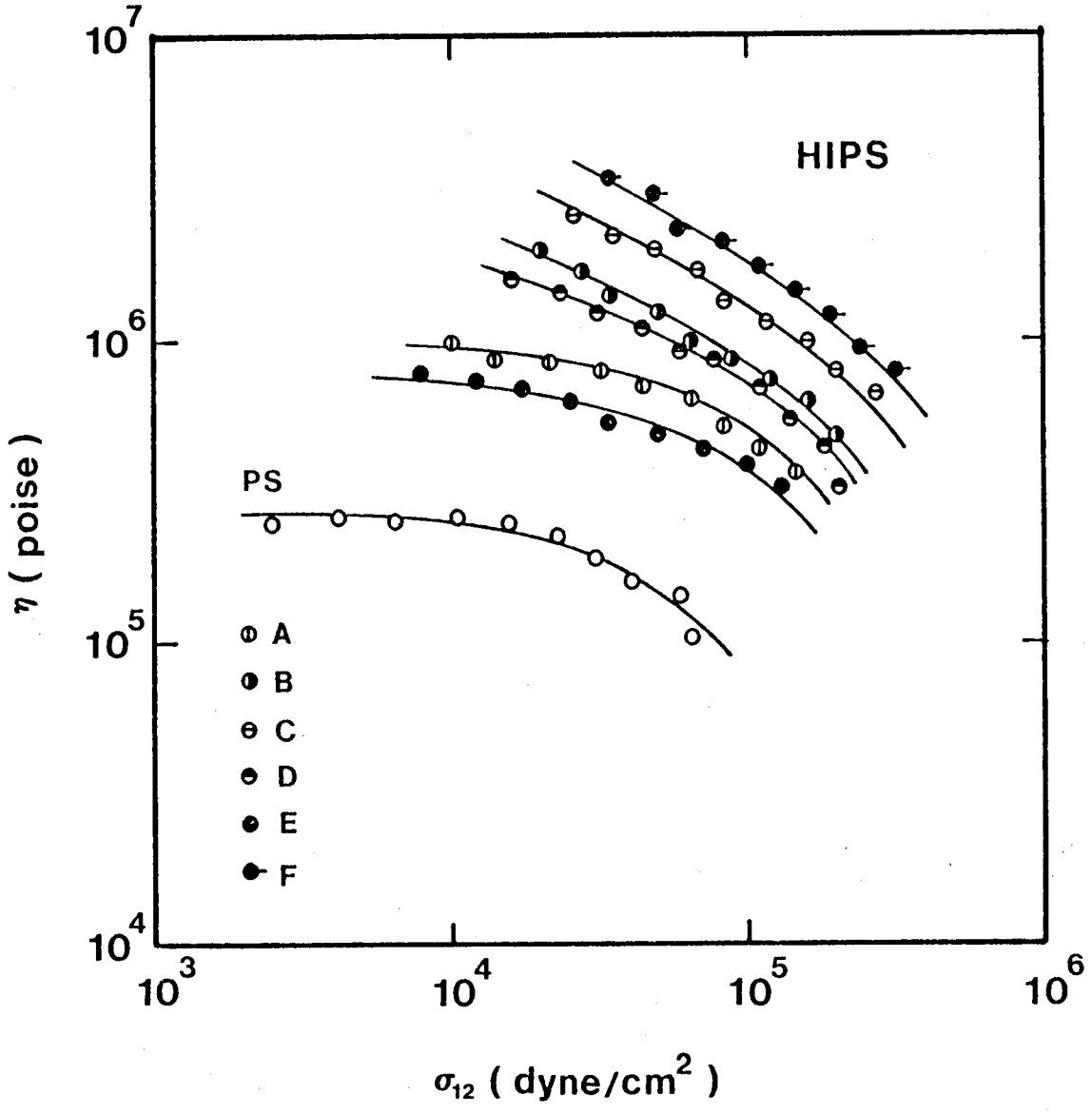

Figure V.9. Shear Viscosity as a Function of Shear Stress for HIPS Melts.

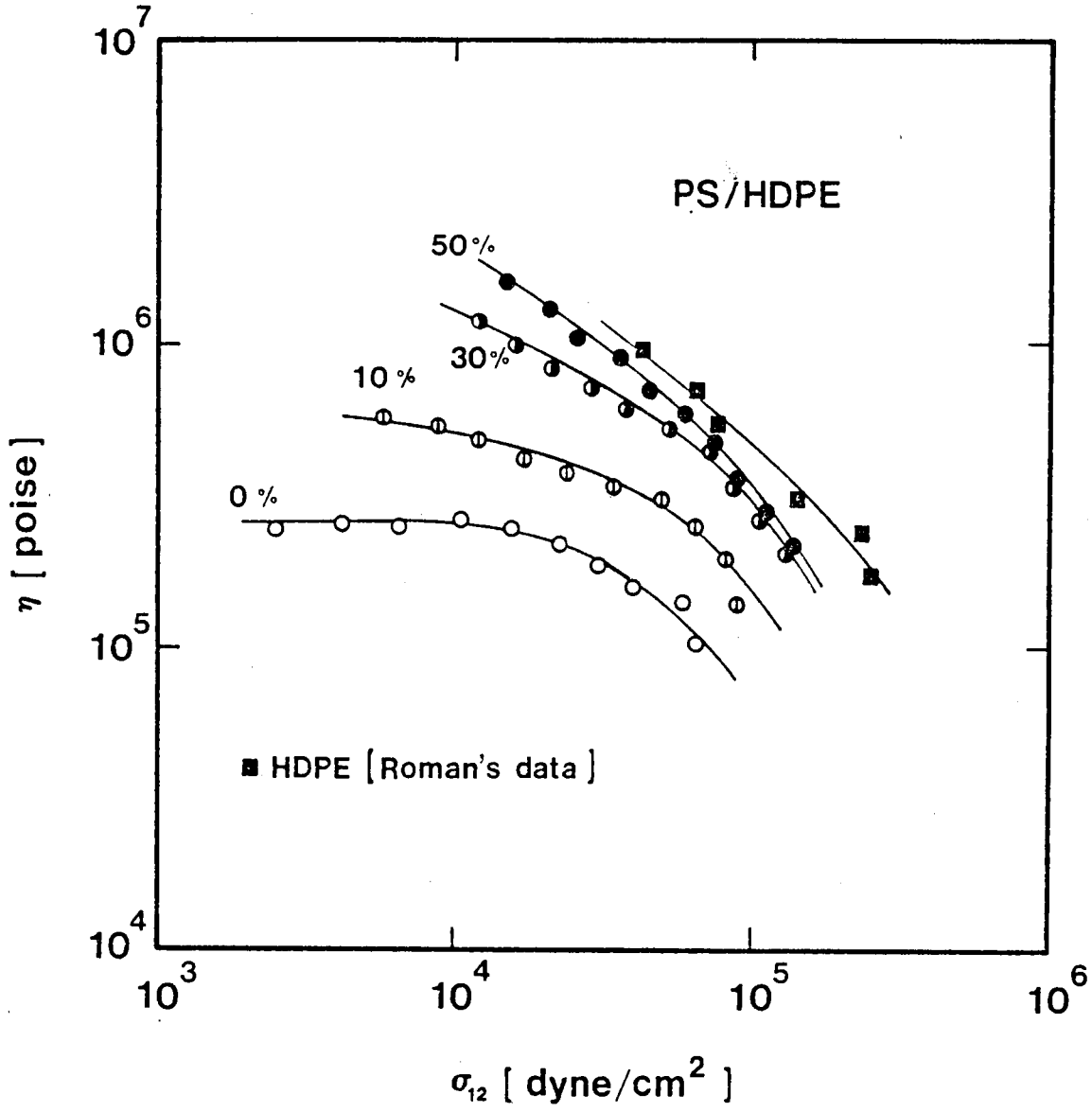

Figure V.10. Shear Viscosity as a Function of Shear Stress for HDPE/PS Melts.

(193) (222). This system tends not to show a Newtonian region. In the present work, the viscosity increases with loading level of HDPE. This composition dependence is similar to that by Lee and White (127).

B. First Normal Stress Difference

In this section, the first normal stress difference N_1 and the first normal stress difference coefficient Ψ_1 are discussed.

B.1. Results

B.1.1. PS Melts Reinforced with Small Rigid Particles

Figures V.11 to V.13 represent the plot of the first normal stress difference against the shear rate. Except for the surface treated $CaCO_3$, it is found to be raised with loading level at low shear rates but to approach to the value of PS melts at high shear rate limit.

The first normal stress difference is plotted against the shear stress in Fig. V.14 to Fig. V.16. Loading of small rigid particles decreases the normal stress at a fixed shear stress.

The first normal stress difference coefficient is plotted against the shear rate in Fig. V.17 to Fig. V.19. Very high values of Ψ_1 can be seen at low shear rates for highly-filled systems except for the surface treated $CaCO_3$. In the high shear rate region, there is no significant difference between loaded and unloaded systems.

B.1.2. HIPS Melts

The corresponding experimental data for HIPS melts are shown in Fig. V.20, Fig. V.21 and Fig. V.22. The first normal stress differences

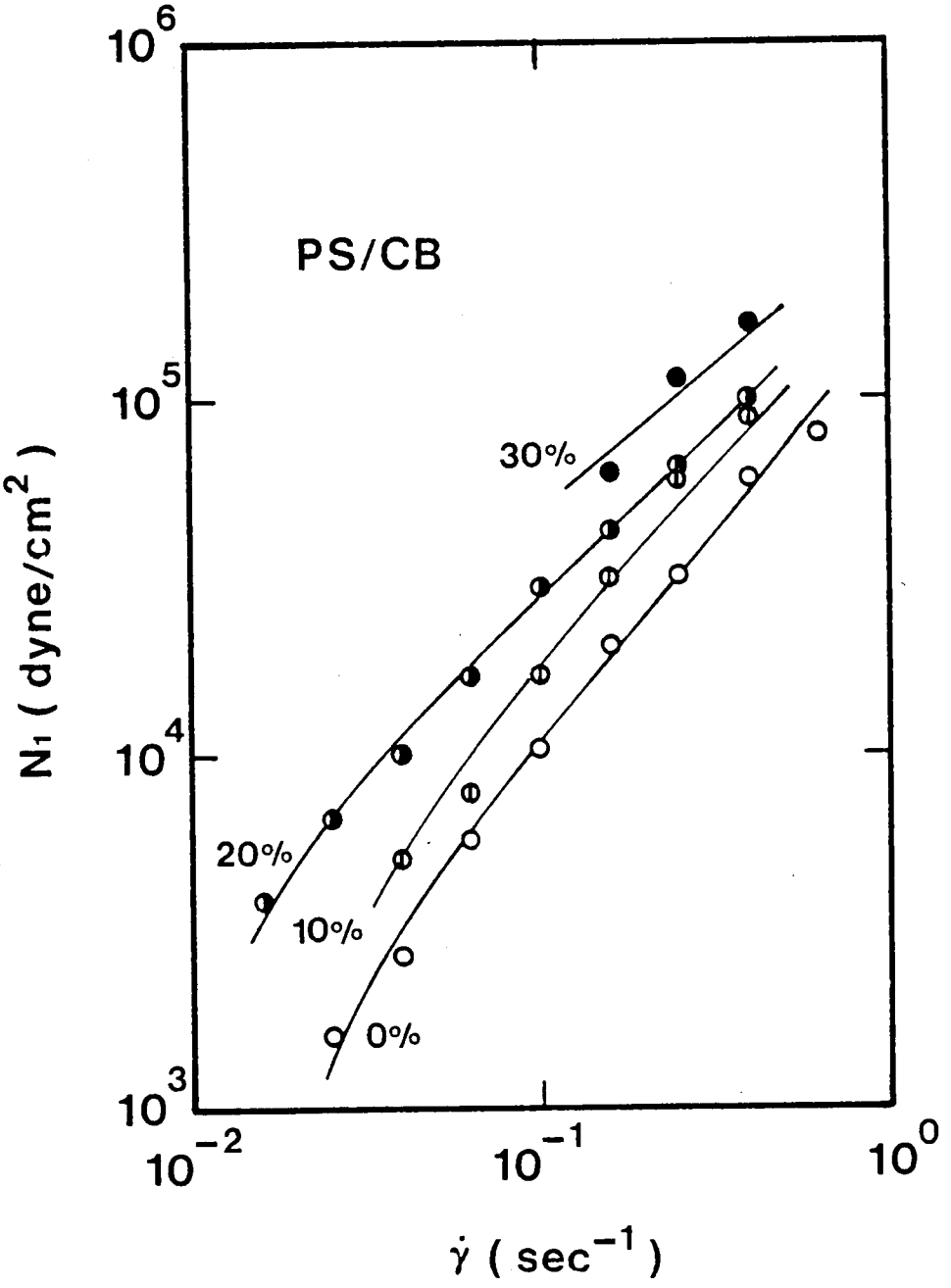

Figure V.11. First Normal Stress Difference as a Function of Shear Rate for CB-Filled PS Melts.

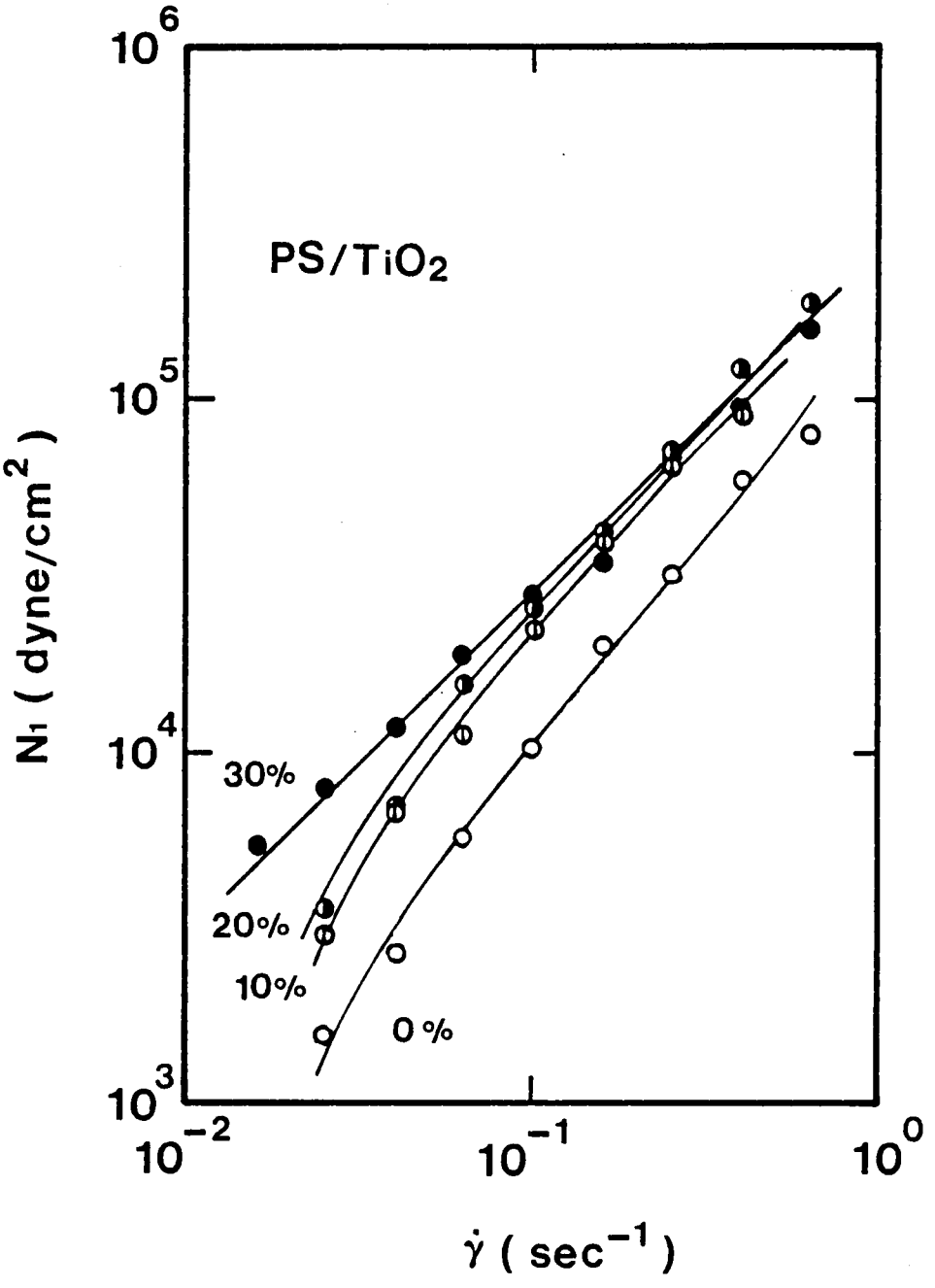

Figure V.12. First Normal Stress Difference as a Function of Shear Rate for TiO_2-Filled PS Melts.

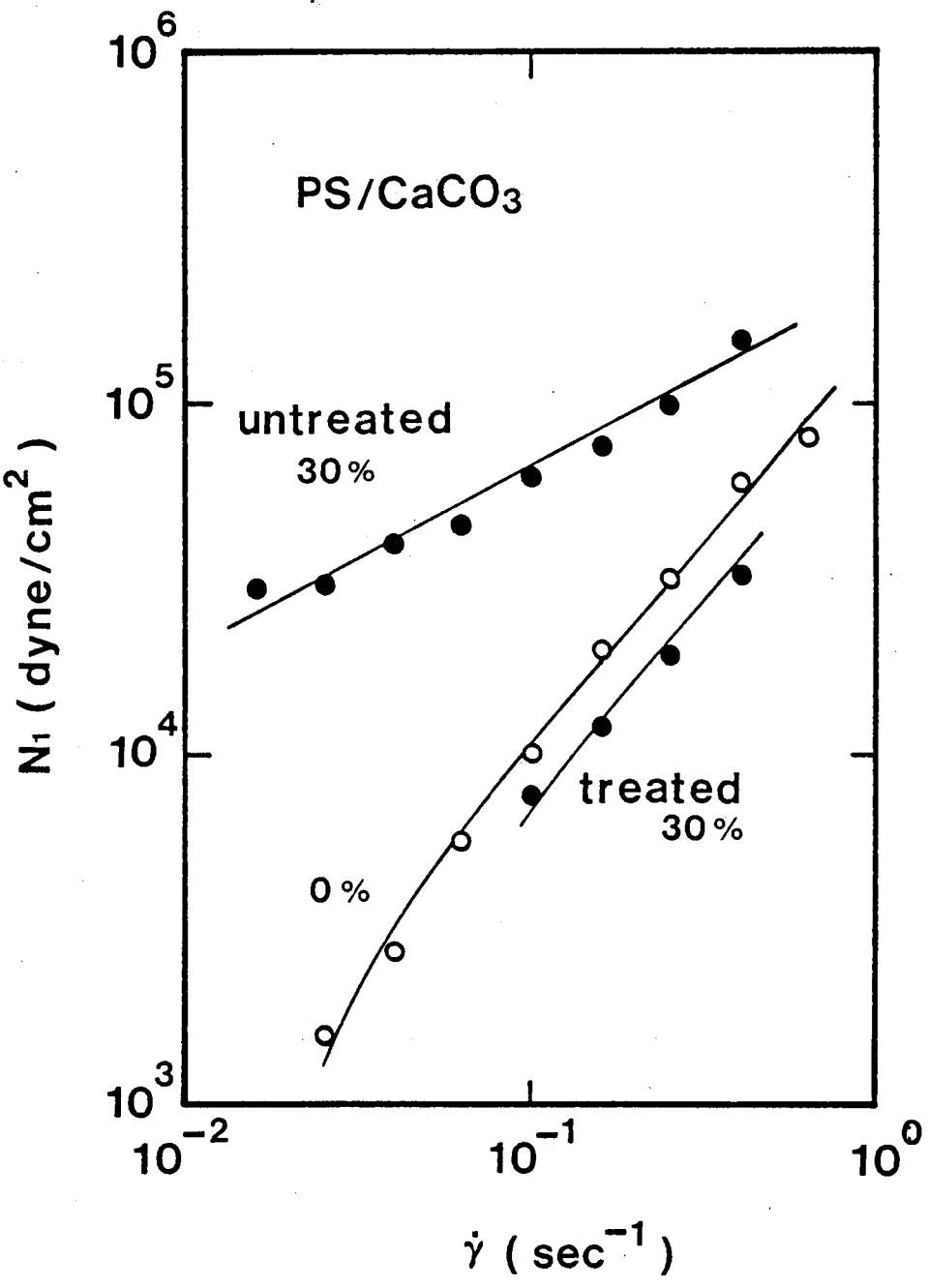

Figure V.13. First Normal Stress Difference as a Function of Shear Rate for $CaCO_3$-Filled PS Melts.

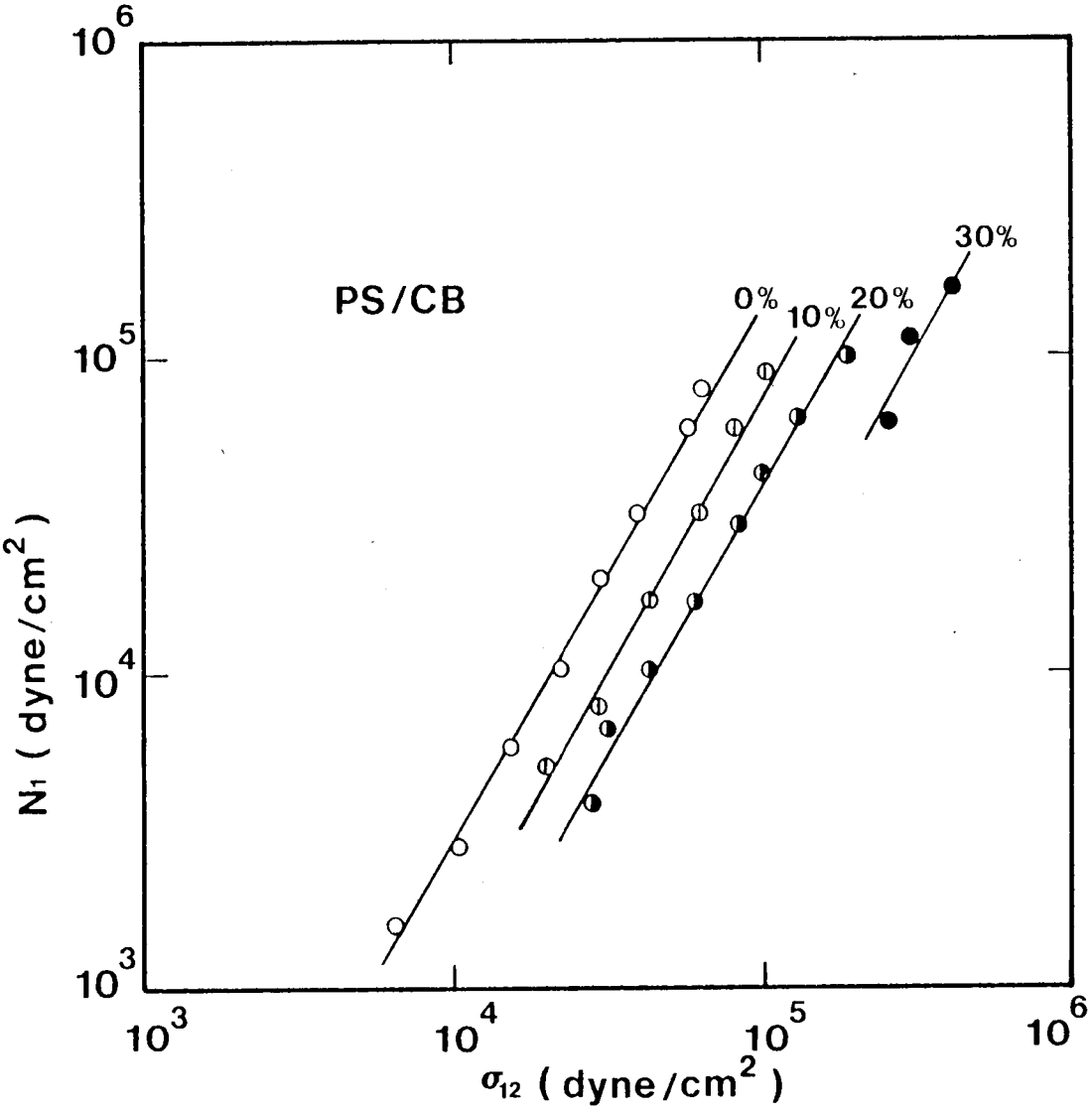

Figure V.14. First Normal Stress Difference as a Function of Shear Stress for CB-Filled PS Melts.

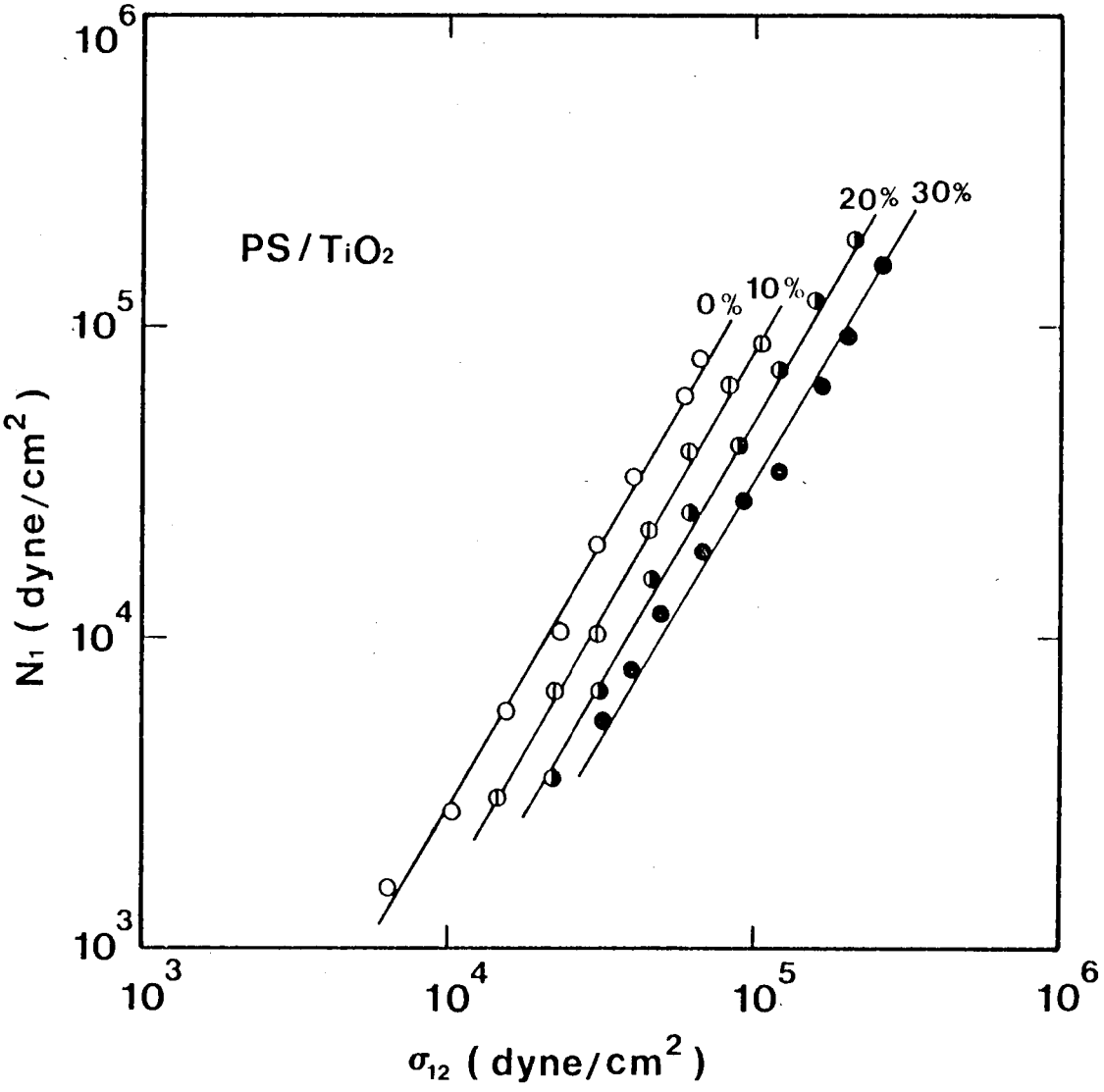

Figure V.15. First Normal Stress Difference as a Function of Shear Stress for TiO_2-Filled PS Melts.

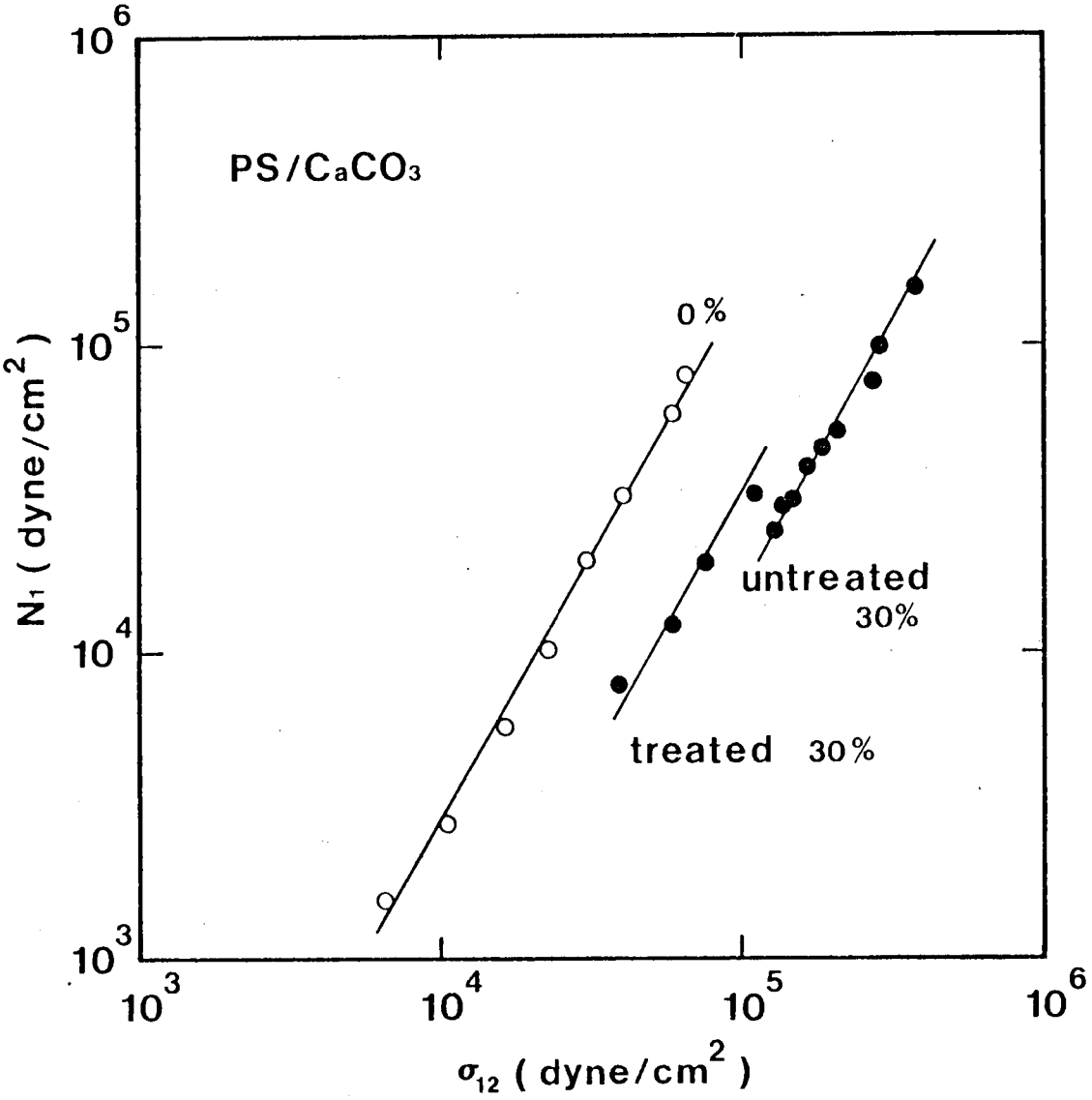

Figure V.16. First Normal Stress Difference as a Function of Shear Stress for $CaCO_3$-Filled PS Melts.

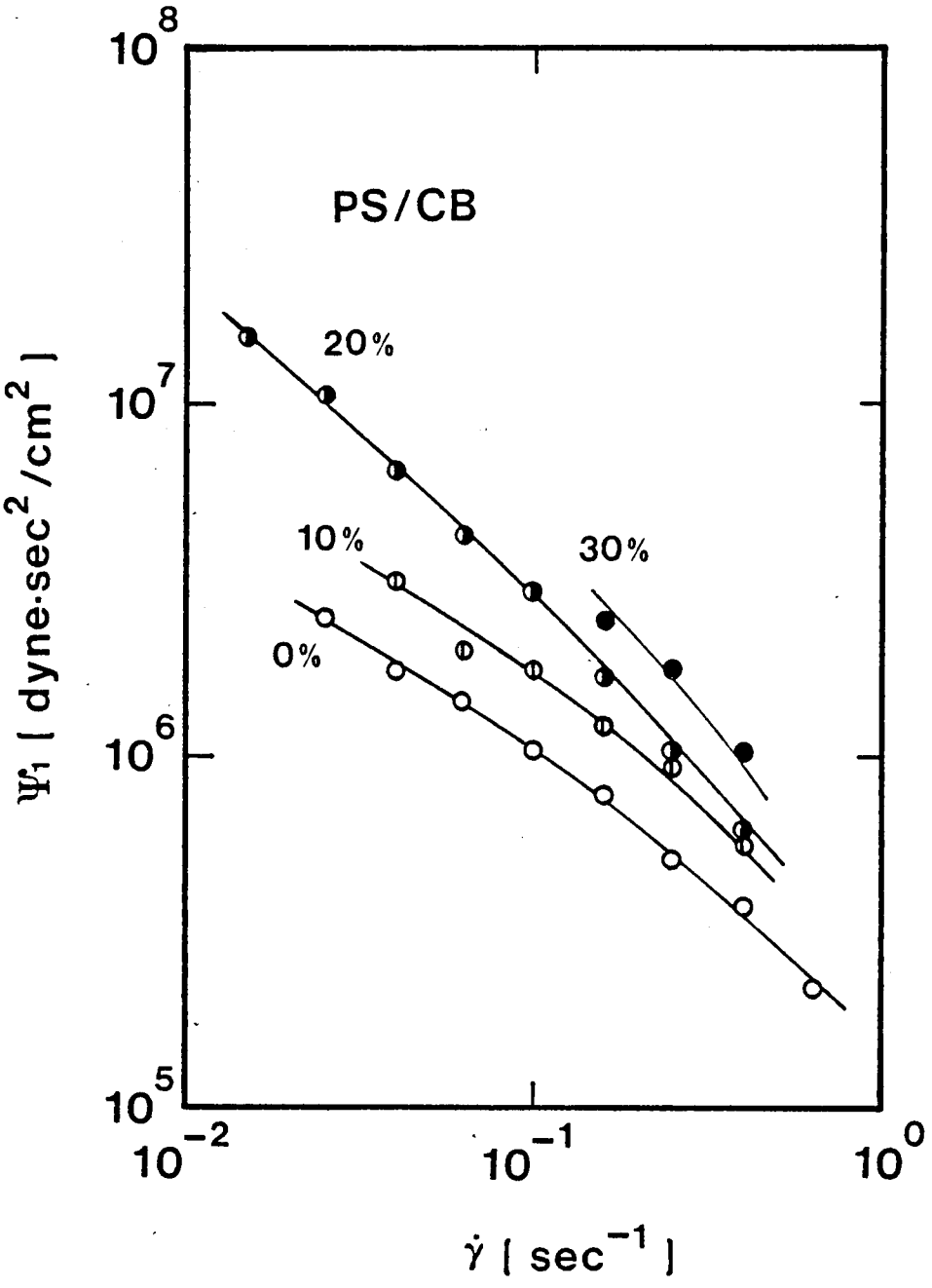

Figure V.17. First Normal Stress Difference Coefficient as a Function of Shear Rate for CB-Filled PS Melts.

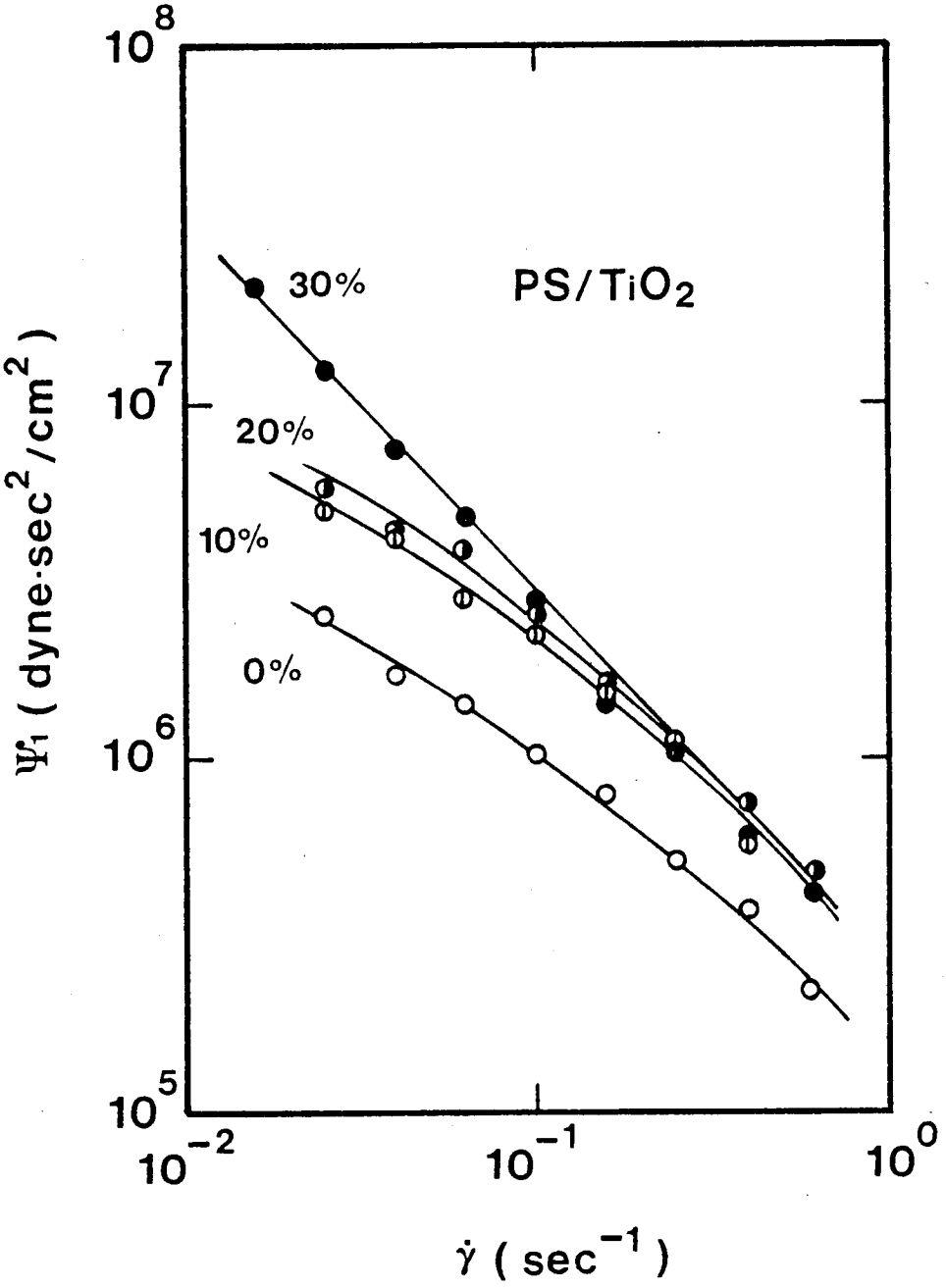

Figure V.18. First Normal Stress Difference Coefficient as a Function of Shear Rate for TiO_2-Filled PS Melts.

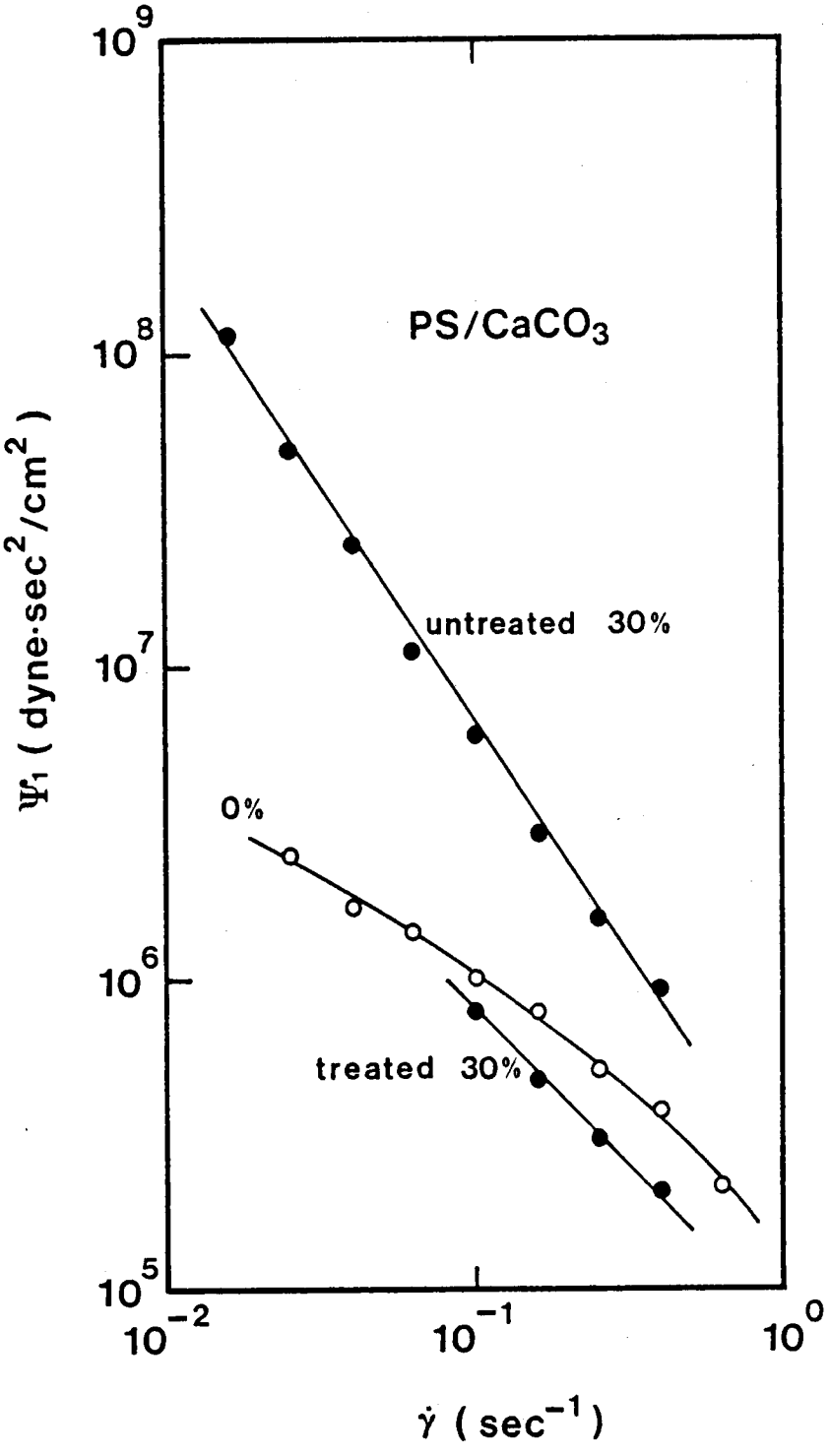

Figure V.19. First Normal Stress Difference Coefficient as a Function of Shear Rate for $CaCO_3$-Filled PS Melts.

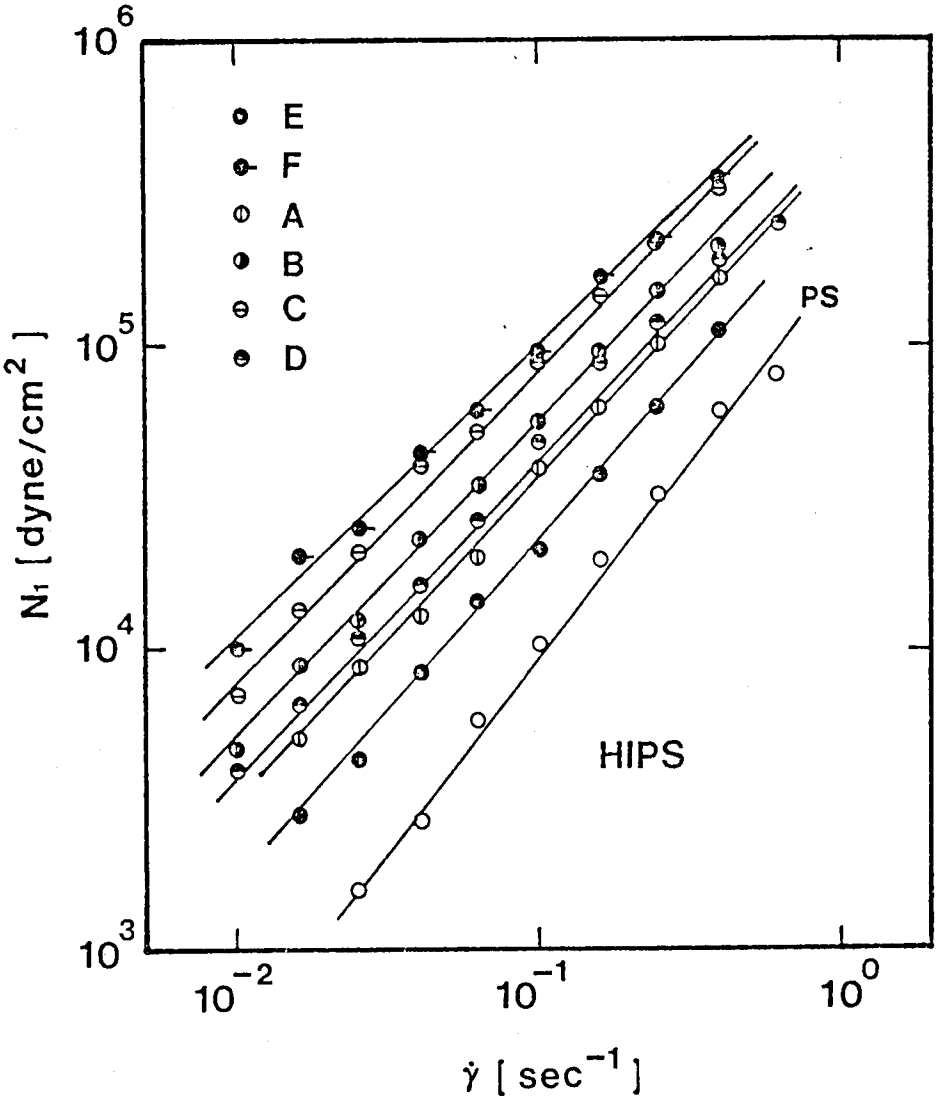

Figure V.20. First Normal Stress Difference as a Function of Shear Rate for HIPS Melts.

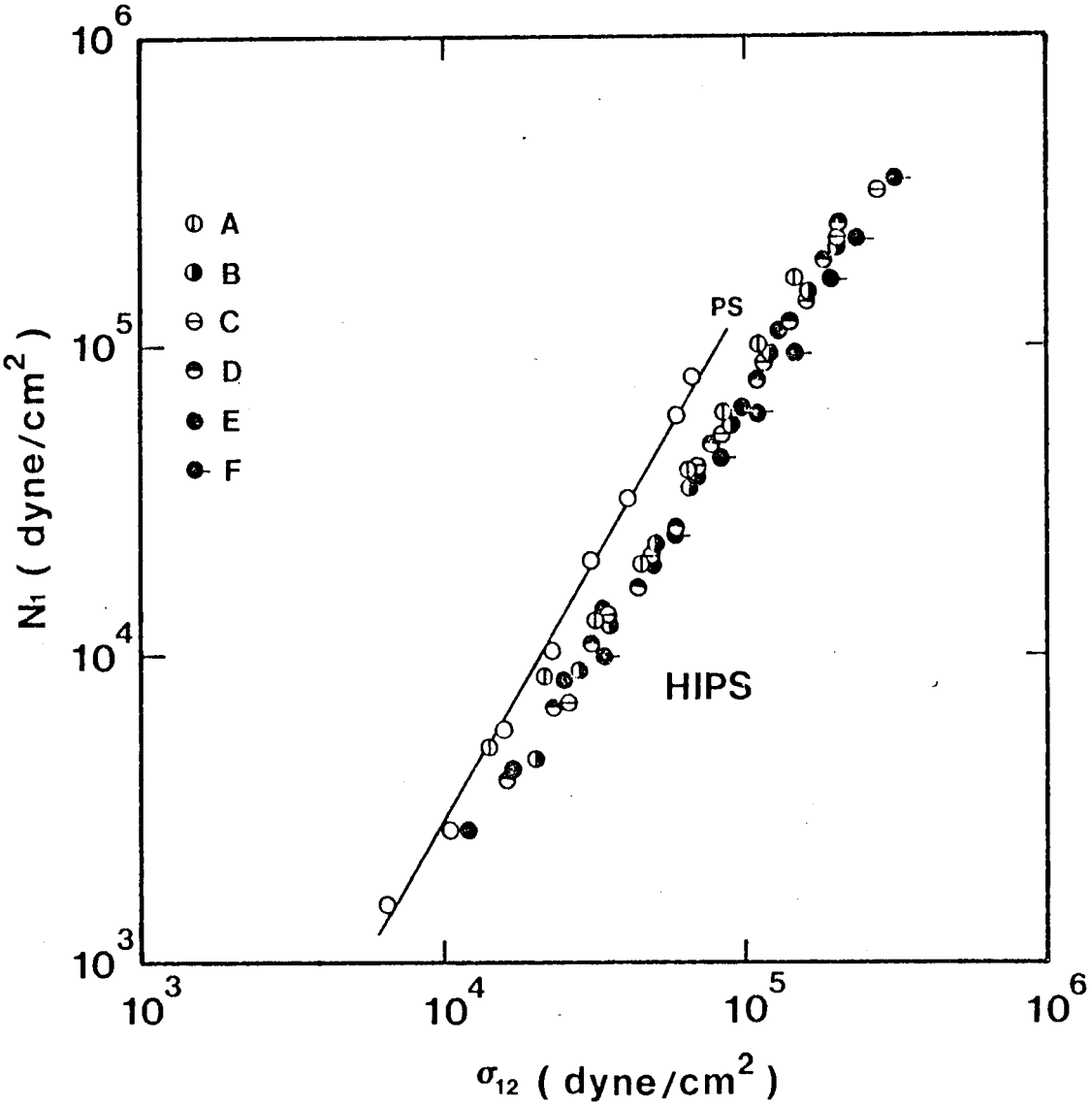

Figure V.21. First Normal Stress Difference as a Function of Shear Stress for HIPS Melts.

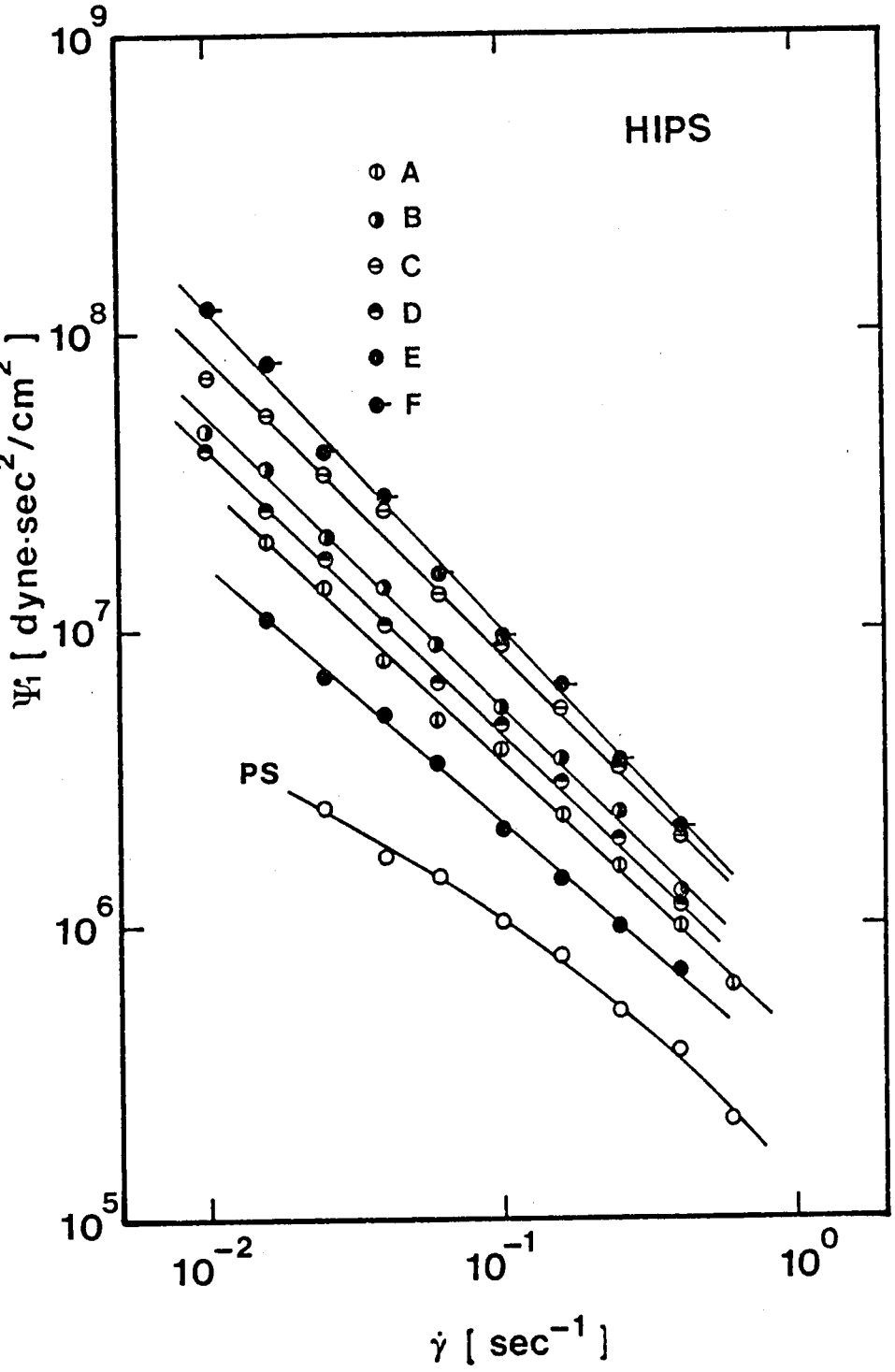

Figure V.22. First Normal Stress Difference Coefficient as a Function of Shear Rate for HIPS Melts.

of HIPS melts are greater at a fixed shear rate, but smaller at a fixed shear stress than those of pure PS melts.

The first normal stress difference coefficient takes much higher values compared with PS melts.

B.1.3. HDPE-PS Blend Polymer Melts

Figure V.23 and Fig. V.24 represent the first normal stress difference plotted against the shear rate and the sheer stress, respectively. In the same figure, the values for pure HDPE by Minagawa and White (151) are also plotted. In the present system, N_1 increases with volume fraction of HDPE.

The first normal stress difference coefficient is plotted as a function of the shear rate in Fig. V.25. In the loading level studied, Ψ_1 is found to increase with it,

B.2. Discussion

As mentioned in Chapter II, there exists some difficulties in cone-and-plate rheometer measurement of materials having yield values (18) (97) (98) (131). This is due to the residual stress in the samples at the beginning of the measurement, which does not give a proper zero point, it is very difficult to measure the normal stress especially at low shear rates for highly-filled systems. This residual stress was found to be released by applying the shear force. Therefore, normal stress measurement at the conditions mentioned above was not possible.

As pointed out by Oda, White and Clark (167), the plot of the normal stress against the shear stress is more useful than that against

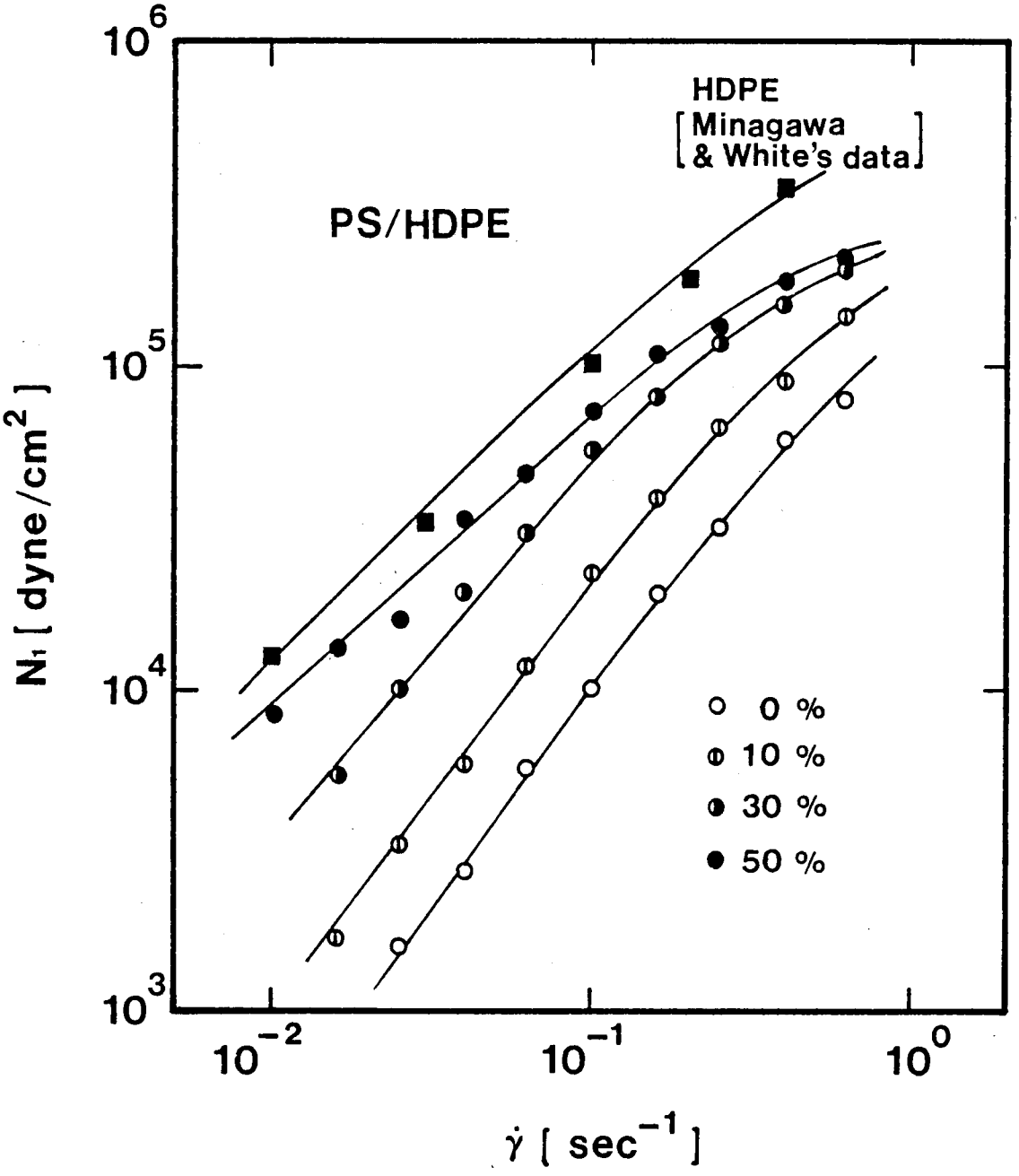

Figure V.23. First Normal Stress Difference as a Function of Shear Rate for HDPE/PS Melts.

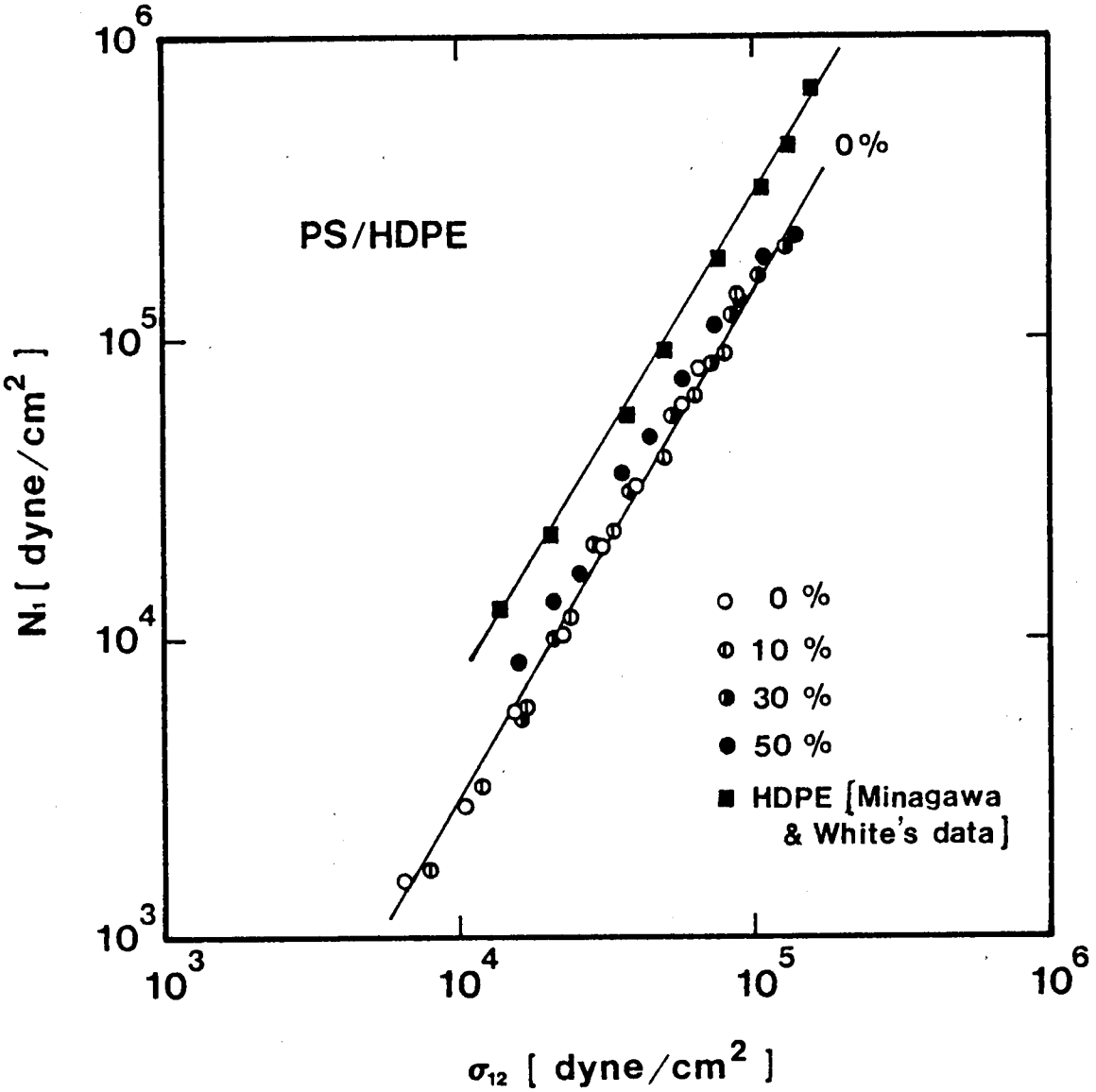

Figure V.24. First Normal Stress Difference as a Function of Shear Stress for HDPE/PS Melts.

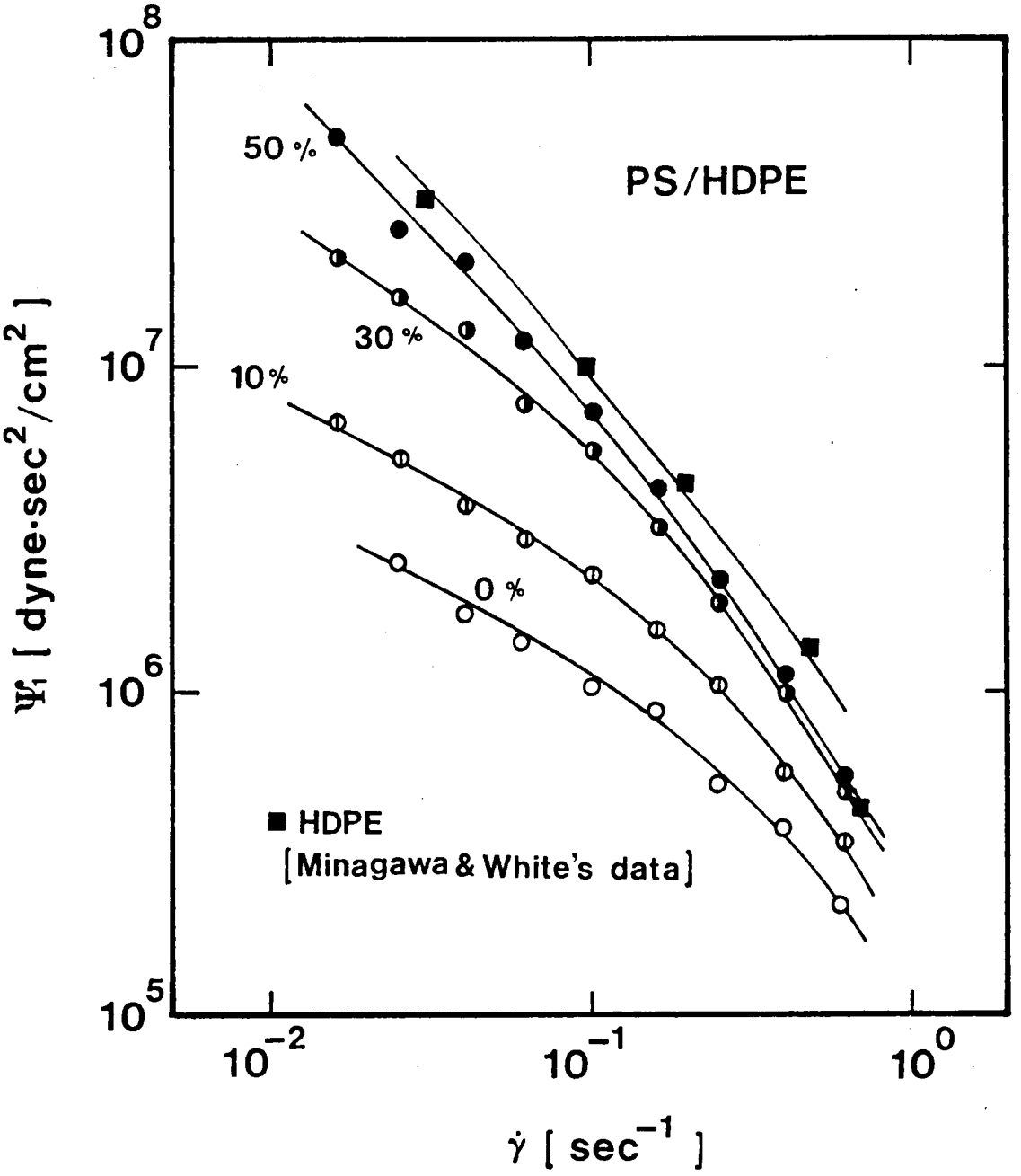

Figure V.25. First Normal Stress Difference Coefficient as a Function of Shear Rate for HDPE/PS Melts.

the shear rate. It is independent of temperature and molecular weight, but is dependent upon molecular weight distribution. They have reported that this plot could be interpreted in terms of steady state compliance. The usefulness of this plot has also been described by Han (76).

B.2.1. PS Melts Reinforced with Small Rigid Particles

As shown in Fig. V.14 to Fig. V.16 (pp. 109-111), normal stresses decrease with loading level. This is the same trend as observed by Lobe and White (131) and Han (75). In order to look at the effect of different particles, normal stresses as a function of shear stress are plotted at a constant loading level in Fig. V.26. N_1 decreases in magnitude in the order of

$$\text{treated } CaCO_3 \approx TiO_2 > \text{untreated } CaCO_3 \geq CB \ .$$

This is essentially the same order as increases in viscosity and yield values. Clearly increasing yield values may decrease normal stresses.

If the data of CB-filled PS melts is compared with those by Lobe and White (131), we can say that a smaller particle shows a lower normal stress. For unfilled melts extrudate swell from long die correlates with normal stresses. The particle size effect on normal stresses is similar to that observed by White and Crowder (219) who observed a similar trend for extrudate swell.

Figure V.16 (p. 111) shows that surface treatment for particles tends to slightly increase the normal stress. This is a similar result to the extrudate swell experiments on $CaCO_3$-filled polyvinylchloride reported by Zolotor (231).

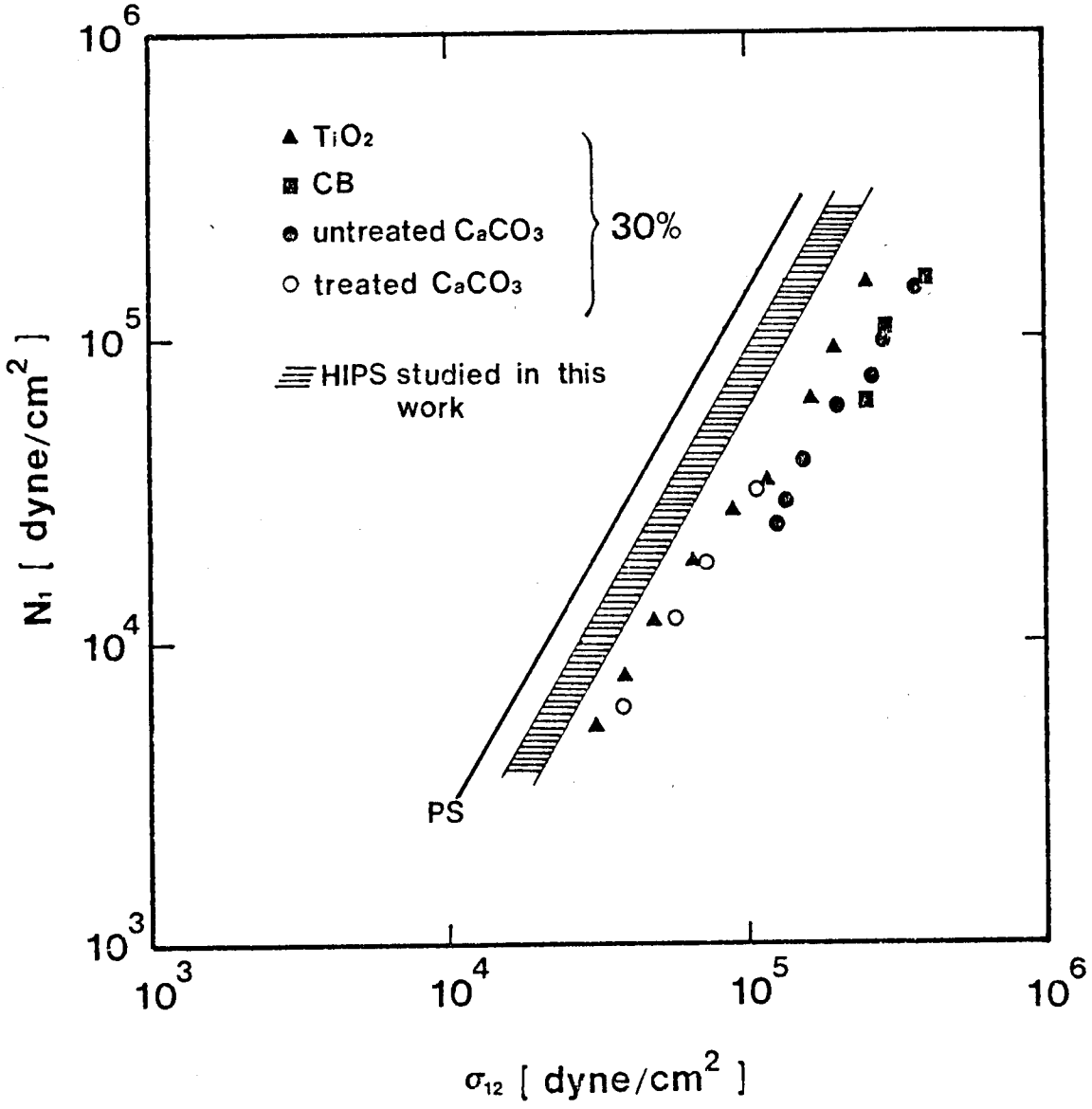

Figure V.26. First Normal Stress Difference as a Function of Shear Stress for Various Filled PS Melts at the Same Loading Level.

To make sure of the low shear limit behavior for Ψ_1 as well as the shear viscosity, the first normal stress difference coefficient was replotted against the shear stress in Fig. V.27 to Fig. V.29. These figures show the existence of yield values for highly-loaded systems.

B.2.2. HIPS Melts

It is evident from Fig. V.21 (p. 116) that HIPS melts show a reduced normal stress compared with PS, namely, rubber modification decreases elastic properties of polymer melts. This trend can be seen in the literature reported (34) (74) (157) (158).

Differences between effects of rubber and rigid particles on normal stresses can be recognized from Fig. V.26. HIPS exhibits higher values of N_1 compared to rigid particle-filled PS. For the systems studied in this work, the normal stress takes the following order in magnitude at the same loading level.

PS > HIPS > PS reinforced with small rigid particles

B.2.3. HDPE-PS Blend Polymer Melts

Figure V.24 (p. 120) reveals that blending of HDPE increases elastic properties of PS melts in the loading level studied in the present work. In order to obtain the complete composition dependence of N_1, we need more additional experiments.

As indicated by Han (78) (79), the viscoelastic properties of polymer blend melts depend on the type of morphology, i.e., the mode of dispersion.

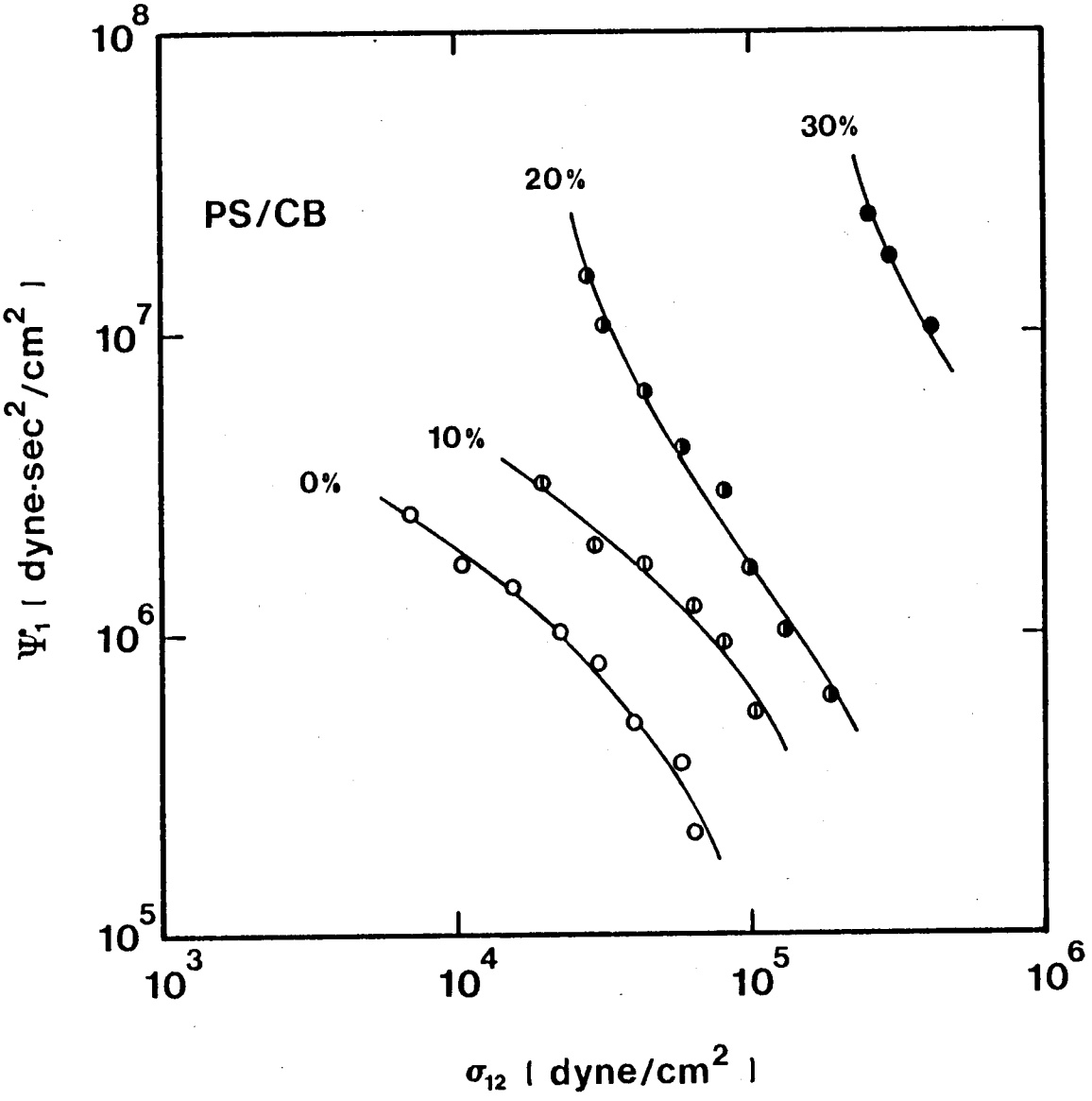

Figure V.27. First Normal Stress Difference Coefficient as a Function of Shear Stress for CB-Filled PS Melts.

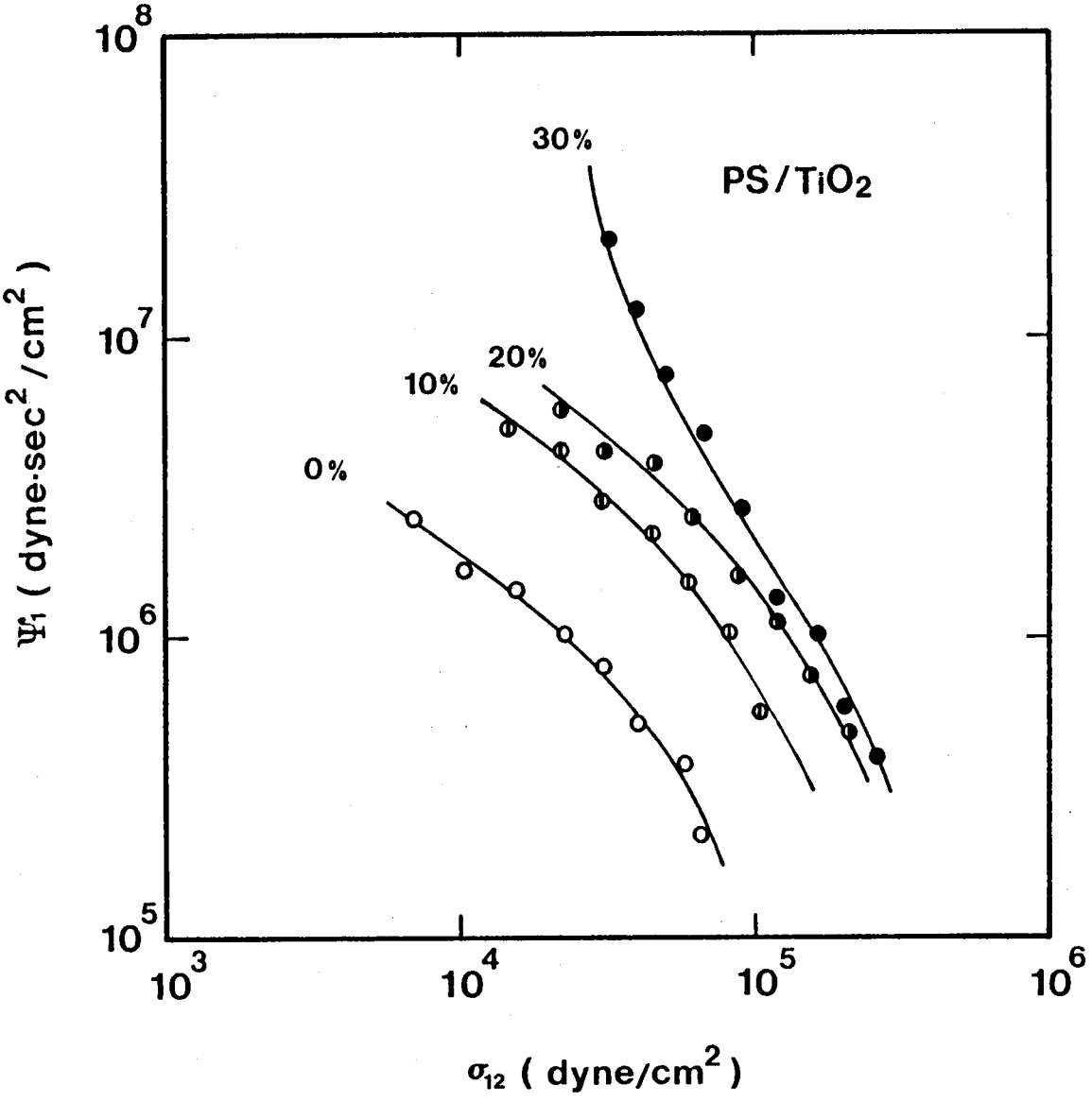

Figure V.28. First Normal Stress Difference Coefficient as a Function of Shear Stress for TiO_2-Filled PS Melts.

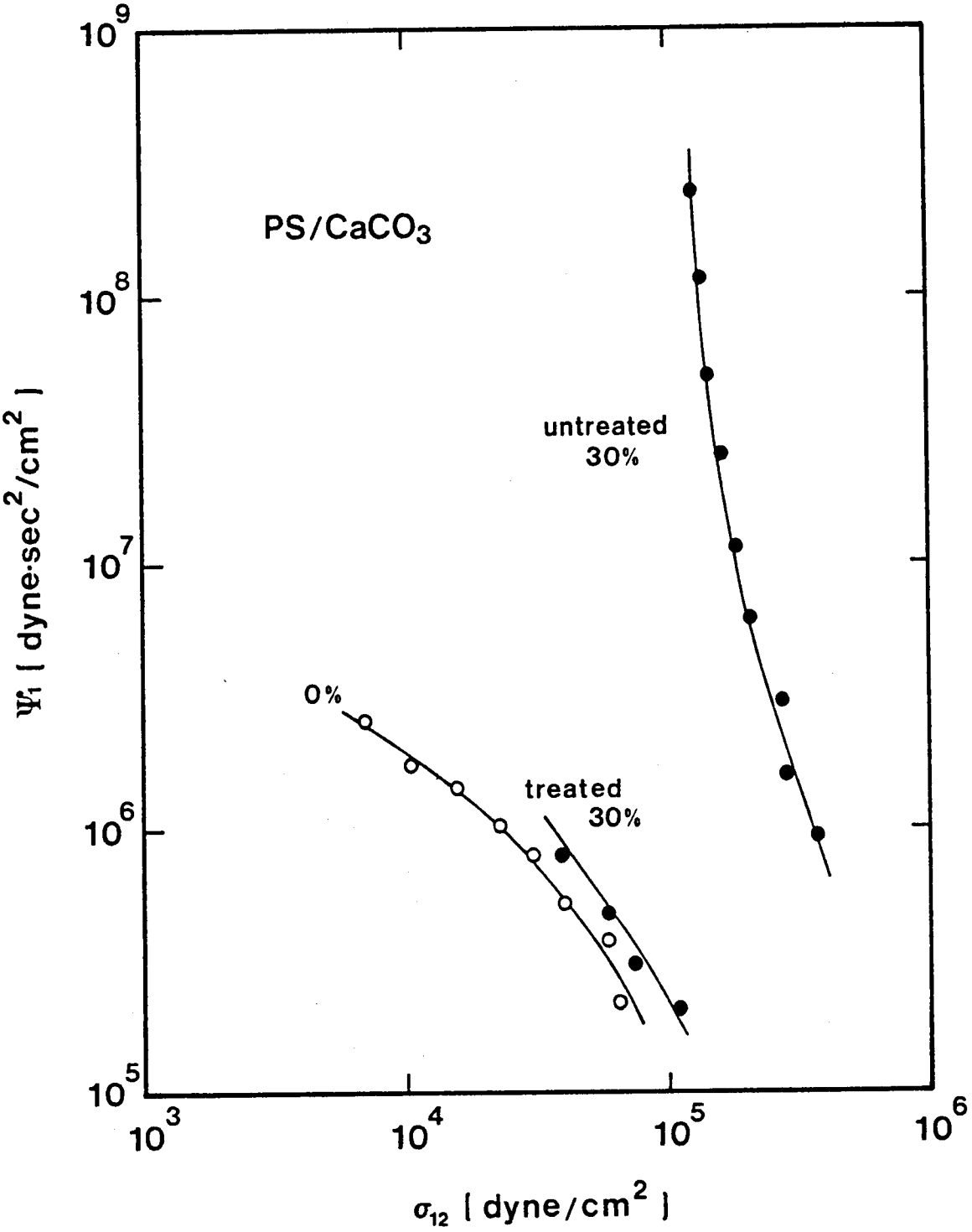

Figure V.29. First Normal Stress Difference Coefficient as a Function of Shear Stress for $CaCO_3$-Filled PS Melts.

CHAPTER VI

EXPERIMENTAL STUDIES ON ELONGATIONAL FLOW

The rheological responses of uniaxial elongational flow of filled polymer melts are presented in this chapter. The elongational viscosity χ and elongation to break L_B/L_0 are considered.

A. Transient Elongational Viscosity

A.1. Results

Figure VI.1 to Fig. VI.8 show the transient elongational viscosity, $\chi(\dot{E},t)$ for PS and small rigid particles-reinforced PS samples. $\chi(\dot{E},t)$ is found to increase to steady state value for all elongational rates measured. With the exception of the PS, the steady state values decrease with elongational rate.

$\chi(\dot{E},t)$ for HIPS samples is shown in Fig. VI.9 and Fig. VI.10. As seen in these figures, the steady state can be achieved.

Figure VI.11 shows $\chi(\dot{E},t)$ for 50% HDPE-blended PS melts. In this system, $\chi(\dot{E},t)$ increases very monotonically with time to steady state compared with other filled systems mentioned above.

A.2. Discussion

In pure PS, $\chi(\dot{E},t)$ increases to steady state values, almost equal to $3\eta_0$ at low elongational rates. At high $\dot{E}$, $\chi(\dot{E},t)$ increases very

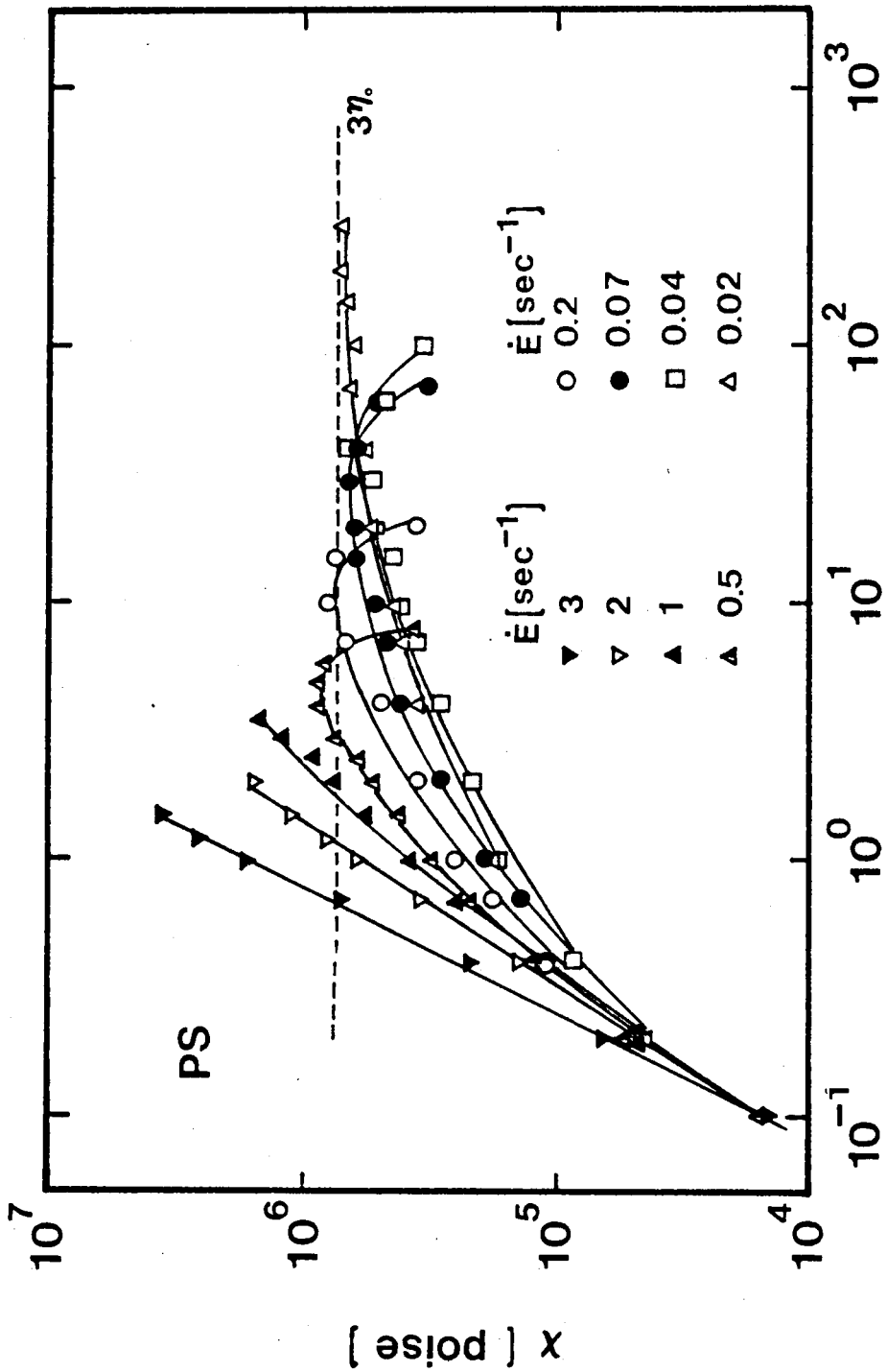

Figure VI.1. Transient Elongational Viscosity at Various Elongational Rates for PS Melt.

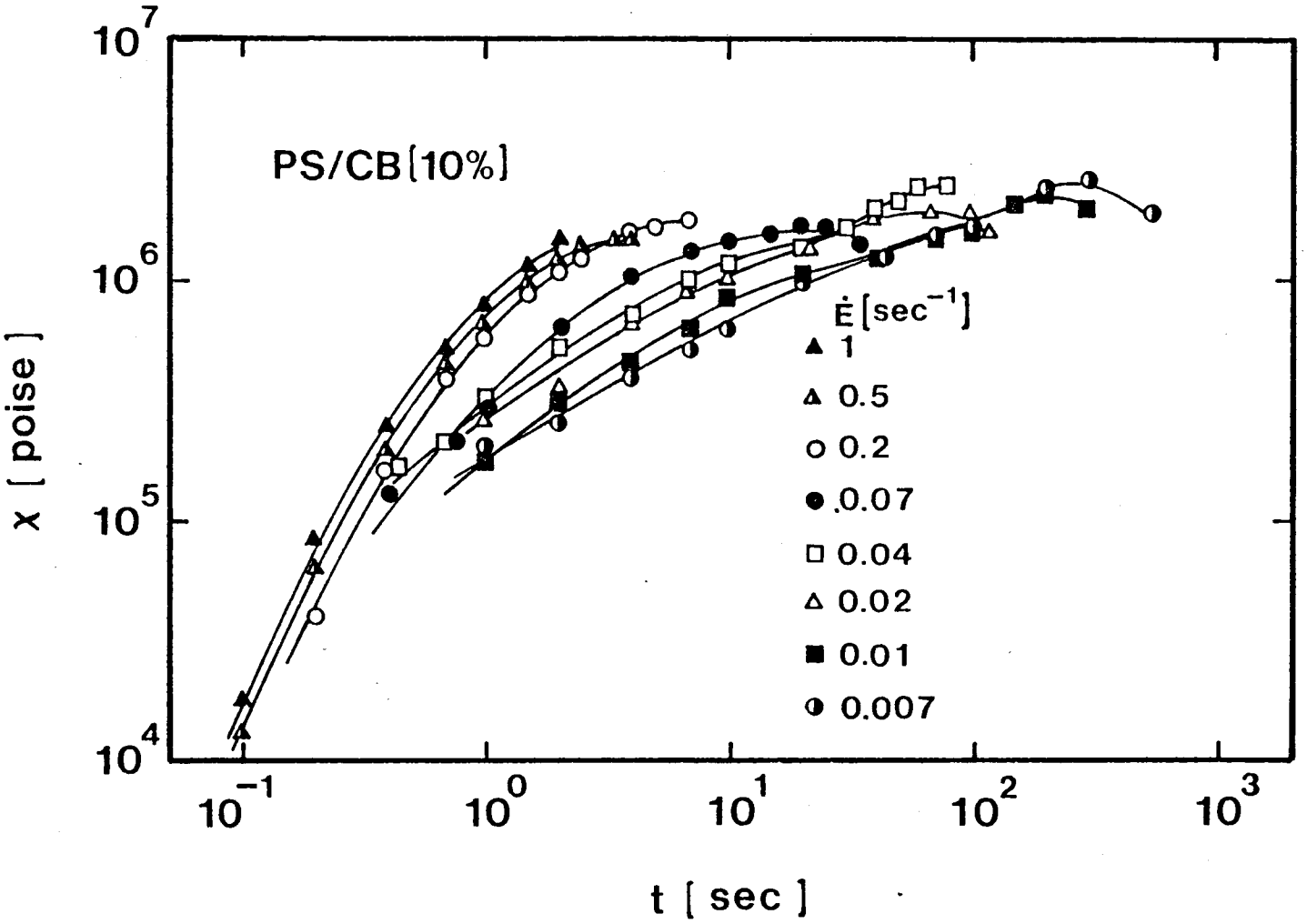

Figure VI.2. Transient Elongational Viscosity at Various Elongational Rates for 10% CB-Filled PS Melt.

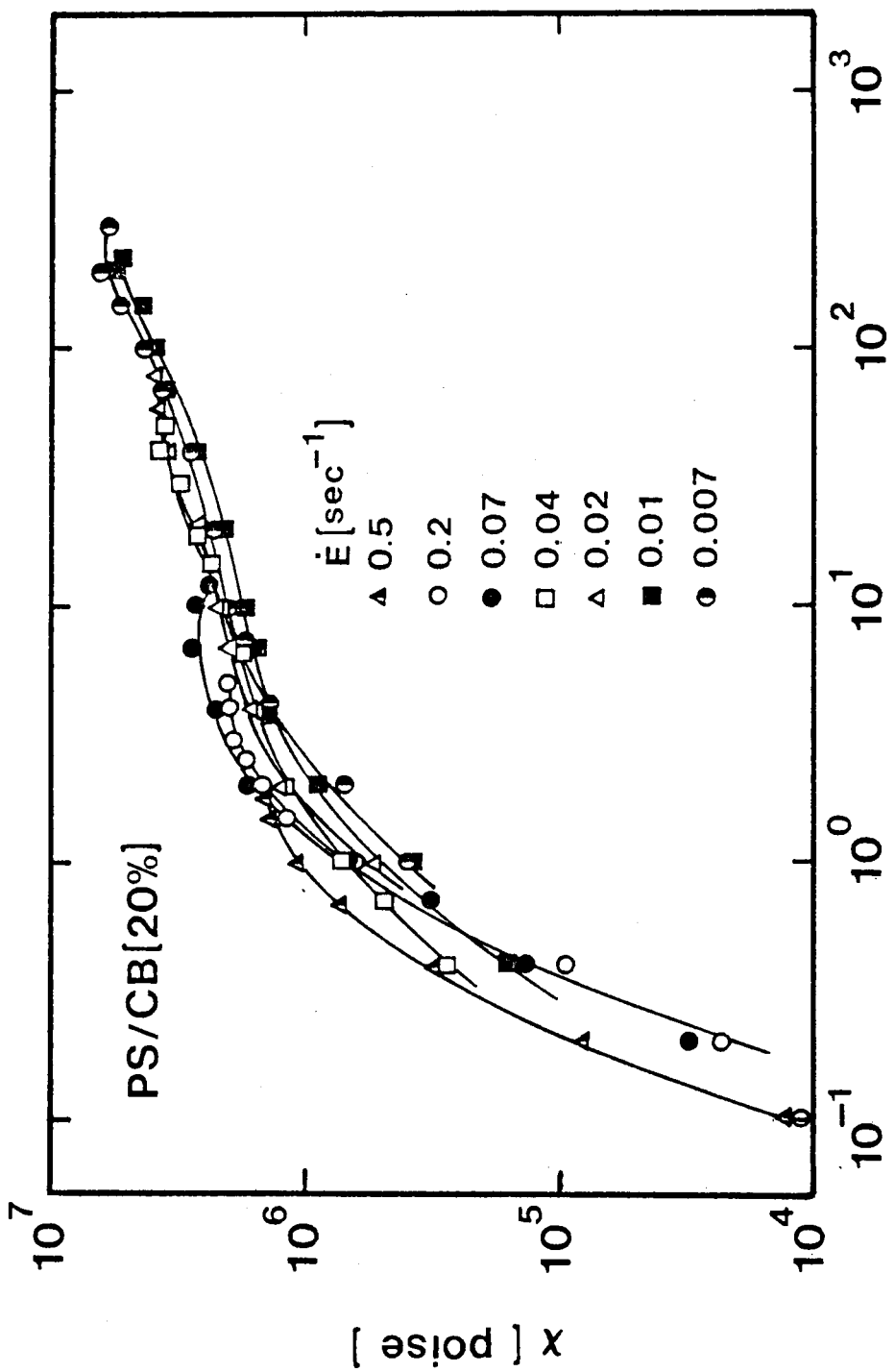

Figure VI.3. Transient Elongational Viscosity at Various Elongational Rates for 20% CB-Filled PS Melt.

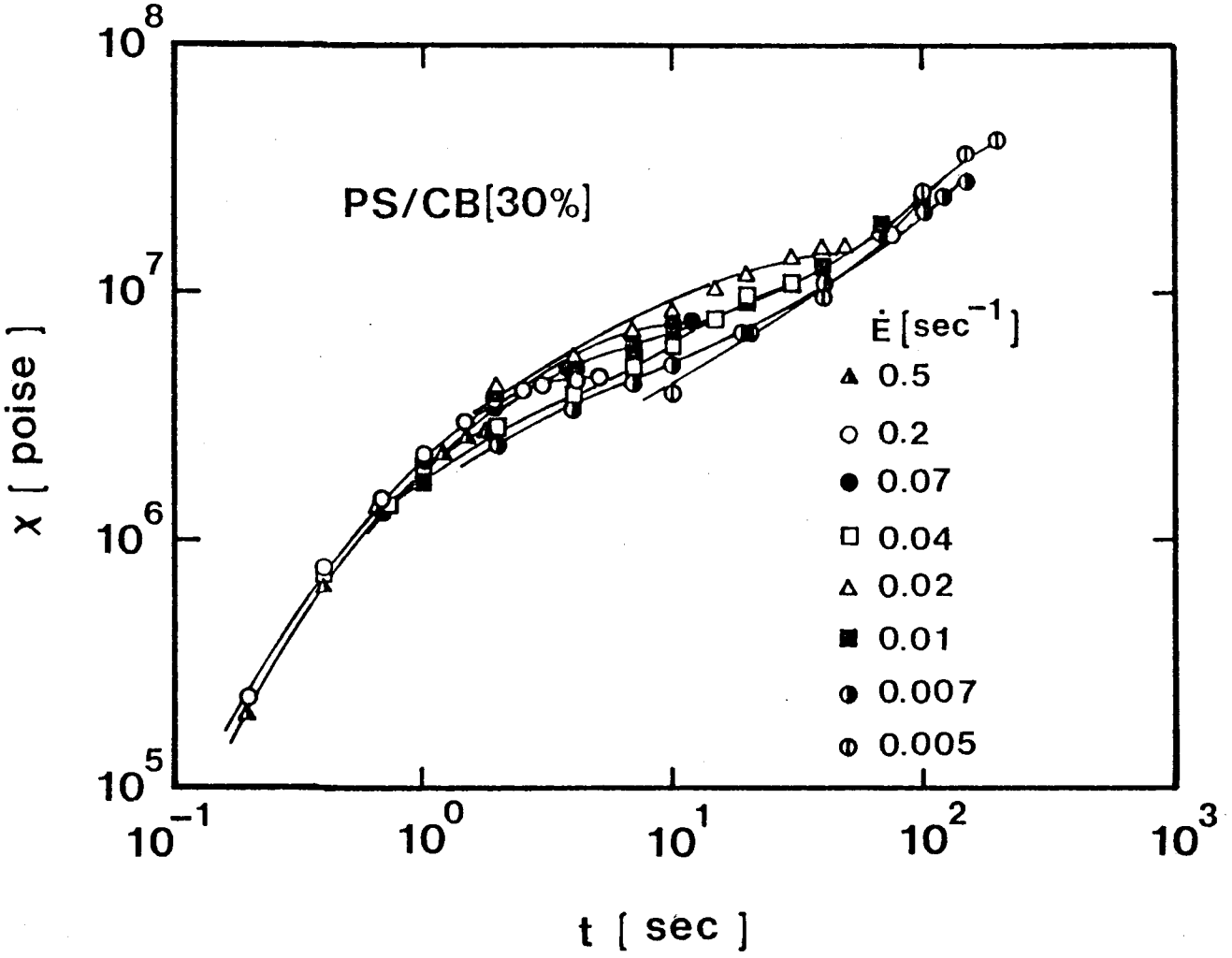

Figure VI.4. Transient Elongational Viscosity at Various Elongational Rates for 30% CB-Filled PS Melt.

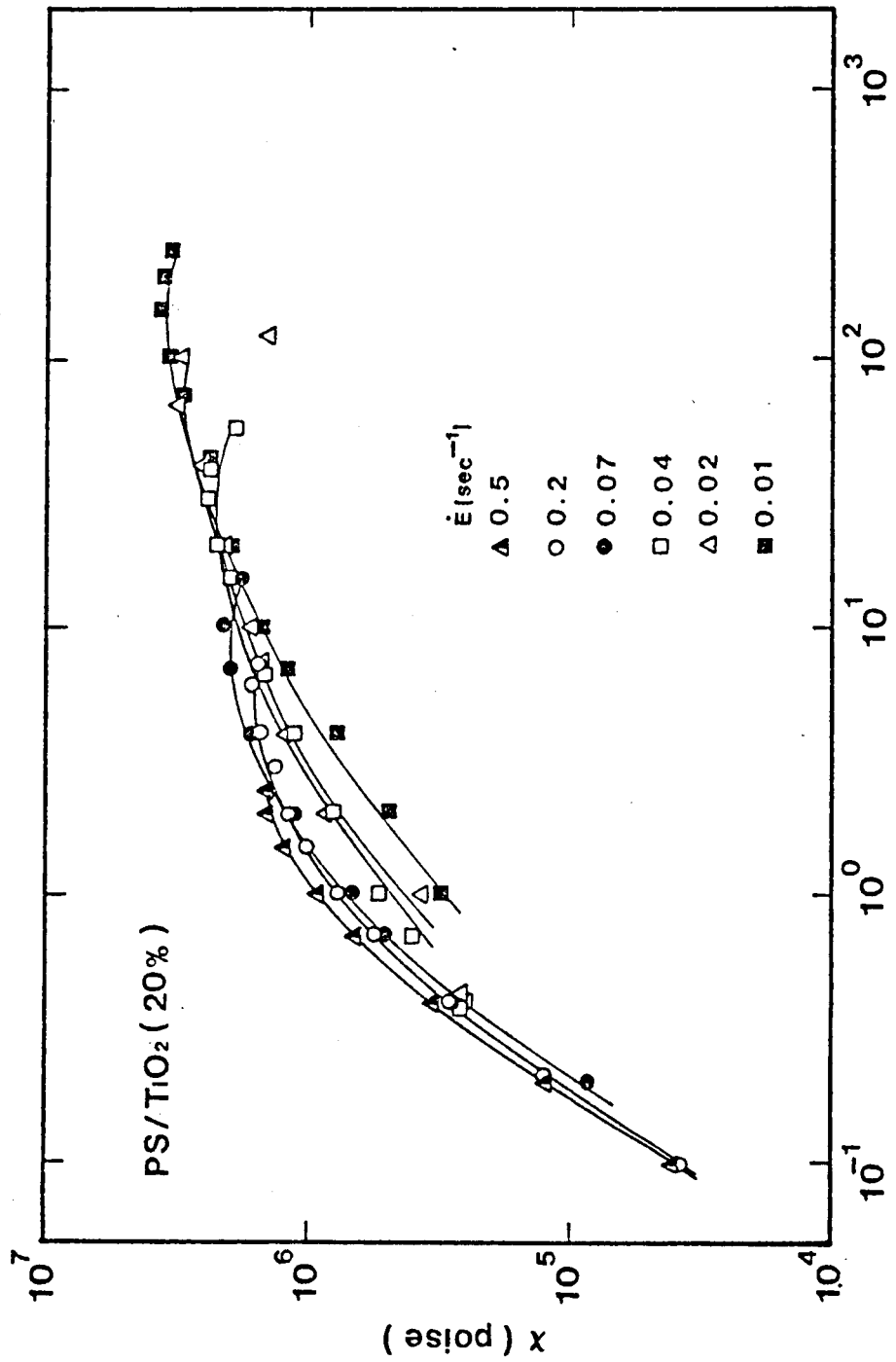

Figure VI.5. Transient Elongational Viscosity at Various Elongational Rates for 20% TiO_2-Filled PS Melt.

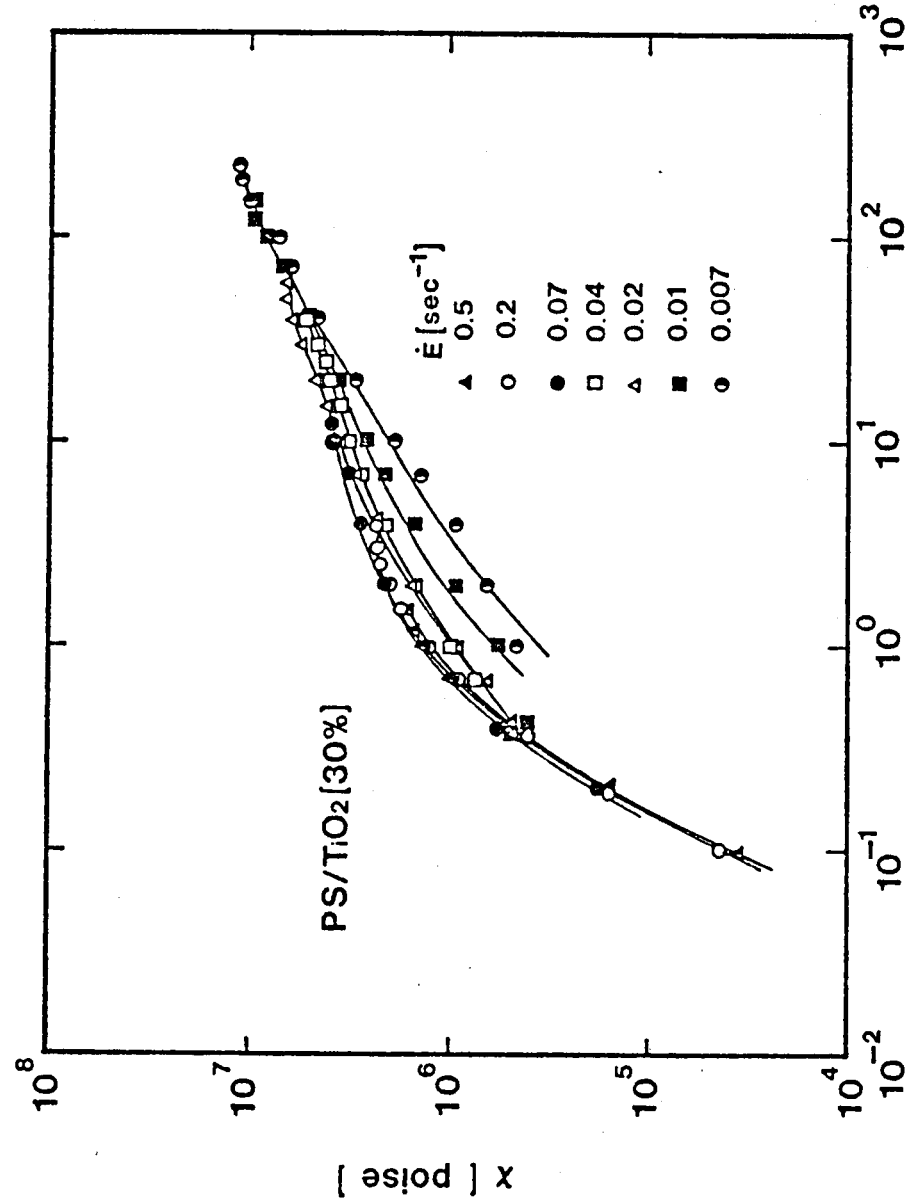

Figure VI.6. Transient Elongational Viscosity at Various Elongational Rates for 30% TiO_2-Filled PS Melt.

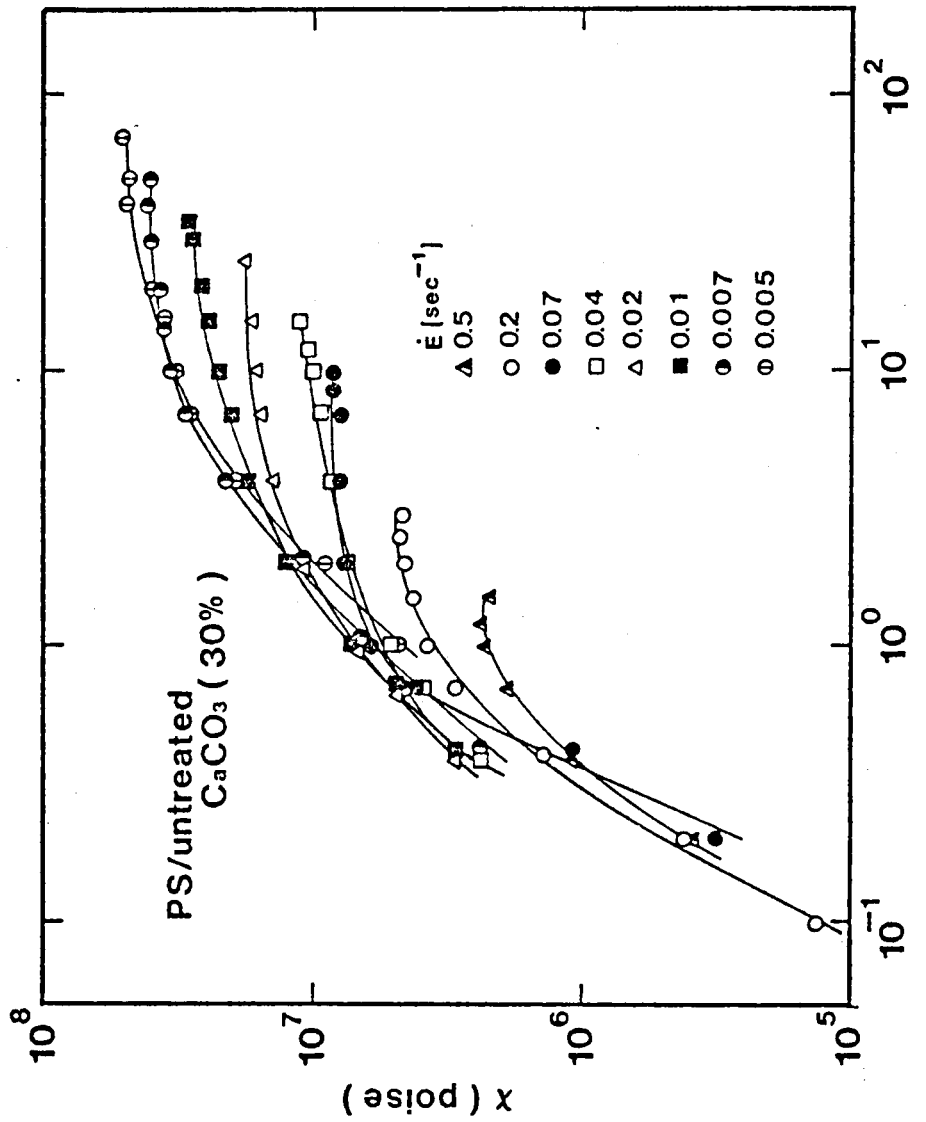

Figure VI.7. Transient Elongational Viscosity at Various Elongational Rates for 30% Untreated $CaCO_3$-Filled PS Melt.

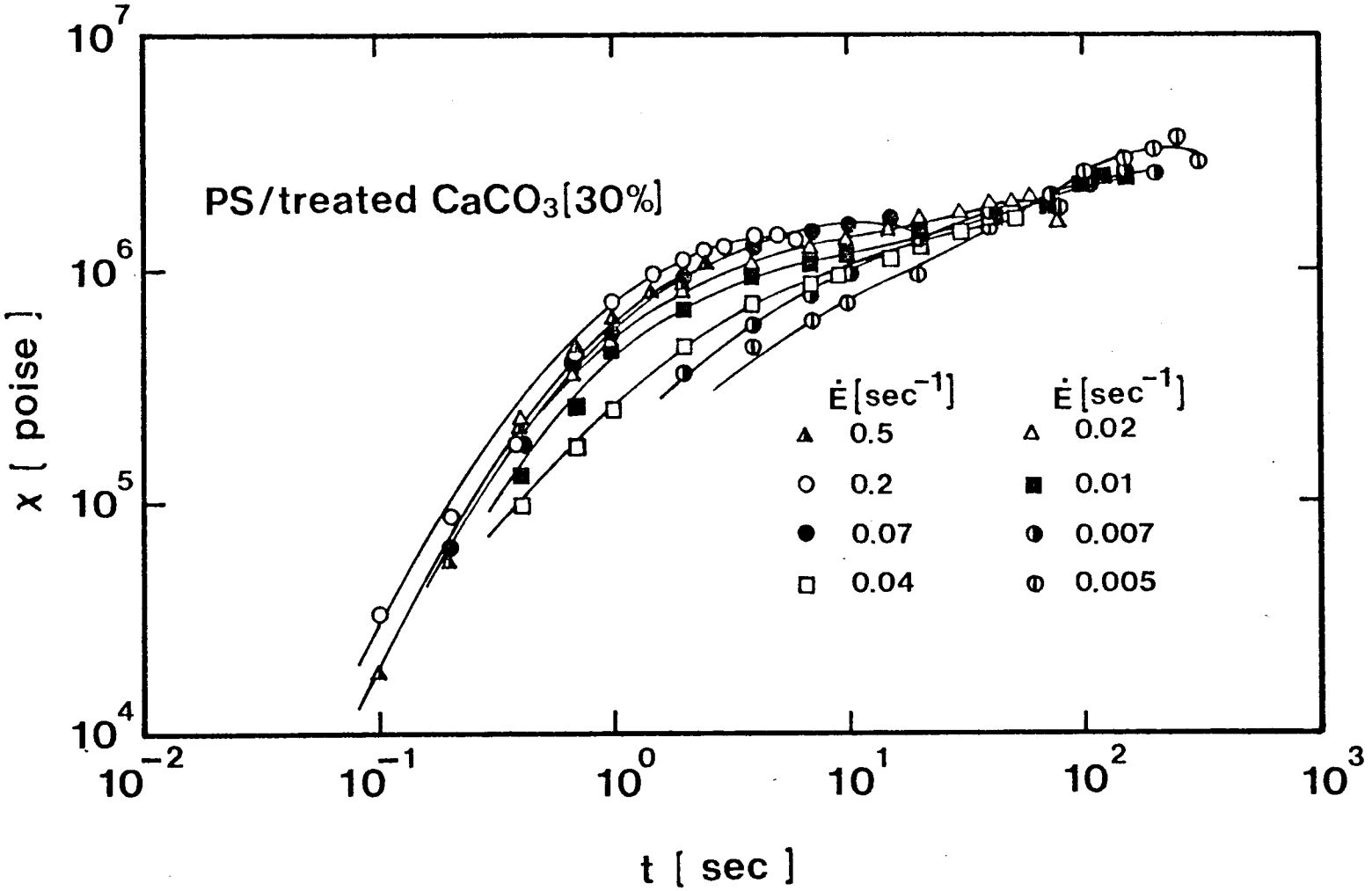

Figure VI.8. Transient Elongational Viscosity at Various Elongational Rates for 30% Treated $CaCO_3$-Filled PS Melt.

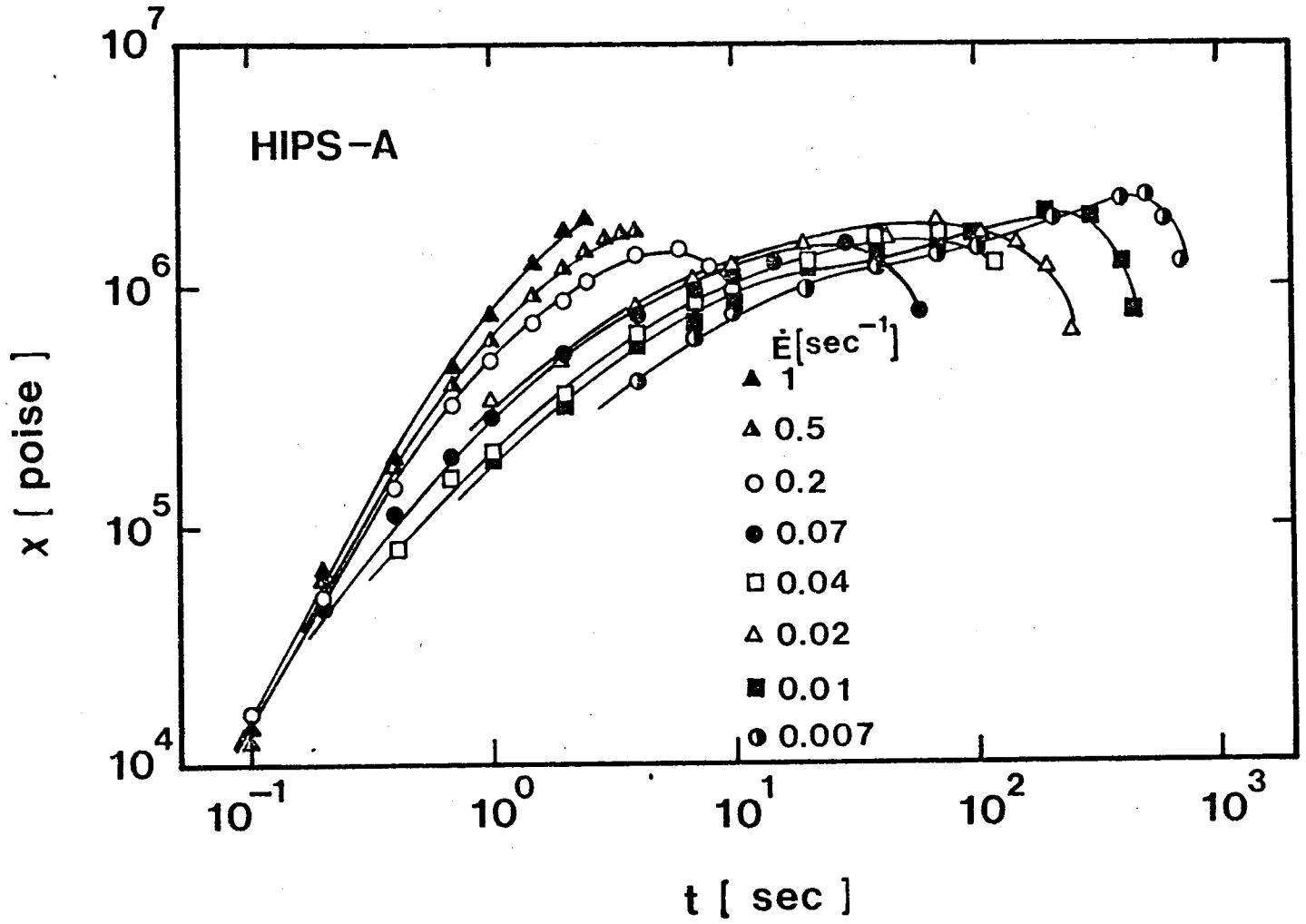

Figure VI.9. Transient Elongational Viscosity at Various Elongational Rates for HIPS-A Melt.

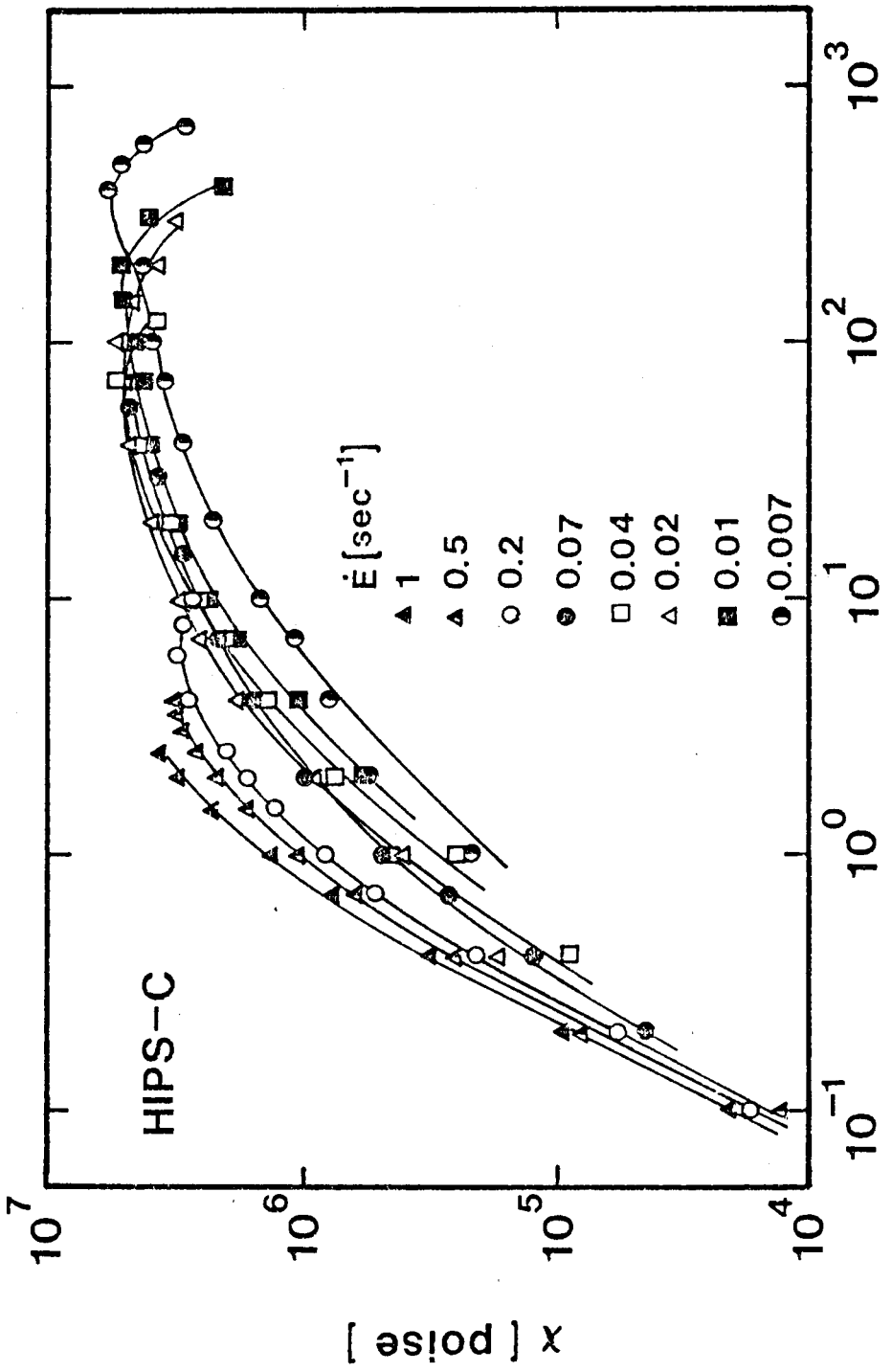

Figure VI.10. Transient Elongational Viscosity at Various Elongational Rates for HIPS-C Melt.

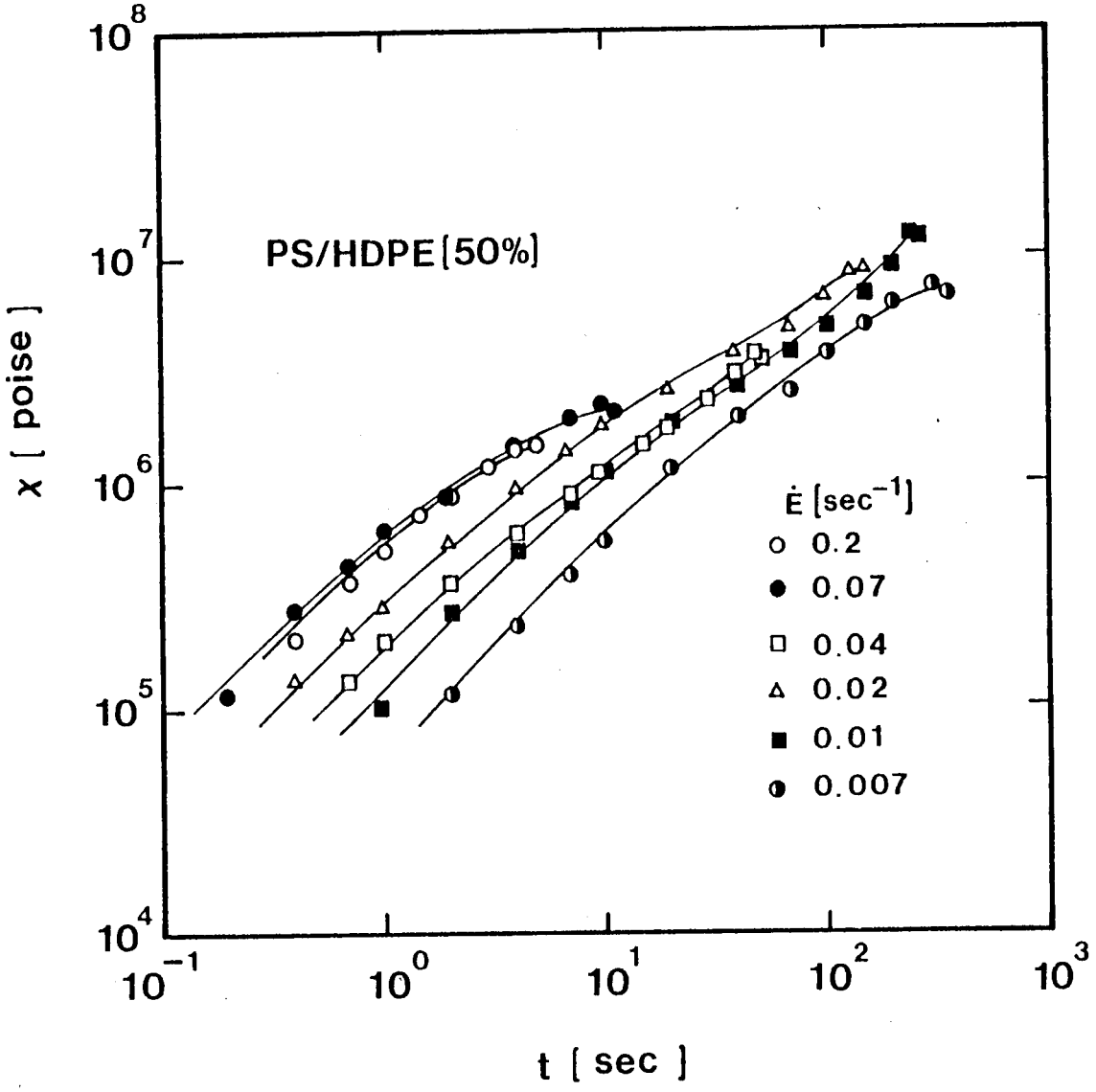

Figure VI.11. Transient Elongational Viscosity at Various Elongational Rates for 50% HDPE-Blended PS Melt.

monotonically with time. Such behavior is almost similar to reported ones (99) (101) (102) (124) (125) (131) (145) (146).

For reinforced systems, the present data show that steady states are attainable as seen in Fig. VI.2 to Fig. VI.8. The results are similar to those of Lobe and White (131). This is in contrast with Cotten and Thiele's data (48), who have reported that steady state cannot be achieved for CB-reinforced unvulcanized rubber.

It was impossible to measure the elongational viscosity for the TiO_2-filled PS at very low elongational rate, for this sample tended to sink in silicone oil.

In the HDPE/PS, the samples showed a tendency to break at the clamp at high elongational rates. As a result, the reproducible data were not obtainable for the corresponding region. However, within the measurable range, steady states were attained.

B. Steady State Elongational Viscosity

B.1. Results

The steady state elongational viscosity χ independent of time can be determined for each elongational rate from the above figures. The maximum values were assumed to be the steady state ones for PS at high elongational rates where $\chi(\dot{E},t)$ increased with time and might not reach the steady state.

B.1.1. PS Melts Reinforced with Small Rigid Particles

Figure VI.12 to Fig. VI.14 give the plot of χ versus $\dot{E}$ for small rigid particle-reinforced systems. In PS, χ takes the constant value at low $\dot{E}$, and then increases with it. In filled systems, χ, which increases with loading level, shows very high values at low deformation rates and decreases with increasing it.

B.1.2. HIPS Melts

Figure VI.15 plots the steady state elongational viscosity as a function of elongational rate for HIPS melts. The present samples tend to take constant values at low elongational rates.

B.1.3. HDPE-PS Blend Polymer Melts

The corresponding plot for a blend system is shown in Fig. VI.16. Also the same behavior, very high viscosities at low $\dot{E}$, is observable. Values for pure HDPE measured by Ide (99) is also given in the same figure although measuring temperature is different.

B.2. Discussion

To understand the nature of the abnormal high viscosity at low elongational rate, steady state elongational viscosities are plotted against tensile stress σ_{11}.

B.2.1. PS Melts Reinforced with Small Rigid Particles

Plots of χ versus σ_{11} for these systems are given in Fig. VI.17 to Fig. VI.19. The steady state elongational viscosity for highly-filled

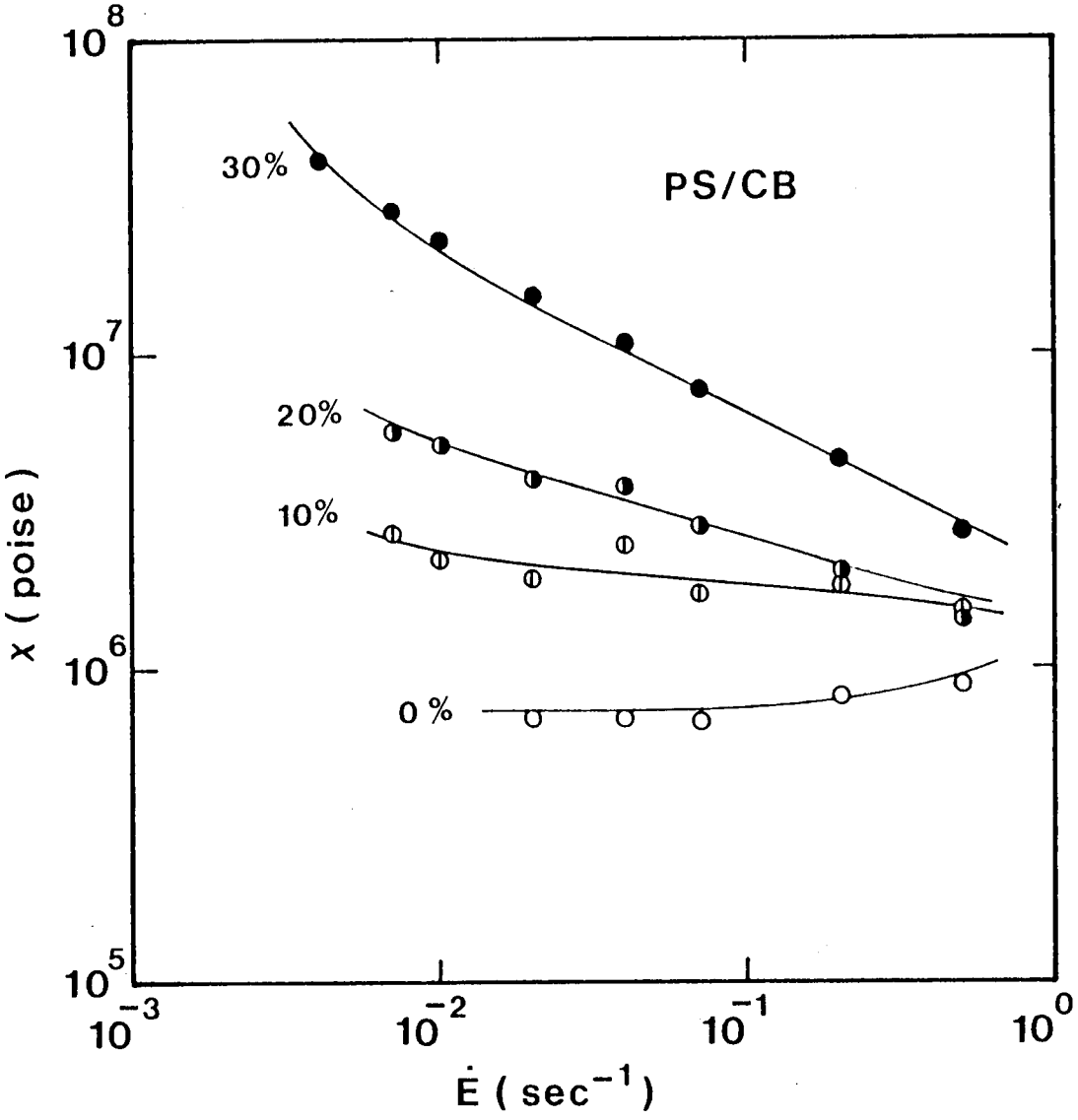

Figure VI.12. Steady State Elongational Viscosity as a Function of Elongational Rate for CB-Filled PS Melts.

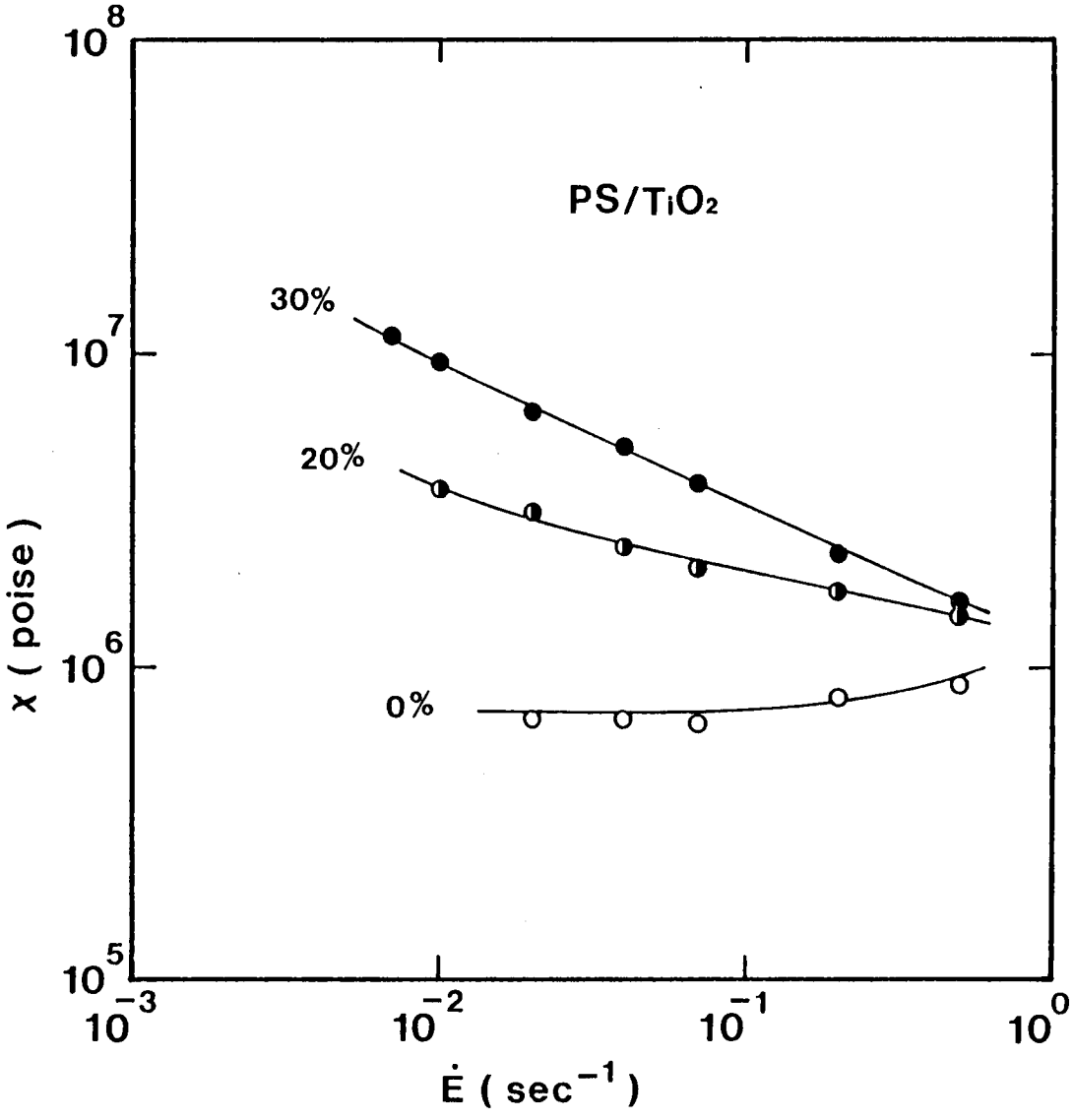

Figure VI.13. Steady State Elongational Viscosity as a Function of Elongational Rate for TiO_2-Filled PS Melts.

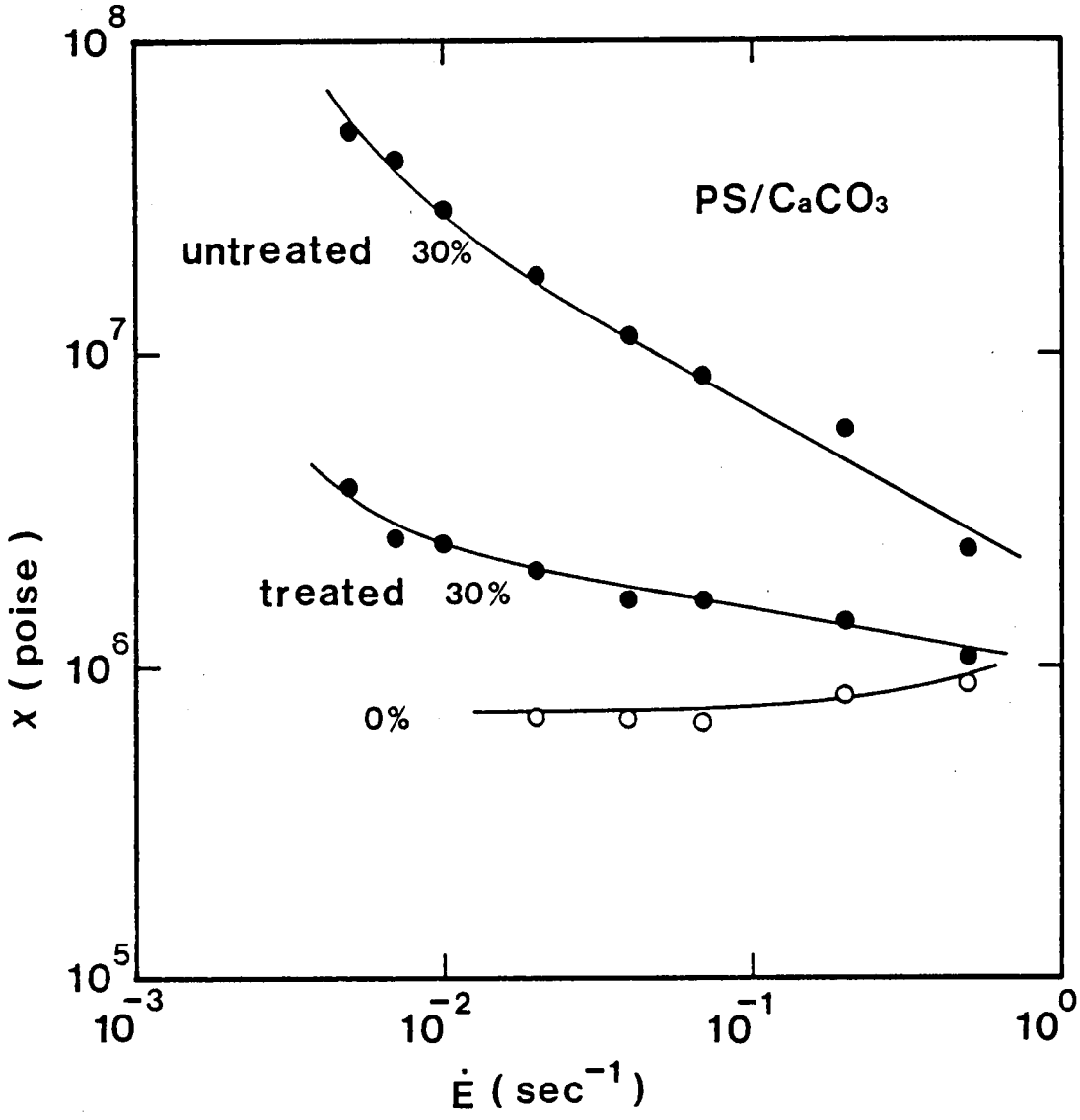

Figure VI.14. Steady State Elongational Viscosity as a Function of Elongational Rate for $CaCO_3$-Filled PS Melts.

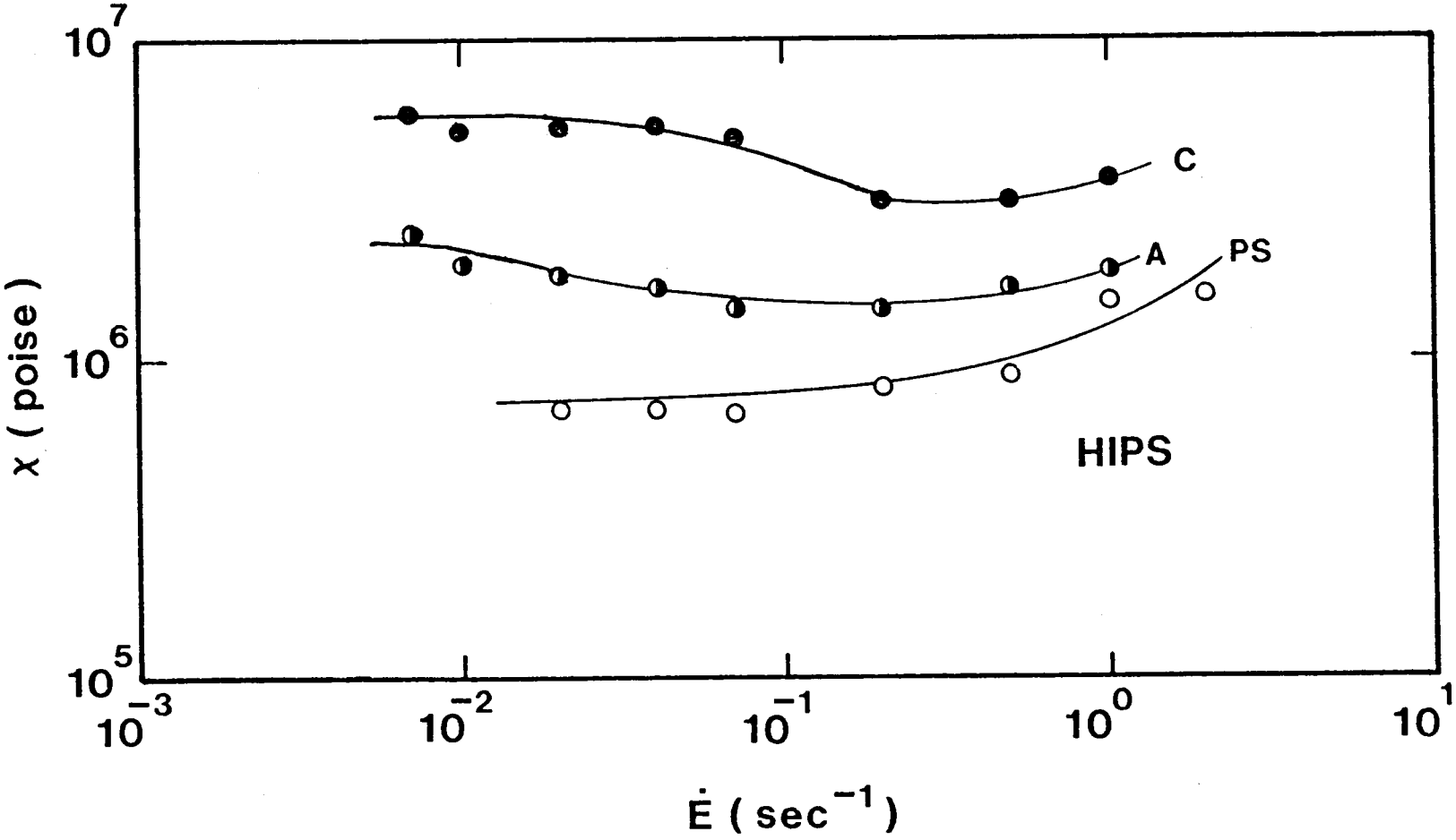

Figure VI.15. Steady State Elongational Viscosity as a Function of Elongational Rate for HIPS Melts.

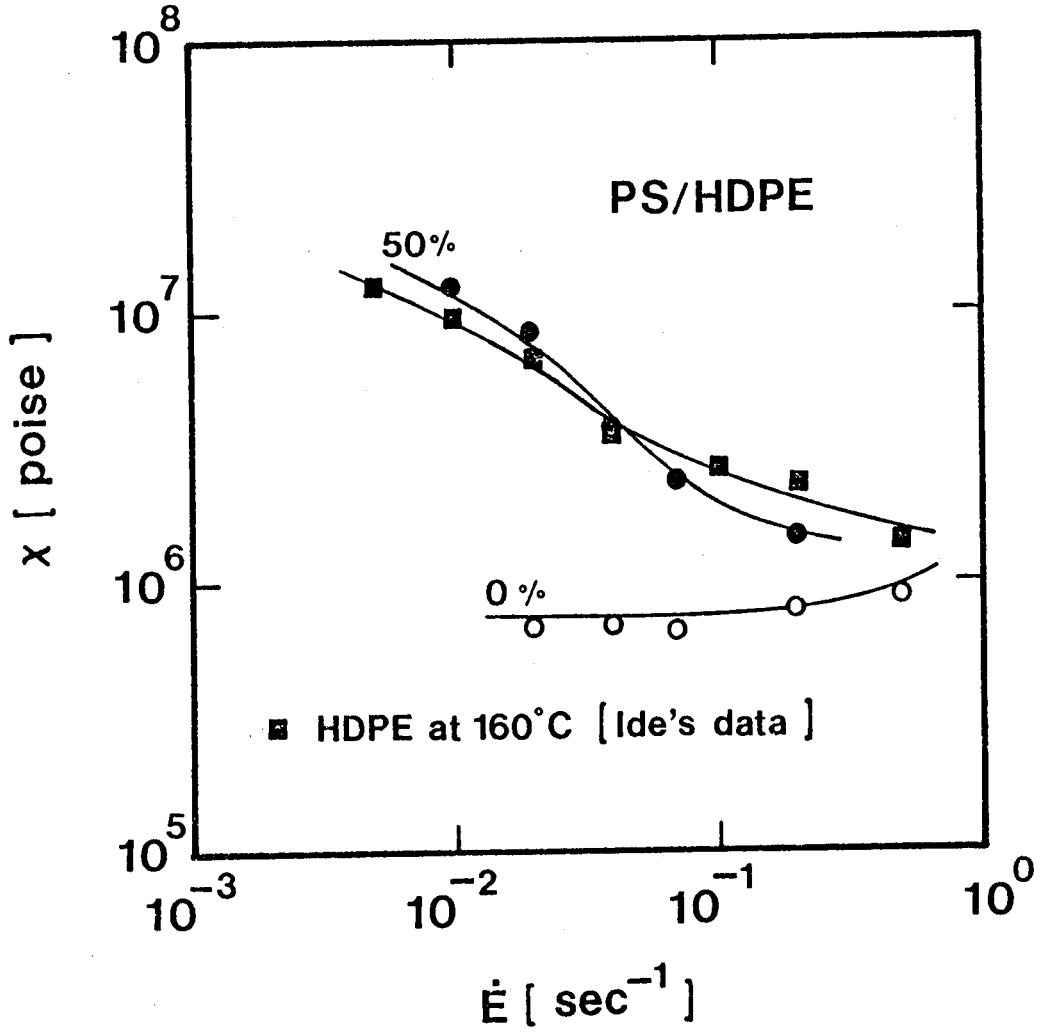

Figure VI.16. Steady State Elongational Viscosity as a Function of Elongational Rate for HDPE/PS Melts.

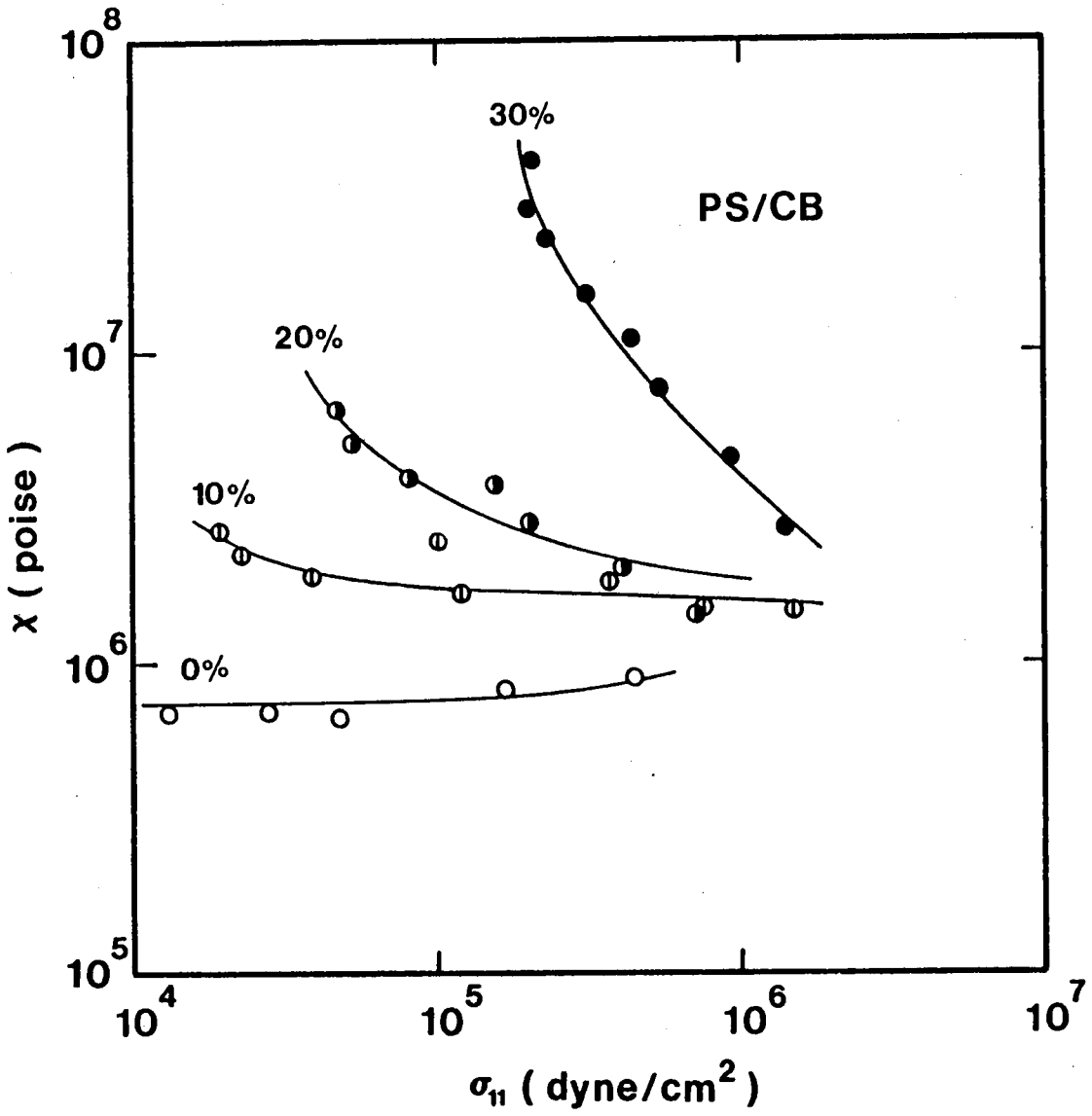

Figure VI.17. Steady State Elongational Viscosity as a Function of Tensile Stress for CB-Filled PS Melts.

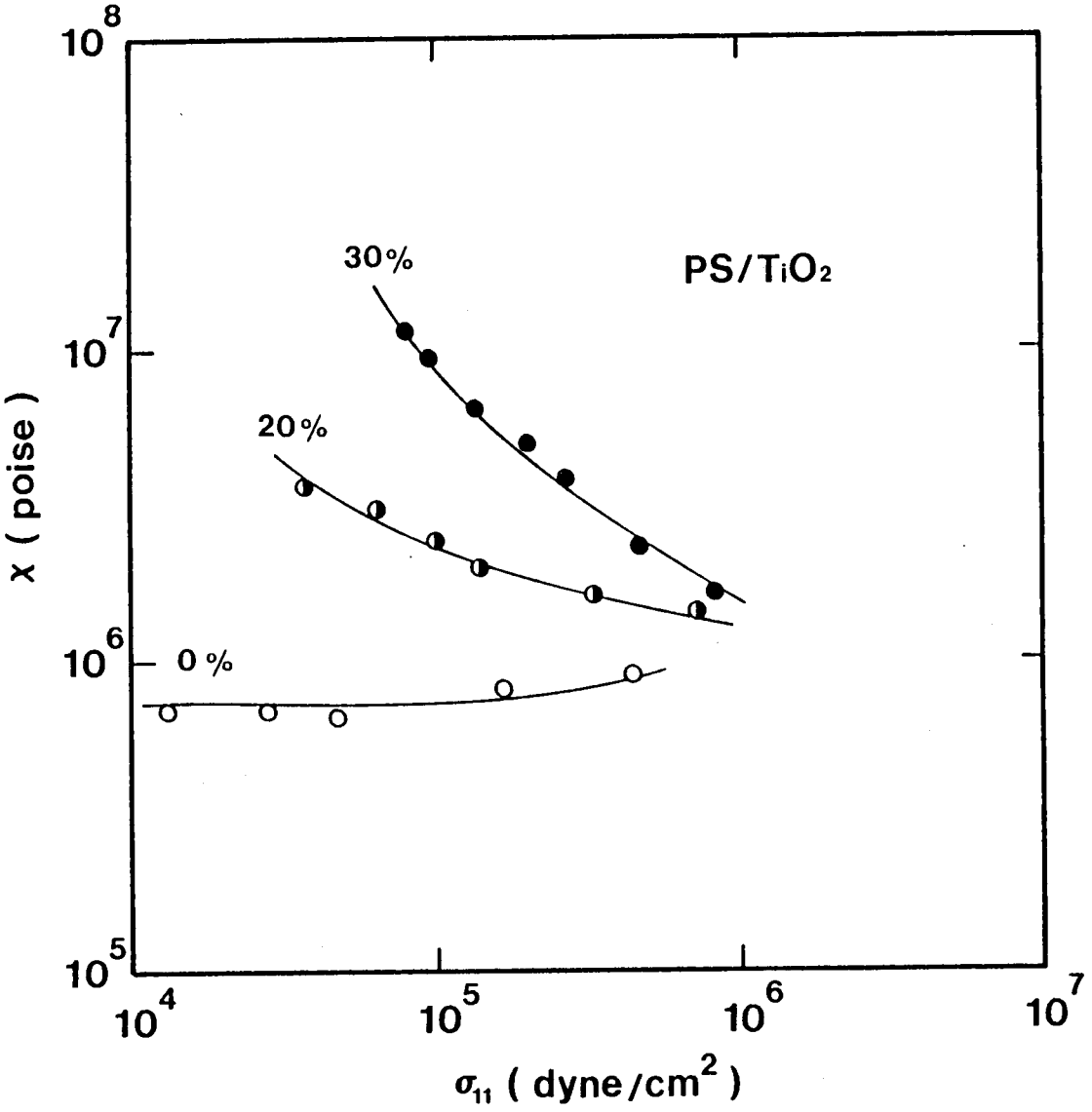

Figure VI.18. Steady State Elongational Viscosity as a Function of Tensile Stress for TiO_2-Filled PS Melts.

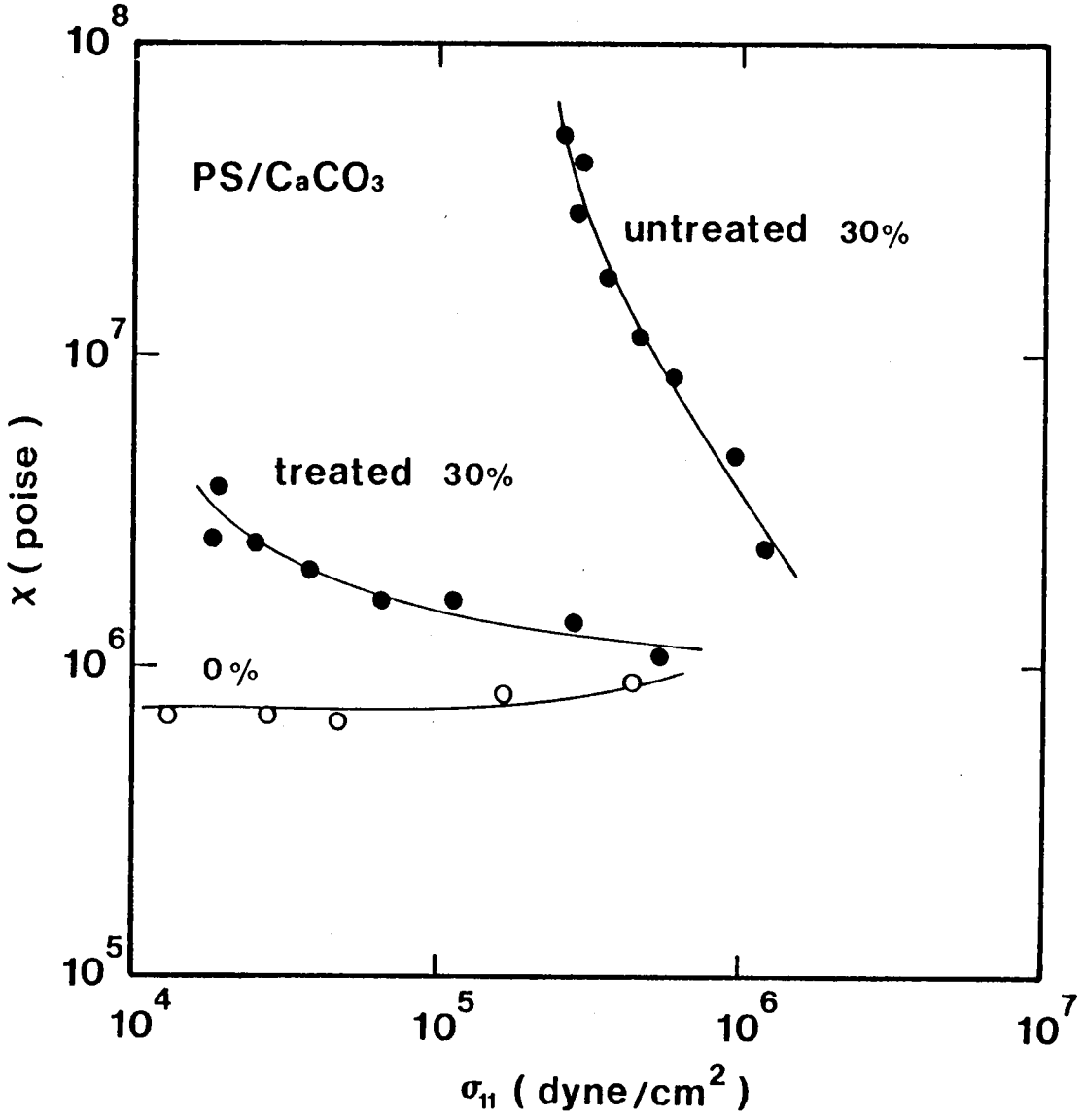

Figure VI.19. Steady State Elongational Viscosity as a Function of Tensile Stress for $CaCO_3$-Filled PS Melts.

systems tends to take an infinite value at a certain tensile stress level. This means the presence of a yield value during elongational flow.

The above figures enable us to discuss the effects of the particle characteristics used. A comparison of the elongational viscosity data of different systems at the same loading level and the elongational rate reveals that X increases in magnitude in the order

$$CB \geq \text{untreated } CaCO_3 > TiO_2 > \text{treated } CaCO_3 .$$

This order is exactly the same as in shear viscosity described in the previous chapter.

Comparing the present data on CB-filled PS with those of Lobe and White (131), we again conclude that the smaller the particle size, the higher the elongational viscosity, and smaller particles may lead to higher yield stresses.

Figure VI.14 and Fig. VI.19 reveal the effect of surface treatment. It seems to decrease the yield stress in addition to lowering the elongational viscosity.

Figure VI.17 to Fig. VI.19 show that loading level increases yield stress level as well as viscosity. These results are entirely the same as those in shear flow.

B.2.2. HIPS Melts

Figure VI.20 plots the steady state elongational viscosity versus the tensile stress. Trends toward yield values are not seen.

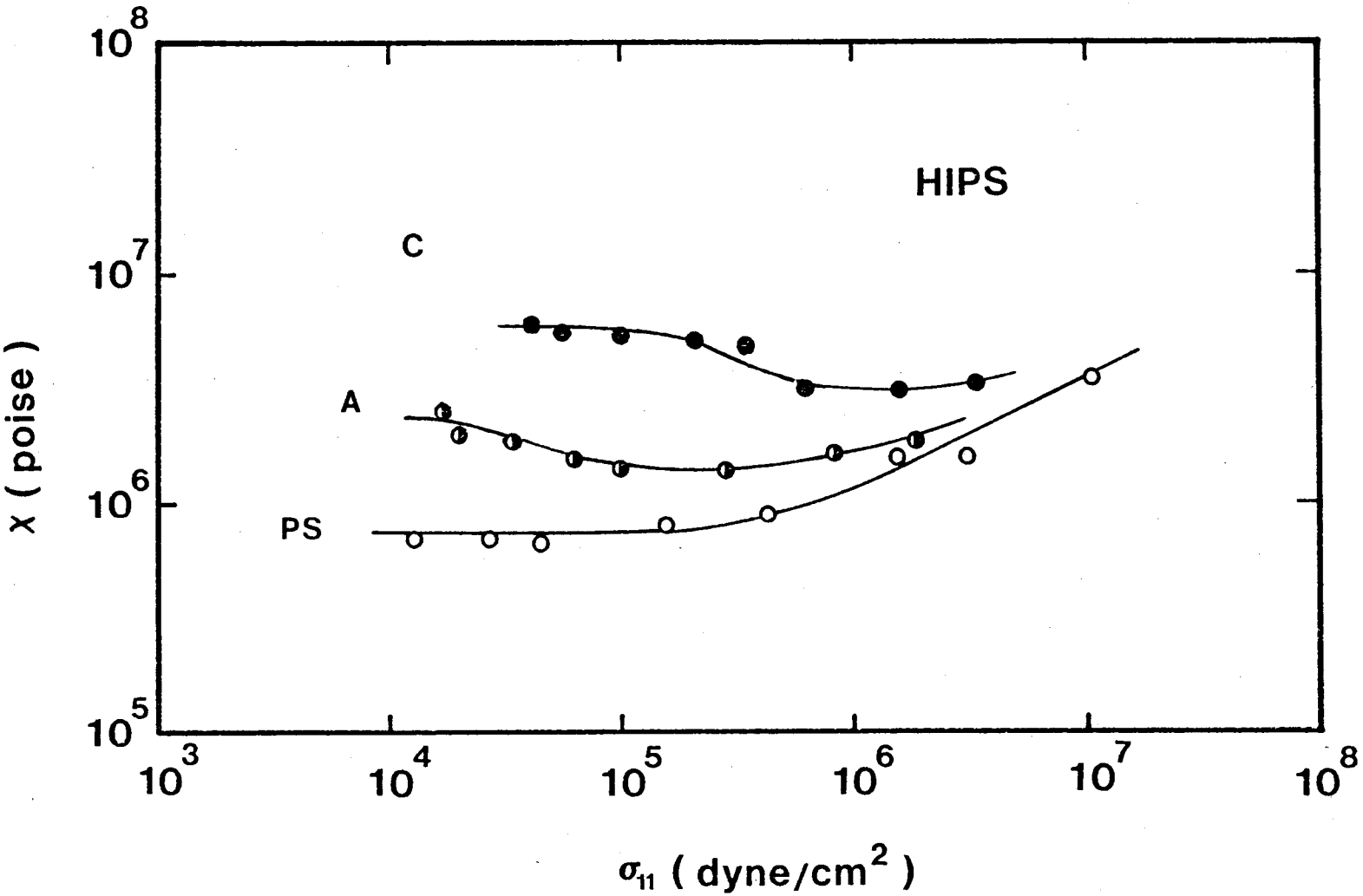

Figure VI.20. Steady State Elongational Viscosity as a Function of Tensile Stress for HIPS Melts.

Cogswell (44) has suggested the existence of a yield value for ABS melts during elongational flow. Since details on rubber morphology of the samples are not clear, we cannot discuss the relationship between rubber particle shape and viscosity behavior. However, the nonexistence of yield values in the present data may be due to the large rubber particle size as mentioned in the section of shear viscosity.

B.2.3. HDPE-PS Blend Polymer Melts

Figure VI.21 gives a plot of χ versus σ_{11} for HDPE-PS blend polymer melt. This system shows very high viscosities at low stress levels, which is similar behavior to that of pure HDPE. However, it is unable to say from only this figure whether the system exhibits a yield value or not.

C. Elongation to Break

C.1. Results

Figure VI.22 to Fig. VI.24 plot elongation to break versus elongational rate for rigid particle-filled systems. Elongation to break decreases with loading level.

The plot for HIPS melts is shown in Fig. VI.25. Rubber modification appears to decrease the elongation to break of PS.

Figure VI.26 shows elongation to break as a function of elongational rate for HDPE-PS blends. Elongation to break of pure HDPE at 160°C presented in the same figure shows Ide's data (99).

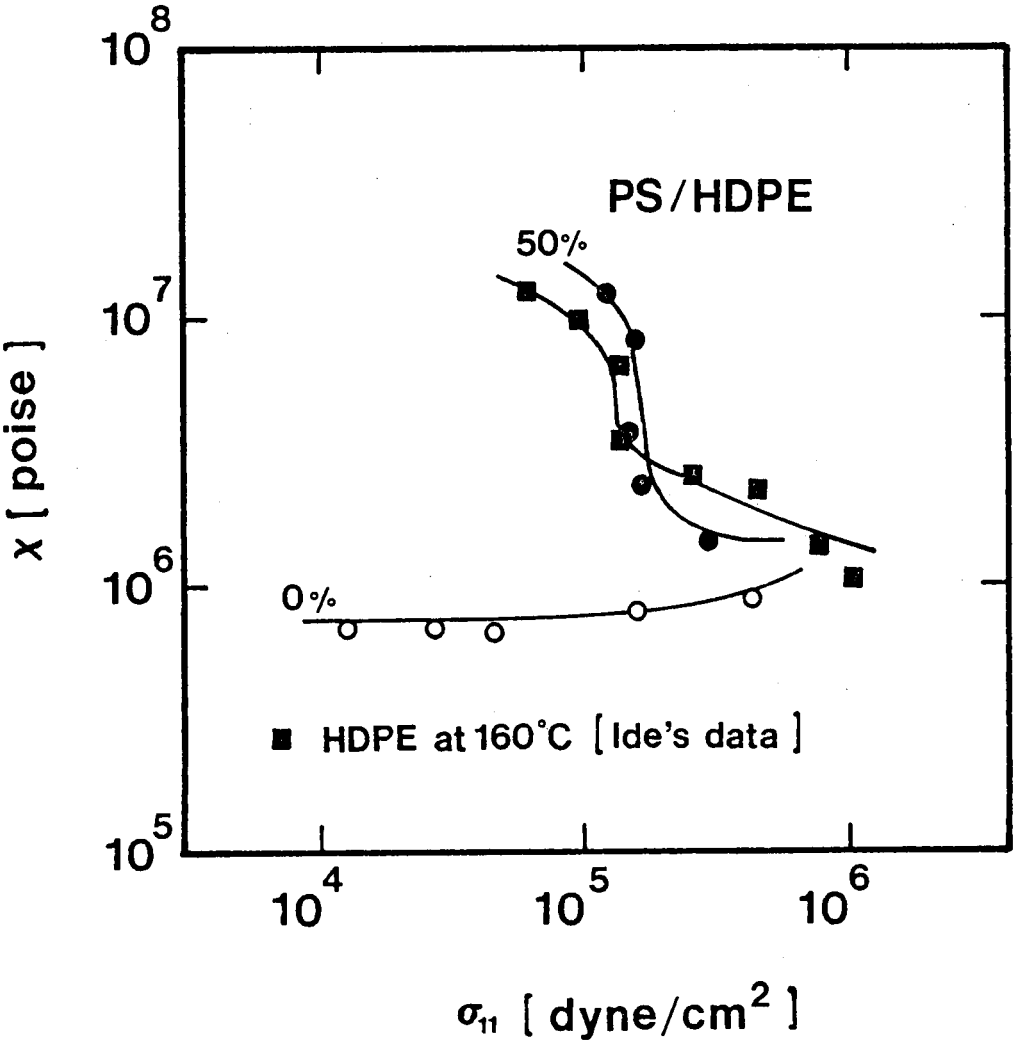

Figure VI.21. Steady State Elongational Viscosity as a Function of Tensile Stress for HDPE/PS Melts.

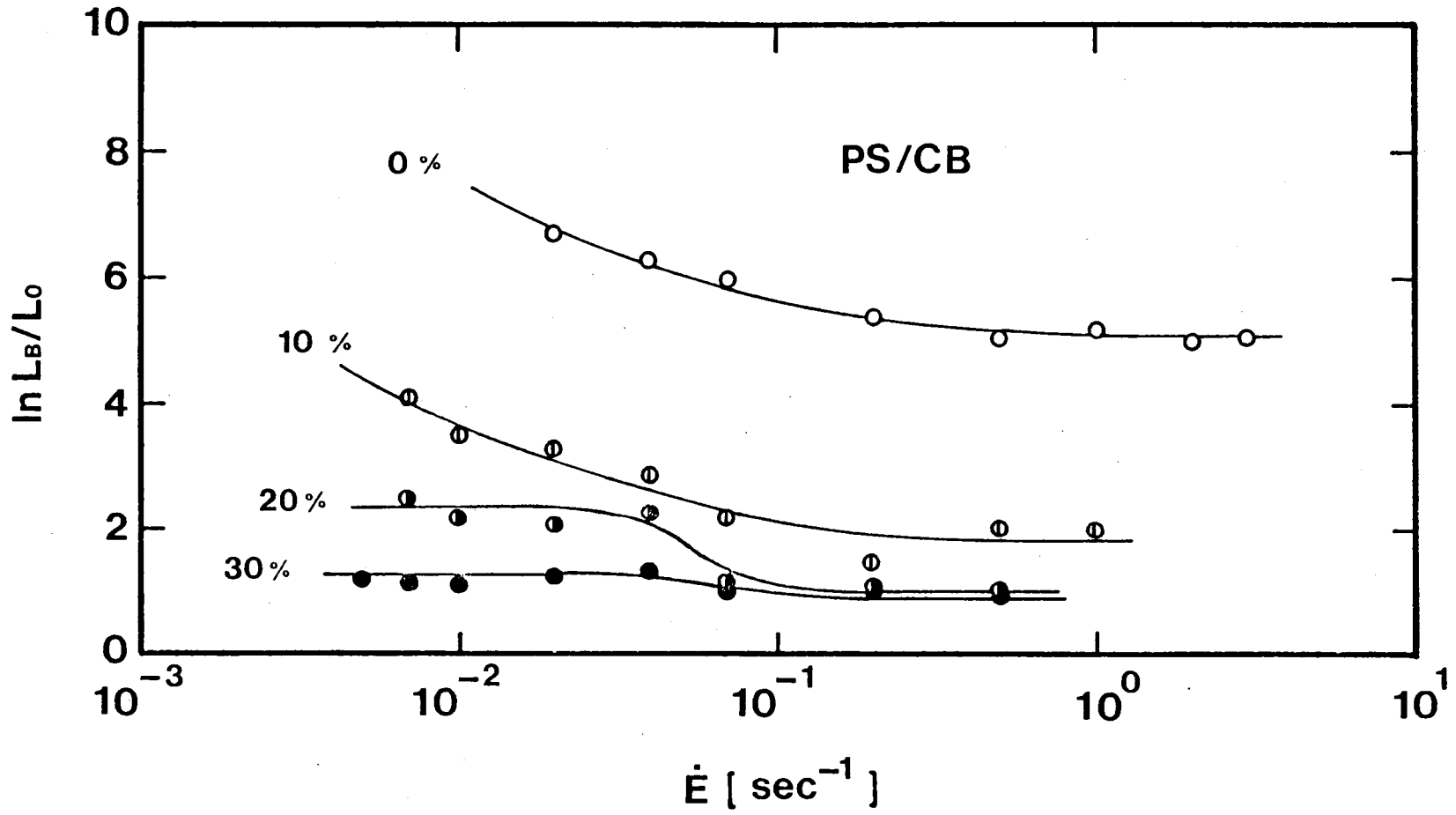

Figure VI.22. Elongation to Break as a Function of Elongational Rate for CB-Filled PS Melts.

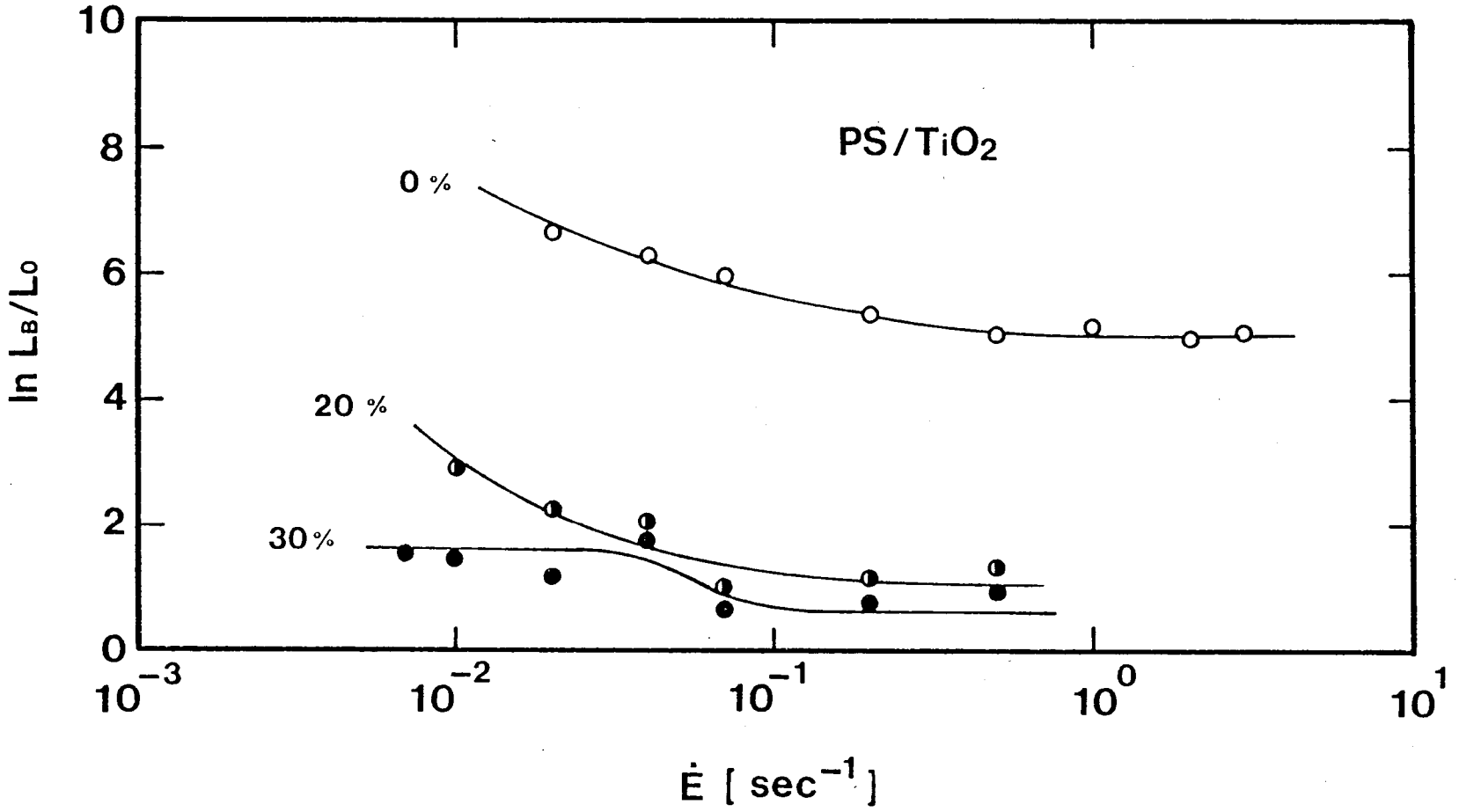

Figure VI.23. Elongation to Break as a Function of Elongational Rate for TiO_2-Filled PS Melts.

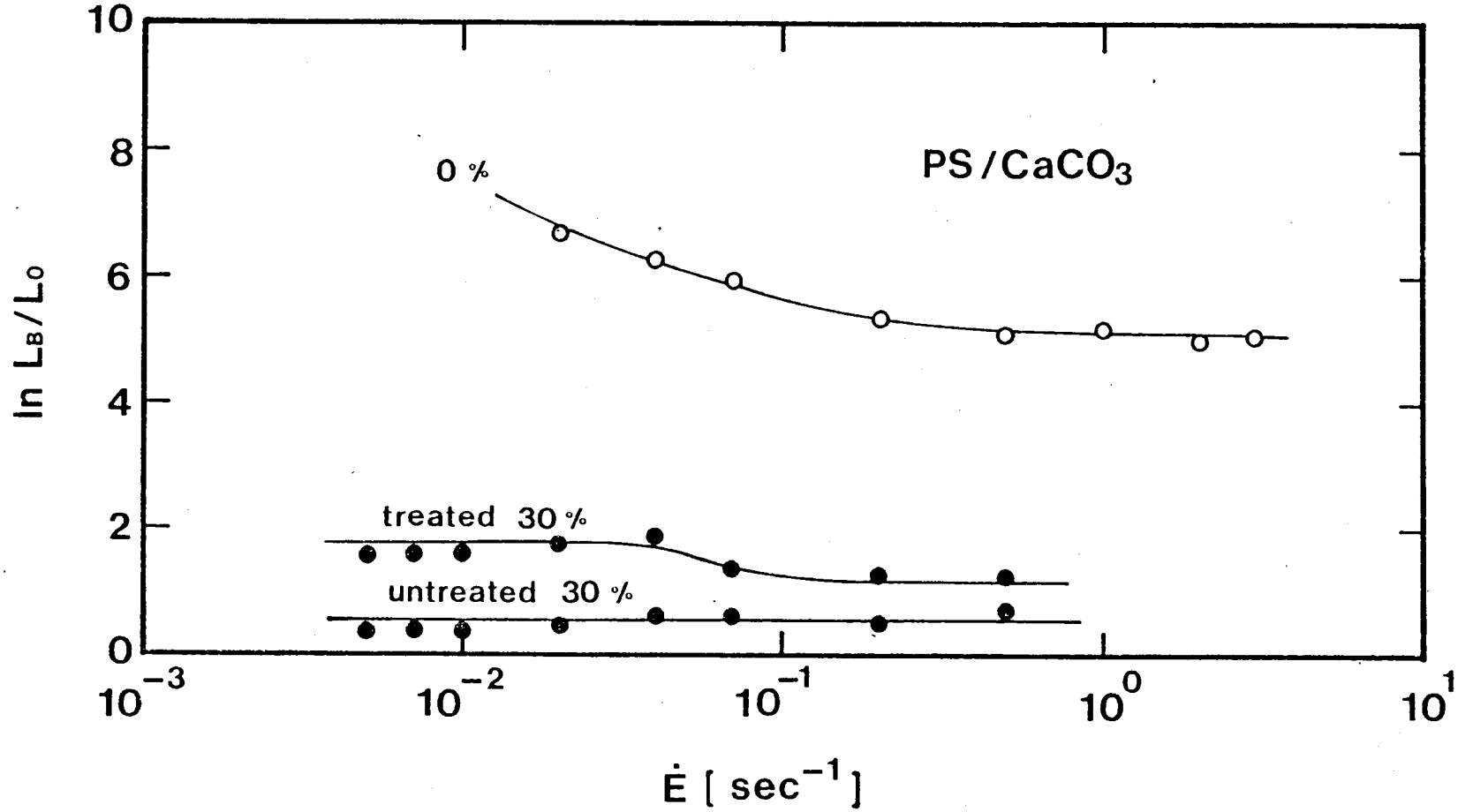

Figure VI.24. Elongation to Break as a Function of Elongational Rate for $CaCO_3$-Filled PS Melts.

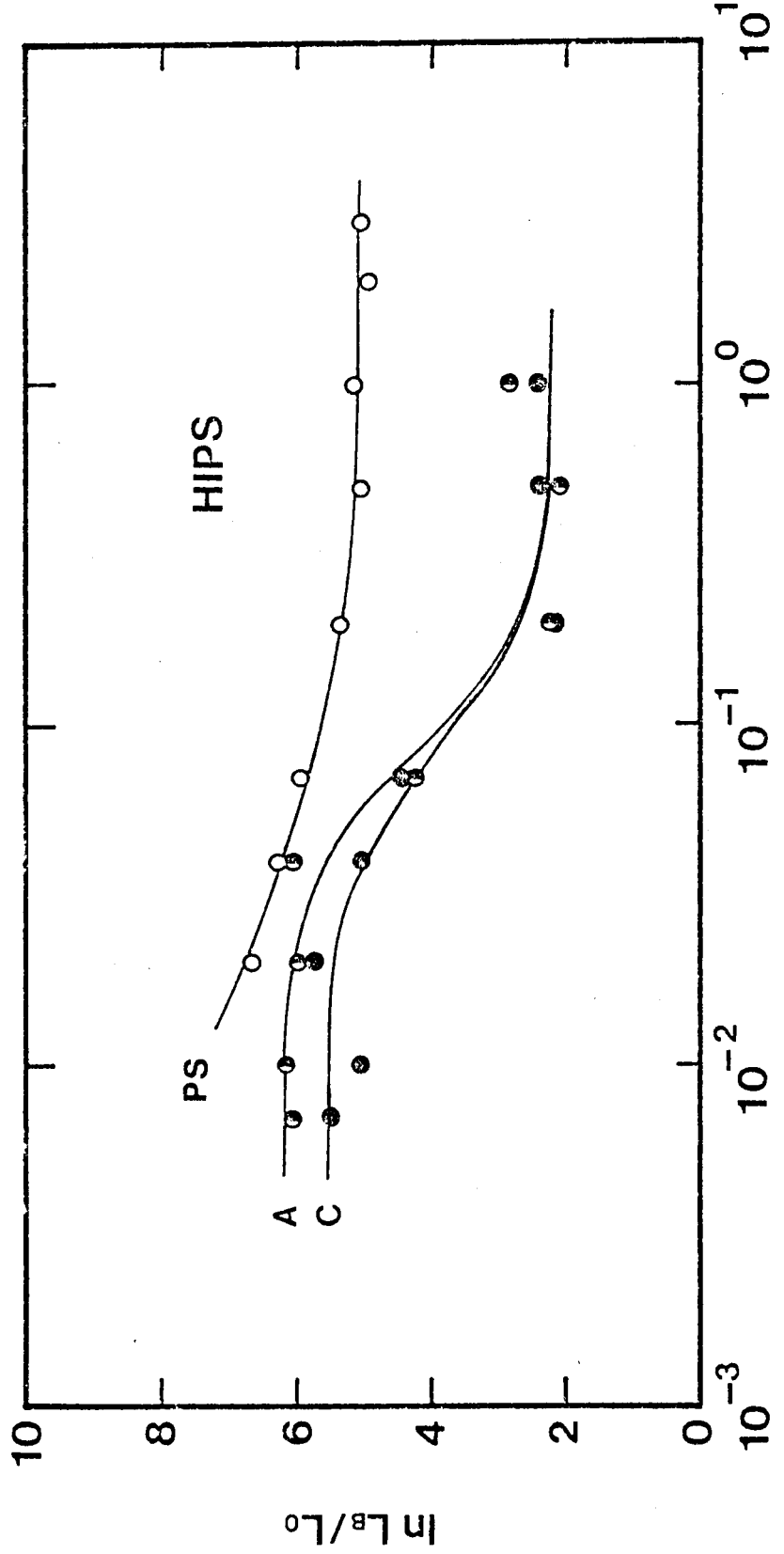

Figure VI.25. Elongation to Break as a Function of Elongational Rate for HIPS Melts.

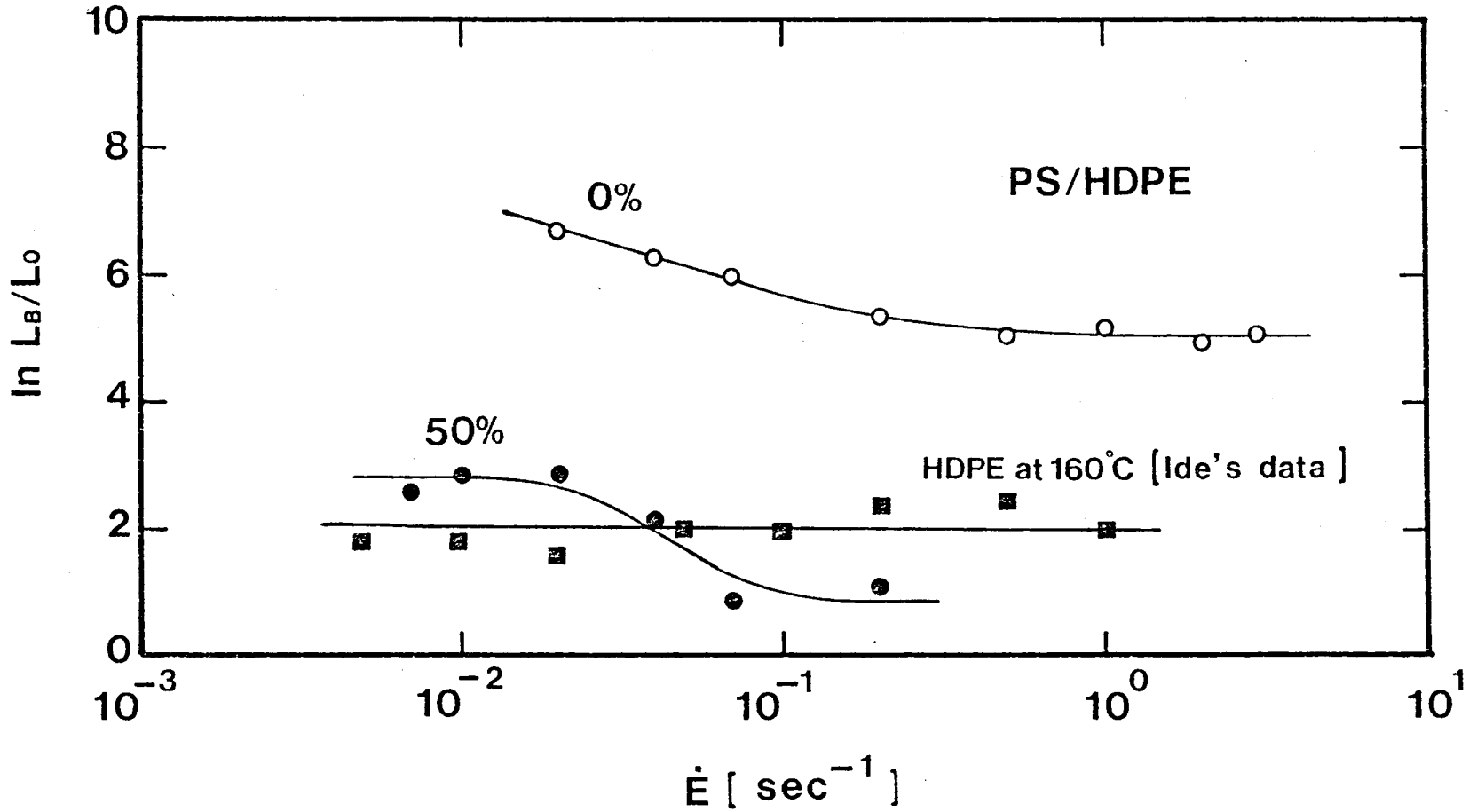

Figure VI.26. Elongation to Break as a Function of Elongational Rate for HDPE/PS Melts.

C.2. Discussion

C.2.1. PS Melts Reinforced with Small Rigid Particles

For both filled and unfilled systems, elongation to break at high elongational rates become constant. However, the values at low elongational rates tend to constant in highly-filled systems in contrast to unfilled systems in which it seems to increase with decreasing elongational rate.

Figure IV.22 to Fig. VI.24 reveal that as loading level increases, elongation to break decreases. In addition, surface treatment is found to increase extensionability of filled polymer melts as mentioned in Fig. VI.24.

Figure VI.27 shows elongation to break for PS melts reinforced with different fillers at the same loading level. It changes in magnitude in the order of

$$\text{untreated } CaCO_3 < TiO_2 \approx CB < \text{treated } CaCO_3 < PS$$

C.2.2. HIPS Melts

Similar trends to those seen in rigid particle-filled systems are found. Rubber modification decreases elongation to break, and the value at low elongational rates become constant.

C.2.3. HDPE-PS Blend Polymer Melts

Blending of HDPE decreases elongation to break of PS melts. The blended system shows a constant elongation to break at low deformation rates, similar to the behavior of pure HDPE.

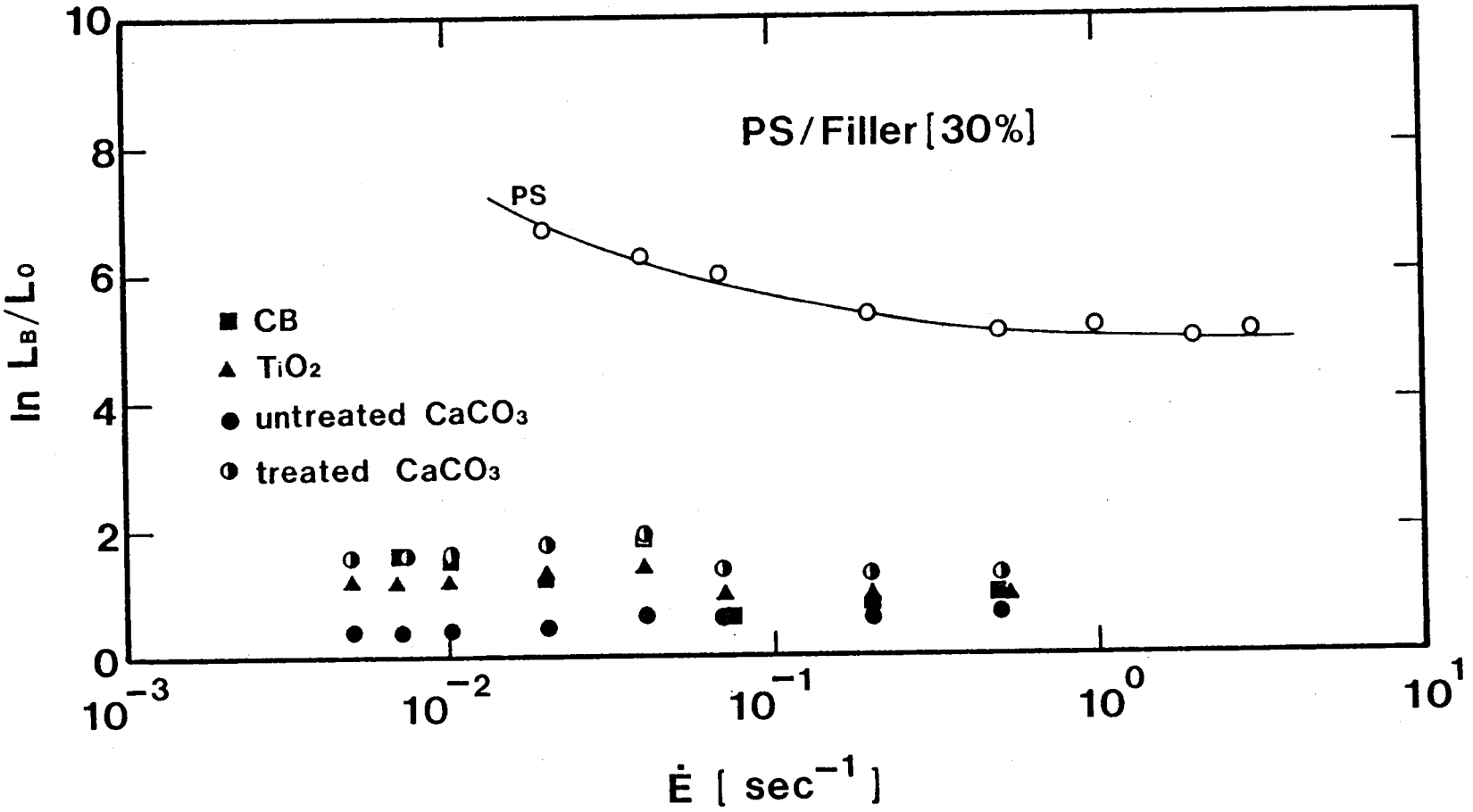

Figure VI.27. Elongation to Break as a Function of Elongational Rate for Various Filled PS Melts at the Same Loading Level.

CHAPTER VII

COMPARISON OF EXPERIMENTAL DATA WITH RHEOLOGICAL THEORIES

A. Yield Surface

In order to determine the yield surface mentioned in Chapter II, many experiments are required. However, we are unable to perform such a range of experiments with our systems because of our inability to carry out such experiments. We seem to be limited to simple shear and uniaxial elongational flow.

Although there have appeared several investigations on yield surfaces of metal and solid polymers, there have been no studies for particle reinforced polymer melts. The present work will be the first such investigation.

Figure VII.1 to Fig. VII.4 show typical plots of viscosity versus stress for both shear and elongational flow for highly-filled systems.

The ratio of the tensile to the shear yield stress, Y_e/Y_s, is given in Table VII.1. Data by Lobe and White (131) are also included in the same table.

All experimental yield values in Table VII.1 were plotted against particle size in Fig. VII.5.

The Y_e/Y_s values of Lobe and White (131) are smaller than our data. Table VII.1 shows values are approximately equal to $\sqrt{3}$, i.e., 1.73. The

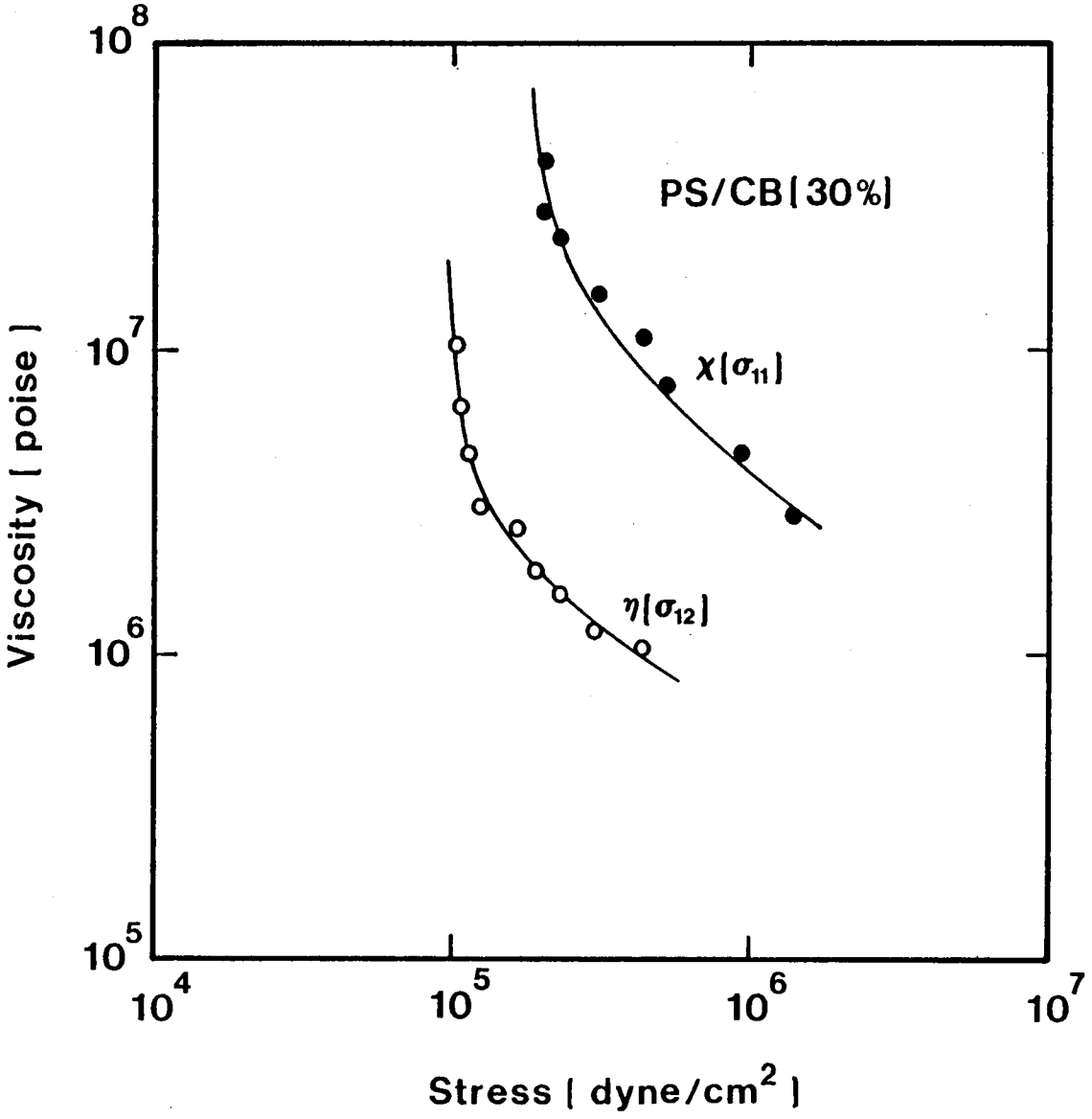

Figure VII.1. Viscosity as a Function of Stress During Both Shear and Elongational Flow for 30% CB-Filled PS Melt.

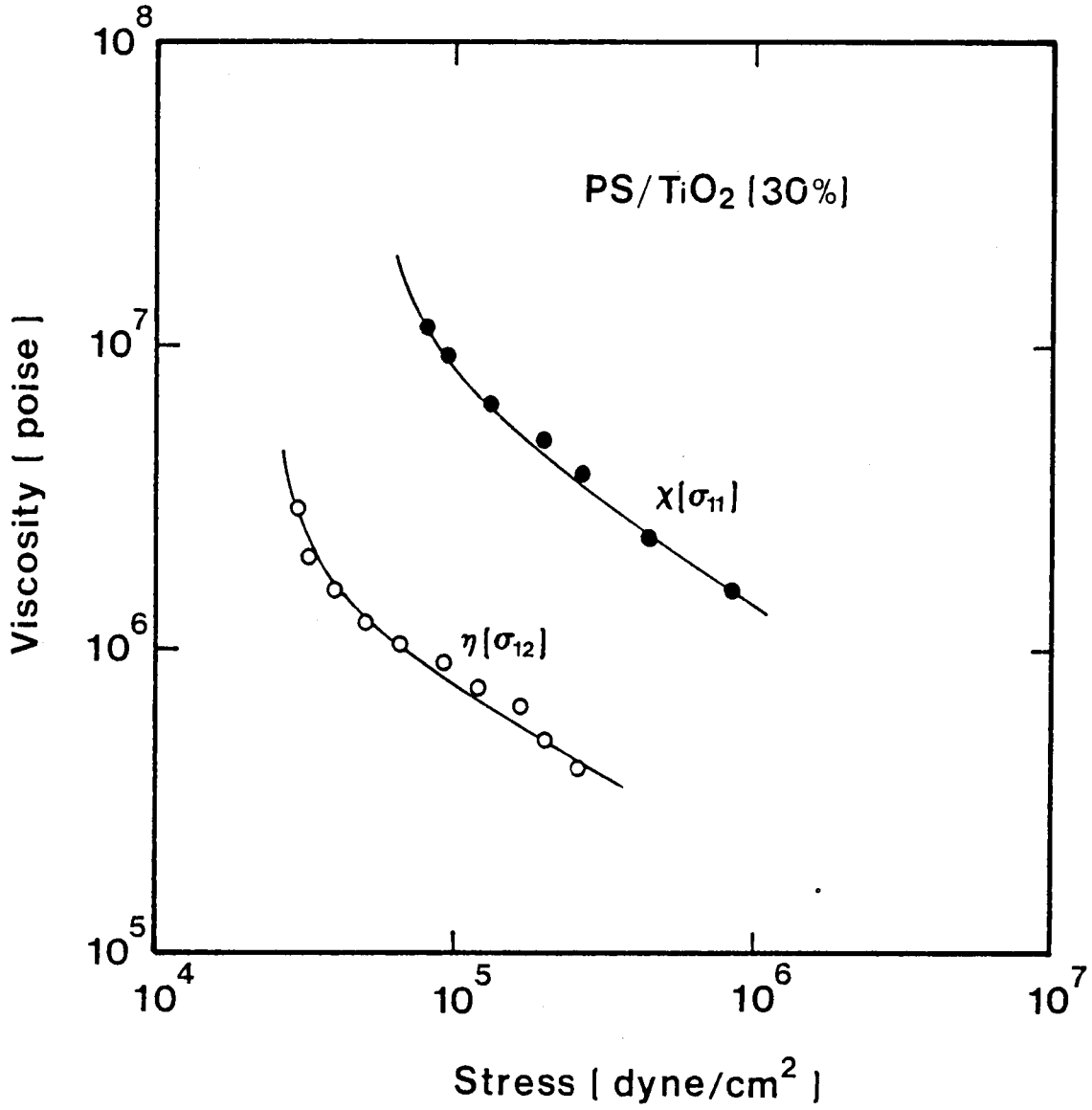

Figure VII.2. Viscosity as a Function of Stress During Both Shear and Elongational Flow for 30% TiO_2-Filled PS Melt.

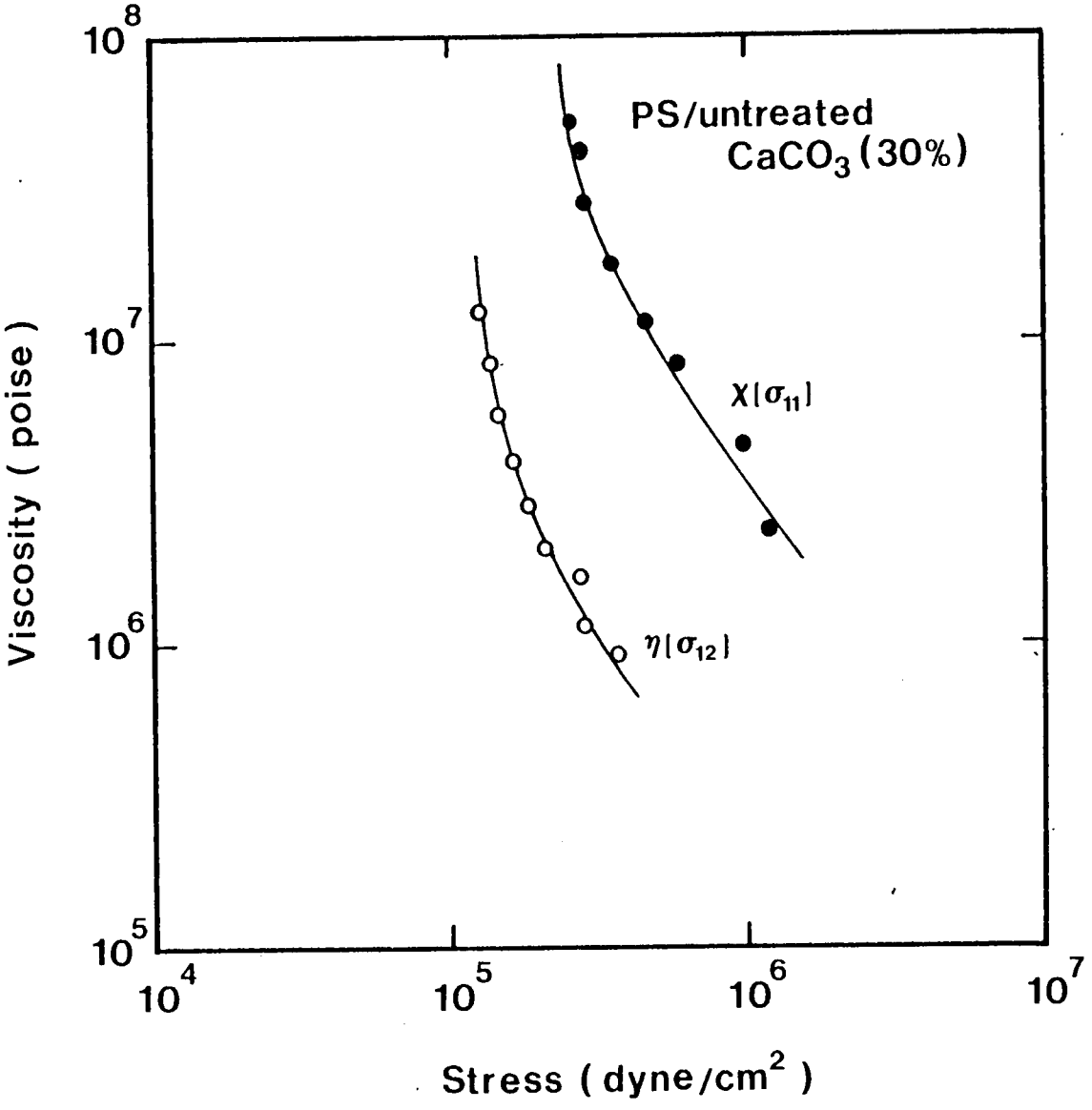

Figure VII.3. Viscosity as a Function of Stress During Both Shear and Elongational Flow for 30% Untreated $CaCO_3$-Filled PS Melt.

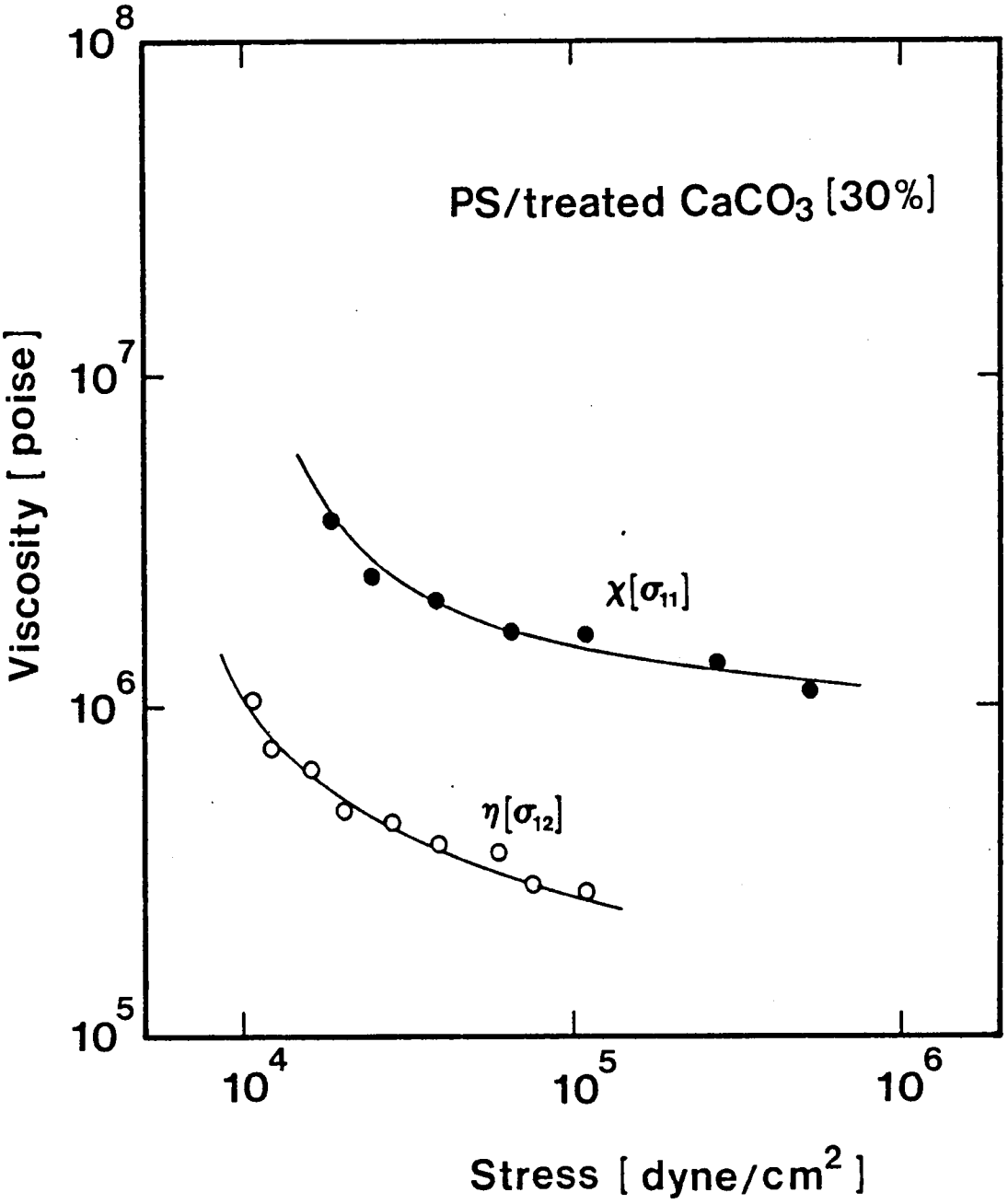

Figure VII.4. Viscosity as a Function of Stress During Both Shear and Elongational Flow for 30% Treated $CaCO_3$-Filled PS Melt.

Table VII.1. Experimental Yield Values

Filler	Particle Size (μ)	Matrix	Temperature (°C)	Loading (Vol.%)	$Y_s \times 10^{-4}$ $\frac{dyne}{cm^2}$	$Y_e \times 10^{-4}$ $\frac{dyne}{cm^2}$	Y_e/Y_s	References
Carbon black	0.1	PIB		29[a]	3			Zakharenko et al.(229)
Carbon black	0.02	PIB	22,60	9[a]	1.0			Vinogradov et al.(213)
Carbon black	0.02	PIB	22,60	13[a]	2.6			Vinogradov et al.(213)
Carbon black	0.025	PS	170	20	12	18	1.5	Lobe and White(131)
Carbon black	0.025	PS	170	25	60	70	1.2	Lobe and White(131)
Carbon black	0.045	PS	180	20	2.5			The present work
Carbon black	0.045	PS	180	30	9	17	1.9	The present work
TiO_2	0.18	LDPE	180	22	2.5			Minagawa and White(151)
TiO_2	0.18	HDPE	180	24	0.5			Minagawa and White(151)
TiO_2	0.18	PS	180	20	~1			The present work
TiO_2	0.18	PS	180	30	2.2	4	1.8	The present work
Untreated $CaCO_3$	0.5	PS	180	30	12	22	1.8	The present work
Treated $CaCO_3$	0.5	PS	180	30	~0.4	~0.7	~1.75	The present work
Talc	?	PP	200	17[b]	0.14			Chapman and Lee(40)

[a]Calculated using $\rho_{PIB\ 20°C} = 0.92\ g/cm^3$ and $\rho_{carbon\ black} = 1.8\ g/cm^3$.

[b]Calculated using $\rho_{pp\ 200°C} = 0.75\ g/cm^3$ and $\rho_{talc} = 2.4\ g/cm^3$.

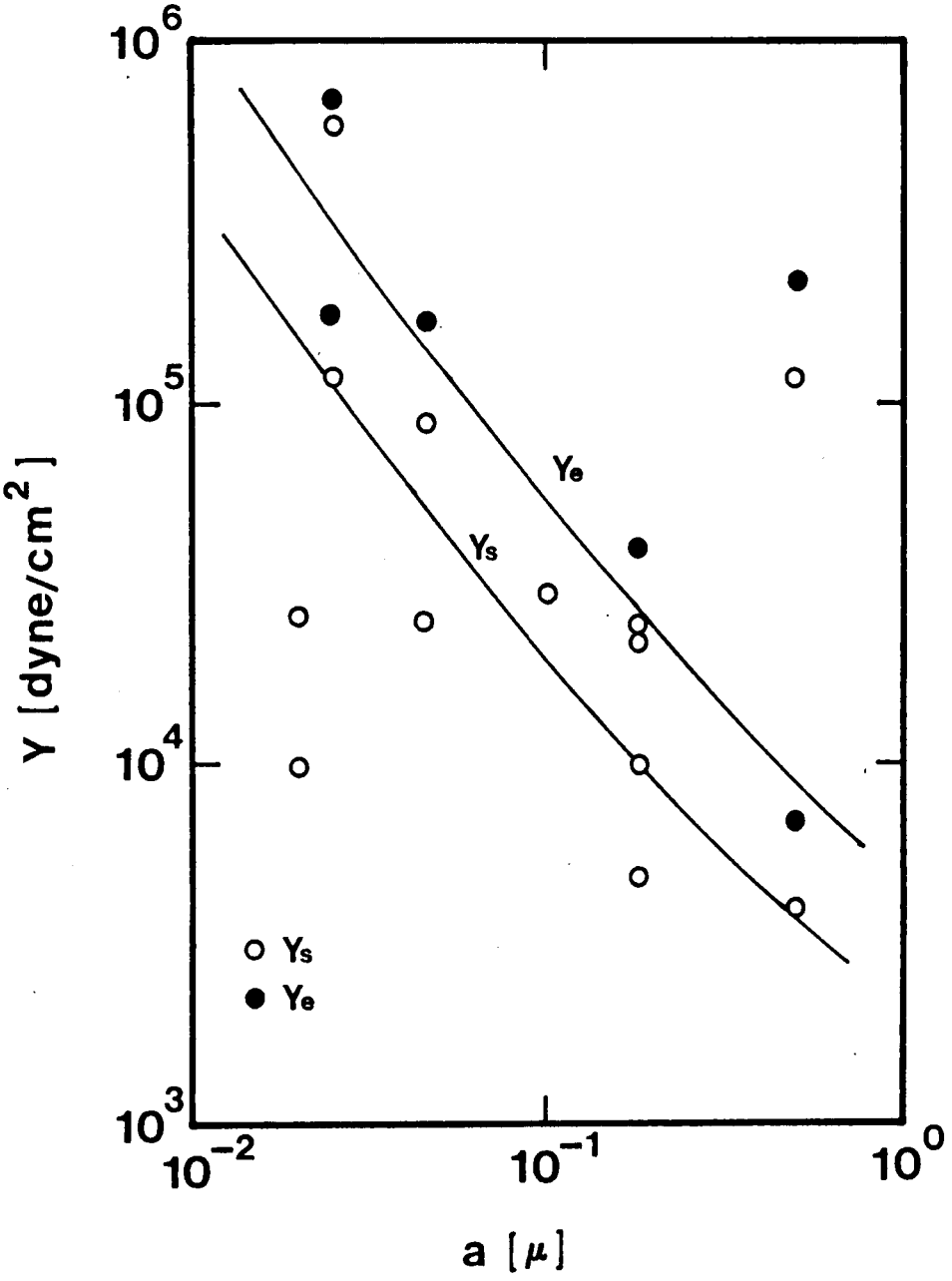

Figure VII.5. Empirical Correlations Between Yield Stress and Particle Size.

results suggest the yield values of these polymer melt systems obey von Mises yield criterion as determined by Equation II.50.

A theoretical interpretation of the von Mises yield criterion has been given by Hencky (87), who has shown it is equivalent to a critical distortional strain energy. From such a point of view, the existence of the von Mises yield criterion is of interest. It seems a reasonable criterion for the break up of a gel due to interparticle forces. This suggests the yield stress is related to the particle-particle interaction energy per unit volume. In addition, we note that phenomenological constitutive equation proposed by White (217) is based on the von Mises yield criterion.

However, as seen from comparison between Equation II.50 and Equation II.52, it is very rash to conclude which criterion would be satisfied in yielding of these systems from results of only two types of flow. In order to determine a reliable yield surface, we need very accurate experimental data and additional information on other types of flow.

Figure VII.5 suggests that yield stresses are strongly dependent upon particle size. The curves obtained represent empirical correlations between yield stress and particle size, and are approximately inversely proportional. In addition, Y_e is always greater than Y_s, and seems to be approximately equal to $\sqrt{3}\, Y_s$.

B. Comparison of Mechanistic Theory with Experiment

From the view of structure and mechanism of concentrated suspensions of small rigid particles a theory for shear viscosity was proposed in Chapter III. In this section, we try to make a quantitative comparison of the experimental data with the theory with respect to yield stress and viscosity-shear rate behavior.

B.1. Yield Stress

We must first discuss the values of the system parameters. Since PS is a nonpolar polymer and rigid particles used here are considered noncharged particles in PS matrix, the electroviscous effect due to an elastic double layer may be negligible compared to van der Waals effect. As a result, from Equation III.53b, yield stress is given by

$$Y \sim \frac{A}{a^3 y^2} . \qquad \text{(VII.1)}$$

As mentioned in Chapter II, the maximum volume fraction ϕ_m, is dependent on the arrangement of particles, for instance, 0.52 for the simple-cubic array and 0.74 for a cubical or hexagonal closest-packed array.

The influence of loading level on yield stress can be obtained from data for different loading level systems. Our experimental data show $Y(\phi=0.3)/Y(\phi=0.2) = 3.6$ and 2.2 for CB and TiO_2-filled PS, respectively. In addition, Table VII.1 (p. 166) gives $Y(\phi=0.13)/Y(\phi=0.09) = 2.6$ and $Y(\phi=0.25)/Y(\phi=0.2) = 5.0$ in Vinogradov et al. (213) and Lobe and White (131) studies for CB-filled polymer melts, respectively.

Theoretical predictions of the loading level dependence of yield stress give the relationship from calculation using Equation III.53c: $Y(\phi=0.3)/Y(\phi=0.2)$, $Y(\phi=0.25)/Y(\phi=0.20)$, and $Y(\phi=0.13)/Y(\phi=0.09)$ take 3.6, 1.8 and 1.8, respectively, in cubic packing, and 2.3, 1.6 and 1.7 in the hexagonal close packed array. It is difficult to compare between data and the theory without any information about the packing of particles. However, the data would be in good agreement with predictions.

Comparison of the present CB-filled PS data with those of Lobe and White (131) gives information about the effect of particle size on yield values, although the measurement temperature is not quite the same. Table VII.1 (p. 166) gives $Y(0.025\mu)/Y(0.045\mu) = 4.8$ for the same loading level systems, 20% CB-filled PS melts.

With no electroviscous effect, the theory developed in this thesis suggests that yield stress is inversely proportional to the third-power of particle diameter. Therefore, the predicted ratio, $Y(0.025\mu)/Y(0.045\mu)$ is nearly equal to 5.8. An agreement between them is presumed to be satisfactory within experimental error.

As described in Chapter V, surface treatment lowers the yield stress level. The present data for $CaCO_3$-filled PS show that yield value for the treated system is almost 1/30 of that of untreated system.

Surface treatment modifies the interparticle interaction. It would presumably influence on Hamaker's constant A representing van der Waals force constant between two particles, i.e., to lower its value. However, there is no information available for the effect of surface treatment on A. Therefore, no theoretical value can be determined. In any case,

experimental results can be quantitatively explained by reduced Hamaker's constant.

Approximate yield stresses can be calculated using Equation VII.1. Usually, a Hamaker's constant has been reported to be $10^{-12} \sim 10^{-13}$ erg. (73). A comparison between experimental data and calculated values is given in Table VII.2. Although calculations were carried out for both simple cubic and the closest packing, the values obtained are included in the range shown.

Except for the untreated $CaCO_3$-filled system, there seems a good agreement. This system shows a very high yield stress in spite of the large particle size, perhaps other factors as well as van der Waals forces which influence the yield stress should be taken into account.

B.2. Viscosity-Shear Rate Behavior

In Chapter III, we derived an expression for the shear viscosity for concentrated suspensions of small particles using a mechanistic approach. Using a power law approximation as a suspending medium viscosity, we obtained a modified Bingham type equation. In this subsection, a comparison between data and the theory of the viscosity-shear rate behavior will be made.

Figure VII.6 shows η^*, determined by $\eta - \frac{Y}{\dot{\gamma}}$, as a function of shear rate for the systems exhibiting yield stresses. This figure reveals that η^* possesses a definite "Newtonian" value, η_0^* at low $\dot{\gamma}$.

Figure VII.7 plots $\eta^*(\dot{\gamma})/\eta_0^*$ against $\dot{\gamma}$. It would appear that this plot is independent of the fillers used and loading level in the shear rate range studied.

Table VII.2. Comparison of Experimental Yield Stress with Theoretical Value

Systems	Y_{exp} $\left(\frac{dyne}{cm^2}\right)$	Y_{cal} $\left(\frac{dyne}{cm^2}\right)$
PS/CB (0.2)	2.5×10^4	$(0.1 \sim 1.0) \times 10^4$
PS/CB (0.3)	9.0×10^4	$(1.0 \sim 10) \times 10^4$
PS/TiO_2 (0.2)	1×10^4	$(0.01 \sim 0.1) \times 10^4$
PS/TiO_2 (0.3)	2.2×10^4	$(0.1 \sim 1.0) \times 10^4$
PS/untr. $CaCO_3$ (0.3)	12×10^4	$(0.01 \sim 0.1) \times 10^4$

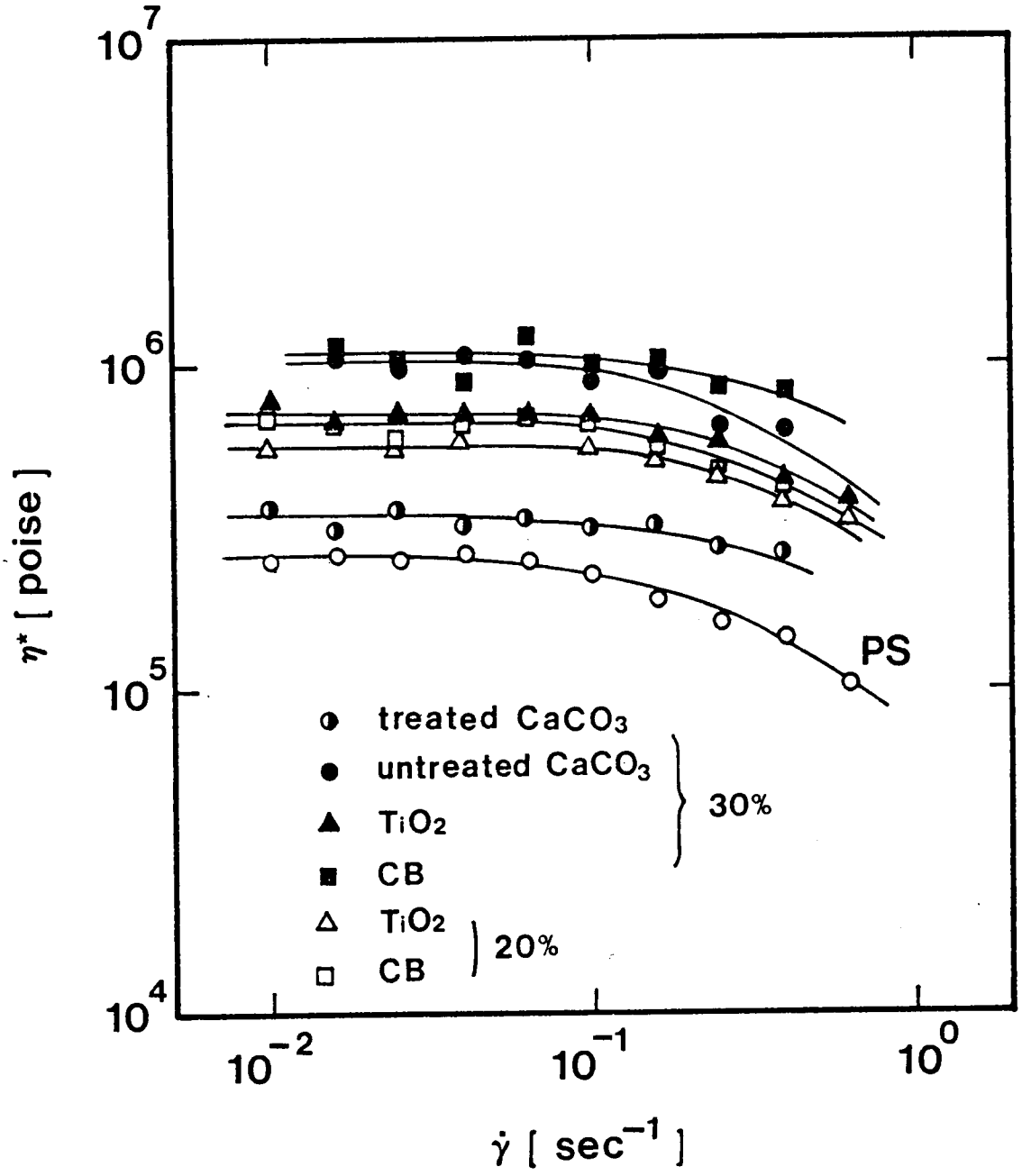

Figure VII.6. Plot of η^* versus Shear Rate for Small Rigid Particle-Filled PS Melts.

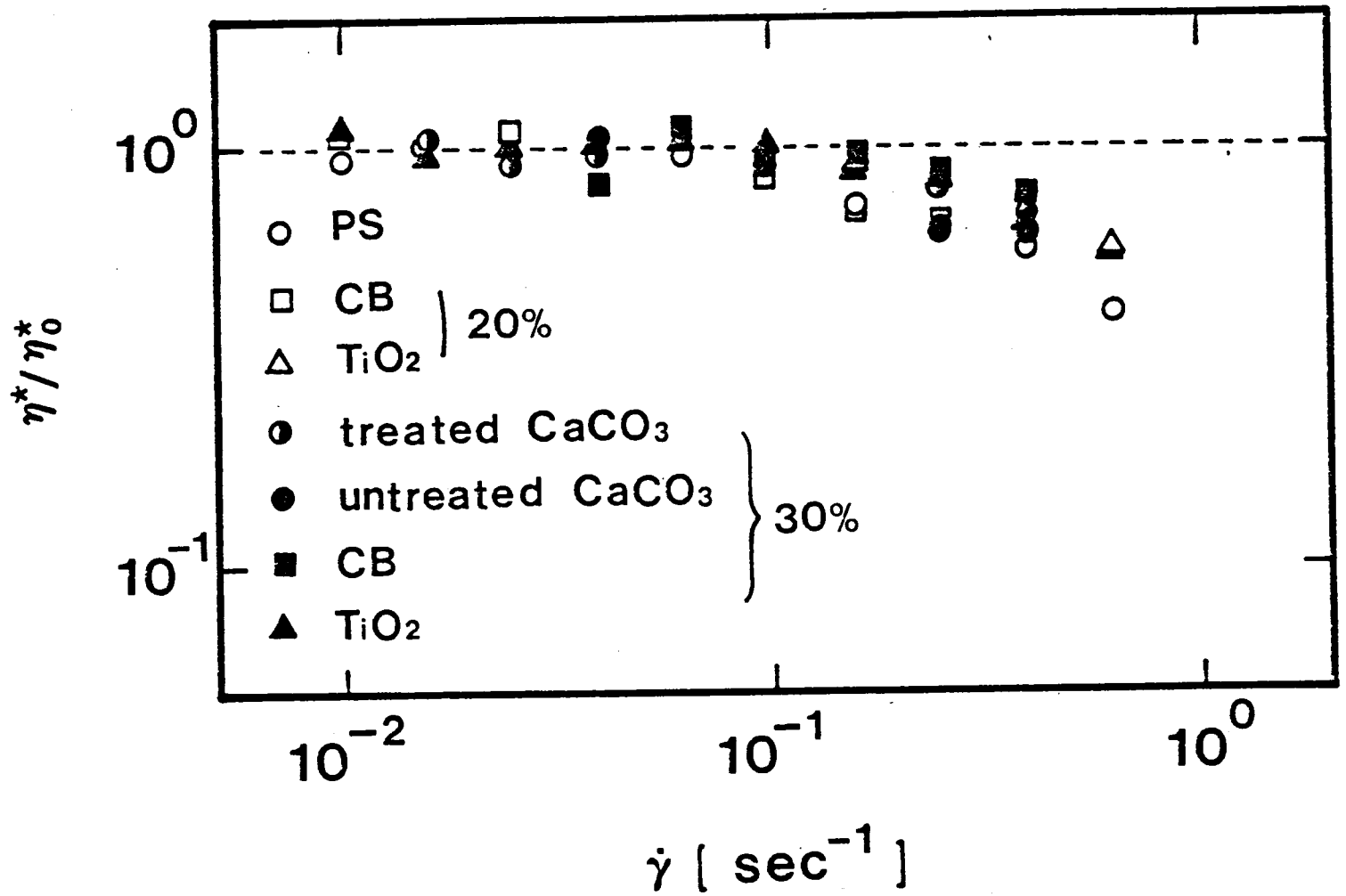

Figure VII.7. Plot of n^*/n_0^* versus Shear Rate for Small Rigid Particle-Filled PS Melts.

Figure VII.8 gives a plot of $\eta^*(\dot{\gamma})/\eta^0(\dot{\gamma})$ versus $\dot{\gamma}$. These values seem to be dependent on loading level and independent of shear rate except treated $CaCO_3$-filled system.

$\eta^*(\dot{\gamma})/\eta^0(\dot{\gamma})$ determined from Fig. VII.8 was plotted against volume fraction in Fig. VII.9. The behavior for $\eta^*(\dot{\gamma})$ giving a definite value at low $\dot{\gamma}$ is the same as for unfilled polymer melts such as PS shown in Fig. VII.6. In other words, $\eta^*(\dot{\gamma})$ seems to be due to pure hydrodynamic interaction. As indicated in Chapter III, the shear viscosity for concentrated suspensions of small particles is considered to be composed of two terms, i.e., hydrodynamic and nonhydrodynamic interaction, Fig. VII.6 may allow us to conclude that the term, $\frac{\gamma}{\dot{\gamma}}$, represents a nonhydrodynamic effect. Therefore, the present experimental data suggest that the proposed form, Equation III.54, would be reasonable.

Results given in Fig. VII.7 may satisfy the relationship expressed by Equation III.56, i.e., $\eta^*(\dot{\gamma})/\eta_0^*$ should be equal to $\eta^0(\dot{\gamma})/\eta_0^0$ independent of shear rate. This agreement between data and the prediction may conclude the correctness of Equation III.53a. In order words, $\eta^*(\phi,\dot{\gamma})$ can be expressed by $\eta^0(\dot{\gamma})f(\phi)$.

This can also be proved in Fig. VII.8. η^*/η^0 is found to be dependent of ϕ, and almost independent of shear rate except for the surface treated $CaCO_3$-filled PS melt.

Thomas (207) has attempted to make a master curve for relationship between relative viscosity and volume fraction for suspensions of spherical particles by removing the effects of particle size and shear rate. He obtained the limiting value for relative viscosity in small

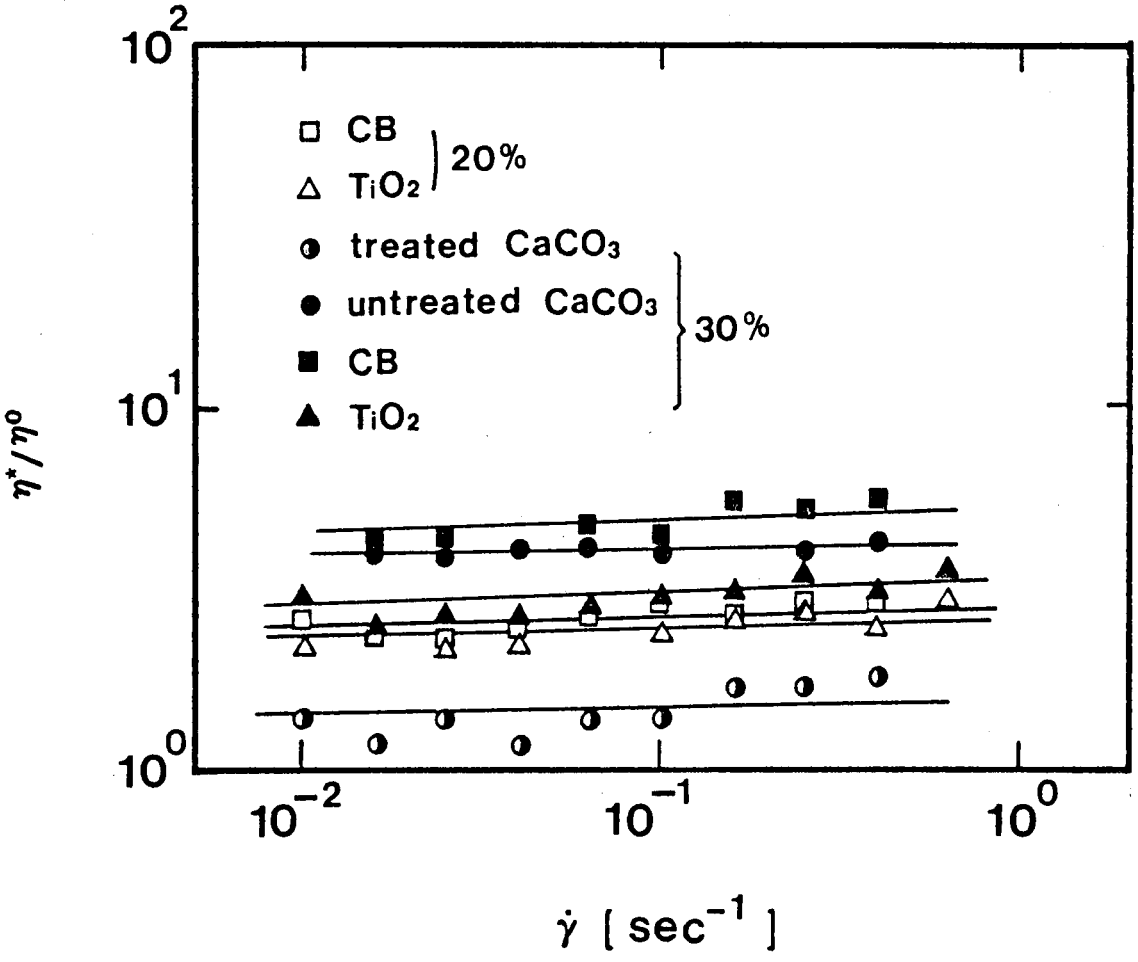

Figure VII.8. Plot of η^*/η^0 versus Shear Rate for Small Rigid Particle-Filled PS Melts.

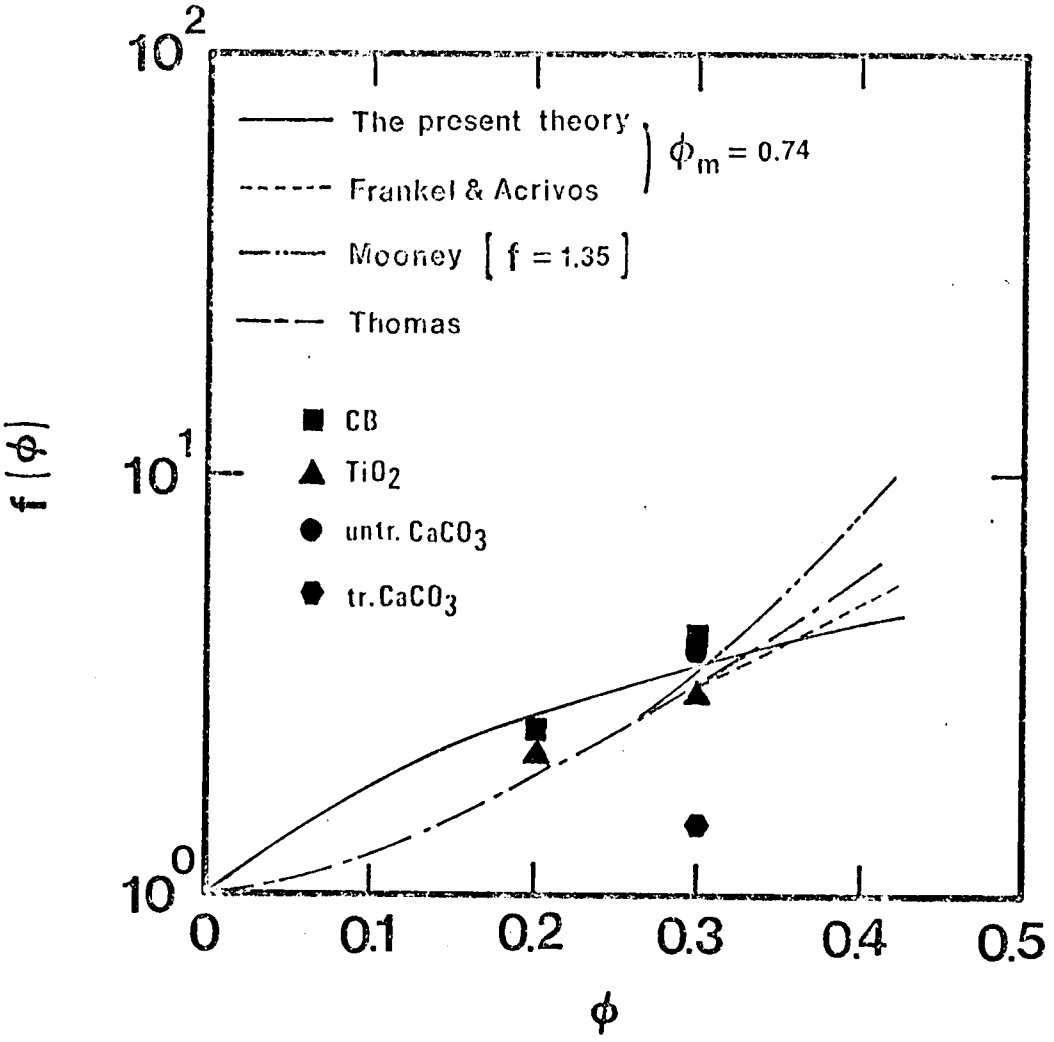

Figure VII.9. $f(\phi)$ as a Function of Volume Fraction of Small Rigid Particles.

particles, from an intercept of the plot of relative viscosity versus $\frac{1}{\dot{\gamma}}$, i.e., $\lim_{\dot{\gamma}\to\infty} \eta/\eta^0$. Since for suspensions of small particles ($a < 1\mu$) particle-particle interaction is dominant at low shear rates, this limiting value corresponds to a purely hydrodynamic contribution to viscosity, which can be dominant at high shear rates. Therefore, if we use the present mechanistic theory, this would become to be

$$\lim_{\dot{\gamma}\to\infty} \eta/\eta^0 = \frac{\eta^*}{\eta^0} = f(\phi) \ . \qquad \text{(VII.2)}$$

The theory developed in Chapter III predicts the volume fraction dependence of η^*/η^0. This is plotted in Fig. VII.9 and compared with our data on different systems. The agreement is satisfactory except for the surface treated $CaCO_3$.

Thomas (207) has proposed for the relative viscosity as a function of ϕ,

$$\eta/\eta^0 = 1 + 2.5\phi + 10.05\phi^2 + 0.00273\, e^{16.6\phi} \ . \qquad \text{(VII.3)}$$

In Fig. VII.9. η^*/η^0 determined from Fig. VII.8, independent of shear rate, is plotted against volume fraction for different systems. As indicated by Equation VII.2, the left side of Equation VII.3 is equivalent to $\lim_{\dot{\gamma}\to\infty} \eta/\eta^0$, i.e., η^*/η^0 in the case of small particles. Thus, a calculated curve from Thomas equation, Equation VII.3, is also shown in Fig. VII.9. In addition, Mooney's empirical equation, Equation II.61, can also be plotted by an empirical parameter $f(1.35 \leq f \leq 1.91)$ being equal to 1.35. Except for the treated $CaCO_3$-filled system, a satisfactory

agreement between data points and calculated curves is obtainable. In the volume fraction range in this figure, there is no distinct difference between both predicted curves. A η^*/η^0 value for the treated $CaCO_3$-filled PS melt appears to be smaller than calculated one from empirical equations.

In the above discussions, we have assumed that the macroscopic shear rate is equivalent to that between particles. However, the latter is in general supposed to be greater than the former (50) (219). If k is a constant greater than unity, η^* should be written as

$$\eta^*(\phi, k\dot{\gamma}) = f(\phi)\ \eta^0(k\dot{\gamma}) \ . \qquad \text{(VII.4)}$$

Then, the shear viscosity of suspensions is

$$\eta(\phi, \dot{\gamma}) = f(\phi)\ \eta^0(k\dot{\gamma}) + \frac{\gamma}{\dot{\gamma}} \ . \qquad \text{(VII.5)}$$

Figure VII.10 plots η^*/η^0 against $\eta_0^*\dot{\gamma}$ for various systems. It seems to give a universal curve independent of the systems within experimental errors except for the PS. This type of plot of composite systems has been discussed by Czarnecki and White (50) for fiber-reinforced polymer melts.

C. Comparison of Phenomenological Theory with Experiment

In a previous section, it was found that the proposed mechanistic theory for suspension viscosity was in a satisfactory agreement with

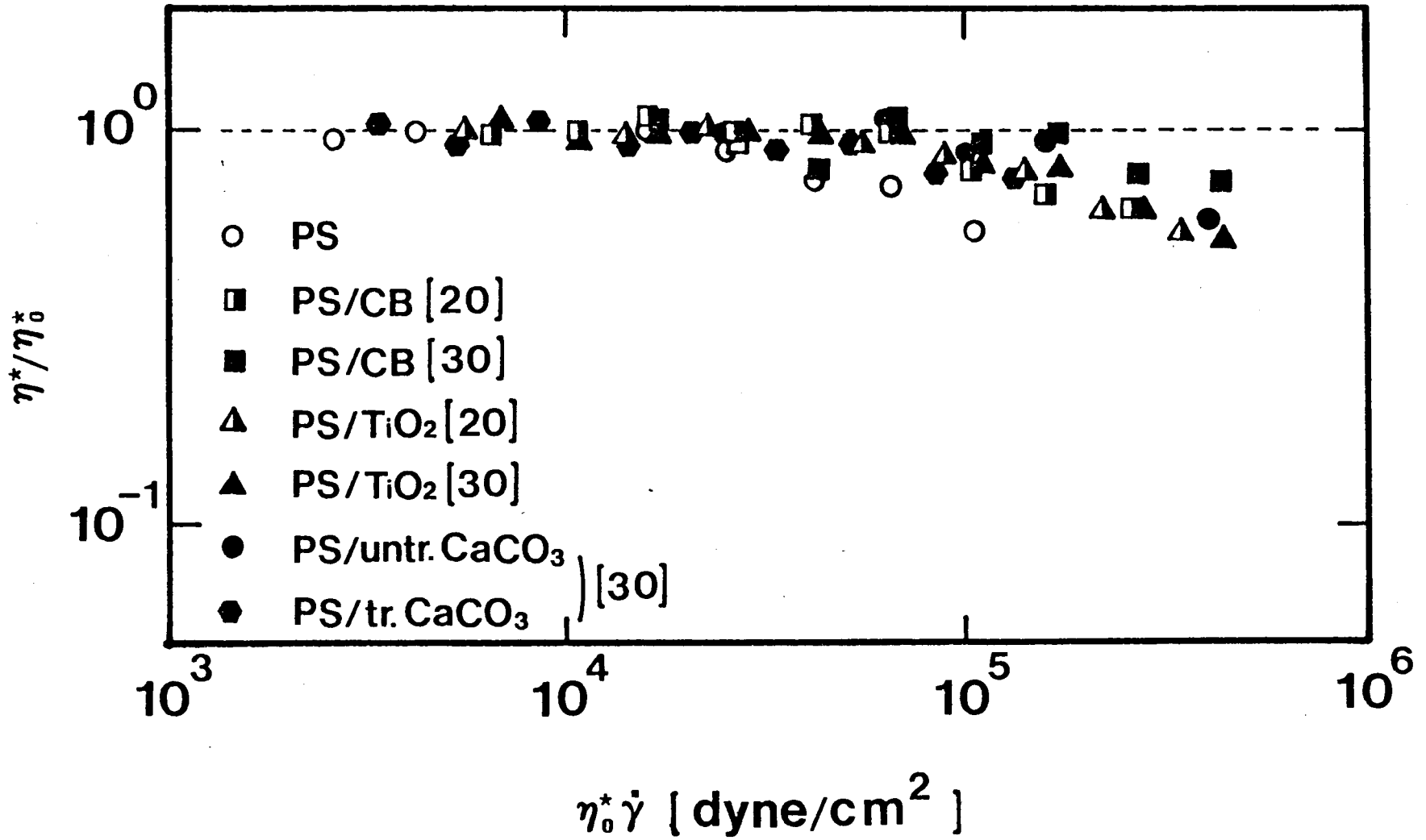

Figure VII.10. η^*/η^0 as a Function of $\eta_0^*\dot{\gamma}$ for Small Particle-Filled PS Melts.

experimental data. Essentially, phenomenological theory must be consistent with the mechanistic theory. Therefore, the deviatoric stress tensor, $\underset{\sim}{P}$ given by Equation II.33b in the limit of yield stress, $Y \to 0$, i.e., the tensor $\underset{\sim}{H}$ representing memory integral should correspond to the stress fields associated with hydrodynamic interactions, depending upon volume fraction of small particles. If we use a one-element Maxwellian memory function, the constitutive equation may be expressed by

$$\underset{\sim}{P}\left(1 - \frac{Y}{II_p^{1/2}}\right) = \int_0^\infty \frac{G(\phi)}{\tau(\phi)} e^{-z/\tau(\phi)} \overline{\underset{\sim}{C}}^{-1} dz \text{ for } II_p \geq Y^2 . \qquad \text{(VII.6)}$$

Assuming

$$G(\phi) = f(\phi)G^0 \qquad \text{(VII.7a)}$$

$$\tau(\phi) = \tau^0(\equiv\tau) \qquad \text{(VII.7b)}$$

where "0" refers to unfilled systems, and $f(\phi)$ denotes the composition dependence of the term η^* in shear viscosity, we obtain the following relationships for $II_p \geq Y^2$,

$$\sigma_{12} = G^0 f(\phi)\tau\dot{\gamma} + \frac{Y}{\sqrt{1 + \frac{4}{3}\tau^2\dot{\gamma}^2}} \qquad \text{(VII.8a)}$$

$$\eta = G^0 f(\phi)\tau + \frac{Y}{\dot{\gamma}\sqrt{1 + \frac{4}{3}\tau^2\dot{\gamma}^2}} \qquad \text{(VII.8b)}$$

$$N_1 = 2G^0 f(\phi)\tau^2\dot{\gamma}^2 + \frac{2\tau Y\dot{\gamma}}{\sqrt{1 + \frac{4}{3}\tau^2\dot{\gamma}^2}} \qquad \text{(VII.8c)}$$

$$\chi = \frac{3G^0 f(\phi)\tau}{(1-2\tau\dot{E})(1+\tau\dot{E})} + \frac{\sqrt{3}\, Y}{\dot{E}} . \qquad \text{(VII.8d)}$$

If we consider a system without a yield value,

$$G^0\tau = \eta^0(\dot{\gamma}) \qquad \text{(VII.9a)}$$

$$2G^0\tau^2\dot{\gamma}^2 = N_1{}^0(\dot{\gamma}) \qquad \text{(VII.9b)}$$

$$\frac{3G^0\tau}{(1-2\tau\dot{E})(1+\tau\dot{E})} = \chi^0(\dot{E}) \qquad \text{(VII.9c)}$$

and assume the following equations

$$\eta^*(\phi,\dot{\gamma}) = \eta^0(\dot{\gamma})f(\phi) = G(\phi)\tau \qquad \text{(VII.10a)}$$

$$N_1^*(\phi,\dot{\gamma}) = N_1{}^0(\dot{\gamma})f(\phi) = 2G(\phi)\tau^2\dot{\gamma}^2 \qquad \text{(VII.10b)}$$

$$\chi^*(\phi,\dot{E}) = \chi^0(\dot{E})f(\phi) = \frac{3G(\phi)\tau}{(1-2\tau\dot{E})(1+\tau\dot{E})} \qquad \text{(VII.10c)}$$

finally for $II_p \geq Y^2$ we obtain,

$$\sigma_{12} = \eta^*\dot{\gamma} + \frac{Y}{\sqrt{1 + \frac{4}{3}\tau^2\dot{\gamma}^2}} \qquad \text{(VII.11a)}$$

$$\eta = \eta^* + \frac{Y}{\dot{\gamma}\sqrt{1 + \frac{4}{3}\tau^2\dot{\gamma}^2}} \qquad \text{(VII.11b)}$$

$$N_1 = N_1^* + \frac{2\tau Y\dot{\gamma}}{\sqrt{1 + \frac{4}{3}\tau^2\dot{\gamma}^2}} \qquad \text{(VII.11c)}$$

$$\chi = \chi^* + \frac{\sqrt{3}\,Y}{\dot{E}} . \qquad \text{(VII.11d)}$$

In these equations, the first and second terms in the right side represent hydrodynamic and particle-particle interaction, respectively. At low shear rate region, Equation VII.11b is equivalent to that obtained from the mechanistic theory, i.e., Equation III.54 because $\sqrt{1 + \frac{4}{3}\tau^2\dot{\gamma}^2} \approx 1$.

Following the form of Bogue and White (25) given by Equation II.13b, Ide and White (101) proposed

$$\tau = \frac{\tau_0}{1 + a\tau_0\langle II_d^{1/2}\rangle} \qquad \text{(VII.12)}$$

for τ in a one-element Maxwell model, where τ_0 is a zero shear relaxation time. In the case of constant deformation rate, the above equation reduces to

$$\tau = \frac{\tau_0}{1 + a\tau_0\dot{\gamma}} \quad \text{for shear flow} \qquad \text{(VII.13a)}$$

$$\tau = \frac{\tau_0}{1 + a\sqrt{3}\,\tau_0\,\dot{E}} \quad \text{for elongational flow .} \qquad \text{(VII.13b)}$$

In a one-element Maxwell model, τ is equal to a characteristic relaxation time, $\bar{\tau}$ defined by

$$\bar{\tau} = \frac{N_1}{2\eta\dot{\gamma}^2} = \frac{\bar{\tau}_0}{1 + a\bar{\tau}_0\dot{\gamma}} \qquad \text{(VII.14)}$$

where $\bar{\tau}_0$ is a zero shear characteristic relaxation time.

In our comparison between the theory and experiments, we will use $\eta(\dot{\gamma})$ and $N_1(\dot{\gamma})$ of the matrix PS melt to predict the behavior of $\eta(\dot{\gamma})$, $N_1(\dot{\gamma})$ and $\chi(\dot{E})$ of the filled melts.

The zero shear viscosity, η_0 has the value 2.6×10^5 poise. Figure VII.11 shows a plot of $\frac{N_1}{2\eta\dot{\gamma}^2}$ or $\bar{\tau}$ versus $\dot{\gamma}$ for the matrix PS melt. If we assume that $\bar{\tau}_0$ can be approximated by $\bar{\tau}$ at low $\dot{\gamma}$, for example, 0.01 sec^{-1}, we obtain $\bar{\tau}_0 = \tau_0 = 4$ sec, therefore $G^0 = 6.5 \times 10^4$ $dyne/cm^2$ from Equation VII.9a.

The function, $f(\phi)$, representing the composition dependence of shear viscosity term, η^*, can be obtained from Fig. VII.9 (p. 177).

Theoretical values were calculated for two cases: a = 0.4 and a = 1.0. The results are shown in Fig. VII.12 to Fig. VII.14 for shear viscosity, elongational viscosity and normal stress.

Good agreement between data and prediction is observable for a = 0.4 in η and for a = 1.0 in χ. The plot of N_1 vs. σ_{12} seems not sensitive to "a". Therefore, the "a" value for a best fit is probably between 0.4 and 1.0.

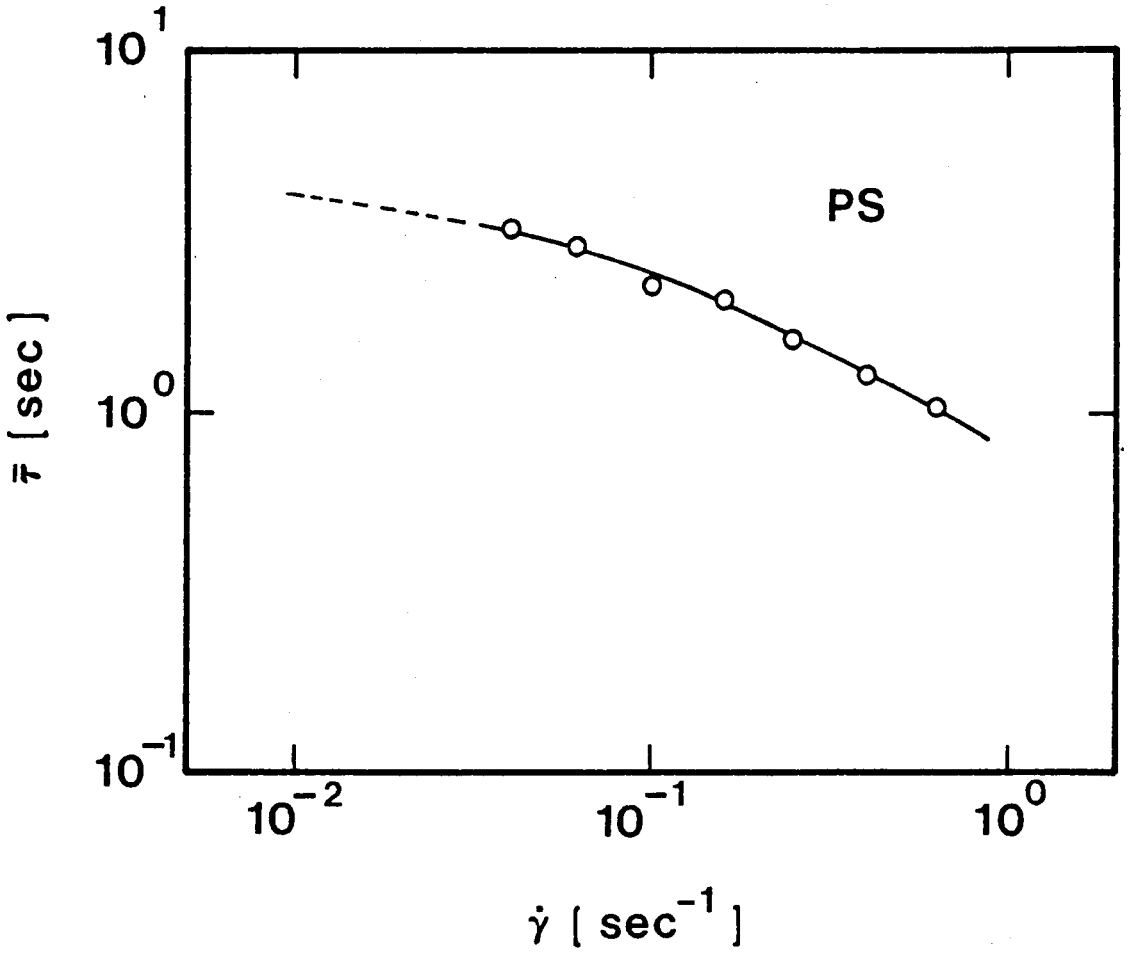

Figure VII.11. Characteristic Relaxation Time as a Function of Shear Rate for Matrix PS Melt.

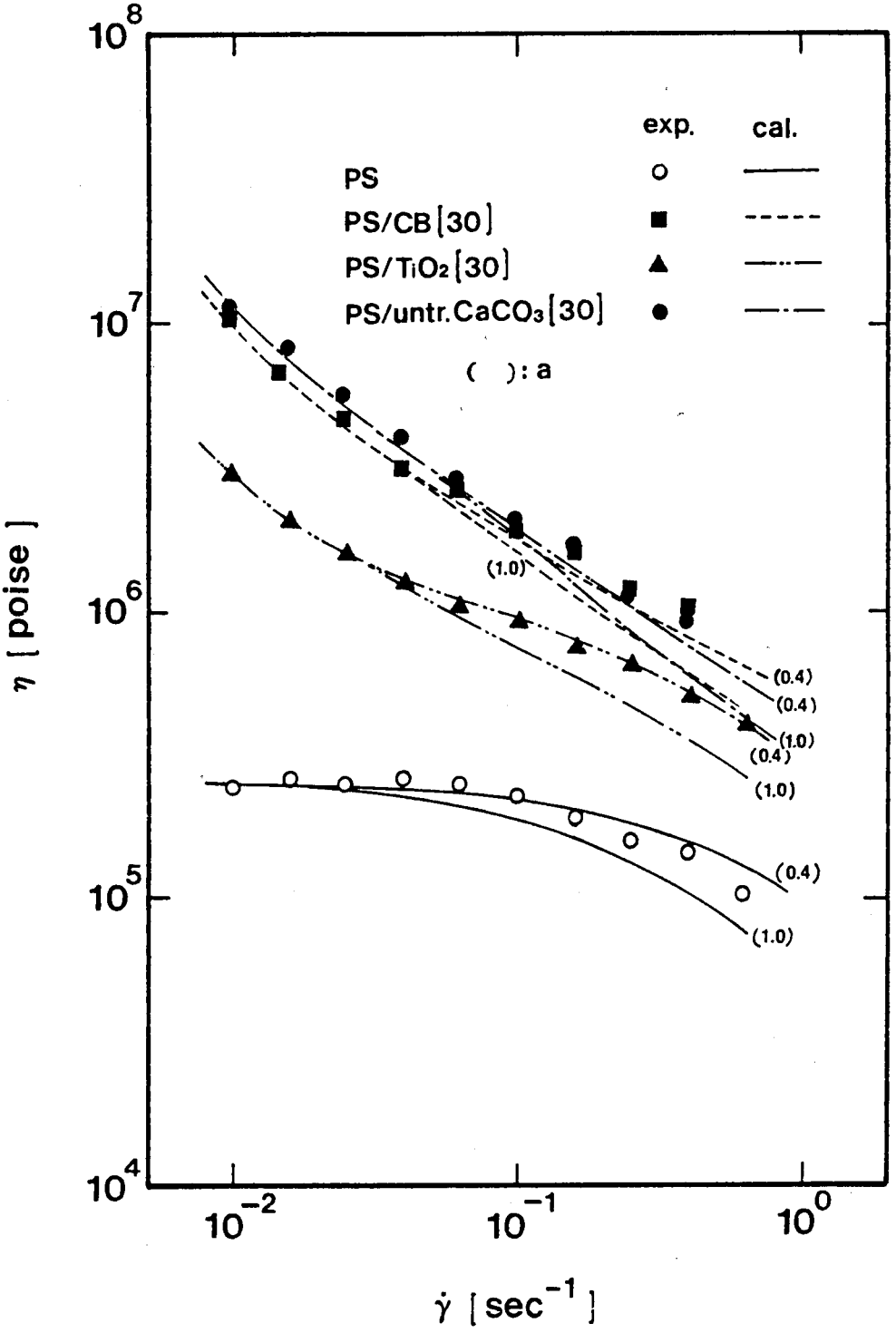

Figure VII.12. Comparison of Experimental Data with Phenomenological Theory for Plot of Shear Viscosity versus Shear Rate.

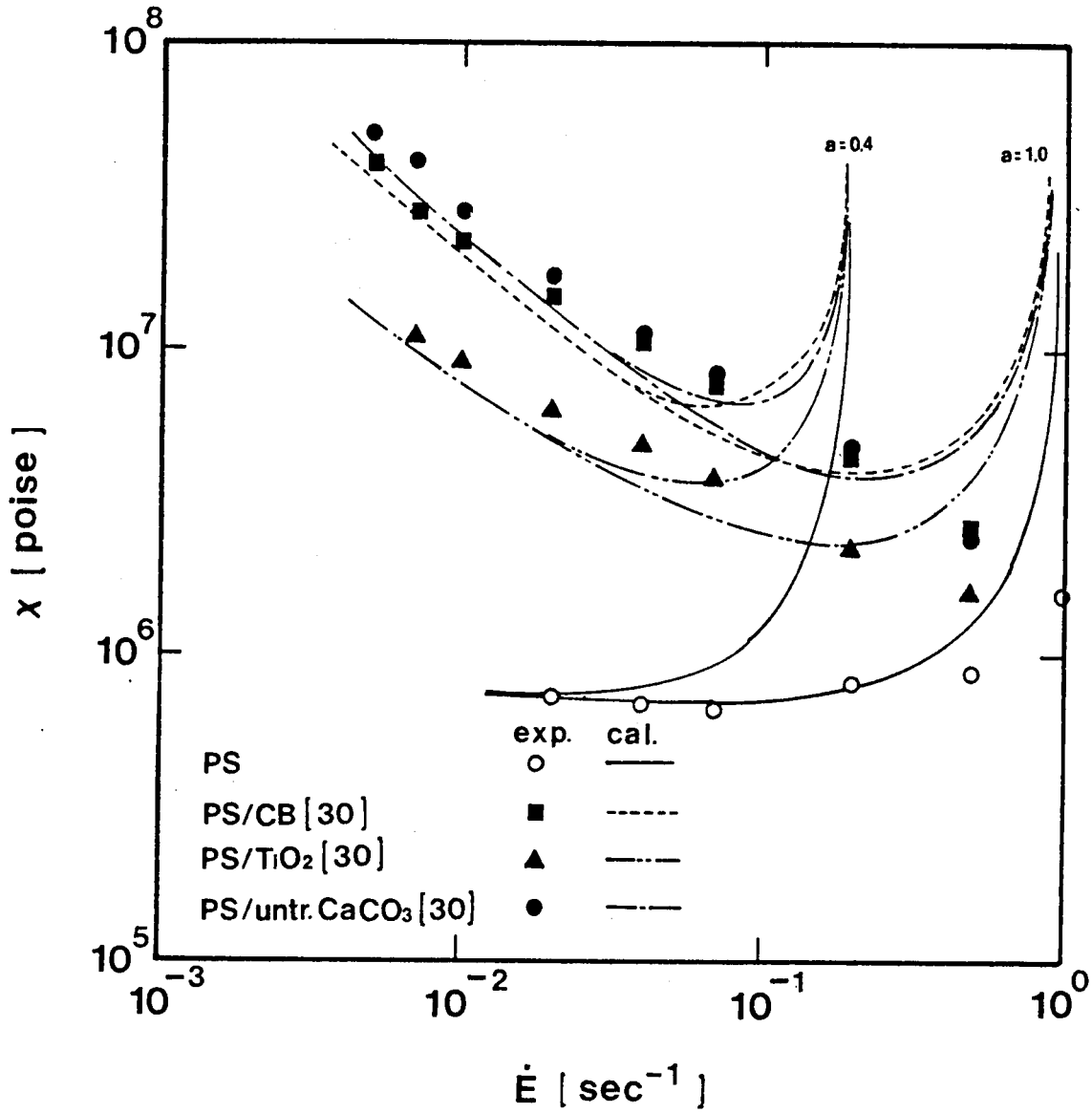

Figure VII.13. Comparison of Experimental Data with Phenomenological Theory for Plot of Elongational Viscosity versus Elongational Rate.

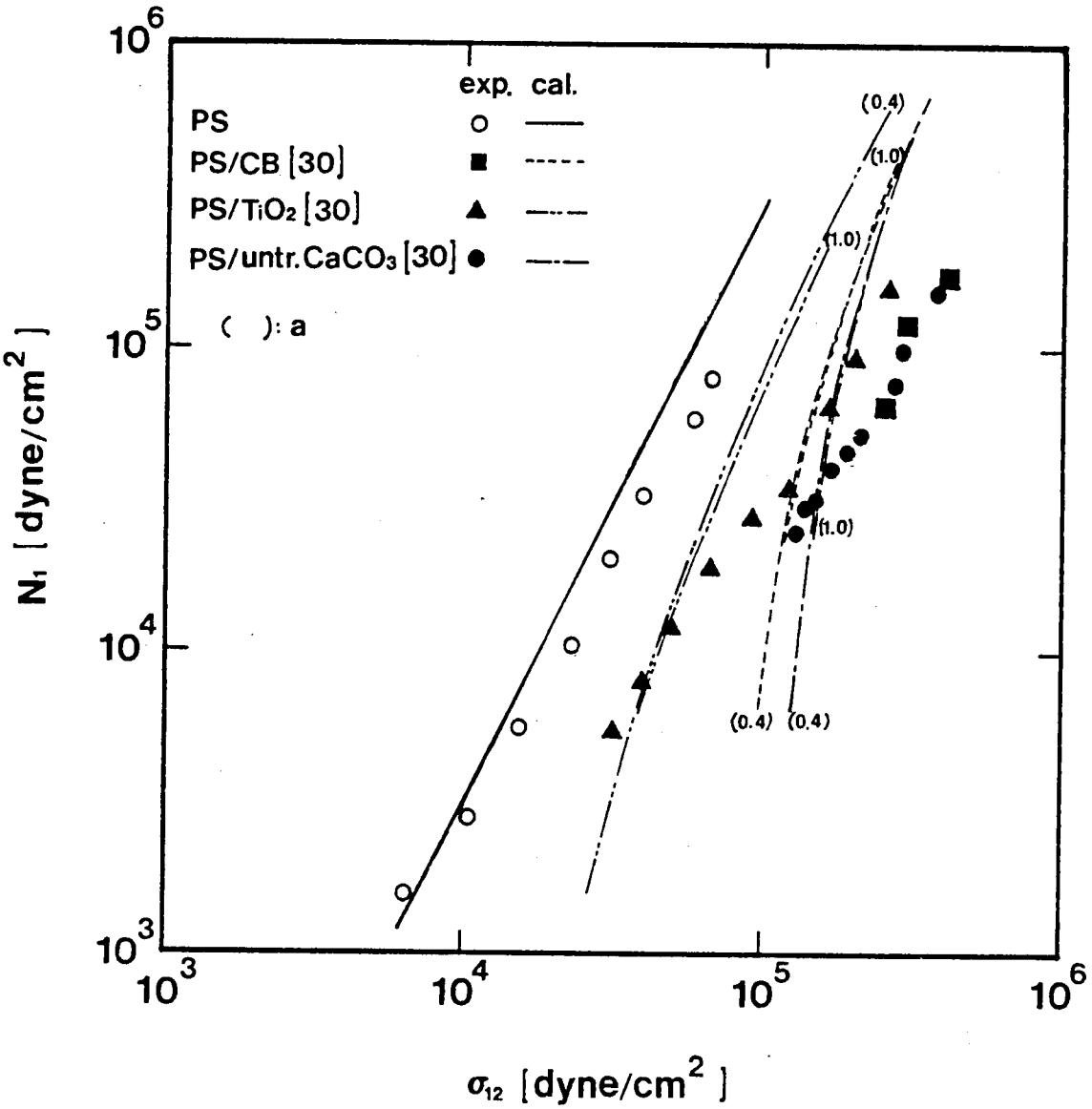

Figure VII.14. Comparison of Experimental Data with Phenomenological Theory for Plot of First Normal Stress Difference versus Shear Stress.

A theoretical curve for elongational viscosity shows that it goes to infinity at $\dot{E} = \frac{1}{(2-a\sqrt{3})\tau_0}$. As a result, the present phenomenological theory using a one-element Maxwellian memory function does not predict correctly the elongational viscosity at high $\dot{E}$, but it gives a satisfactory agreement with data at low $\dot{E}$.

In normal stress $\sim$ shear stress relationship there are some discrepancies between data and the theory for filled systems. Experimental data show lower N_1 at high σ_{12} compared with predicted values. Also, a yield value is not clear. These are presumed to be due to difficulty in normal stress measurement for highly-filled systems as mentioned in Chapter V.

As discussed in the section of mechanistic theory, the actual shear rate between particles is higher than the macroscopic value. This makes $\tau(\dot{\gamma})$ lower than it should be. This trend was argued by White and Crowder (219), who report that the deformation rates in the matrix surrounding small particles are more severe than the averaged behavior of the entire composite system. Therefore, Equation VII.10 should be rewritten as follows, similarly to Equation VII.4,

$$N_1^*(\phi, k\dot{\gamma}) = N_1^0(k\dot{\gamma}) f(\phi) \qquad \text{(VII.15a)}$$

$$\chi^*(\phi, k\dot{E}) = \chi^0(k\dot{E}) f(\phi) \qquad \text{(VII.15b)}$$

where $k > 1$. As a result, Equation VII.11 can also be reformulated

$$\sigma_{12} = \eta^*(\phi, k\dot{\gamma})\dot{\gamma} + \frac{Y}{\sqrt{1 + \frac{4}{3}\tau^2(k\dot{\gamma})\dot{\gamma}^2}} \tag{VII.16a}$$

$$\eta = \eta^*(\phi, k\dot{\gamma}) + \frac{Y}{\dot{\gamma}\sqrt{1 + \frac{4}{3}\tau^2(k\dot{\gamma})\dot{\gamma}^2}} \tag{VII.16b}$$

$$N_1 = N_1^*(\phi, k\dot{\gamma}) + \frac{2\tau(k\dot{\gamma})Y\dot{\gamma}}{\sqrt{1 + \frac{4}{3}\tau^2(k\dot{\gamma})\dot{\gamma}^2}} \tag{VII.16c}$$

$$X = \chi^*(\phi, k\dot{E}) + \frac{\sqrt{3}\,Y}{\dot{E}} . \tag{VII.16d}$$

From the following relationships for pure matrix PS melt

$$\eta^0(k\dot{\gamma}) < \eta^0(\dot{\gamma}) \tag{VII.17a}$$

$$N_1^0(k\dot{\gamma}) > N_1{}^0(\dot{\gamma}) \tag{VII.17b}$$

$$\chi^0(k\dot{E}) > \chi^0(\dot{E}) \tag{VII.17c}$$

$$\tau(k\dot{\gamma}) < \tau(\dot{\gamma}) \tag{VII.17d}$$

the actual predicted values are larger for elongational viscosity and normal stress, and smaller for shear viscosity than the phenomenological theory developed here.

In the above discussions, rheological theories derived from both mechanistic and phenomenological approach which are consistent with

each other were found to be in an almost good agreement with experimental data. Here, a mechanism for flow behavior of these systems is proposed. Nonhydrodynamic particle-particle interaction such as van der Waals and electrostatic force is significantly important at low stress level. This results in the formation of a gel structure associated with a yield stress. Therefore, the yield stress is related to the interparticle interaction depending upon particle characteristics loaded. The gel formed is disrupted if a distortional strain energy stored in the material reaches a certain critical value. After break-up, the systems behave as viscoelastic fluids in which purely hydrodynamic interaction mainly depending upon volume fraction of fillers is dominant.

CHAPTER VIII

MELT SPINNING

A. Introduction

We often make use of polymer processing techniques based on uniaxial elongational flow, for example, melt spinning, flat film extrusion, extrusion coating and so on. Filled and rubber modified polymers are widely used in these processing fields.

As a simple version of these processing techniques, we investigate melt spinning here. In this chapter, we study both stable and unstable spinline behavior during isothermal melt spinning, and determine the spinline elongational viscosity. Then, unstable spinline behavior during nonisothermal conditions is investigated.

B. Spinline Elongational Viscosity During Isothermal Melt Spinning

B.1. Results

Isothermal melt spinning experiments were carried out for PS, HIPS and HDPE/PS blend samples. However, the last systems showed too high tension to be measured by a 10 gm full scale tensiometer in a stable spinline region. As a result, the spinline elongational viscosity was determined only for PS and HIPS samples. The experiments were carried out at draw ratio, v_L/v_0 of 1.68 through a distance of about 60 cm.

A "k" value in Equation IV.19, representing friction between thread and the two teflon rods, was determined by the calibration method described previously (152). It was 0.71 for all samples except HIPS-C for which it was 0.76. As a result, the following values as a take-up force, F_L were obtained: 1.41 gm (1.38×10^3 dyne) for PS, 1.17 gm (1.15×10^3 dyne) for HIPS-A, 1.22 gm (1.20×10^3 dyne) for HIPS-B and 1.63 gm (1.60×10^3 dyne) for HIPS-C.

Next, F_{drag} and F_{inert} were calculated. F_{drag} was approximately 1.7 dyne and 3.8 dyne between fiber and water, and between fiber and air, respectively. F_{inert} was of order 1.2×10^{-3} dyne.

Figure VIII.1 shows a typical photograph of the spinline during isothermal melt spinning. Using the diameter distribution along spinline, F_{grav} was calculated from Equation IV.14. It is of order 3.4 to 5.1 dyne at 1 mm from the die exit, its maximum value. Therefore, F_{drag}, F_{inert} and F_{grav} can be neglected compared with F_L.

Figure VIII.2 and Fig. VIII.3 show profiles of fiber diameter and fiber velocity along spinline, respectively. Also Fig. VIII.4 gives the profiles of elongational rate. Finally, the spinline elongational viscosity is shown as a function of elongational rate in Fig. VIII.5.

Figure VIII.6 shows a comparison between steady state elongational viscosity obtained in Chapter VI and the spinline elongational viscosity. This figure reveals that spinline viscosity is much higher than the steady state viscosity in magnitude especially at low deformation rates. In the HIPS samples, the spinline elongational viscosity decreases rapidly with elongational rate. As compared with this, the steady state

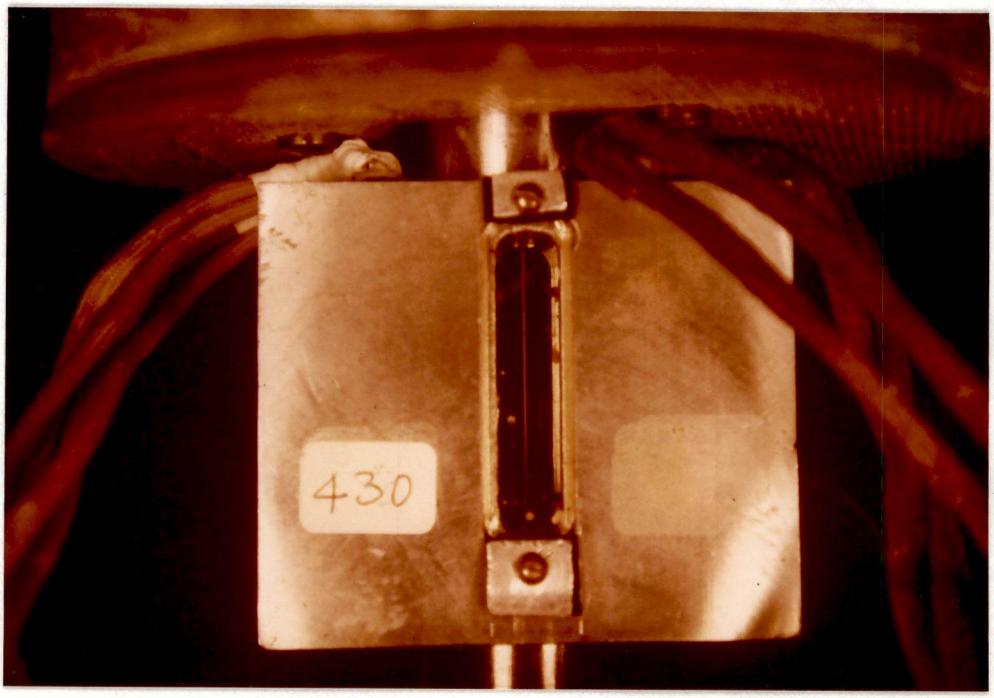

Figure VIII.1. Typical Photograph of the Spinline During the Isothermal Melt Spinning for HIPS-A.

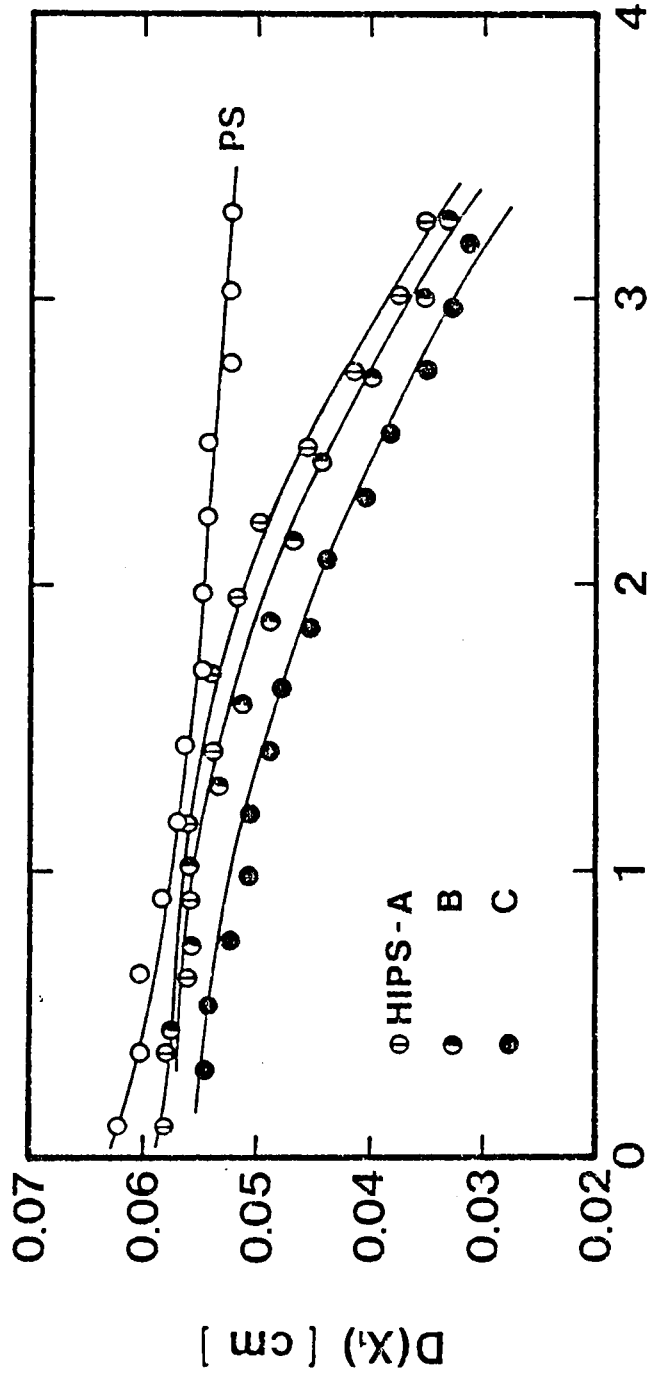

Figure VIII.2. Profiles of Fiber Diameter along Spinline for HIPS under Isothermal Conditions.

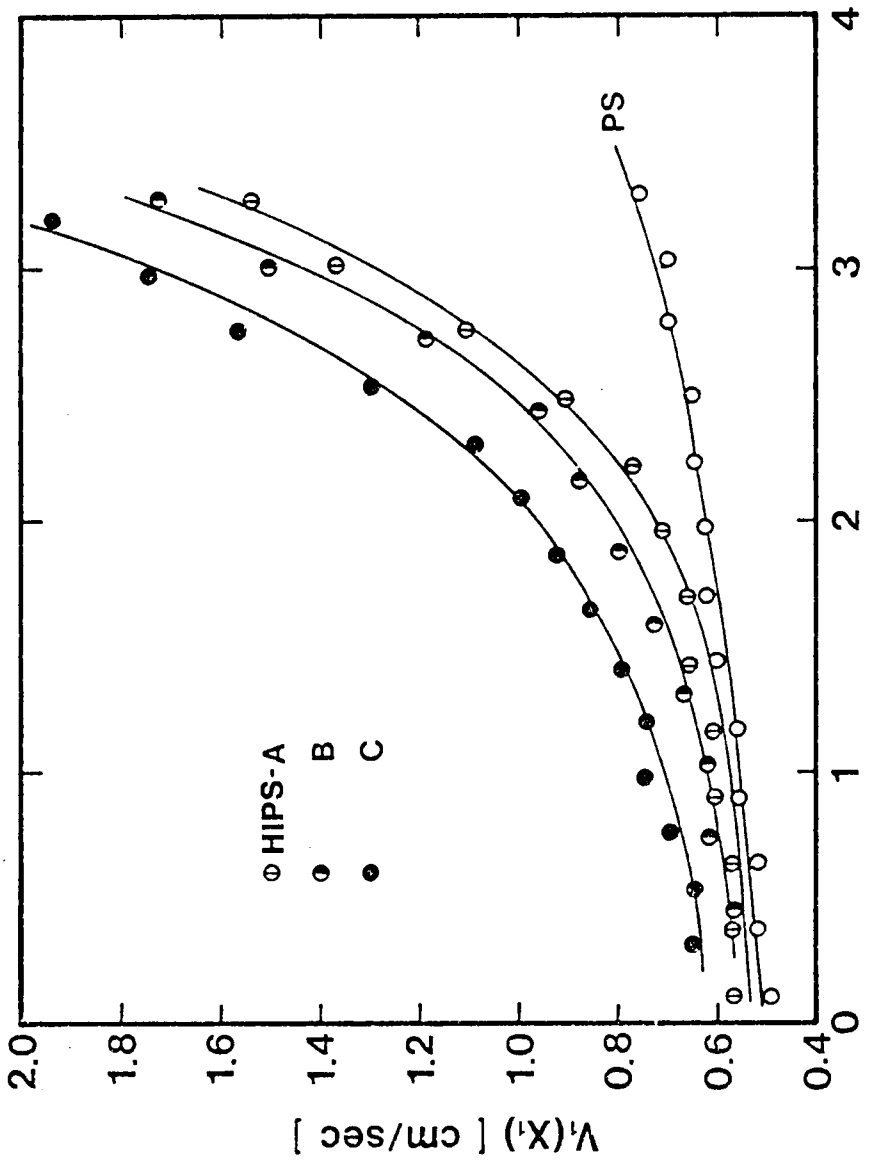

Figure VIII.3. Profiles of Fiber Velocity along Spinline for HIPS under Isothermal Conditions.

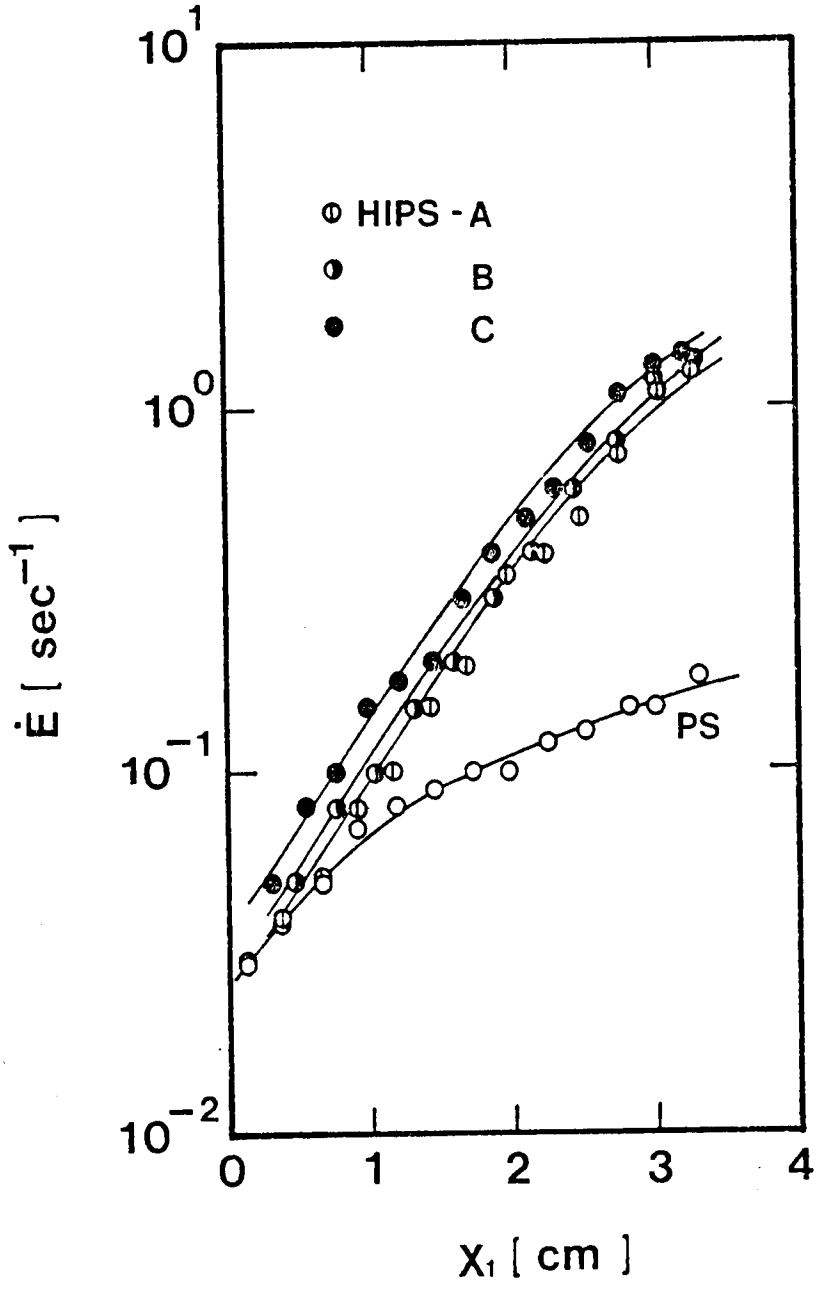

Figure VIII.4. Profiles of Elongational Rate along Spinline for HIPS under Isothermal Conditions.

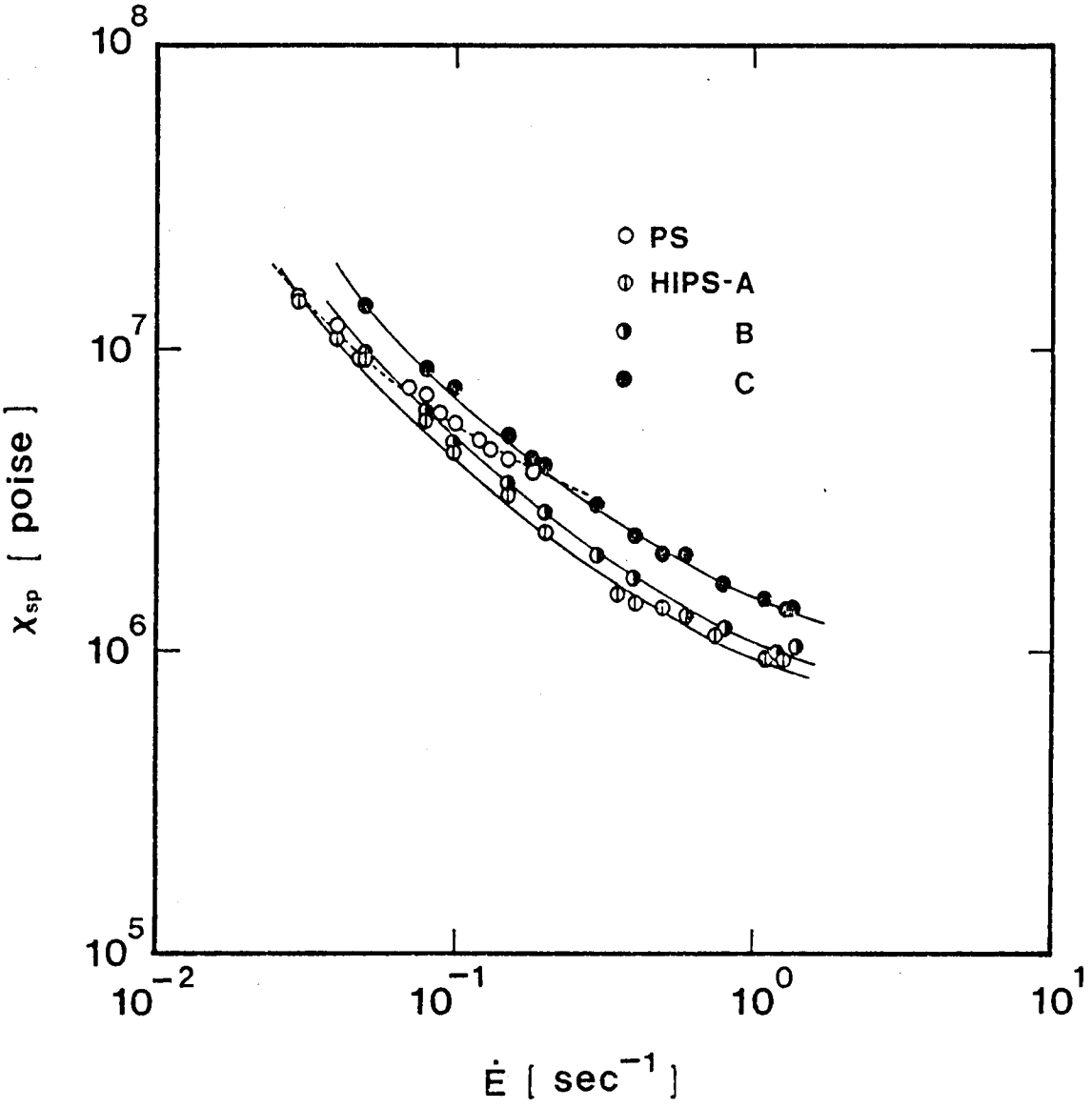

Figure VIII.5. Spinline Elongational Viscosity as a Function of Elongational Rate for HIPS.

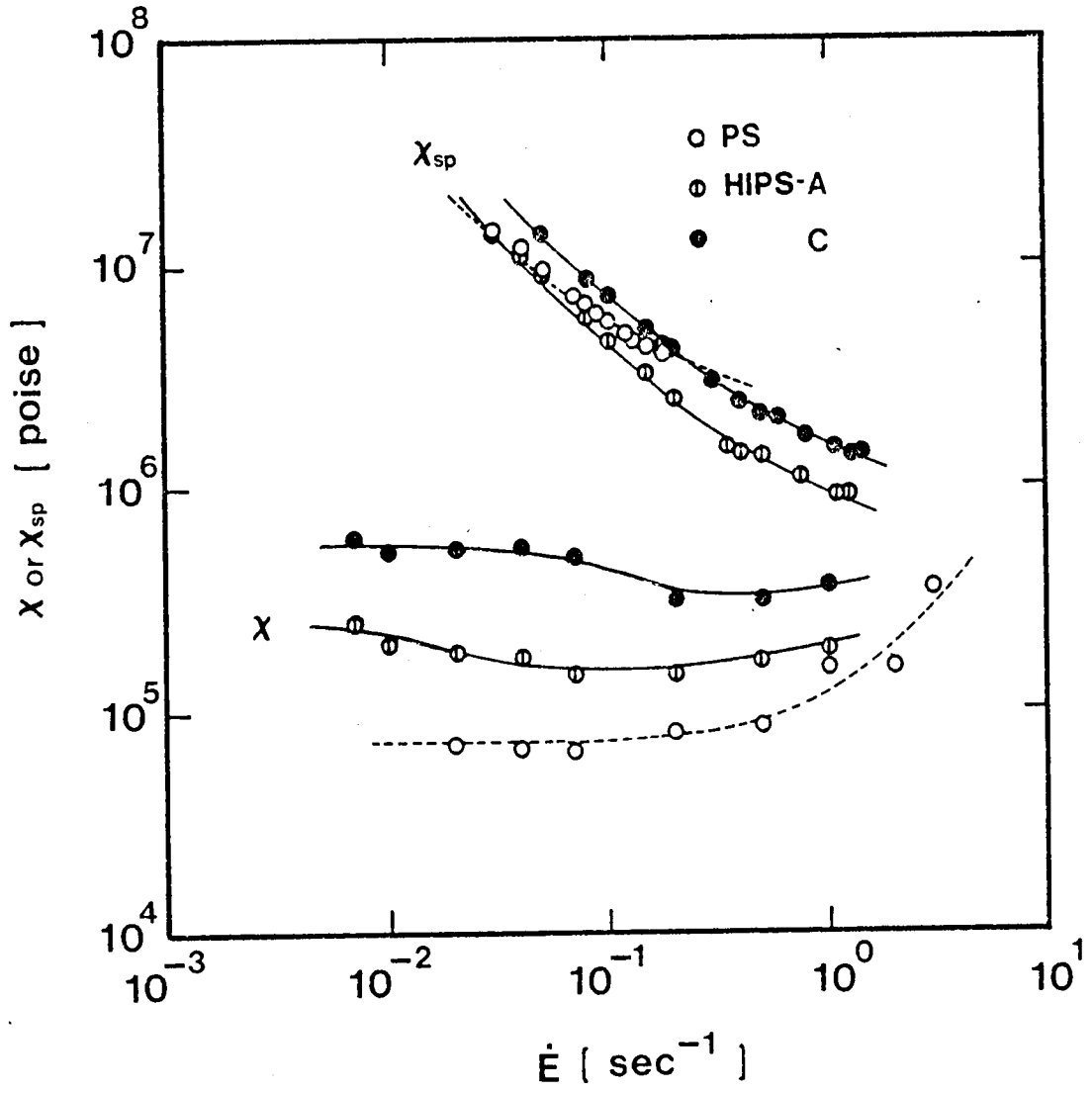

Figure VIII.6. Comparison of Spinline Elongational Viscosity with Steady State Elongational Viscosity for HIPS.

elongational viscosity tends to decrease more slowly with elongational rate.

B.2. Discussion

It can be seen that HIPS fiber has a quite different profile from that of PS at a distant position from the die exit. It shows a more striking decrease in diameter and a more rapid increase in velocity along the spinline can be observed. This behavior may be more distinctly in the profiles of elongational rate. In the case of HIPS, elongational rate increases more rapidly along the spinline compared with PS, i.e., the deformation rate is very nonuniform along spinline.

In the present systems the spinline elongational viscosity may be seen to be a decreasing function of elongational rate. It should be noted that the rate of decrease with elongational rate for HIPS is more rapid than for PS. In the case of PS, the values are presumed to approach a constant at high elongational rate. This behavior has been reported by several investigators (1) (80).

A similar effect of small particles in decreasing the rate of change of the spinline elongational viscosity of a polypropylene melt has been reported for $CaCO_3$-filled polypropylene by Han and Kim (77).

Comparison of Fig. VIII.4 and Fig. VIII.5 reveals that in the case of HIPS the spinline elongational viscosity decreases rapidly with elongational rate which increases along the spinline. In contrast to this, the spinline elongational viscosity of PS decreases slowly with spinline position. These differences are presumably reflected in spinline stability characteristics as discussed later.

It should be mentioned that the spinline elongational viscosity probably has complex effects of prehistory in both the die region and spinline. Rigorously speaking, it is not adequate to correspond the spinline elongational viscosity to steady state one determined from a constant elongational rate experiment.

However, the observed behavior of the spinline elongational viscosity, χ_{sp}, should be similar to that of steady state elongational viscosity, χ. In the present study, χ_{sp} is found to be larger than χ especially at low $\dot{E}$. This trend has also been reported in polypropylene melts (154).

In the case of PS melts reinforced with small particles, the elongational viscosity decreases more rapidly with increasing elongational rate compared with PS melts. This is observed with both χ_{sp} and χ.

C. Draw Resonance Phenomena

Fluctuations of fiber diameter have been studied by many investigators. They may be classified into two types: There are what may be called forced oscillation fluctuations due to random fluctuations in spinline tension, output, cooling conditions, melt temperature, etc., and give small irregularities in diameter occurring at any draw ratio. The second type of diameter fluctuations is the so-called "draw resonance phenomenon" occurring at a critical draw ratio dependent on the rheological properties of polymer melts during melt spinning. Draw resonance shows regular diameter variations. The considerable theoretical

and experimental literature on draw resonance have been reviewed by Petrie and Denn (180).

C.1. Draw Resonance During Isothermal Melt Spinning

C.1.1. Results

Figure VIII.7 shows typical tension fluctuations of a HIPS fiber for both stable and unstable isothermal melt spinning conditions.

Table VIII.1 gives the critical draw ratio, the onset of draw resonance, for PS, HIPS and HDPE/PS blend fibers during isothermal melt spinning. An exact critical draw ratio for HDPE/PS blend systems could not be obtained because of the high levels of spinline tension in the stable region.

C.1.2. Discussion

From Table VIII.1, an incorporation of rubber globules or blending of HDPE to PS decreases a critical draw ratio, that is, tends to make the spinline unstable during isothermal melt spinning. This can be interpreted in terms of elongational viscosity behavior discussed in terms of elongational viscosity behavior discussed in a previous section. In the HIPS, spinline elongational viscosity decreases rapidly with increasing elongational rate which increases quickly along spinline, i.e., the system shows an "elongational rate thinning."

Pearson and Shah (179) (198), Han, Lamonte and Shah (81) and Kase (110) have reported that on the stability of fiber spinning of power law fluids taking into account rate-dependent elongational viscosity behavior.

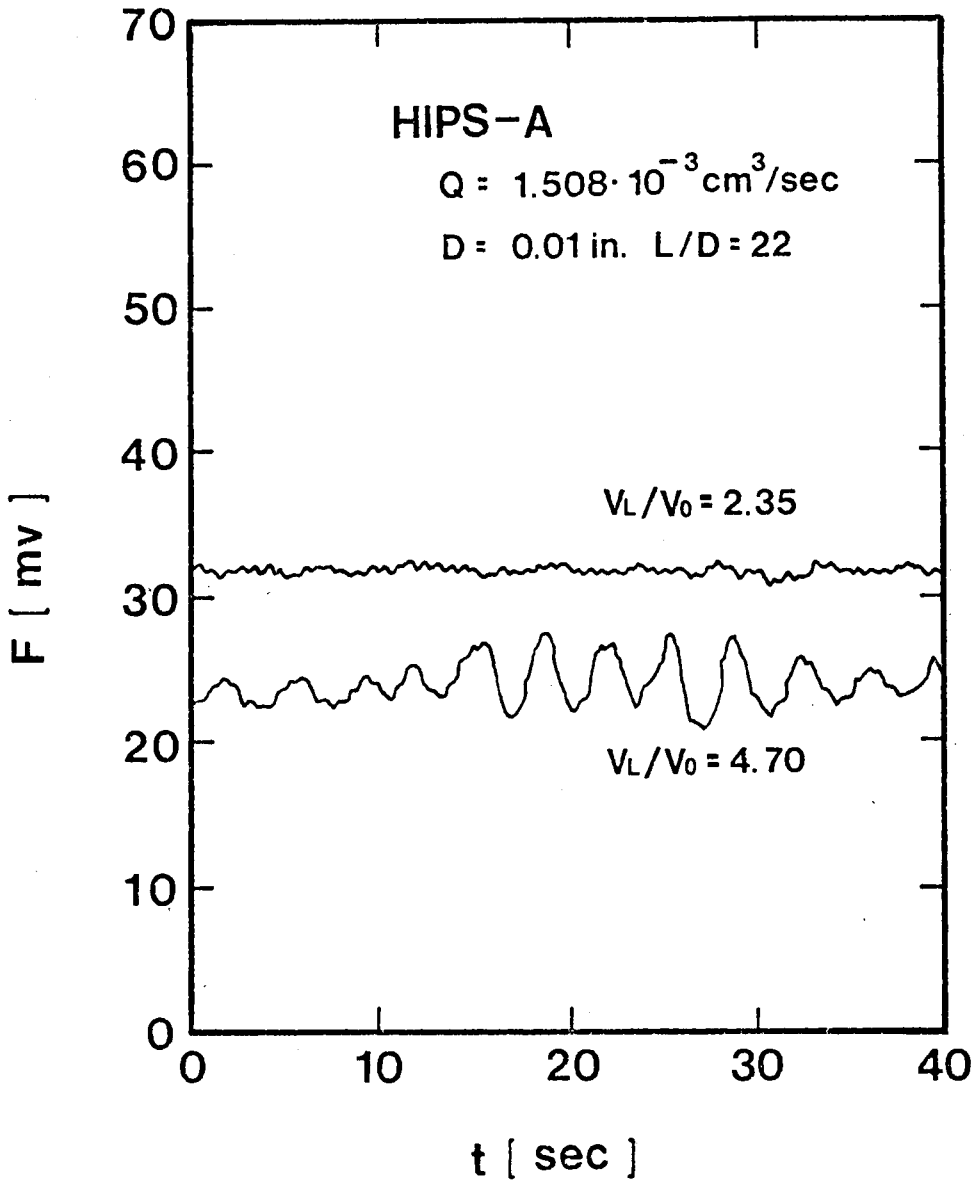

Figure VIII.7. Typical Spinline Tension Variation with Time under Isothermal Conditions for HIPS-A.

Table VIII.1. Critical Draw Ratio During Isothermal Melt Spinning

Sample	Critical Draw Ratio
PS	6.0
HIPS-A	4.7
HIPS-B	2.7
HIPS-C	2.4
PS/HDPE (10%)	1.5>

They point out that "elongational rate thinning" fluids are unstable at smaller draw ratio than "elongational rate thickening" fluids under both isothermal and nonisothermal conditions.

A linear analysis of spinning stability of a viscoelastic fluids has been carried out by Fisher and Denn (60) (61) for an "elongational rate thinning" generalization of the Maxwell fluid in which viscosity obeys a power law.

Using viscoelastic fluid mechanics and the convected Maxwell model, White and Ide (220) have argued that the polymer melts exhibiting "deformation softening" tend to show low critical draw ratio in isothermal conditions. This is supported by experimental results for polypropylene fibers (154).

The present experimental results are consistent with the above theories based on rate-dependent elongational viscosity behavior. In "elongational rate thinning" fluids, the accumulation of the material in the threadline causing draw resonance is prone to occur. In other words, loading of small particles to polymer melts may result in a nonhomogeneous local deformation in the threadline which is initiated by forced oscillations.

C.2. Draw Resonance During Nonisothermal Melt Spinning

C.2.1. Results

The effects of fillers (loading level: 10%) and loading level on draw resonance during nonisothermal melt spinning were studied.

Table VIII.2 shows the critical draw ratio for the samples used. The relative amplitude, D_{max}/D_{min} is shown as a function of draw ratio in Fig. VIII.8. An addition of fillers decreases the critical draw ratio and increases draw resonance in magnitude. PS melts reinforced with deformable particles such as HIPS and HDPE/PS blends tend to show smaller diameter fluctuations than those with rigid particles.

Figure VIII.9 and Fig. VIII.10 show the period, T, and the wavelength, λ, to spinline length, L, of draw resonance occurring under nonisothermal conditions as a function of draw ratio, respectively. It seems to be difficult to find any differences in the period among the samples used. However, some effects of small particles on the wavelength can be noticed in Fig. VIII.10. Highly-filled systems increase the value, λ/L of draw resonance particularly at high draw ratio spinning.

C.2.2. Discussion

As discussed in a previous section, the introduction of small particles to polymers tends to result in a rapid decrease in the spinline elongational viscosity with increasing elongational rates, i.e., "elongational rate thinning," causing diameter fluctuations of fibers. The similar trends observed in Fig. VIII.8 and Table VIII.2 can be interpreted in terms of the same arguments. Nonuniformities in elongational rates along the spinline and a strong "elongational rate thinning" behavior leads to the heterogeneous local deformation in the threadline by forced oscillations. Therefore, the present experimental results are consistent with the theory associated with rate-dependent elongational viscosity characteristics mentioned before.

Table VIII.2. Critical Draw Ratio During Nonisothermal Melt Spinning

Sample	Critical Draw Ratio
PS	40
PS/CB (10%)	7
PS/CB (20%)	5
PS/TiO_2 (10%)	10
PS/TiO_2 (20%)	10
PS/treated $CaCO_3$ (10%)	10
PS/treated $CaCO_3$ (20%)	6
PS/HDPE (10%)	20
HIPS-C	25

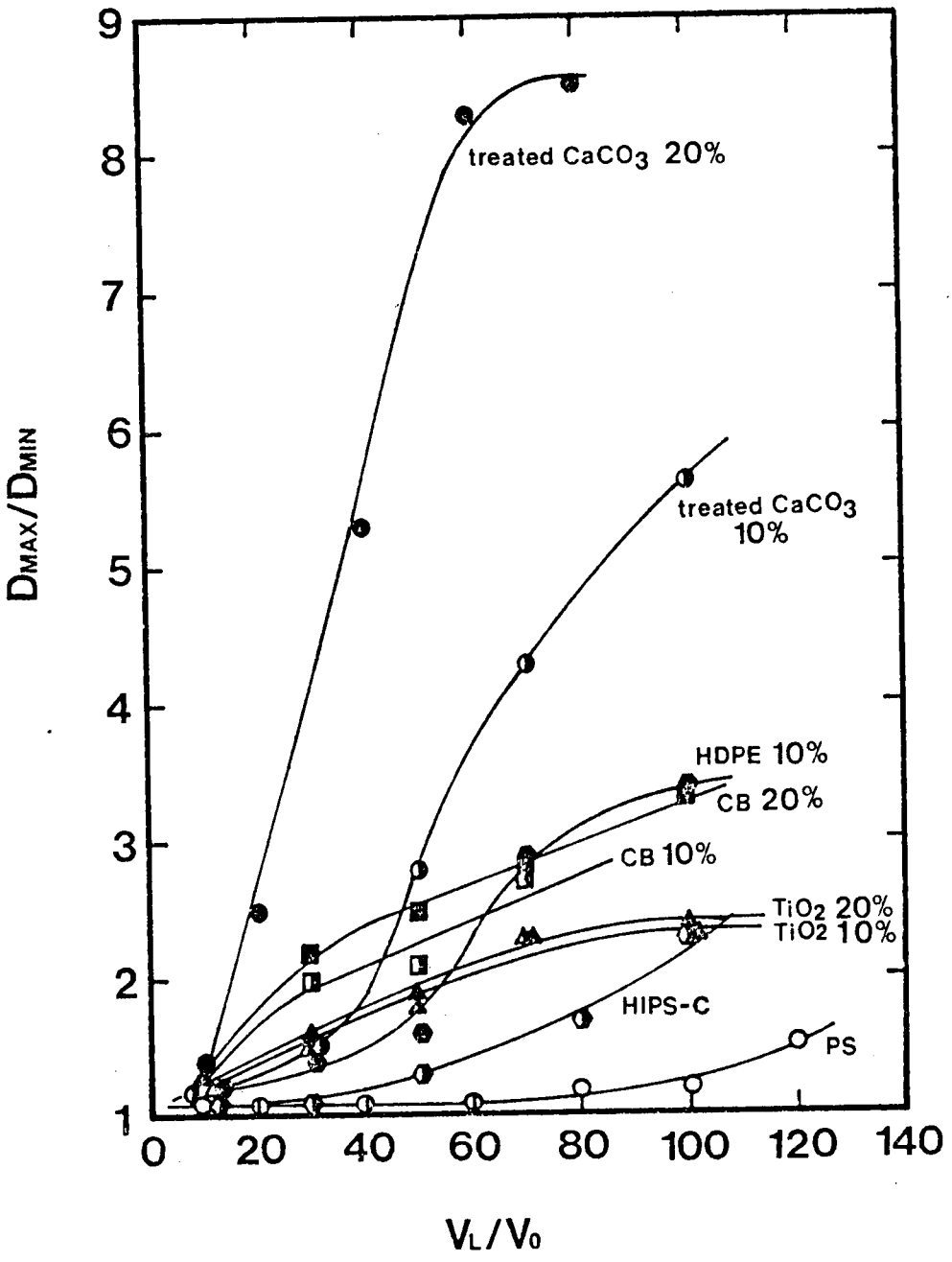

Figure VIII.8. Diameter Fluctuation as a Function of Draw Ratio for Various Filled PS under Nonisothermal Conditions.

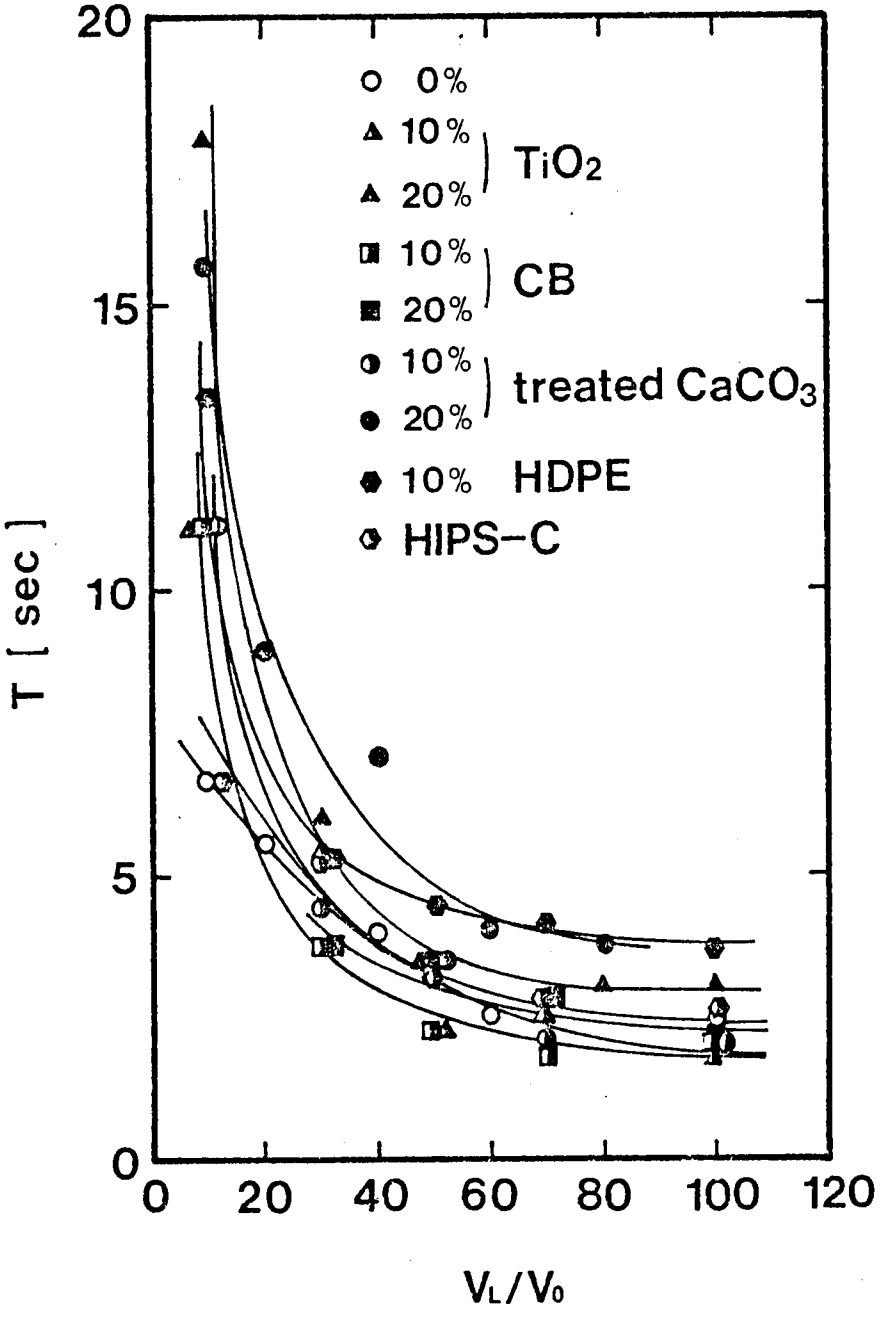

Figure VIII.9. Period of Draw Resonance as a Function of Draw Ratio for Various Filled PS under Nonisothermal Conditions.

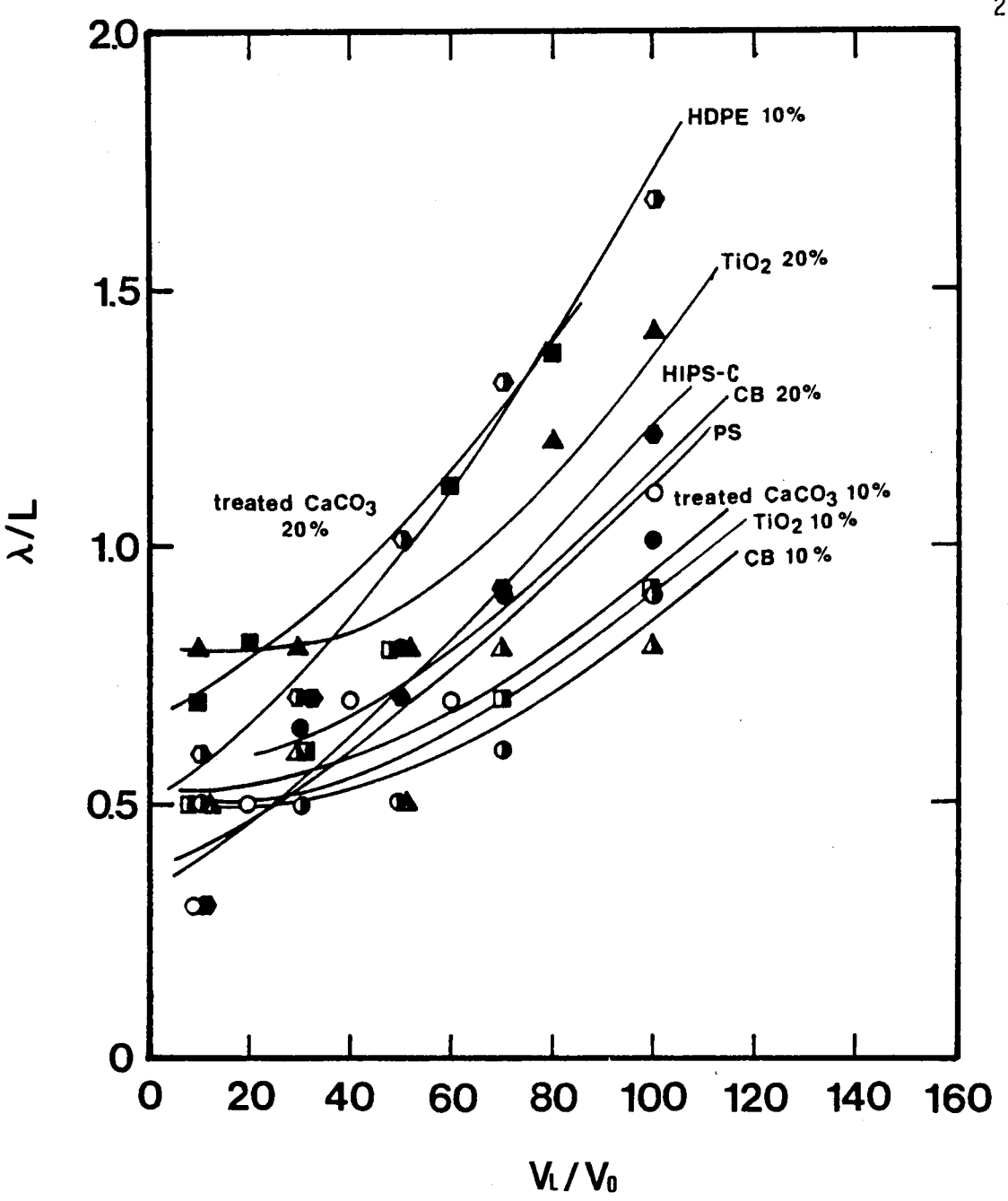

Figure VIII.10. Ratio of Wavelength of Draw Resonance to Spinline Length as a Function of Draw Ratio for Various Filled PS under Nonisothermal Conditions.

If we correspond the steady state elongational viscosity to the spinline one, differences in diameter fluctuations observed between rigid and deformable particle-reinforced systems can be interpreted in terms of those in "elongational rate thinning" behavior which can be seen in Chapter VI. The former shows a stronger "elongational rate thinning" and a more unstable spinline behavior than the latter. However, the reason for enhanced diameter fluctuations for treated $CaCO_3$-reinforced systems is not clear.

Figure VIII.9 and Fig. VIII.10 show that the value, λ/L, is almost inversely proportional to the period, T. A highly loading of small particles may increase the value λ/L as well as the amplitude of diameter fluctuations, i.e., decreases the period. In other words, the fiber diameter tends to show periodical fluctuations.

Ishihara and Kase (104) have solved the equations of continuity and momentum with the power law viscosity model for nonlinear limit cycle solutions (103) using different values of the power law exponent and steady state draw ratio. They have found that only these two parameters affect the normalized wave form of the limit cycle solutions under isothermal conditions, and show that the fluids with small power law exponents, i.e., "elongational rate thinning" fluids tend to take a wave form with a larger amplitude and a longer wavelength compared to "elongational rate thickening" fluids. Therefore, the trends on wavelength mentioned above agree well with Ishihara and Kase's theoretical analysis. Thus, the effects of an introduction of small particles to polymers on draw resonance, i.e., periodical diameter fluctuations, may

be interpretable in terms of the rate-dependent elongational viscosity behavior, in other words, "elongational rate thinning" effects.

White and Ide (220) have related the spinline residence time to draw resonance behavior, i.e., as it increases, draw resonance is prone to occur. In Fig. VIII.10, to obtain the same resonance wavelength, $(v_0)_{filled}$ should be higher than $(v_0)_{unfilled}$ at a constant L, and $(L)_{filled}$ should be shorter than $(L)_{unfilled}$ at a constant v_L/v_0. In the melt spinning of filled systems, we need to shorten the spinline residence time compared with pure systems because of draw resonance.

CHAPTER IX

CONCLUSIONS AND RECOMMENDATIONS

A. Conclusions

Rheological properties including both shear and elongational flow and melt spinning characteristics for PS melts reinforced with small particles were studied. Shear viscosity, normal stress, elongational viscosity and elongation to break were measured. In the melt spinning experiments, unstable spinline behavior, i.e., draw resonance was studied. Furthermore, the spinline elongational viscosity was determined under isothermal conditions.

For the shear viscosity of concentrated suspensions containing small particles, a theoretical mechanistic analysis was attempted, taking into account particle-particle interactions. Then, constitutive equations consistent with the mechanistic theory were discussed. Comparisons of experimental data with the theories were made.

For the experimental studies of the PS melts with small particles the main conclusions which were obtained are:

1. The shear viscosity increases with increasing loading level and decreasing particle size. Surface treatment of $CaCO_3$ decreases the shear viscosity.

2. These highly-filled systems exhibit yield values during shear flow, that is, they do not show the Newtonian viscosity. The yield

value increases with increasing loading level and decreasing particle size. Surface treatment of $CaCO_3$ decreases the yield value.

3. The steady state elongational viscosity, which was achieved in the present study, increases with increasing loading level and decreasing particle size. Surface treatment of $CaCO_3$ decreases the elongational viscosity.

4. The elongational flow yield value increases with increasing loading level and decreasing particle size. Surface treatment of $CaCO_3$ decreases the yield value.

5. The ratio of tensile yield stress to shear yield stress is close to $\sqrt{3}$. This suggests that these systems may obey von Mises yield criterion.

6. The first normal stress difference at constant shear stress decreases with increasing loading level and decreasing particle size. Surface treatment increases slightly the first normal stress difference.

7. Elongation to break in elongational flow experiments decreases with increasing loading level. Surface treatment increases elongation to break.

8. Experimental data on the effects of loading level and particle size on shear viscosity are consistent with the prediction from the proposed mechanistic theory. However, the theory seems not to fully predict shear viscosity behavior for surface treated filler-loaded systems.

9. Results on both shear and elongational flow mentioned above agree well with the phenomenological theory of White based on the

von Mises yield criterion. However, some discrepancies between data and theory in normal stress were observed. This is probably in part due to the effect of yield stress on the normal stress measurements for highly-filled systems.

10. Loading of small particles increases draw resonance during both isothermal and nonisothermal melt spinning.

11. Spinline elongational viscosity for small particle-filled systems tends to show a strong "elongational rate thinning" behavior compared with unfilled systems, the same tendency as in the steady state elongational viscosity. Loading of small particles makes profiles of elongational rate along spinline nonuniform.

12. High impact polystyrene melts used in this study appear not to exhibit yield values. This is probably due to large rubber particle size.

B. Recommendations

The following studies on rheological properties and processing characteristics of polymer melts reinforced with small particles are recommended for future works:

1. More extensive studies of the effect of particle characteristics are needed, particularly surface character.

2. The determination of an accurate yield surface is desirable. More experiments are needed.

3. Theoretical studies on more general constitutive equation for concentrated suspensions of small particles.

4. We need to investigate further the effects of mixing or mastication processes on rheological properties.

5. Investigations on processing characteristics of highly-filled polymer melts.

LIST OF REFERENCES

LIST OF REFERENCES

1. Acierno, D., J. N. Dalton, J. M. Rodriguez and J. L. White, J. Appl. Polymer Sci., 15, 2395 (1971).

2. Adler, P. M., Rheol. Acta, 17, 288 (1978).

3. Aoki, Y., J. Soc. Rheol., Japan, 7, 20 (1979).

4. Bagchi, A. K. and K. K. Sirkar, J. Appl. Polymer Sci., 23, 1653 (1979).

5. Bankar, V. G., J. E. Spruiell and J. L. White, J. Appl. Polymer Sci., 21, 2135 (1977).

6. Barthés-Biesel, D. and A. Acrivos, Int. J. Multiphase Flow, 1, 1 (1973).

7. Batchelor, G. K., J. Fluid Mech., 41, 545 (1970).

8. Batchelor, G. K., J. Fluid Mech., 46, 813 (1971).

9. Batchelor, G. K., Ann. Rev. Fluid Mech., 6, 227 (1974).

10. Batchelor, G. K. and J. T. Green, J. Fluid Mech., 56, 401 (1972).

11. Bauer, W. H. and E. A. Collins, "Rheology," Vol. 4, ed. by F. R. Eirich, Academic Press, New York (1967).

12. Bauwens, J. C., J. Polymer Sci., Part A-2, 5, 1145 (1967).

13. Bauwens, J. C., J. Polymer Sci., Part A-2, 8, 893 (1970).

14. Bell, G. M., S. Levine and L. M. McCartney, J. Colloid and Interface Sci., 33, 335 (1970).

15. Berko-Boateng, V., M.S. Thesis, The University of Tennessee, Knoxville (1977).

16. Bernstein, B., E. A. Kearsley and L. J. Zapas, Tran. Soc. Rheol., 7, 391 (1963).

17. Binding, D. M., J. M. Davies and K. Walters, J. Non-Newtonian Fluid Mech., 1, 259 (1976).

18. Binding, D. M., J. F. Hutton and K. Walters, Rheol. Acta., 15, 540 (1976).

19. Bingham, E. C., "Fluidity and Plasticity," McGraw-Hill, NY (1922).

20. Bingham, E. C. and H. S. Green, Proc. ASTM, 19, 640 (1919).

21. Bird, R. B., W. E. Stewart and E. N. Lightfoot, "Transport Phenomena," John Wiley, New York (1960).

22. Boaira, M. S. and C. E. Chaffey, Polymer Eng. Sci., 17, 715 (1977).

23. Bogue, D. C., Ind. Eng. Chem. Fund., 5, 253 (1966).

24. Bogue, D. C., "Tensile Viscosity," Polymer Science and Engineering Report, No. 123, The University of Tennessee, Knoxville (1978).

25. Bogue, D. C. and J. L. White, "Engineering Analysis of Non-Newtonian Fluid," NATO Agardograph, No. 144 (1970).

26. Boltzmann, L., Sitzungber. Akad. Wiss., Wien, 70, 275 (1874).

27. Booth, F., Proc. Roy. Soc., London, A203, 533 (1950).

28. Booth, F., Nature, 161, 83 (1948).

29. Brandrup, J. and E. H. Immergut, "Polymer Handbook," 2nd ed., Wiley-Interscience, New York (1975).

30. Brindley, C., J. M. Davies and K. Walters, J. Non-Newtonian Fluid Mech., 1, 19 (1976).

31. Brodnyan, J. G., Tran. Soc. Rheol., 12, 357 (1968).

32. Brodnyan, J. G. and E. L. Kelley, J. Colloid Sci., 20, 7 (1965).

33. Burgers, J. M., "Second Report on Viscosity and Plasticity," Amsterdam, North-Holland (1938).

34. Casale, A., A. Moroni and C. Spreafico, ACS Poly. Prepr., 15 (1), 334 (1974).

35. Casson, N., "Rheology of Disperse Systems," Pergamon, London (1959).

36. Chan, F. S., J. Blachford and D. A. I. Goring, J. Colloid and Interface Sci., 22, 378 (1966).

37. Chan, Y., M.S. Thesis, The University of Tennessee, Knoxville (1977).

38. Chan, Y., J. L. White and Y. Oyanagi, Trans. Soc. Rheol., 22, 507 (1978).

39. Chang, E. P. and A. Takahashi, Polymer Eng. Sci., 18, 350 (1978).

40. Chapman, F. M. and T. S. Lee, SPE J., 26, 37 (1970).

41. Chen, I. J. and D. C. Bogue, Trans. Soc. Rheol., 16, 59 (1972).

42. Chen, I. J., G. E. Hagler, L. E. Abott, D. C. Bogue and J. L. White, Trans. Soc. Rheol., 16, 473 (1972).

43. Christensen, H., J. Lubrication Tech., 92, 145 (1970).

44. Cogswell, F. N., Appl. Polymer Symp., No. 27, 1 (1975).

45. Coleman, B. D., H. Markovitz and W. Noll, "Viscoelastic Flow of Non-Newtonian Fluid," Springer Verlag, NY (1966).

46. Coleman, B. D. and W. Noll, Arch. Rat. Mech. Anal., 6, 355 (1960).

47. Collins, E. A. and J. T. Oetzel, Rubber Age, March (1970).

48. Cotten, G. R. and J. L. Thiele, Rubber Chem. Tech., 51, 749 (1978).

49. Coulomb, C. A., Mém. Math. et Phys., 7, 343 (1773).

50. Czarnecki, L. and J. L. White, "Experimental Studies of the Shear Flow Rheological Properties, Fiber Damage Characteristics and Mastication Effects of Kevlar®, Glass and Cellulose Fiber Reinforced Polystyrene Melts," Polymer Science and Engineering Report, No. 131, The University of Tennessee, Knoxville (1979).

51. Czarnecki, L. and J. L. White, unpublished data (1979).

52. Derjaguin, B., Kolloid Z., 69, 155 (1934).

53. Derjaguin, B., Trans. Faraday Soc., 36, 203 (1940).

54. Eilers, H., Kolloid Z., 102, 154 (1943).

55. Einstein, A., Ann. Physik, 19, 289 (1906).

56. Einstein, A., Ann. Physik, 34, 591 (1911).

57. Ericksen, J. L., Arch. Rat. Mech. Anal., 4, 231 (1960).

58. Ericksen, J. L., Kolloid Z., 173, 117 (1960).

59. Faulkner, D. L. and L. R. Schmidt, Polymer Eng. Sci., 17, 657 (1977).

60. Fisher, R. J. and M. M. Denn, AIChE J., 22, 236 (1976).

61. Fisher, R. J. and M. M. Denn, AIChE J., 23, 23 (1977).

62. Frankel, N. A. and A. Acrivos, Chem. Eng. Sci., 22, 847 (1967).

63. Freundlich, H. and F. Juliusberger, Trans. Faraday Soc., 31, 920 (1935).

64. Freundlich, H. and H. L. Roder, Trans. Faraday Soc., 34, 308 (1938).

65. Frisch, H. L. and R. Simha, "Rheology," Vol. 1, ed. by F. Eirich, Academic Press, New York (1966).

66. Fryling, C. F., J. Colloid Sci., 18, 713 (1963).

67. Furuta, I., V. M. Lobe and J. L. White, J. Non-Newtonian Fluid Mech., 1, 207 (1976).

68. Green, A. E. and R. S. Rivlin, Arch. Rat. Mech. Anal., 1, 1 (1957).

69. Goddard, J. D., J. Non-Newtonian Fluid Mech., 1, 1 (1976).

70. Goddard, J. D., J. Non-Newtonian Fluid Mech., 2, 169 (1977).

71. Goddard, J. D., SM Arch., 2, 403 (1977).

72. Guth, E. and R. Simha, Kolloid Z., 74, 266 (1936).

73. Hamaker, H. C., Physica, 4, 1058 (1937).

74. Han, C. D., J. Appl. Polymer Sci., 15, 2591 (1971).

75. Han, C. D., J. Appl. Polymer Sci., 18, 821 (1974).

76. Han, C. D., "Rheology in Polymer Processing," Academic Press, New York (1976).

77. Han, C. D. and Y. W. Kim, J. Appl. Polymer Sci., 18, 2589 (1974).

78. Han, C. D. and Y. W. Kim, Trans. Soc. Rheol., 19, 245 (1975).

79. Han, C. D., Y. W. Kim and S. J. Chen, J. Appl. Polymer Sci., 19, 2831 (1975).

80. Han, C. D. and R. R. Lamonte, Trans. Soc. Rheol., 16, 447 (1972).

81. Han, C. D., R. R. Lamonte and Y. T. Shah, J. Appl. Polymer Sci., 16, 3307 (1972).

82. Han, C. D., C. Sandford and H. J. Yoo, Polymer Eng. Sci., 18, 850 (1978).

83. Hand, G. L., Arch. Nat. Mech. Anal., 7, 6 (1961).

84. Hand, G. L., J. Fluid Mech., 13, 33 (1962).

85. Happel, J., J. Appl. Phys., 28, 1288 (1957).

86. Happel, J. and H. Brenner, "Low Reynolds Number Hydrodynamics," Prentice-Hall, Englewood Cliffs, NJ (1965).

87. Hencky, H., Z. Angew. Math. und Mech., 4, 322 (1924).

88. Hencky, H., Ann. Phys., 2, 617 (1929).

89. Hill, R., "Mathematical Theory of Plasticity," Oxford Univ. Press London (1950).

90. Hinch, E. J. and L. G. Leal, J. Fluid Mech., 71, 481 (1975).

91. Hinch, E. J. and L. G. Leal, J. Fluid Mech., 76, 187 (1976).

92. Hoffman, R. L., Trans. Soc. Rheol., 16, 155 (1972).

93. Hoffman, R. L., J. Colloid and Interface Sci., 46, 491 (1974).

94. Hogg, R., T. W. Healy and D. W. Fuerstenau, Trans. Faraday Soc., 62, 1638 (1966).

95. Hohenemser, K. and W. Prager, Z. Angew. Math. und Mech., 12, 216 (1932).

96. Hopper, J. R., Rubber Chem. Tech., 40, 403 (1967).

97. Hutton, J. F., "The Rheology of Lubricants," Appl. Sci. Pub. (1973).

98. Hutton, J. F., Rheol. Acta, 14, 979 (1975).

99. Ide, Y., Ph.D. Dissertation, The University of Tennessee, Knoxville (1976).

100. Ide, Y. and J. L. White, J. Appl. Polymer Sci., 20, 2511 (1976).

101. Ide, Y. and J. L. White, J. Non-Newtonian Fluid Mech., 2, 281 (1977).

102. Ide, Y. and J. L. White, J. Appl. Polymer Sci., 22, 1061 (1978).

103. Ishihara, H. and S. Kase, J. Appl. Polymer Sci., 21, 169 (1977).

104. Ishihara, H. and S. Kase, J. Appl. Polymer Sci., 19, 557 (1975).

105. Itoyama, K. and A. Soda, J. Appl. Polymer Sci., 23, 1723 (1979).

106. Jeffrey, D. J. and A. Acrivos, AIChE J., 22, 417 (1976).

107. Jeffrey, G. B., Proc. Roy. Soc., London, A102, 161 (1923).

108. Jinescu, V. V., Int. Chem. Eng., 14, 397 (1974).

109. Kachanov, L. M., "Foundations of the Theory of Plasticity," North-Holland, Amsterdam (1971).

110. Kase, S., J. Appl. Polymer Sci., 18, 3279 (1974).

111. Kataoka, T., T. Kitano and T. Nishimura, Rheol. Acta, 17, 626 (1978).

112. Kataoka, T., T. Kitano, M. Sasahara and K. Nishijima, Rheol. Acta, 17, 149 (1978).

113. Katz, H. S. and Y. V. Milewski, "Handbook of Fillers and Reinforcements for Plastics," von Nostrand Reinhold Company, NY (1978).

114. Krasny-Ergen, W., Kolloid Z., 74, 172 (1936).

115. Krieger, I. M., Adv. Colloid Interface Sci., 3, 111 (1972).

116. Krieger, I. M. and M. Eguiluz, Trans. Soc. Rheol., 20, 29 (1976).

117. Kruse, R. L. and J. H. Southern, Paper presented at American Institute of Chemical Engineers Meeting, Miami Beach (1978).

118. Kuhn, W., Kolloid Z., 68, 2 (1934).

119. Kuhn, W. and H. Kuhn, Helv. Chim. Acta, 28, 97 (1945).

120. Lamb, H., "Hydrodynamics," Dover, New York (1945).

121. Landau, L. D. and E. M. Lifshitz, "Fluid Mechanics," Vol. 6, Pergamon Press, New York (1959).

122. Langlois, W. E., "Slow Viscous Flow," Macmillan, New York (1964).

123. Langmuir, I., J. Chem. Phys., 6, 873 (1938).

124. Laun, H. M. and H. Münstedt, Rheol. Acta, 15, 517 (1976).

125. Laun, H. M. and H. Münstedt, Rheol. Acta, 17, 415 (1978).

126. Lee, T. S., Proc. 5th Int. Rheol. Cong., 4, 421 (1970).

127. Lee, B. L. and J. L. White, Trans. Soc. Rheol., 19, 481 (1975).

128. Leider, P. J., Ind. Eng. Chem. Fund., 13, 342 (1974).

129. Leider, P. J. and R. B. Bird, Ind. Eng. Chem. Fund., 13, 336 (1974).

130. Lobe, V. M., Ph.D. Dissertation, The University of Tennessee, Knoxville (in preparation).

131. Lobe, V. M. and J. L. White, Polymer Eng. Sci. (in press).

132. Lodge, A. S., Proc. 2nd Int. Rheol. Cong., 229 (1952).

133. Lodge, A. S., Trans. Soc. Rheol., 52, 120 (1956).

134. Lodge, A. S., "Elastic Liquid," Academic Press, NY (1964).

135. Malvern, L. E., "Introduction to the Mechanics of a Continuous Medium," Prentice-Hall, Englewood Cliffs, NJ (1969).

136. Mandelkern, L., "Crystallization of Polymers," McGraw-Hill, New York (1964).

137. Maron, S. H. and S. M. Fok, J. Colloid Sci., 10, 482 (1955).

138. Maron, S. H., B. P. Madow and I. M. Krieger, J. Colloid Sci., 6, 584 (1951).

139. Maron, S. H. and A. W. Sisko, J. Colloid Sci., 12, 99 (1957).

140. Matsumoto, T., Ph.D. Dissertation, Kyoto University, Japan (1973).

141. Matsumoto, T., C. Hitomi and S. Onogi, Trans. Soc. Rheol., 19, 541 (1975).

142. Matsumoto, T., A. Takashima, T. Masuda and S. Onogi, Trans. Soc. Rheol., 14, 617 (1970).

143. Maxwell, J. C., Phil. Trans. Roy. Soc., 157, 249 (1866).

144. McCabe, C. C. and N. Mueller, Trans. Soc. Rheol., 5, 329 (1961).

145. Meissner, J., Rheol. Acta, 10, 230 (1971).

146. Meissner, J., Trans. Soc. Rheol., 16, 405 (1972).

147. Metzner, A. B. and M. Whitlock, Trans. Soc. Rheol., 2, 239 (1958).

148. Middleman, S., Trans. Soc. Rheol., 13, 123 (1969).

149. Mikami, Y., T. Matsumoto and S. Onogi, J. Soc. Rheol. Japan, 4, 149 (1976).

150. Minagawa, N. and J. L. White, Polymer Eng. Sci., 15, 825 (1975).

151. Minagawa, N. and J. L. White, J. Appl. Polymer Sci., 20, 501 (1976).

152. Minoshima, W., M.S. Thesis, The University of Tennessee, Knoxville (1978).

153. Minoshima, W., J. S. White and J. E. Spruiell, Polymer Eng. Sci. (in press).

154. Minoshima, W., J. L. White and J. E. Spruiell, "Experimental Investigations of the Influence of Molecular Weight Distribution on Melt Spinning and Extrudate Swell Characteristics of Polypropylene," Polymer Science and Engineering Report, No. 128, The University of Tennessee, Knoxville (1979).

155. Mises, R. von, Nachr. d. Gesellschaft der Wissenschaft zu Göttingen Math. Phys. Klasse (1913).

156. Mooney, M., J. Colloid Sci., 6, 162 (1951).

157. Münstedt, H., Proc. 7th Int. Rheol. Cong., 496 (1976).

158. Münstedt, H., Paper presented at International Conference on "Toughening Plastics" in London (1978).

159. Nadai, A., "Theory of Flow and Fracture of Solid," 2nd ed., McGraw-Hill, New York (1950).

160. Nakajima, N. and E. A. Collins, Rubber Chem. Tech., 48, 615 (1975).

161. Nakajima, N., H. H. Bowerman and E. A. Collins, Proc. Int. Rubber Conf., Tokyo, 15-3-20 (1975).

162. Nakajima, N., H. H. Bowerman and E. A. Collins, J. Appl. Polymer Sci., 21, 3063 (1977).

163. Newman, S. and Q. A. Trementozzi, J. Appl. Polymer Sci., 9, 3071 (1965).

164. Nicodemo, L. and L. Nicolais, J. Appl. Polymer Sci., 18, 2539 (1974).

165. Nicodemo, L. and L. Nicolais, Polymer, 15, 589 (1974).

166. Noll, W., Rat. Mech. Anal., 4, 13 (1955).

167. Oda, K., J. L. White and E. S. Clark, Polymer Eng. Sci., 18, 25 (1978).

168. Oldroyd, J. G., Proc. Camb. Phil. Soc., 43, 100 (1947).

169. Oldroyd, J. G., Proc. Camb. Phil. Soc., 43, 396 (1947).

170. Oldroyd, J. G., Proc. Camb. Phil. Soc., 43, 521 (1947).

171. Oldroyd, J. G., Proc. Camb. Phil. Soc., 44, 200 (1948).

172. Oldroyd, J. G., Proc. Camb. Phil. Soc., 44, 214 (1948).

173. Oldroyd, J. G., Proc. Roy. Soc., London, A200, 523 (1950).

174. Onogi, S., T. Masuda and T. Matsumoto, Trans. Soc. Rheol., 14, 275 (1970).

175. Onogi, S., T. Matsumoto and Y. Warashina, Trans. Soc. Rheol., 17, 175 (1973).

176. Onogi, S., Y. Mikami and T. Matsumoto, Polymer Eng. Sci., 17, 1 (1977).

177. Payne, A. R., J. Appl. Polymer Sci., 3, 127 (1960).

178. Payne, A. R., J. Appl. Polymer Sci., 6, 57 (1962).

179. Pearson, J. R. A. and Y. T. Shah, Ind. Eng. Chem. Fund., 13, 134 (1974).

180. Petrie, C. J. S. and M. M. Denn, AIChE J., 22, 209 (1976).

181. Pfizer Inc., Technical Paper.

182. Plochocki, A. P., Trans. Soc. Rheol., 20, 287 (1976).

183. Polakowski, N. H. and E. J. Ripling, "Strength and Structure of Engineering Materials," Prentice-Hall, Englewood Cliffs, NJ (1966).

184. Prager, S., Trans. Soc. Rheol., 1, 53 (1962).

185. Prager, W., "Rheology," Vol. 1, ed. by F. R. Eirich, Academic Press, New York (1966).

186. Prager, W., "Introduction to Mechanics of Continua," Ginn New York (1961).

187. Quemada, D., Rheol. Acta, 16, 82 (1977).

188. Quemada, D., Rheol. Acta, 17, 632 (1978).

189. Quemada, D., Rheol. Acta, 17, 643 (1978).

190. Rehbinder, P., Discuss. Faraday Soc., 18, 151 (1954).

191. Reiner, M., "Deformation, Strain and Flow," H. K. Lewis and Co., London (1969).

192. Reynolds, O., Phil. Mag., 20, 469 (1885).

193. Roman, J. F., M.S. Thesis, The University of Tennessee, Knoxville (1974).

194. Russel, W. B., J. Colloid and Interface Sci., 55, 590 (1976).

195. Russel, W. B., J. Fluid Mech., 85, 209 (1978).

196. Sano, Y. and K. Orii, Seni Gakkaishi, Japan, 24, 212 (1968).

197. Schofield, A. N. and C. P. Wroth, "Critical State Soil Mechanics," McGraw-Hill, New York (1968).

198. Shah, Y. T. and J. R. A. Pearson, Polymer Eng. Sci., 12, 219 (1972).

199. Simha, R., J. Appl. Phys., 23, 1020 (1952).

200. Spriggs, T. W. and R. B. Bird, Ind. Eng. Chem. Fund., 4, 182 (1964).

201. Spriggs, T. W., Chem. Eng. Sci., 20, 931 (1965).

202. Takaki, T. and D. C. Bogue, J. Appl. Polymer Sci., 19, 419 (1975).

203. Tanner, R. I., Trans. Soc. Rheol., 12, 155 (1968).

204. Tanner, R. I., AIChE J., 15, 177 (1969).

205. Taylor, G. I., Proc. Roy. Soc., London, A138, 41 (1932).

206. Taylor, G. I., Proc. Roy. Soc., London, A146, 501 (1934).

207. Thomas, D. G., J. Colloid Sci., 20, 267 (1965).

208. Tresca, H., C. R. Acad. Sci. (Paris), 59, 754 (1864).

209. Tresca, H., C. R. Acad. Sci. (Paris), 64, 809 (1867).

210. Umeya, K., T. Kanno, M. Wagatsuma and H. Igarashi, J. Soc. Rheol., Japan, 3, 145 (1975).

211. Umeya, K., J. Soc. Rheol., Japan, 4, 91 (1976).

212. Verwey, E. J. W. and J. Th. G. Overbeek, "The Theory of the Stability of Lyophobic Sols," Elsevier, Amsterdam (1948).

213. Vinogradov, G. V., A. Ya. Malkin, E. P. Plotnikova, O. Yu. Sabsai and N. E. Nikolayeva, Int. J. Poly. Mater., 2, 1 (1972).

214. Ward, I., "Mechanical Properties of Solid Polymers," Wiley-Interscience, NY (1971).

215. Weltmann, R. N., "Rheology," Vol. 3, ed. by F. R. Eirich, Academic Press, New York (1967).

216. White, J. L., Appl. Polymer Symp., 33, 31 (1978).

217. White, J. L., J. Non-Newtonian Fluid Mech., 5, 177 (1979).

218. White, J. L., Y. Chan and Y. Oyanagi, J. Soc. Rheol., Japan, 6, 1 (1978).

219. White, J. L. and J. W. Crowder, J. Appl. Polymer Sci., 18, 1013 (1974).

220. White, J. L. and Y. Ide, J. Appl. Polymer Sci., 22, 3057 (1978).

221. White, J. L. and A. B. Metzner, J. Appl. Polymer Sci., 8, 1367 (1963).

222. White, J. L. and J. F. Roman, J. Appl. Polymer Sci., 20, 1005 (1976).

223. White, J. L. and N. Tokita, J. Appl. Polymer Sci., 12, 1589 (1968).

224. Williams, M. C. and R. B. Bird, Phys. Fluid, 5, 1126 (1962).

225. Winspear, G. G., "Rubber Handbook," R. T. Vanderbilt Company Inc. (1968).

226. Yamamoto, M., J. Phys. Soc., Japan, 11, 413 (1956).

227. Yamamoto, M., J. Phys. Soc., Japan, 12, 1148 (1957).

228. Yamamoto, M., "Buttai no Henkeigaku," Seibundo, Tokyo (1972).

229. Zakharenko, N. V., F. S. Tolstukhina and G. M. Bartenev, Rubber Chem. Tech., 35, 326 (1962).

230. Zaremba, S., Bul. Acad. Cracovie, 594 (1903).

231. Zolotor, A. M., Mod. Plastics, 68 (1970).

232. Zosel, A., Rheol. Acta, 11, 229 (1972).

APPENDIX

APPENDIX

Using the approximation, Equation III.22, f(x) reduces to

$$f(x) = \int_x^1 \frac{x(1-x^2)^{\frac{n-1}{2}}}{(B-x)^{2n+1}}\,dx \sim \int_x^1 \frac{x}{(B-x)^{2n+1}}\,dx$$

$$= -\frac{1}{2n-1}\left[\left(\frac{1}{B-1}\right)^{2n-1} - \left(\frac{1}{B-x}\right)^{2n-1}\right] + \frac{B}{2n}\left[\left(\frac{1}{B-1}\right)^{2n} - \left(\frac{1}{B-x}\right)^{2n}\right] .$$

Therefore

$$f(0) - f(x) = -\frac{1}{2n-1}\left(\frac{1}{B-x}\right)^{2n-1} + \frac{B}{2n}\left(\frac{1}{B-x}\right)^{2n} + \frac{1}{(2n)(2n-1)}\left(\frac{1}{B}\right)^{2n-1} .$$

Furthermore

$$\int_0^1 x\{f(0) - f(x)\}dx = -\frac{1}{2n-1}\int_0^1 \frac{x}{(B-x)^{2n-1}}\,dx + \frac{B}{2n}\int_0^1 \frac{x}{(B-x)^{2n}}\,dx$$

$$+ \frac{1}{2n(2n-1)}\left(\frac{1}{B}\right)^{2n}\int_0^1 x\,dx .$$

After tedious calculations, we obtain

$$\int_0^1 x\{f(0) - f(x)\}dx = -\frac{1}{(2n-1)(2n-2)}\frac{B}{(B-1)^{2n-2}} + \frac{1}{(2n-1)(2n-3)}\left(\frac{1}{B-1}\right)^{2n-3}$$

$$- \frac{1}{(2n-1)(2n-2)(2n-3)}\left(\frac{1}{B}\right)^{2n-3} + \frac{1}{(2n)(2n-1)}\frac{B^2}{(B-1)^{2n-1}}$$

$$- \frac{1}{(2n)(2n-2)} \frac{B}{(B-1)^{2n-2}} + \frac{1}{(2n)(2n-1)(2n-2)} \left(\frac{1}{B}\right)^{2n-3}$$

$$+ \frac{1}{4n(2n-1)} \left(\frac{1}{B}\right)^{2n-1} .$$

From $2n-2 \leq 0$ and $2n-3 < 0$,

$$\lim_{B\to 1} \frac{B}{(B-1)^{2n-2}} = 0$$

$$\lim_{B\to 1} \left(\frac{1}{B-1}\right)^{2n-3} = 0 .$$

Therefore, for $\frac{h_0}{a} \to a$, i.e., $B \to 1$

$$\lim_{B\to 1} \int_0^1 x\{f(0) - f(x)\}dx = \lim_{B\to 1} \frac{1}{(2n)(2n-1)} \frac{B^2}{(B-1)^{2n-1}}$$

$$\simeq \frac{1}{(2n)(2n-1)} \lim_{B\to 1} \left(\frac{B}{B-1}\right)^{2n-1}$$

$$= \frac{1}{(2n)(2n-1)} 2^{2n-1} \left(\frac{a}{h_0}\right)^{2n-1} .$$

F given by Equation III.20, using Equation III.19a, is

$$F = \int_0^a (p(r) - p_0) 2\pi r dr = 2\pi K \left[\frac{(n+1)(2n+1)}{n}\right]^n u^n 2^{-2n-1} a^{2-n} \int_0^1 x\{f(0) - f(x)\}dx.$$

We can calculate E

$$E = \left|\frac{1}{2} uF\right| = \pi K\left[\frac{(n+1)(2n+1)}{n}\right]^n u^n 2^{-2n-1} a^{2-n}\left|\int_0^1 x\{f(0) - f(x)\}dx\right|.$$

Therefore

$$\lim_{\substack{h_0 \\ \overline{a} \to 0}} E = \lim_{B\to 1} E = \pi K\left[\frac{(n+1)(2n+1)}{n}\right]^n u^{n+1} 2^{-2n-1} a^{2-n}\left|\lim_{B\to 1}\int_0^1 x\{f(0) - f(x)\}dx\right|.$$

Substituting the equation derived above,

$$\lim_{\substack{h_0 \\ \overline{a} \to 0}} E = \pi K\left[\frac{(n+1)(2n+1)}{n}\right]^n u^{n+1} 2^{-2n-1} a^{2-n}\left|\frac{1}{(2n)(2n-1)}\right| 2^{2n-1} \left(\frac{a}{h_0}\right)^{2n-1}$$

$$= \alpha K a^{2-n} u^{n+1} \left(\frac{a}{h_0}\right)^{2n-1}$$

where

$$\alpha = \frac{\pi}{4}\left[\frac{(n+1)(2n+1)}{n}\right]^n \left|\frac{1}{(2n)(2n-1)}\right|.$$

VITA

The author, Hideho Tanaka, was born in Hamamatsu, Japan, on September 16, 1945, as the oldest son of Mr. and Mrs. Yoshizo Tanaka. After completing his basic education from elementary school to high school in Hamamatsu, Japan, he was admitted to Nagoya University in April 1964. He studied polymer fractionation under Professor Mitsuru Nagasawa for his bachelor thesis at the University and received a Bachelor of Engineering in Synthetic Chemistry in March 1968. He entered UBE Industries, LTD. in April 1968. Since then, he has been working for Hirakata Plastics Laboratory, UBE Industries, LTD., Osaka, Japan. He got married with Toshiko Noda in October 1973. They have two daughters, Eriko (4 years) and Yuriko (2 years). Then, he entered The University of Tennessee in September 1977. After getting a degree of Master of Science, he will rejoin Hirakata Plastics Laboratory in order to continue his work.